Hydrotropic Action and Solubilization of Sparingly Soluble Drugs

A Thesis Submitted

in Partial Fulfillment of the Requirements

for the Degree of

DOCTOR OF PHILOSOPHY

by

Shubhadip Das

to the

Department of Chemistry

Indian Institute of Technology Guwahati, India

2017

DEDICATED TO
MY BELOVED PARENTS

Declaration

I hereby declare that the matter manifested in this thesis entitled "*Hydrotropic Action and Solubilization of Sparingly Soluble Drugs*" is the result of research carried out by me in the Department of Chemistry, Indian Institute of Technology Guwahati, India under the supervision of Prof. Sandip Paul.

In keeping with the general practice of reporting scientific observations, due acknowledgement has been made wherever the work described is based on the findings of other investigators.

Shubhadip Das
IIT Guwahati

Certificate

It is certified that the work contained in this thesis entitled, "*Hydrotropic Action and Solubilization of Sparingly Soluble Drugs*" has been carried out by Mr. Shubhadip Das for the Degree of Doctor of Philosophy under my supervision and the same has not been submitted elsewhere for a degree.

Prof. Sandip Paul
Thesis Supervisor
Department of Chemistry
Indian Institute of Technology Guwahati
Guwahati-781039, India

Preface

On accomplishment of my doctorate studies, I would like to express my sincere gratitude to everyone who directly or indirectly helped me during this wonderful journey of my research career. Firstly, I would like to thank my thesis supervisor, Prof. Sandip Paul for guiding and supporting me over the years. I have been extremely lucky to have a supervisor who cared so much about my work, and who responded to my questions and queries so promptly. Prof. Paul introduced me to the world of computer simulations and was always willing to provide insightful comments on my research and encouragement throughout the research process. He gave me the freedom to pursue the research ideas I found most interesting. He also motivated me to pay careful attention to every detail of my research, and worked very hard to provide feedback on each of the articles, reports, and talks I have prepared over the past five years.

I would like to acknowledge my sincere gratitude to the doctoral committee chair and members, Prof. Arun Chattopadhyay, Dr. Subhradip Ghosh, Dr. Sumana Dutta and Dr. Manabendra Sarma for periodically assessing my work and providing valuable suggestions for its improvement. My sincere thanks go to all other faculty members in the department for their kind help at various stages of my doctoral work. I am very grateful to the Ministry of Human Resource and Development (MHRD), India for financial support and IIT Guwahati for all the facilities that were made available to me. I am also grateful to the Center for Development of Advanced Computing (CDAC), Pune and PARAM-ISHAN HPC, IIT Guwahati, for the computational support.

Further, I would like to thank all my past and present group members for their support, helpful discussions and creating a wonderful environment in the lab. A big thanks to Dr. Rahul Sarma, Dr. Subrata Paul, Dr. Bhanita Sharma and Dr. Gargi Borgohain for their help, suggestions and sharing their many experiences during my work. I am also very grateful to all other group members Krishna, Srijita, Saikat, Rabindranath, Shubhajit and Vikram.

I extend my sincere thanks to Dr. Renjith Bhaskaran, Dr. Debashis Koner, Dr. Harikrishna Sahu for their suggestions throughout my work and my friends Uday, Shilaj, Anindya, Soumen, Keshab, Gourab and the other research scholars of Chemistry department who have shared their thoughts and views with me and all the joyful moments we shared in this campus.

I take this opportunity to express my sincere thanks to all my teachers in school, college, and university days for helping and encouraging me in various aspects of my life and academics. All the learning from them will be an asset in every walk of my life.

Finally, my Ph.D. endeavor could not have been completed without the endless love, support, and blessings from my family members. I am truly grateful to my parents for their immeasurable love and care. They have always encouraged me to explore my potential and pursue my dreams. They helped me a lot to reach this stage in my life. I would also like to thank my sisters for their everlasting encouragement and supports. At the end I owe my deepest gratitude towards my better half for her eternal support and understanding of my goals and aspirations. Her infallible love and support has always been my strength.

Shubhadip Das

2017

"Natural science, does not simply describe and explain nature; it is part of the interplay between nature and ourselves."

— Werner Karl Heisenberg

Outline of the Thesis

Chapter 1

Introduction

" Expenses for pharmacological drug development of new entities are constantly rising, as the vast majority of structures fail on their way to approval. Progressively, emphasis is set on small organic molecule drugs and with this, low water solubility emerges as one of the key problems, resulting in poor bioavailability and undesirable pharmaceutical profiles. To improve solubility of small molecule compounds and reduce failure risks, the development of delivery systems and formulation additives has been the center of attention."

— S. Wieczorek et al. *J. Am. Chem. Soc.* **138**, 9349 (2016)

■ MECHANISM OF HYDROTROPIC PHENOMENON

Solubility is the phenomenon of dissolution of solute in solvent to give a homogeneous system. It is one of the most critical preformulation properties which shows significant impact on performance of a molecule. Solubility and permeability build the backbone of Biopharmaceutics Classification System (BCS). About 70% of newly developed drugs in pharmaceutical industry possess low aqueous solubility. Pharmaceutical solid oral dosage forms must undergo dissolution in the intestinal fluids of the gastrointestinal tract before they can be absorbed and reach the systemic circulation. Orally administered solid drugs will completely absorb only when they show high solubility in the gastrointestinal tract and such drugs display high bioavailability. Bioavailability depends on several factors, drug solubility in an aqueous environment and drug permeability through lipophilic membranes being the important ones. Therefore, dissolution is a critical part of the drug-delivery process and a major challenge for the formulation scientist. Various techniques can be adapted to improve solubilization of poor water soluble drug and further to improve its bioavailability. These techniques are selected on the basis of definite characteristics such as properties of drug under consideration, nature of excipients to be selected and nature of intended dosage form. The techniques generally used for solubilization of drug include chemical modification, pH adjustment, solid dispersion, complexation, co-solvency, micellar solubilization, hydrotropy etc. Pharmaceutical industries make practical and effective use of hydrotropy technique to increase the water solubility of poorly water soluble drug molecule to preclude the use of organic and costlier solvents.

Hydrotropes are substances that improve the solubility of sparingly soluble solute molecules in water. Hydrotropy is the term originally introduced by Neuberg in 1916 to describe the increase in the solubility of hydrophobic substances by the addition of fairly high concentrations of alkali metal salts of various organic acids [1]. Shortly thereafter, in 1927, Freundich and Traube separately describe the phenomenon of hydrotropy [2, 3]. “Hydro” means “water” and “tropes” mean “something other”. The phenomenon of increasing solubility of normally insoluble or sparingly soluble compounds in water by a third component or additive is termed as hydrotropy or hydrotropism. The molecular characteristic of a hydrotropic molecule is that it is a saturated hydrotropic ring and ionic compound [4]. Hydrotropes normally comprise of hydrophilic and hydrophobic moieties and the hydrophobic part is generally too small. Thus, hydrotropes are a special class of small amphiphilic organic molecules, and they resemble close structural features with classical surfactants as

well as they exhibit distinct solution properties. Hydrotropes can be ionic or nonionic and exist in a range of structures. Although the classifications of hydrotropes, based on their molecular structures, are very difficult, the most studied and effective hydrotropes are alkyl benzenesulfonates based on toluene, xylene and cumene, polyhydroxybenzene, sodium salts of lower alkanols, and derivatives of aromatic acids [5]. Furthermore, the hydrotropic actions of aromatic hydrotropes with anionic head groups are widely studied because of the fact that for them large number of isomers are possible, and the availability of interactive π orbitals is believed to be the main reason behind their hydrotropic actions. Hydrotropes with cationic hydrophilic group, for example, salts of aromatic amines and so on, are barely studied [6].

Hydrotropes have a wide range of industrial applications. The hydrotrope additives have effectiveness in both aqueous and oil phases, therefore, they have been used in detergent industries. Moreover, they are extensively used as solubilizing agents to solubilize drugs, biochemicals and organic compounds and also used in the formulation of pharmaceuticals [7-10]. It can be used in quantitative estimations of poorly water soluble drugs by UV-visible spectrophotometric analysis precluding the use of organic solvents [11]. Furthermore, hydrotropes are used for extractive separation of mixtures [12-14], for cleaning, washing and cosmetics purposes [15]. They are also used in paper and pulp industries [16]. They can influence the micelle formation of classical surfactants, phase manifestation of multicomponent systems with reference to nanodispersions and conductance percolation, clouding of surfactants and polymers [5]. As hydrotropes also possess some catalytic properties, they can be used to execute organic synthetic reactions [17, 18]. Aqueous solutions of hydrotropes can be used as alternative reaction media for organic synthesis because they are cheap, non-toxic and environment friendly. Previously, various organic transformation reactions were carried out in aqueous hydrotropic solutions [19]. Beside these, micelle and microemulsion formation can also be influenced by hydrotropes [20-22]. Their biological actions have also received wide attention [23].

It has been reported that hydrotropic solubilization is superior than the other solubilization techniques such as miscibility, micellar solubilization, cosolvency and salting in [24]. There are many advantages of hydrotropic solubilization technique, such as: (i) The solvent character is independent of pH, has high selectivity and does not require emulsification. (ii) It is cheap and easily available. (iii) It is non toxic and non reactive. (iv) It is insensitive to temperature effects, when dissolved in water. (v) It does not produce any heat when dissolved in water. (vi) It may reduce the large total concentration of hydrotropic

agents necessary to produce modest increase in solubility by employing combination of agents in lower concentration.

Although hydrotropes are usually considered as primitive amphiphiles, they have similarities and differences in terms of molecular structure and nature of self-association with that of regular amphiphiles. Furthermore, despite having a polar headgroup and a hydrophobic tail, the main structural difference between a surfactant and a hydrotrope lies in the fact that the former possesses a much longer tail alkyl chain ($C_8 - C_{20}$) whereas the latter has a relatively shorter alkyl chain ($C_0 - C_4$) [25, 26]. As a result, in hydrotropes a much higher hydrophile/lipophile balance (HLB) is observed as compared with that of surfactants. Thus, in order to solubilize an insoluble solute in water a relatively higher concentration level is required for hydrotropes than that of surfactants. In addition to that, some hydrotropes have been known to increase the solubility of organic solutes more than normal surfactants. As the surfactant forms a micelle above its critical micelle concentration (CMC) hydrotrope also shows aggregation behavior above its minimum hydrotrope concentration (MHC) [27, 28]. The dissolved solute is precipitated on dilution of hydrotrope solution, whereas in case of surfactant dilution leads to emulsification with consequent problem of separation. Unlike the micelle forming surfactants, the aqueous solution of hydrotropes do not contain any lamellar liquid crystal region. Therefore, the phase diagram of aqueous solution of hydrotropes show a single continuous isotropic liquid phase [5]. Analogous to surfactants, hydrotropes also reduce the surface tension of water in the region of 20 mN/m depending on their chemical structures and types [29]. These observations raise questions about the chemical structure regarding at what point hydrotrope becomes surfactant and when does the switch from hydrotropy to micellar behavior take place. Balasubramanian et al. [30] reported the results of a homologous series of sodium benzenesulfonate solutions, and they found that the aggregation pattern in that homologous series changes somewhat sharply around sodium butyl benzenesulfonate and sodium pentyl benzenesulfonate.

Despite intermittent attempts have been made overall the years, there is no over consensus on the mechanism of hydrotropy. Mckee reported that concentrated aqueous solutions of soluble neutral salts of organic acids such as sodium benzoate, sodium salicylate, sodium benzenesulfonate, sodium p-toluenesulfonate, sodium xylenesulfonate and sodium cumenesulfonate increase the solubility of various organic and inorganic compounds in water [23]. In contrast to the earlier views of Neuberg and others, Mckee suggested that not only the organic compounds but also some inorganic substances (e.g alkali iodides,

thiocyanates, oxalates and bicarbonates) can act as hydrotropes [23]. He pointed out that the hydrotropic phenomenon is similar to "salting in" process. According to Bancroft, the phenomenon of hydrotropy could be explained based on the theory of mixed solvents [31]. Later Booth and Everson reported that the increased solubility accomplished by xylenesulfonate is neither linear nor monotonic, but displays a sigmoidal behavior as a function of hydrotrope concentration [32]. According to Winsor hydrotropy is quite similar to cosolvency [33]. In 1950, Licht and Wiener [34] and in 1963, Deno and Spink [35] have attributed the hydrotropic solubilization as salt effect. Ueda pointed out that the hydrotrope forms a complex with the solubilizate (the component that undergoes solubilization) and also decreases the activity coefficient of the latter in water, both of which lead to an increase in solubility [36]. Rath suggested the possibility of intermolecular interaction between hydrotrope and the solute [37]. To gain insight into the mechanism of hydrotropic solubilization Rawat et al. used various hydrotropes (nicotinamide, sodium benzoate and sodium salicylate) and drugs (rofecoxib, celecoxib and meloxicam) and their results indicate that the enhanced solubility of these drugs in the presence of hydrotropes in low concentration is due to weak ionic interaction whereas at high hydrotropic concentration the formation of molecular aggregation appears to be the possible mechanism of solubilization [38]. Poochikian et al. investigated the solubilization of chartreusin by hydroxybenzoate. According to them plane to plane orientation of ligand molecules and chartreusin brought them together by intermolecular electrostatic and hydrophobic interactions [39]. Badwan et al. studied the solubility of benzodiazepine derivatives in aqueous hydrotrope solutions and they observed an enhancement in the solubility of the benzodiazepine derivatives from a certain hydrotrope concentration [40]. Later, Balasubramanian et al. also found that a minimum concentration of hydrotrope was necessary in the aqueous phase to initiate the solubilization of the solute and they termed this threshold concentration as MHC. Here it is to be noted that experimentally reported MHC values of some hydrotropes are found to be inconsistent with each other [29, 41]. It is further to be noted that the mechanism of hydrotropic action is different from cosolvency. Cosolvents enhance drug solubility by minimizing the polarity gap between the solvent and the drug molecules but hydrotropes preferentially concentrate nearby the drug molecules [42]. So far three general hypotheses have been proposed for explain the mechanism of hydrotropic actions. We first summarize briefly these three classical hypotheses on the mechanism of hydrotropy.

Self-Aggregation Hypothesis: This hypothesis based on the assumption that the hydrotrope molecules self-associate among themselves to form organized aggregates or clusters in bulk solution. It is this hydrotrope aggregates that promotes the solubility of the insoluble molecules by incorporating the insoluble solutes into the cage of these hydrotrope clusters [26, 41, 43]. This scenario is quite similar to the solubilization by micelles. Indeed, the concentration of hydrotrope in the aqueous phase from which the solubilization of the insoluble solute actually takes place (known as MHC) which suggests a resemblance to the CMC. Balasubramanian et al. and Loh et al. suggested the view of a gradual stepwise association of hydrotropes [41, 42]. They proposed that changes in properties spread over a wide range of concentrations and were consistent with continuous stepwise aggregation, rather than "on-off" association seen with classical surfactants when crossing the CMC. From X-ray diffraction studies of solid hydrotropes, Balasubramanian et al. also concluded that lamellar-type association structures formed in dilute hydrotrope solutions [44]. Using the small-angle neutron scattering (SANS) technique, Triolo et al. proved that hydrotrope self-aggregates in D_2O solution [45]. They also reported that aggregation number of the cluster (spheroidal or ellipsoidal) is low.

Water Structure Breaking Hypothesis: This hypothesis assumes that the hydrotropes do not bind directly to the insoluble or sparingly soluble solutes [46]. Therefore, the solute-water interaction is indirectly affected by hydrotropes [43]. The theme of water structure breaking hypothesis of hydrotrope molecules was suggested by Frank and Franks [47]. As per their view, hydrotropes break the structure of water and prevent iceburg formation around hydrophobic insoluble molecules.

Solute-Hydrotrope Complexation Hypothesis: This hypothesis claims that the low stoichiometry complexes between the solute and the hydrotrope (such as 1:1 or 1:2) are the origin of hydrotropy [48, 49]. Korenmann suggested that the solubilization may be due to the formation of weak complexes between the hydrophobic compound and the hydrotrope [50]. Riboflavin-caffeine complexation supports this hypothesis [49] and the complexation takes place via π-stacking interactions between them [48, 49]. Rasool et al. also suggested that the aromaticity of the pyridine ring which promote the complexation through stacking interactions [51]. Coffman et al. investigated the effect of hydrotrope nicotinamide on the solubility of sparingly soluble riboflavin drug molecules in various solvents [43]. They proposed that the mechanism for hydrotropic solubilization is complexation between hydrotrope and drug molecules.

Recently Shimizu et al. [52] employed a rigorous theoretical framework of the Fluctuation Theory of Solution (FTS), which is an exact statistical thermodynamic theory, to study the mechanism of hydrophobic drug solubilization by small molecule hydrotrope and to analyze the experimental data within this framework. In their theoretical calculations [53, 54] they concluded that the preferential interactions between solute and hydrotrope is responsible for solubilization of solutes not the aggregation of hydrotropes. Zemb and coworkers [55] accepted that hydrotropes have solubilization property but they opposed the self-aggregation hypothesis of hydrotropes. These solubilization mechanism are opposite to that of the popular hypothesis of hydrotropy. Indeed, they showed that the self-association of the hydrotropes is induced by the presence of the hydrophobic solute in a nonstoichiometric ratio.

Each hydrotropic agent is fruitful in increasing the water solubility of specified hydrophobic drugs. No general hydrotropic agent has been found which is successful in increasing the aqueous solubility all hydrophobic drugs. Thus in order to find the hydrotropic agent for a poorly water-soluble drug requires screening of large number of potential candidate hydrotropes. However, once the effectual hydrotropic agent is recognized for a series of structurally different hydrophobic drugs, the structure activity relationship can be established.

There are various shortcoming of the previously proposed mechanisms. Hydrotrope molecules possess short hydrophobic chains which are unlikely to form micellar structures. So how these hydrotrope molecules self-associate in aqueous solution need to be answered. There are controversies over the MHC regions of hydrotrope molecules and also the reason for the inaction of hydrotropes below MHC values is not clear. Explanation also needed for the increased solubilization of the insoluble solute with increase in hydrotrope concentration. Here, it is worth noting that although hydrotropes are important but unlike surfactants (which are vastly studied) they are somewhat neglected class of amphiphiles. Thus, the generalized picture of hydrotropic behavior has not yet emerged mainly because of the fact that hydrotropes have a broad range of structures and very little academic research have been devoted in search of the mechanism of hydrotropy. The accurate mechanism of hydrotropy, and the structural characteristics that make a true hydrotrope are still issues under debate. There is no simulation or theoretical works has been done to investigate the mechanism of hydrotropy. Again it is very difficult to understand the microstructure of the aggregate and the details of molecular interactions within this hydrotropic system from an experimental point of view. From the above discussions it is also clear that the

mechanism of hydrotropic actions of hydrotropes for the enhancement in the solubility of a sparingly soluble molecule in water is way far from conclusive. This motivates us to examine the mechanism of hydrotropy (of hydrotropes) through a combined approach of classical molecular dynamics (MD) simulations as well as via Flory-Huggins (FH) theory.

The physico-chemical origin and mechanism of hydrotropic action has been a subject of academic debate and controversy for many years. In the current study, an attempt has been made to propose a mechanism of hydrotropic phenomenon. First, we anticipate the results for binary and ternary solutions of hydrotrope and hydrotrope-hydrophobic solute. Then the mechanism lying behind the hydrotrope induced solubilization of hydrophobic molecules is investigated and illustrated. The simulation works and concluding remarks are presented in the subsequent six chapters. The next section of the present chapter deals with the basic techniques of MD simulation and FH theory that is employed in our work. The detail analyses of the applications of these techniques for specific systems are given in later chapters. This is followed by a brief description of the work presented in the current thesis.

■ METHODOLOGY

In this thesis, we have used classical MD simulation technique. It has been widely used to investigate the structure and dynamics of biomolecular systems, such as proteins, nucleic acids, and small molecules like amino acids, sugars and drugs. In MD simulation, the potential energy function (U) is described by all interactions between the atoms that are covalently bonded as well as non-bonded interactions between atoms and molecules in the condensed phase. The interactions between particles are governed by the so-called force field parameterization [56].

The potential energy function is written as a sum of bonded and non-bonded interaction terms

$$U = U_{bond} + U_{angle} + U_{dihedral} + U_{vdw} + U_{Coulomb} \tag{1.1}$$

The first three terms (U_{bond}, U_{angle}, $U_{dihedral}$) are the bonded terms, which describe the bond stretching, angle bending, and torsion rotation, and the last two terms are for the non-bonded potential. In bonded terms, the bond and angle contributions are described by harmonic potentials and all of the interactions between directly bonded atoms (1-2 interactions), angles (1-3 interactions, where two atoms bonded to a common atom), and

torsion (interactions between pairs of 1-4 atoms) are defined as:

$$U_{bond} = \sum_{bonds} K_b(b_{ac} - b_{eq})^2 \tag{1.2}$$

$$U_{angle} = \sum_{angles} K_\theta(\theta_{ac} - \theta_{eq})^2 \tag{1.3}$$

$$U_{dihedral} = \sum_{dihedrals} \frac{V_n}{2}(1 + cos(n\phi - \delta)) \tag{1.4}$$

The letters b, θ, ϕ, and δ represent the bond length, bond angle, dihedral angle, and phase angle, respectively. The subscripts ac stands for actual and eq stands for equilibrium. The parameters K_b, K_θ, and V_n are the force constants for bond, bond angle, and dihedral angle, respectively.

The non-bonded potentials are calculated using two terms, the first one is the Lennard-Jones term (U_{vdw}) [57] describing the van der Waals interaction [58], and the second one is the Coulomb term ($U_{coulomb}$) [59] that deals with the electrostatic interactions between particles having partial charges on them. The non-bonding interaction terms are defined as:

$$U_{vdw} = \sum_i \sum_{i<j} 4\epsilon_{ij}\left[\left(\frac{\sigma_{ij}}{r_{ij}}\right)^{12} - \left(\frac{\sigma_{ij}}{r_{ij}}\right)^{6}\right] \tag{1.5}$$

$$U_{coulomb} = \sum_i \sum_{i<j} [\frac{q_i q_j}{4\pi\epsilon_o r_{ij}}] \tag{1.6}$$

where the overall sum is over all the atom pairs i and j. Lennard-Jones parameters σ and ϵ are the diameter of atomic sites and well depth energy, respectively. r_{ij} is the inter-atomic distance. q_i and q_j are the partial charges on interaction sites i and j and ϵ_o is the electrical permittivity.

The aim of the MD simulation is to observe the evolution of atomic coordinates in time. We consider an N-particle system characterized by the following Hamiltonian

$$H = \sum_{i=1}^{N} \frac{p_i^2}{2m} + U(\mathbf{r}^N) \tag{1.7}$$

where m is the mass of each particle, p_i is the momentum of the i-th particle and $U(\mathbf{r}^N)$ is the total potential energy of the system which includes the all particle-particle interactions. The coordinates of the particles are denoted by $\mathbf{r}^N = \{\mathbf{r}_1, \cdots, \mathbf{r}_N\}$. The position and velocity of i-th particle is represented by $\mathbf{r}_i$ and $\mathbf{v}_i$, respectively. The method of molecular dynamics consists of solving the equation

$$a_i = \frac{\mathbf{F_i}}{m_i} \tag{1.8}$$

where $i = 1, 2, ...N$, m_i is the mass of i-th particle and $\mathbf{F}_i$ is the force acting on particle i. This equation is obtained easily from the Lagrangian

$$L = \frac{1}{2}\sum_{i=1}^{N} m_i \mathbf{v_i}.\mathbf{v_i} - \frac{1}{2}\sum_{i=1}^{N}\sum_{j\neq i}^{N} u(r_{ij}) \tag{1.9}$$

where the potential U has been assumed to be the sum of pair potentials u_{ij}. The Lagrangian equation of motion is

$$\frac{d}{dt}(\frac{\partial L}{\partial \dot{q}_i}) - \frac{\partial L}{\partial \dot{q}_i} = 0 \tag{1.10}$$

It is clear from Eq. 1.10 that the dynamics of particles is described by 3N number of second order differential equations.

It is also possible to write down the Hamiltonian (H) for the system and solve the the Hamiltonian equations of motion

$$\dot{\mathbf{q}}_k = \frac{\partial H}{\partial p_k} \tag{1.11}$$

$$\dot{\mathbf{p}}_k = -\frac{\partial H}{\partial q_k} \tag{1.12}$$

where $\mathbf{q}_k$ and $\mathbf{p}_k$ represent generalized coordinates and momenta. For a system with pairwise interaction potential, the Hamiltonian is

$$H = \frac{1}{2}\sum_{i=1}^{N} m_i \mathbf{v_i}.\mathbf{v_i} + \frac{1}{2}\sum_{i=1}^{N}\sum_{j\neq i}^{N} u(r_{ij}) \tag{1.13}$$

and Eqs. 1.11 and 1.12 yield

$$\frac{dr_i}{dt} = \frac{\mathbf{p_i}}{m_i} \tag{1.14}$$

$$-\dot{\mathbf{p}}_i = -\nabla \mathbf{u} = \mathbf{F_i} \tag{1.15}$$

where i=1,2,....N. There are now $6N$ first order differential equations to be solved.

The equation of motion is solved numerically to yield particle velocities and positions as a function of time. It is usually integrated by using finite difference approach. The Verlet algorithm is one of the most commonly used algorithm for this purpose [60]. The advantage of the use of Verlet algorithm is that its implementation is straightforward and storage requirements are modest. Although, it has the disadvantage of moderate precision during the calculation and velocity does not appear explicitly in the Verlet integration. As an improvement to the Verlet algorithm, the leap-frog algorithm [61] has been developed. But, it has a disadvantage that the positions and velocities are not synchronized. As an

alternative of Verlet or the leapfrog algorithm, Velocity Verlet algorithm has been developed and the following relations are used to calculate new position and velocity at the same time:

$$r(t+dt) = r(t) + v(t)dt + \frac{1}{2}a(t)dt^2 \tag{1.16}$$

$$v(t+dt) = v(t) + \frac{1}{2}[a(t) + a(t+dt)]dt \tag{1.17}$$

To calculate the velocities at time t+dt, this method requires acceleration at time t and t+dt. In the present work, we have employed Velocity Verlet algorithm.

FH theory is a lattice-model based theory and it was developed to understand the non-ideal behavior of polymer solutions [62, 63]. This theory assumes that the arrangements of the molecules in the solution are completely random. Furthermore, according to FH theory, the formation of solution depends mainly on: (i) the transfer of polymer chain from a perfectly ordered pure state to a much disordered state (in the disordered state the polymer attains a freedom to be placed randomly in the lattice) and this is followed by (ii) the process of mixing of the polymer chain with the solvent molecules. According to FH theory, the critical value of Flory-Huggins interaction parameter (χ_{FH}) for phase separation of a polymer-solvent mixture is given by:

$$\chi_{FH} = \frac{1}{2} + \frac{1}{2x} + \frac{1}{\sqrt{x}} \tag{1.18}$$

From equation (1.18) it is obvious that for monomeric mixture ($x = 1$), the value of χ_{FH} is 2. On the other hand when $x \to \infty$, χ_{FH} becomes 0.5. Thus, when χ_{FH} is less than 0.5, the polymer is soluble.

As used before for predicting the solubility of small molecules using MD simulation technique [64], in our study also we consider modified FH theory. Unlike FH theory, the modified Flory-Huggins theory allows us to consider intermolecular interactions between the molecules that are present within the mixture and it also allows us for the determination of χ_{FH} as concentration changes [65]. We calculate χ_{FH}, by using equation (1.19) [64]:

$$\chi_{FH} = \frac{V_{ref}\Delta E_{mix}}{RT} \tag{1.19}$$

where V_{ref} is the smaller volume between the molar volumes of solute-1 and solute-2. This smallest volume is obtained from the experimental density and the molecular weight of the corresponding molecule. ΔE_{mix} is the energy of mixing of solute-1 and solute-2 molecules.

Since the volume change due to mixing is insignificant, therefore, ΔE_{mix} can successfully be replaced by the enthalpy of mixing, ΔH_{mix} [66]. We have calculated ΔH_{mix} from the enthalpy of binding ΔH_{bind} of pure solute-1 molecules ($(\Delta H_{bind})_1$), pure solute-2 molecules ($(\Delta H_{bind})_2$), and solute-1-solute-2 mixture ($(\Delta H_{bind})_{1-2}$), by using equation (1.20) [66-68]:

$$\Delta H_{mix} = (\frac{\Delta H_{bind}}{V})_{1-2} - \phi_1(\frac{\Delta H_{bind}}{V})_1 - \phi_2(\frac{\Delta H_{bind}}{V})_2 \tag{1.20}$$

where ϕ_1 and ϕ_2 are the volume fractions of solute-1 and solute-2 respectively. The total volume of the system is denoted by V. Enthalpy of mixing ΔH_{mix} can be calculated from the long time simulated production phase trajectories with the help of the above equation 1.20. Once the value of ΔH_{mix} is obtained, χ_{FH} parameter can be determined.

Next, we have calculated ΔH_{bind} using MM-GBSA [69] method. ΔH_{bind} is calculated with the help of series of following equations:

$$\Delta H_{bind} = \Delta E_{vac} + \Delta G_{solv} \tag{1.21}$$

where ΔE_{vac} is the energy in vacuum (gas phase) and ΔG_{solv} represents the solvation free energy [67, 70]. They can be calculated as:

$$\Delta E_{vac} = \Delta E_{ele} + \Delta E_{vdw} \tag{1.22}$$

$$\Delta G_{solv} = \Delta G_{GB} + \Delta G_{NP} \tag{1.23}$$

where ΔE_{ele} and ΔE_{vdw} are the electrostatic and van der Waals components of energies. The polar component, ΔG_{GB}, is estimated using generalized-Born (GB) approach [71] and the nonpolar contribution, ΔG_{NP}, of the solvation free energy ΔG_{solv} is calculated as follows [67, 71]:

$$\Delta G_{NP} = \gamma(SASA) + \beta \tag{1.24}$$

where γ=0.005 kcal/Å^2 and β=0.0, and SASA represents the solvent accessible surface area.

■ PRESENT WORK

Hydrotropes are substances that improve the solubility of sparingly soluble solute molecules in water. Hydrotropic solubilization is new, simple, economic, safe method, and widely used to increase the solubility of sparingly soluble drugs. The mechanism by which hydrotrope molecules increase the solubility of insoluble solutes has been investigated. We focus on the effects of anionic, cationic and nonionic hydrotropes on the different hydrophobic as well as sparingly soluble drug molecules and put an effort to uncover the basic mechanism of hydrotropy. **Chapter 1** of the thesis deals with the review of theoretical and experimental works that already exist in the literature and this chapter also explains the basic techniques of MD simulations and FH theory. FH theory allows us to determine whether the interaction between the hydrotrope and insoluble molecule is favorable or not. The reason of choosing modified FH theory over the original FH theory is also explained. In this chapter, we also present a descriptive view of the mechanism of hydrotropic action of different hydrotropes.

Chapters 2 deals with the hydrotropic action of anionic hydrotrope and is divided into two parts: Part A and Part B. In Part A, we investigate the self-aggregation behavior of hydrotrope sodium cumene sulfonate (SCS) in aqueous solution of increasing SCS concentration. The study reveals that SCS molecules start to self-associate at and above its minimum hydrotrope concentration (MHC) and with increasing concentration the self-aggregation propensity of hydrotrope SCS molecules also increases. We have also examined the effect of temperature on the SCS aggregation and the results suggest that the aggregation tendency of SCS increases with increase in temperature. The underlying mechanism behind the enhanced solubility of a solute in water (in presence of hydrotropes) has been explored in Part B. To examine the mechanism of hydrotropy we have used di-t-butyl-methane (DTBM) as a model hydrophobic solute and SCS as hydrotrope and the outcome is presented here. We find that above minimum MHC, the self-aggregation of SCS starts and the aggregated SCS creates a micellar like environment in which the hydrophobic tail part of SCS points inward while its hydrophilic sulfonate group points outward to make favorable contact with water molecules. The formation of the hydrophobic core of SCS cluster also creates a hydrophobic environment where the hydrophobic DTBM molecules are encapsulated. An insight picture of the temperature- and concentration-dependent aggregation behavior of hydrotrope is also obtained by examining the direct interactions of the hydrotrope with hydrotrope and hydrotrope with solvent. The ther-

modynamic properties like partial molal volume, and apparent molal volume of SCS, and osmotic coefficient are estimated. Then, the accumulation or depletion of solution species near the hydrophobic solute is examined by calculating time-averaged normalized ratio of water oxygen, and hydrophobic tail part carbon atoms of SCS in different solutions. The usual water oxygen−oxygen radial distribution function (rdf) is used to describe water structure breaking ability of hydrotrope molecules. Finally, the hydrogen bond properties, cluster structure of hydrotrope and Flory-Huggins interaction parameters are studied to describe molecular behavior of hydrotrope on the solubilization process.

Similar to the work in **Chapter 2B**, the effect of hydrotrope SCS on the solubility of a sparingly water-soluble drug, griseofulvin, is studied in **Chapter 3**. The main observations from this study are the following: (i) The SCS molecules self-aggregate through its small hydrophobic tail above the MHC causes the formation of micellar-like frameworks, and (ii) interestingly, though the drug griseofulvin drug molecule possesses both polar and nonpolar groups, it prefers to get encapsulated inside the hydrophobic core of SCS aggregates. The formation of SCS aggregates is investigated thoroughly by cluster structure analysis method. To shed light on the encapsulation of griseofulvin molecules, we have also calculated here the average number of griseofulvin drug molecules that are incorporated in the cage of SCS cluster. And then, preference of solution species near the drug is examined by calculating time-averaged normalized ratio of water oxygen and hydrophobic tail part carbon atoms of SCS molecule in different solutions. The hydrogen bond properties are also examined. Flory-Huggins interaction parameter and van der Waals and electrostatic interaction energy between drug and hydrotrope are also calculated to shed light on the mechanism of hydrotropy.

In **Chapter 4**, we have examined the effects of cationic hydrotrope on the solubility of sparingly soluble drug molecule by means of classical MD simulation technique. We have used p-toluidinium chloride (PTOL) as hydrotrope molecule and gliclazide as drug molecule. Our cluster structure analysis results demonstrate that PTOL starts to self aggregate above its MHC. Further, these PTOL aggregates create a mixed micellar type framework in which the hydrophobic small tail parts of most of the PTOL molecules direct inside whereas in order to make favorable contact with water molecules its hydrophilic ammonium group points outward. But electrostatic and van der Waals interaction energy between drug and hydrotrope suggest that in order to make hydrogen bonds with GLC molecules the polar groups of few of the hydrotropes direct inward also. This provides an environment for the incorporation of the drug molecules into the mixed environment (hy-

drophobic as well as hydrophilic core) of PTOL clusters. The analysis of density profiles of water and hydrotrope around the gliclazide drug molecules reveal that water molecules are replaced by the hydrotrope molecules. Flory-Huggins interaction parameters and hydrogen bond properties are also calculated that shed light on the mechanisms of hydrotropic action of cationic hydrotrope.

The effect of non-ionic hydrotrope nicotinamide on the solubilization of sparingly soluble riboflavin drug molecule is investigated in **Chapter 5**. The calculation of orientational preference of aromatic planes constituting the nicotinamide with respect to the another nicotinamide or riboflavin molecule indicate that nicotinamide molecules self-associate through stacking of their pyridine rings and they also form complexes with riboflavin molecules in 1:1 and 1:2 ratio. The analyses of density profiles of water and nicotinamide ensure that water molecules only prefer to stay at the periphery of the riboflavin molecules and they are replaced by the hydrotrope molecules with increasing concentration of solution. The roles of van der Waals and electrostatic interactions between the drug and hydrotrope molecules on the solubilization process are also analyzed. The estimations of intra- and inter- molecular hydrogen bonds and Flory-Huggins interaction parameters are also employed to analyze the mechanisms of hydrotropy.

In **Chapter 6**, we have emphasized the drug releasing ability hydrotrope clusters. The goal of this study is to investigate the release of griseofulvin drug into situ. In brief, we investigated the binding of the drug griseofulvin molecule (after releasing from the hydrotrope cluster) to the different binding sites of the protein γ-tubulin via classical MD simulation and MM-GBSA method. We have calculated the root mean square deviation (RMSD) of C_α atoms, radius of gyration and solvent accessible surface area (SASA) of the protein to see the conformational stability of γ-tubulin protein in presence of bare drug and hydrotrope encapsulated drug molecules. The release of drug griseofulvin from the SCS cluster has been confirmed by the time-averaged coordination number analysis. Analyses of root mean square fluctuation (RMSF) and average secondary structure of the protein give an idea about the possible binding sites protein. We observe that the binding pockets are mainly formed by the H8, H9 helices and S7, S8, S14 strands of γ-tubulin protein and the van der Waals interactions between the drug and γ-tubulin protein drive the binding process. Moreover, hydrotrope molecules alter the binding sites of the protein and a moderate weakening of the drug-protein interactions is also observed.

In **Chapter 7**, we have discussed the results of each of the work and tried to bring our view on the mechanism of hydrotropic action on the solubility of sparingly or insoluble

solute. Since the drug molecules are sparingly soluble in water, here, we also present a promising approach for formulating and achieving delivery of a poorly soluble drug via hydrotrope cluster.

Chapter 2

Insights into the Self-Aggregation Behavior of Anionic Hydrotrope and its Role into the Solubility of Purely Hydrophobic Molecules

"The hydrophobic effect - the tendency for oil and water to segregate - is important in diverse phenomena, from the cleaning of laundry, to the creation of micro-emulsions to make new materials, to the assembly of proteins into functional complexes. This effect is multifaceted depending on whether hydrophobic molecules are individually hydrated or driven to assemble into larger structures. Despite the basic principles underlying the hydrophobic effect being qualitatively well understood, only recently have theoretical developments begun to explain and quantify many features of this ubiquitous phenomenon."

— D. Chandler *Nature* **437**, 640 (2005)

Hydrotropes are mild surface active amphiphilic organic molecules with hydrophobic parts are comparatively smaller than that of a classical surfactant. Although hydrotropes possess some structural similarities with the conventional surfactants but the major difference between a hydrotrope and the surfactants is in the solubility behavior of hydrotropes. Hydrotropes show a higher and often more selective ability to solubilize insoluble molecules.

In literature some experimental evidences exist showing self-aggregation behavior of hydrotrope molecules, hydrotrope induced solubilization of sparingly soluble molecules [28-30]. The findings are substrate specific based on intermolecular interaction mechanism. These studies inspired us to investigate and characterize the self-association and solubilization mechanisms of anionic hydrotrope sodium cumene sulfonate (SCS) and purely hydrophobic solute di-t-butyl-methane (DTBM) at molecular level using simulation technique. To bring out the detailed mechanism of self-aggregation of hydrotrope and their roles in the solubilization of hydrophobic solute are the core objective of this study.

The chapter is divided into two parts. In Part A, we focus on the self-aggregation behavior of hydrotrope molecules in pure aqueous solution. Part B, on the other hand, concentrates on the hydrotropic action of SCS on purely hydrophobic DTBM molecule.

Part A:

Aggregation of Sodium Cumene Sulfonate in Aqueous solution

Overview: In this chapter, we try to understand the underlying mechanism of self-aggregation of anionic hydrotrope sodium cumene sulfonate (SCS) in water. We have carried out classical molecular dynamics simulations of aqueous SCS solutions with a regime of concentrations. Moreover, to examine the effect of temperature change on SCS aggregation, if any, we consider four different temperatures ranging from 298 to 358 K. From the estimation of densities of different solutions we calculate apparent and partial molal volumes of the hydrotrope. The changes in these quantities increase sharply at a characteristic minimum hydrotrope concentration. The determination of molal expansibility at infinite dilution for different temperatures indicates the water structure breaking by SCS molecules, which is further confirmed by the calculations of water-water pair correlation functions. In comparison with typical surfactants in micelles, a slightly lower value of volumetric change upon aggregation per carbon atom suggests the formation of a more closely packed structure of hydrotrope aggregates. A close examination of different structural properties of hydrotrope solutions reveals that the hydrophobic interactions through their hydrophobic tails significantly contribute in hydrotrope aggregation, and the dehydration of hydrophobic tail at elevated temperatures is also visible. Remarkably, the aggregates have little or no impact on the average number of water-SCS hydrogen bonds.

■ INTRODUCTION

The phenomenon of the solubilization of hydrophobic solute in aqueous solution by the self-assembled hydrotropes is widely accepted. Therefore, to understand the hydrotropic action of a hydrotrope, the self-aggregation of hydrotrope molecules, which is sort of a prerequisite for the increased solubility of a solute in water, needs to be clearly examined. Unfortunately, although the thermodynamic properties of medium- and long-chain surfactants are studied extensively and despite the fact that hydrotropes have been known for nearly a century, very little works have been dedicated to studying the thermodynamic properties of hydrotropes and their aggregates [29, 30, 41, 72, 73]. As a result, the exact mechanism of hydrotropy and the structural features that make a true hydrotrope are still issues under debate.

Taking together all of the research to date, on balance it appears that hydrotropes generally aggregate above MHC. However, it is very difficult to understand the microstructure of the aggregate and the details of molecular interactions within this hydrotropic system from an experimental point of view. So to obtain better insight into the molecular details of hydrotropy, we have carried out molecular dynamics simulation of sodium cumene sulfonate (SCS) (Figure 2A-1). SCS is an important hydrotrope and found useful in number of applications such as extraction of natural products [17, 74], chemical reactions [75], etc. By using various experimental techniques like surface tensiometry, volumetric changes, vapor pressure osmometry, fluorescence polarization studies, enthalpy changes and polarizing microscopic studies Wagle et al. [29] characterized the aqueous solution of SCS. They reported that aggregation propensity of SCS molecules increases as a function of temperature and concentration. Balasubramanian et al. [30] also reported the aggregation behavior of aqueous SCS solutions.

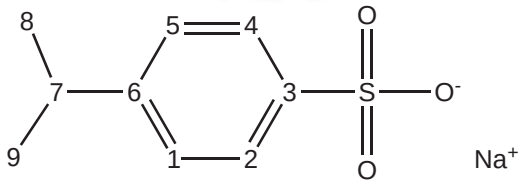

sodium cumene sulfonate

Figure 2A-1. *Structure and atomic number of sodium cumene sulfonate. Hydrogen atoms are left off for clarity.*

Although over the last century few experimental works have been performed to examine the solution-state properties of hydrotropes, to best of our knowledge this is the first molecular dynamics simulation of hydrotrope molecules. The main focus of this study is to examine the molecular mechanism of hydrotrope aggregation, which is yet to be understood clearly. Once this is understood clearly, the next step would be to examine the role of hydrotrope aggregates on the enhanced solubility of a solute molecule in aqueous system. Because experimentally reported MHC values of SCS are found to be inconsistent with each other [29, 41], in this study, we first try to find out the MHC of SCS; then, by examining different structural properties, we extend our investigation toward understanding the molecular details of self-assembly process of hydrotrope SCS in water and the effect of temperature change on it.

The models and simulation details are described in next section, thereafter the results are presented and discussed, and in the last section of this chapter our conclusions are briefly summarized.

■ MODELS AND SIMULATION METHOD

Molecular dynamics simulations were performed for binary hydrotrope SCS-water mixtures at four different temperatures ranging from 298 to 358 K. For each temperature, eight different SCS concentrations were considered. Thus, altogether 32 different systems were studied. The different systems considered in this study are briefly summarized in Table 2A-1. All simulations were performed using the AMBER12 package [76]. The SPC/E model was used for water molecules [77], and for the cumene sulfonate group the CHARMM General Force Field (CGenFF) [78, 79] was adopted. In this study we chose the SPC/E model over TIP3P water due to the fact that when compared with the experimental results the former reproduces better structural (and dynamical) properties over the latter [80]. Here we note that although the use of CHARMM force field in AMBER is not a good practice, in our study the CGenFF force field was adopted for cumene sulfonate group mainly because of the following reasons: (1) the lack of proper force field for cumene sulfonate group in AMBER and (2) the very similar functional form of the potential energy functions (in particular, for "non-biological" systems) of CHARMM and AMBER makes it possible to use the force field for the former in the latter. Indeed, using the CHAMBER toolkit [81] it is possible to enable the CHARMM force field in AMBER12. One Na^+ ion was added to neutralize the single negative charge carried by each sulfonate group of cumene sulfonate. The initial configurations of all systems were prepared using the PACKMOL program [82].

Furthermore, to calculate the density of pure water at different temperatures considered here, we separately carried out another four simulations for the systems containing water only, and the details of these systems are also included in Table 2A-1. Each of these simulations was performed using cubic box, and periodic boundary conditions were applied in all three directions. At first the systems were energy minimized for 10000 steps, of which the first 4000 steps in steepest descent method were followed by 6000 steps in the conjugate gradient method. Thereafter, to avoid void formation, in canonical ensemble (NVT) each system was heated slowly from 0 K to the desired temperature for 320 ps at 1 atm pressure. Then, the systems were equilibrated in an isothermal-isobaric (NPT) at P = 1.0 atm for 5 ns. Finally, to calculate different structural properties, the production runs were performed for 40 ns in NPT ensemble. The temperature was controlled by using the Langevin dynamics method with collision frequency of 1 ps^{-1}, and a time step of 2 fs was used. To maintain the physical pressure of each system, we used a Berendsen barostat [83] with a pressure relaxation time of 2 ps. The SHAKE algorithm [84] was used to constrain the covalent bonds between hydrogen atoms and heavy atoms, and a cutoff distance of 10 Å was defined for all nonbonded interactions. The long-ranged nonbonding interactions were treated using the particle mesh Ewald method. All pure water simulations were carried out in an NPT ensemble for 1 ns equilibration, followed by 8 ns production runs. The Ptraj program of the AMBER12 toolkit was used to analyze the trajectories obtained from the production run, and visual molecular dynamics (VMD) [85] was used to analyze the hydrogen-bond properties.

Table 2A-1. Overview of Systems[a]

			Volume(nm^3)				
System	N_{SCS}	N_{wat}	298 K	318 K	338 K	358 K	m
S0	5	3600	109.08	110.31	112.33	113.59	0.077
S1	8	3600	109.83	111.28	112.89	114.44	0.123
S2	12	3600	110.25	112.46	113.45	115.57	0.185
S3	24	3600	113.38	114.65	116.00	118.59	0.370
S4	36	3600	116.43	117.86	119.90	121.80	0.556
S5	48	3600	118.80	120.48	122.54	124.33	0.741
S6	60	3600	121.95	124.03	125.52	128.18	0.926
S7	72	3600	124.92	126.58	128.40	130.79	1.111
S8		500	14.89	15.16	15.44	15.70	

[a] N_{SCS} and N_{wat}, respectively, are the number of sodium cumene sulfonate and water molecules. m is the molal concentration of SCS.

■ RESULTS AND DISCUSSION

Apparent and Partial Molal Volumes

Partial molal volume is an important thermodynamic property that provides information about the interactions between different components in a mixture as well as the local structure of the solvent. For a mixture, because the environment of the molecules changes with a change in the composition of the mixture, the partial molal volumes of the components in a mixture vary with concentration. This change in the molecular environment (and the consequent alteration of the interactions between different species) makes the thermodynamic properties of a mixture change as the composition of the mixture is altered. In this study, because we consider a regime of temperatures, partial molal volume, which is independent of temperature (instead of partial molar volume), of SCS for different systems is calculated. The apparent and partial molal volumes of SCS for different solutions can be estimated from the density measurements [29, 86]. By using Eqs. 2.1 and 2.2, we have calculated apparent molal volume (ϕ_v) and partial molal volume ($\bar{V_2}$) of SCS from the measured densities of the aqueous SCS solutions (ρ) for different molal concentrations and temperatures.

$$\phi_v = M_2/\rho - 1000(\rho - \rho_0)/\rho\rho_0 m \tag{2.1}$$

$$\bar{V_2} = m(d\phi_v/dm) + \phi_v \tag{2.2}$$

where M_2 is the molecular weight of SCS and ρ_0 and m are the density of pure water and the molality of the solutions, respectively.

In Figure 2A-2, we have shown how the values of ϕ_v and $\bar{V_2}$ change as the molality of the solution changes. At a fixed temperature, as concentration increases, prominent changes are observed in the apparent and partial molal volumes of SCS up to 0.185m concentration, indicating a major structural reorganization in the aqueous hydrotrope solutions up to this concentration. Furthermore, above 0.370m concentration, the changes in the ϕ_v and $\bar{V_2}$ values are not very dramatic. Because the slopes of pre- and post-aggregation regions are different, the value of MHC for SCS can be estimated from this Figure. True size of the molecule and the free space between the molecules are the two components that contribute to the molal volume of hydrotrope in aqueous solution. In the context of apparent molal volume of hydrotrope, below MHC, the monomer-solvent interaction is the predominant factor, whereas the intermolecular space contributes little to it. With increas-

ing concentration as the aggregation of hydrotropes starts, the growth of the aggregates leads to an increase in ϕ_v value of SCS, but once a critical size is attained, although the number of hydrotrope aggregates increases, the size of the aggregates should not increase much. Considering the influence of temperature on the apparent molal volumes of SCS, we find that for all of the systems considered here there is an increase in ϕ_v values with increasing temperature, and the major structural changes of hydrotrope aggregation are observed up to 0.185m, and this effect is less pronounced above 0.370m. In this context we note that our findings are in qualitative agreement with the reported experimental results (left inset of Figure 2A-2a) [29]. Furthermore, for all temperatures, by extrapolating the $\phi_v - m$ plot, we have calculated the apparent molal volume of SCS at infinite dilution (ϕ_v^0). The value of ϕ_v^0 for SCS is 134.91 cm^3mol^{-1} at 298 K, and it increases with temperature but not exactly in linear fashion (right inset of Figure 2A-2a). We note that our findings are in general agreement with the experimental findings [29], where a nearly linear relationship between ϕ_v^0 and molality was observed. In an attempt to find out the value of molal expansibility at infinite dilution, $E_v^0 = (\partial\phi_v^0/\partial T)_p$, which gives information about how partial molal volume changes as temperature is changed, we have plotted ϕ_v^0 versus T (right inset of Figure 2A-2a). From the slope of the graph, the value of E_v^0 is estimated to be 0.2155 $cm^3K^{-1}mol^{-1}$ for SCS, whereas the reported experimental value is found to be 0.146 $cm^3K^{-1}mol^{-1}$ [29]. Here we note that for different surfactants positive molal expansibility at infinite dilution values with similar magnitudes was also previously observed [87, 88]. To get an idea about the water structure making or breaking ability of SCS molecules, we have further calculated $(\partial E_v^0/\partial T)$. This is important because the sign of $(\partial E_v^0/\partial T)$ suggests whether the solute SCS has any structure making (if positive) or structure breaking (if negative) ability. Here we have found that $(\partial E_v^0/\partial T) = -0.0594$. Although the numerical value is not very high, the significant variation of E_v^0 with temperature gives us an idea about the water structure breaking ability of SCS molecules. This is further confirmed from $O_w - O_w$ radial distribution functions (rdf's) for different systems that we discuss later.

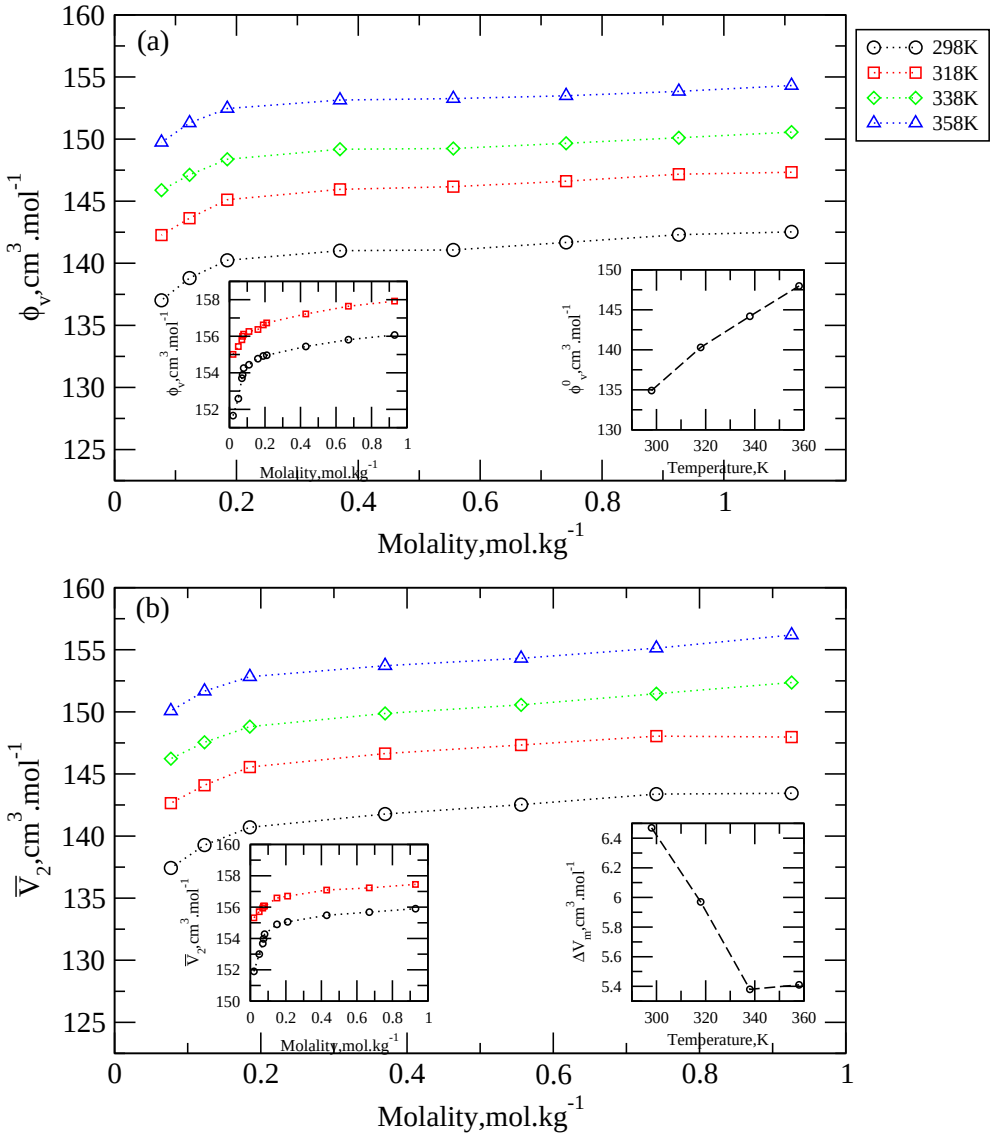

Figure 2A-2. *(a) Apparent molal volume (ϕ_v) versus concentration. Experimental apparent molal volume data (taken from ref 29) are presented in the left inset. The right inset represents the apparent molal volume at infinite dilution (ϕ_v^0) versus temperature in the present work. (b) Partial molal volume ($\bar{V}_2$) versus concentration. Experimental partial molal volume data (taken from ref 29) are shown in the left inset. The right inset represents the volumetric change on aggregation (ΔV_m) versus temperature in the present work.*

The changes in partial molal volumes can give a perception about the changes in aggregation pattern of hydrotropes. Similar to apparent molal volume, the partial molal volume of SCS also increases with an increase in molality of the solution (see Figure 2A-2b), and the increase is more rapid (and in a linear fashion) up to 0.185m concentration, but above 0.370m concentration, the changes in the $\bar{V}_2$ values with molality of the solution are not that remarkable. These observations imply fewer further structural changes in the aggregates above this concentration. Taking into consideration the effect of temperature on partial molal volumes of SCS, we observe an increase in $\bar{V}_2$ values with increasing temperature for all of the systems considered here, but the major structural changes are observed up to 0.185m, and this effect is less prominent after 0.370m. A comparison between our findings and the available experimental $\bar{V}_2$ values [29] (left inset of Figure 2A-2b) reveals that the results obtained in this study are in qualitative accordance with the experimental findings.

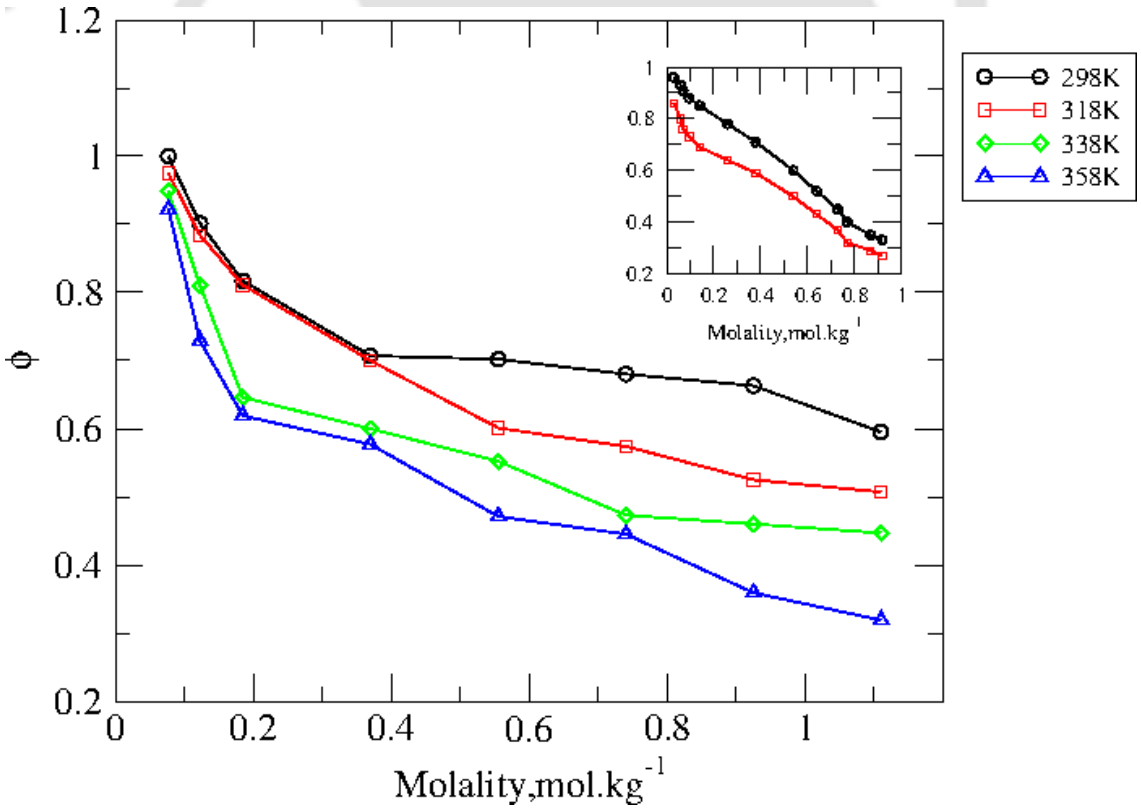

Figure 2A-3. *Osmotic coefficients (ϕ) vs. SCS concentration for different temperatures. The data in the inset represent the experimental osmotic coefficient values taken from ref 29.*

Knowing the partial molal volumes in the aggregated state ($\bar{V_2^m}$) and singly dispersed state ($\bar{V_2^s}$), we further, calculate the volumetric change on aggregation $\Delta V_m = \bar{V_2^m} - \bar{V_2^s}$. For a particular system, the partial molal volume in the singly dispersed state ($\bar{V_2^s}$) is estimated by extrapolating to $m = 0$ concentration of the $\bar{V_2} - m$ plot. The ΔV_m for SCS is found to be 6.47 cm^3mol^{-1} at 298 K, and its value decreases with an increase in temperature up to 338 K, and after that it remains constant. The same is presented in Figure 2A-2b (right inset). The ΔV_m values are within the range of 6.47 to 5.38 cm^3mol^{-1}, and these values are very similar to those already reported values for typical surfactants [89]. Moreover, we have also calculated the value for change in ΔV_m with respect to the number of carbon atoms within the hydrotrope molecule (n), and the value of $\Delta V_m/n$ for SCS is 0.719 cm^3mol^{-1}, whereas typical values of $\Delta V_m/n$ reported for sodium octyl sulfate, sodium decyl sulfate, and sodium dodecyl sulfate, respectively, are 0.78, 0.91, and 0.9 cm^3mol^{-1} [89]. These findings suggest a slightly lower partial volumes of hydrotropes in their aggregated state than those of typical surfactants in their micellar state. This further implies that in the aggregated state hydrotropes have a slightly more close-packed structure. With increasing temperature there is a loss of hydrophobic hydration (which we have elaborately discussed later) of the monomers due to the formation of aggregated structure. As a result, the value of ΔV_m at higher temperature decreases. Again, weakening of hydrogen bonds among water molecules around the small tail part of SCS molecules at higher temperature can further reduce the hydrophobic hydration, which indirectly affects the value of ΔV_m. Moreover, we estimated the value of osmotic coefficients (ϕ) for different solutions and in Figure 2A-3; the same are plotted as a function of solute concentrations. In the inset of the same Figure, we have shown the available experimental osmotic coefficient values for different systems [29]. As concentration of SCS increases, the formation of aggregates (due to solute-solute interactions) leads to a decrease in the ϕ value [90, 91]. The effect of temperature on the aggregation propensity of SCS is also quite evident. In brief, because the aggregation propensity of SCS increases with temperature, for a fixed concentration, we observe a reduction in the ϕ value at higher temperature. In this context it is worth noting that although at pre-aggregation regions the estimated values of ϕ are in good agreement with that of experimental findings, in the post-aggregation regions they differ modestly [29]. The higher osmotic coefficient values in concentrated solution, as estimated here, suggest that the model SCS considered in this study shows less aggregation tendency.

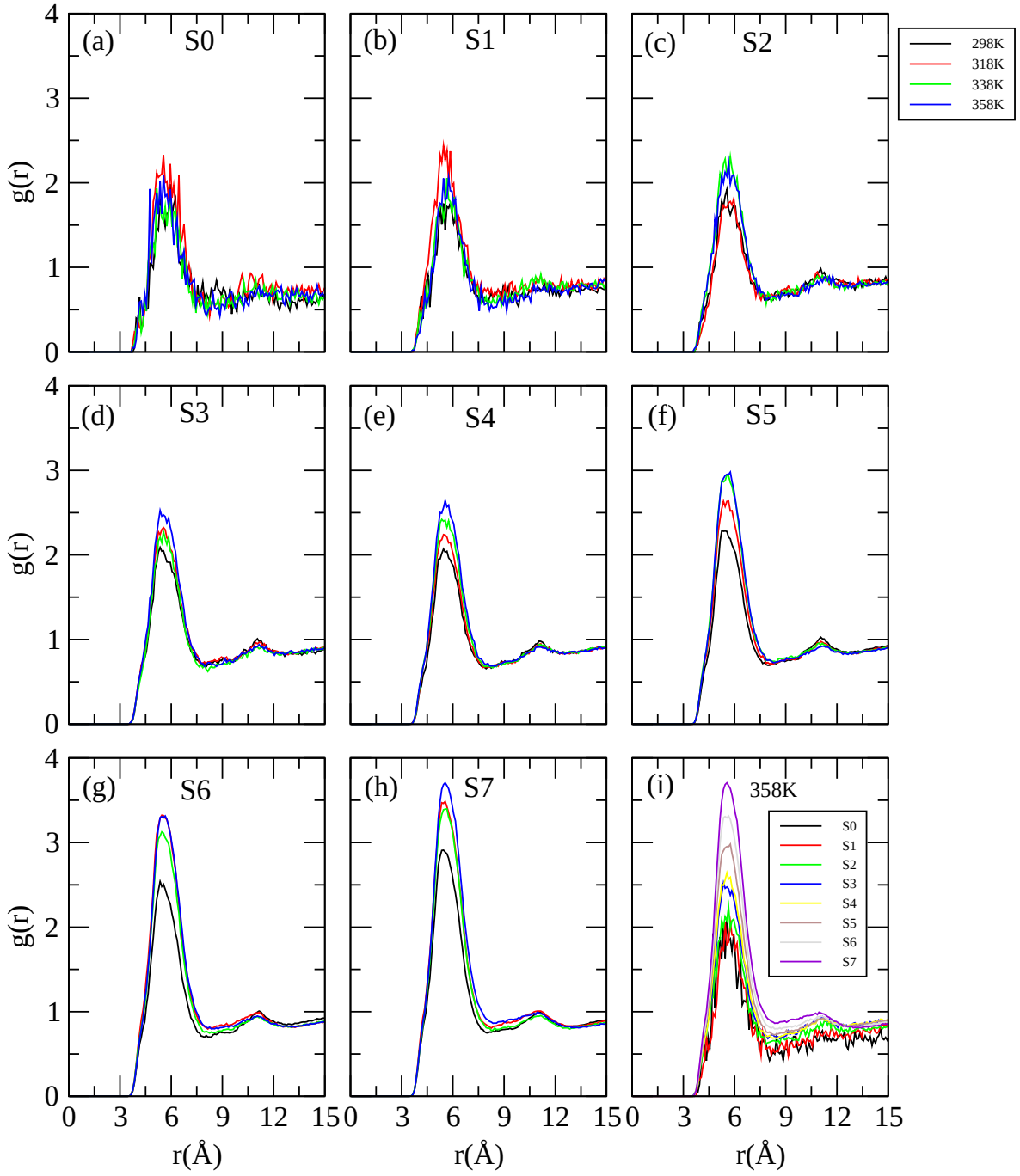

Figure 2A-4. *$C_7 - C_7$ site-site radial distribution functions for different systems (a-h). (i) depicts the change in $C_7 - C_7$ rdf with increasing SCS concentration at temperature 358 K.*

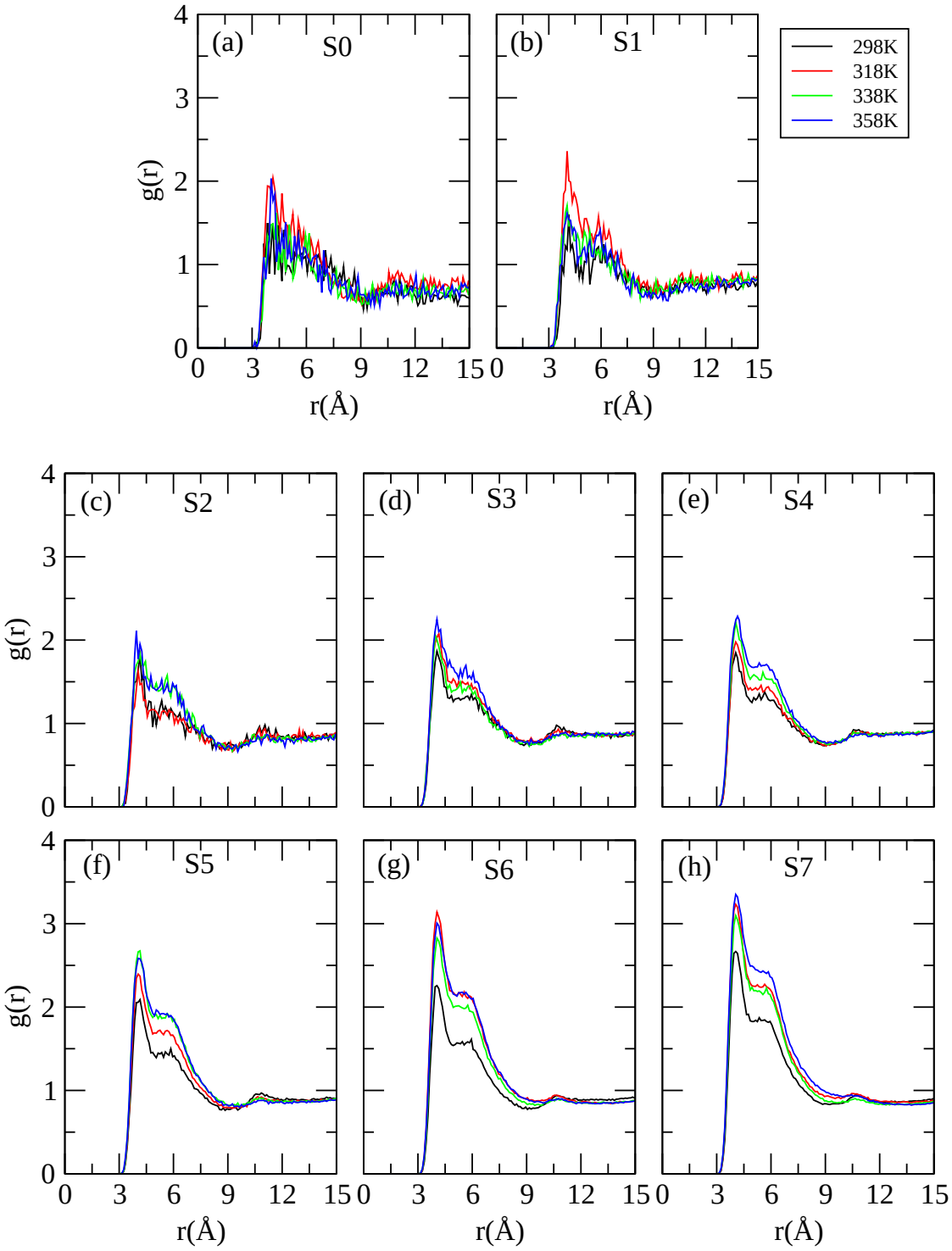

Figure 2A-5. *$C_8 - C_8$ site-site radial distribution functions for different systems.*

Solution Structural Properties

To obtain in detail structural properties of different solutions, we consider selected site-site rdf's involving hydrotrope and water molecules. These distribution functions are shown in Figures 2A-4, 2A-5, 2A-7, 2A-9, and 2A-10.

To get an idea about the aggregation behavior of the hydrotrope through its hydrophobic tail, we first consider distribution functions between $C_7 - C_7$ and $C_8 - C_8$ atoms of SCS with varying concentration and temperature. These rdf's are presented in Figures 2A-4 and 2A-5. Considering $C_7 - C_7$ rdf first, we observe that a strong first peak appears at about 5.45 Å. Furthermore, at a particular temperature as the SCS concentration increases, there is an increase in the first peak height (Figure 2A-4i). Here we note that due to use of small number of SCS molecules in systems S0 and S1 the peaks are a bit noisy. Moreover, keeping the concentration at a fixed value we notice a diminution of the first peak height with the decrease in temperature for all of the systems except for systems S0 and S1. Note that these systems are below the MHC level and they belong to pre-aggregated regions. For $C_8 - C_8$ correlation function (Figure 2A-5), the effect of solute concentration and temperature on it is very similar to that of $C_7 - C_7$ distribution functions. Note that solute-solute rdf's involving other SCS atoms are not shown because they show very little or no concentration and temperature dependency. These observations indicate an enhancement in the solute-solute interactions through nonpolar C_7 and C_8 atomic sites of SCS with increasing concentration and temperature. The temperature and hydrotrope concentration induced aggregation of SCS molecules are further probed by visualizing snapshots of different systems taken at the end of each simulation. In Figure 2A-6a we present the snapshots for systems S0, S2, S4, and S7 for 298 and 358 K temperatures considering SCS molecules only. To have proper visual clarity, water molecules and other systems are left off. We chose the systems in such a manner that the concentration of SCS falls below MHC level for one system (i.e., system S0), significant changes in the apparent and partial molal volumes take place for two systems (i.e., systems S2 and S4), and the concentration of SCS is above MHC level for one system (i.e., system S7). As can be seen, the formation of aggregates of SCS molecules is absent below MHC level (S0), whereas it starts appearing for system S2. For other systems, the presence of a substantial amount of SCS aggregates is quite visible. Furthermore, a close examination of SCS clustering reveals that it is the hydrophobic tail that contributes to the SCS aggregation (Figure 2A-6b).

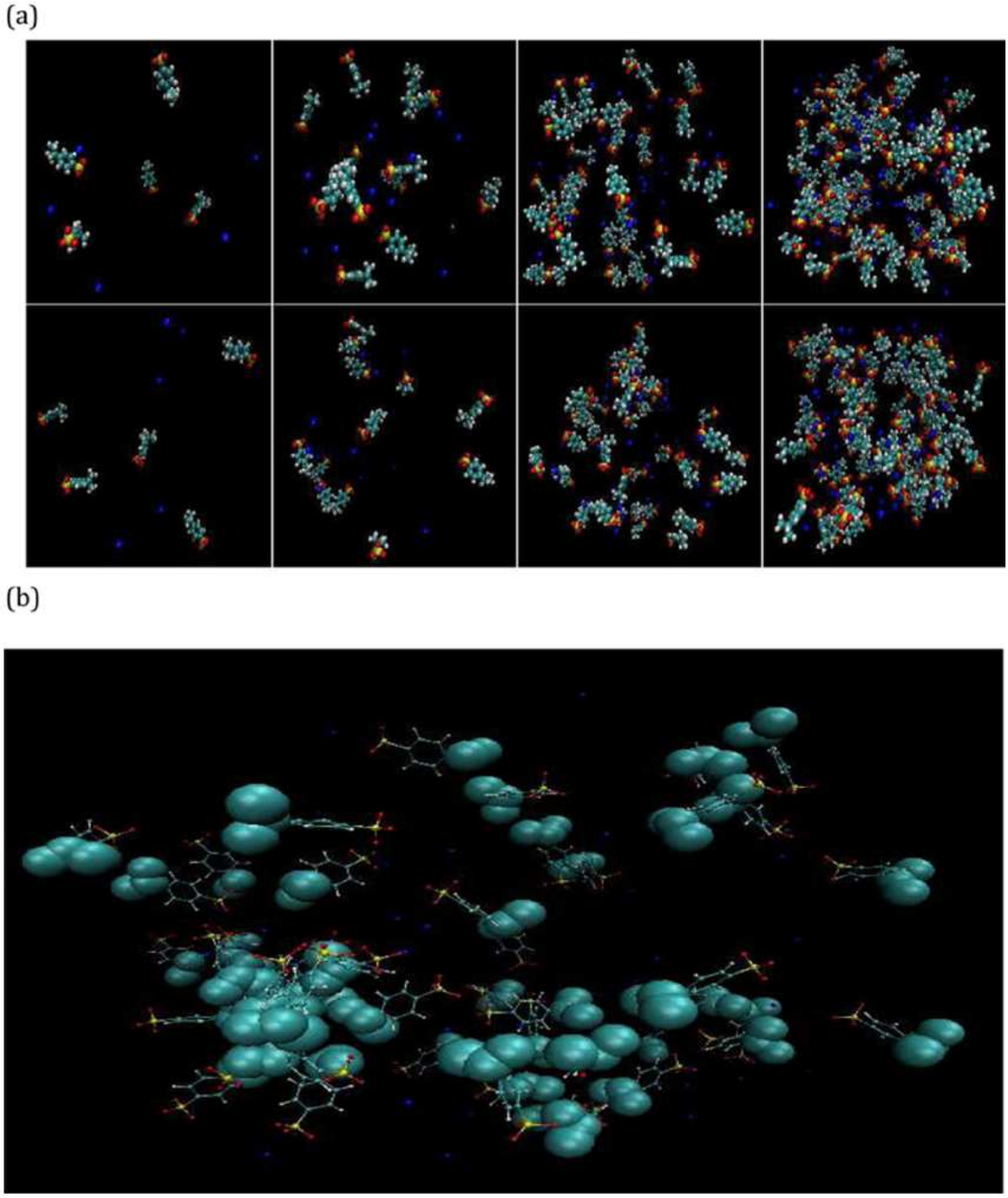

Figure 2A-6. *(a) Snapshots of SCS aggregation for systems S0, S2, S4 and S7 (from left to right) for 298 K and 358 K temperature (top to bottom). Blue balls represent sodium ions. (b) Close view of clustering of SCS molecules through hydrophobic tail (represented by green balls). The system considered is S5 at 338 K temperature. For both snapshots, water molecules are left off to have proper visual clarity.*

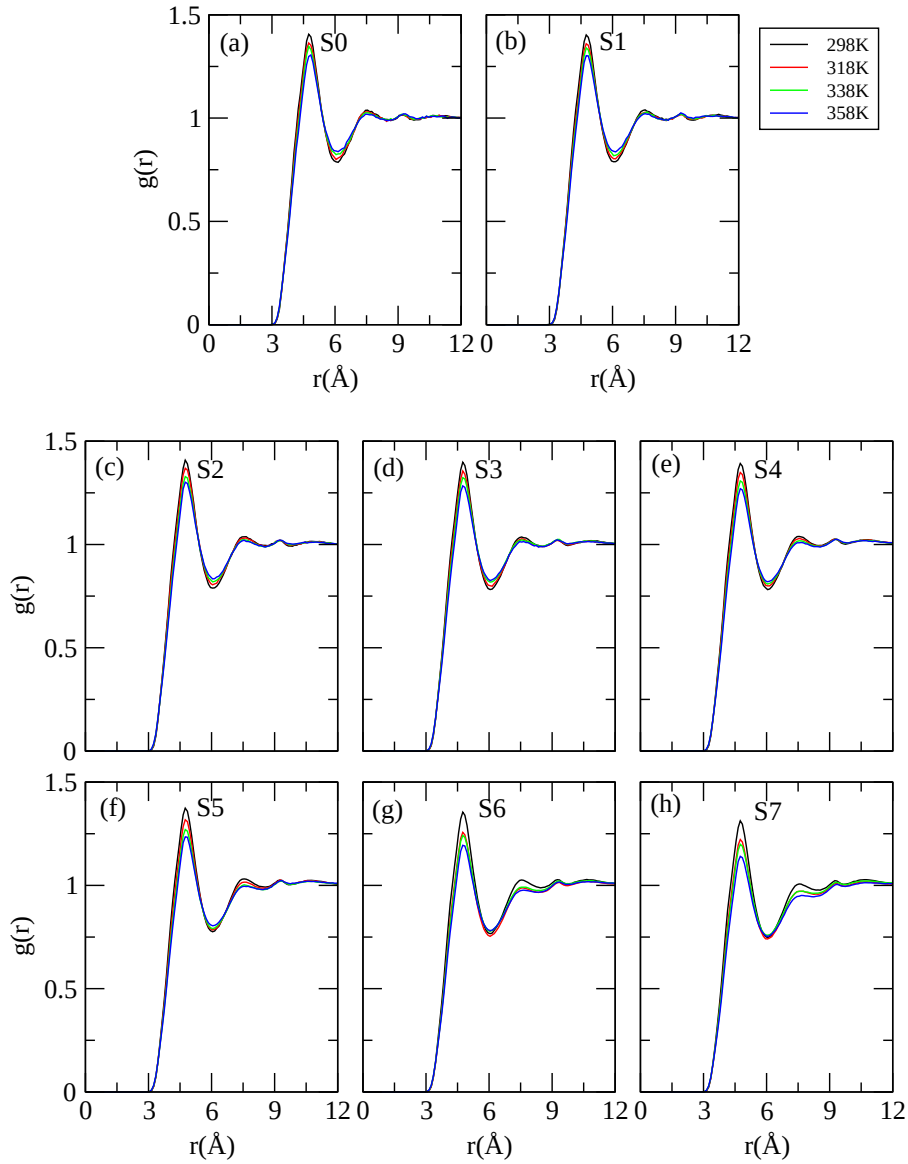

Figure 2A-7. *Site-site radial distribution functions between $C_7 - O_w$.*

Because the self-aggregation propensity of solute SCS molecules in water is reflected in the hydration pattern, we further extend our study to a close examination of distribution functions involving the C_7 atom of SCS and water molecules. Figure 2A-7(a-h) displays the rdf's between the C_7 atom of SCS and the oxygen atom of water. Note that the oxygen atom of water is abbreviated here by O_w. Concentrating on the hydration of C_7 atom of SCS at 298 K first (Figure 2A-7a), we make the following observations: (a) The rdf starts to rise at 3.05 Å and reaches the bulk value (where g(r) = 1) at about 4.25 Å . Hence, below

4.25 Å there is an exclusion of water molecules from the solvation shell of C_7 atoms. (b) The minimum of the first peak position that appears at 6.15 Å indicates the outer limit of first hydration shell of C_7 atom of SCS. (c) The g(r) value of the S0 system is 1.40 at the first maximum, implying that the first peak water density is only 1.40 times that of bulk density. The effect of temperature on this rdf is also quite visible. In brief, for a fixed SCS concentration, increasing temperature causes a depletion in the first peak height. Although this effect is not very remarkable for systems with low SCS concentrations, we do observe a modest change in the first peak height for concentrated solution systems. Furthermore, increased temperature makes the first valley shallower. In regard to the effect of SCS concentration on $C_7 - O_w$ distribution function, we find that on addition of SCS the first peak decreases modestly, especially for concentrated SCS solution systems. These observations imply increased SCS concentration, and elevation of temperature causes a reduction in the number of water molecules in the first solvation shell of C_7 atom of SCS. To verify this we have further estimated the number of water molecules in the solvation shell of hydrophobic C_7 (and C_8) atom by using Eq. 2.3.

$$n_{\alpha\beta} = 4\pi\rho_\beta \int_{r_1}^{r_2} r^2 g_{\alpha\beta}(r) dr \tag{2.3}$$

where $n_{\alpha\beta}$ represents the number of atoms of type β surrounding atom α in a shell extending from r_1 to r_2 and ρ_β is the number density of β in the system. Typical values for r_1 and r_2 are set to zero and the distance of the first minimum in the corresponding distribution function, respectively, to calculate the first solvation shell coordination number.

Table 2A-2. Number of First-Shell Water Molecules around C_7 Atom of Sodium Cumene Sulfonate Molecules[a]

system	298 K	318 K	338 K	358 K
S0	30.32	29.75	29.15	28.47
S1	29.83 (30.11)	29.03 (29.49)	28.66 (29.00)	28.06 (28.26)
S2	29.13 (30.00)	28.67 (29.18)	27.79 (28.86)	27.21 (27.98)
S3	27.06 (29.17)	26.32 (28.62)	25.98 (28.23)	25.11 (27.27)
S4	25.46 (28.41)	24.72 (27.84)	24.02 (27.31)	23.32 (26.55)
S5	23.53 (27.84)	22.63 (27.24)	21.84 (26.72)	21.30 (26.01)
S6	21.82 (27.12)	20.31 (26.46)	20.19 (26.09)	19.42 (25.23)
S7	20.02 (26.47)	18.67 (25.92)	18.40 (25.50)	17.56 (24.73)

[a] Values in the parentheses represent the first-shell coordination number if the only change with added SCS came through the number density change.

Table 2A-3. Number of First-Shell Water Molecules around C_8 Atom of Sodium Cumene Sulfonate Molecules[a]

system	298 K	318 K	338 K	358 K
S0	16.53	16.11	15.78	15.32
S1	16.37 (16.42)	15.85 (15.97)	15.56 (15.70)	15.17 (15.21)
S2	16.06 (16.35)	15.74 (15.80)	15.22 (15.62)	14.82 (15.06)
S3	15.20 (15.90)	14.72 (15.50)	14.45 (15.28)	13.92 (14.67)
S4	14.51 (15.49)	14.06 (15.08)	13.58 (14.78)	13.12 (14.29)
S5	13.63 (15.18)	13.05 (14.75)	12.53 (14.46)	12.17 (14.00)
S6	12.83 (14.78)	11.83 (14.33)	11.71 (14.12)	11.20 (13.58)
S7	11.88 (14.43)	10.99 (14.04)	10.79 (13.80)	10.21 (13.30)

[a] Values in the parentheses represent the first-shell coordination number if the only change with added SCS came through the number density change.

Tables 2A-2 and 2A-3 display the number of water molecules that are present in the first solvation shell of C_7 and C_8 atomic sites of SCS. As can be seen, for a fixed temperature the number of first-shell water molecules around C_7 (and C_8) atom decreases as the concentration of SCS is increased. Note that we have added SCS molecules without replacing water molecules. As a result the box volume increases as one moves from system S0 to system S7, which makes the water number density lower. So, a decrease in the coordination number value is expected because of this change in the box volume. In an attempt to nullify the effect of increased box volume on the coordination number value, we normalized the coordination number value of different systems such that the change in its value purely reflects the effect of added hydrotropes and these normalized coordination number values are also included in the parentheses of the same Tables. For systems up to 0.185m concentration we observe very little change in the coordination number value, whereas a marked change in its number is observed above this concentration. These observations hold true for all temperatures considered in this study. The effect of increased temperature is also quite evident from these Tables. In specific, as temperature increases we observe a modest decrease in the coordination number value. In view of these, by using the VMD program we have further carried out the atomic mass density analysis. Figure 2A-8 represents the mass density map of oxygen atom of water with a cell side of 0.5 Å within 4.75 Å (the position of first peak maximum of $C_7 - O_w$ distribution function) around the C_7 atom of a randomly chosen SCS molecule at different time intervals. For this, we have considered system S3 for two different temperatures (298 and 358 K). Note that in the starting configuration all SCS molecules are dispersed in the solution, and as

the simulation progresses the aggregation of SCS molecules takes place. This can be clearly interpreted from this Figure. At the beginning of the simulation, we observe a very high water density around the SCS molecule, and as soon as aggregates begin to form, a clear depletion in the water density around the C_7 atom is observed. The effect of temperature is also quite apparent. In brief, as temperature increases a lowering of the water density at 358 K (compared with that at 298 K) is also noticed. These facts suggest that elevation in temperature causes an exclusion of more number water molecules from the solvation shell of hydrophobic tail of SCS. These findings also act as corroborative evidence of what we observe in the $C_7 - C_7$ and $C_7 - O_w$ distribution functions.

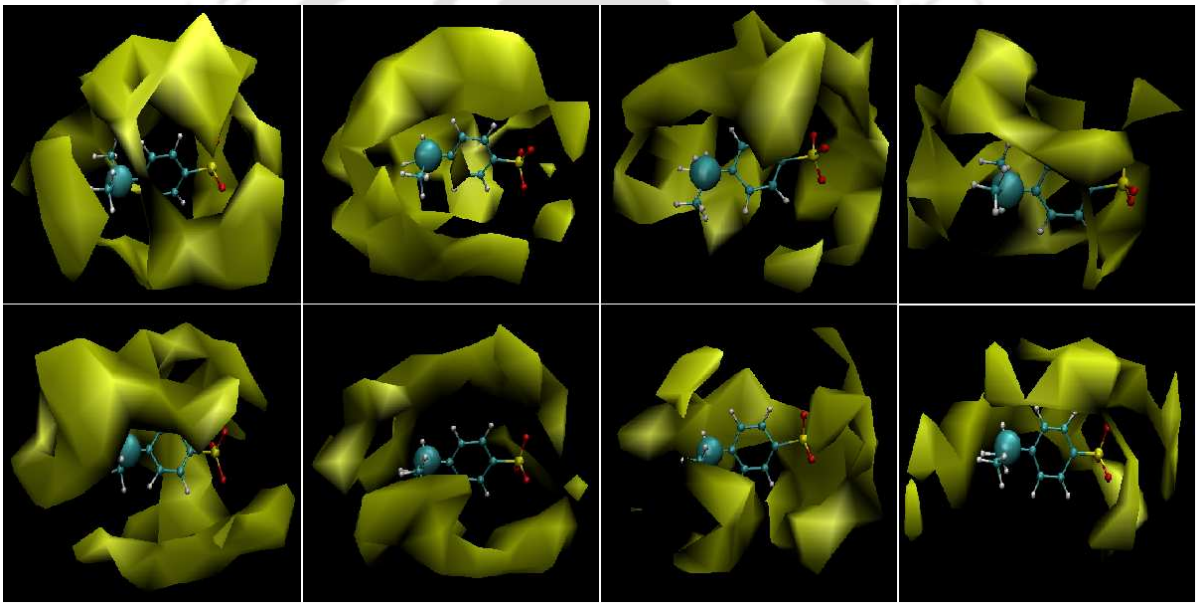

Figure 2A-8. *Contours of solvent water density within 4.75 Å around C_7 atom (large green ball) of a randomly chosen SCS molecule at different time intervals. From left to right: 0, 10, 20, and 40 ns. Top: at 298 K; bottom: at 358 K.*

To investigate the influence of hydrotrope concentration and the effect of temperature on the water structure, we consider water oxygen-water oxygen ($O_w - O_w$) rdf's of different systems (Figure 2A-9). It is important to examine the water-water distribution function because it provides, albeit indirectly, the details of the solvation of hydrotrope SCS. The first and second peak of the $O_w - O_w$ distribution function that appears at 2.75 and 4.55 Å corresponds to the H-bonded first neighbor and the tetrahedrally located second neighbor, respectively. We note that the location of these peaks in the $O_w - O_w$ rdf's

resembles well that already reported elsewhere [92]. As we move from low to high SCS concentration, although a negligibly small enhancement in the first peak height of the $O_w - O_w$ distribution function is observed the first valley becomes shallower and the second peak becomes less pronounced. These suggest some perturbations of tetrahedrally located water structure at higher SCS concentrations. Taking into consideration the effect of temperature at a fixed SCS concentration, we find that the locations of the first and second peak remain unaltered with increasing temperature. However, a depletion in the first and second peak height and a much shallower first valley are observed as the temperature is increased. These results indicate that both increased concentration and elevated temperature bring about the same effect in regards to changes in water structure. The only difference is that the temperature affects both the H-bonded first neighbor and the tetrahedrally located second neighbor, while a change in SCS concentration affects only the tetrahedrally located water structure.

Because the pair correlation function provides information about the probability density distribution of the atoms around a particular site, it is instructive to determine the probability of counterion (Na^+) density around the polar charged site (O atom attached to the sulfur atom) of the sulfonate anion. The rdf's for polar headgroup and counterion ($O - Na^+$) for different systems are presented in Figure 2A-10. Examining the polar headgroup and counterion rdf, we observe that it is a bimodal type distribution with the peaks appearing at 2.35 and 4.65 Å respectively. Unlike unimodal distribution, a bimodal distribution identifies the advent of a dual charge layer around the polar headgroup at two radial locations in space. Although Na^+ ions are attached within the Stern layer of the aggregated systems, they are not able to screen the effect of charged surface completely. In regard to the effect of temperature at a fixed SCS concentration we find that the height of both of these peaks is slightly enhanced as temperature increases (except for systems S0 and S1). Although the addition of SCS causes a small depletion in the first peak height and an enhancement in the second peak height for all systems considered here except for the S0 and S1 systems (which are below MHC level), these are not a strong function of SCS concentration. Nevertheless, these results suggest the enhancement in dual charge layer as the self-aggregation of hydrotropes increases.

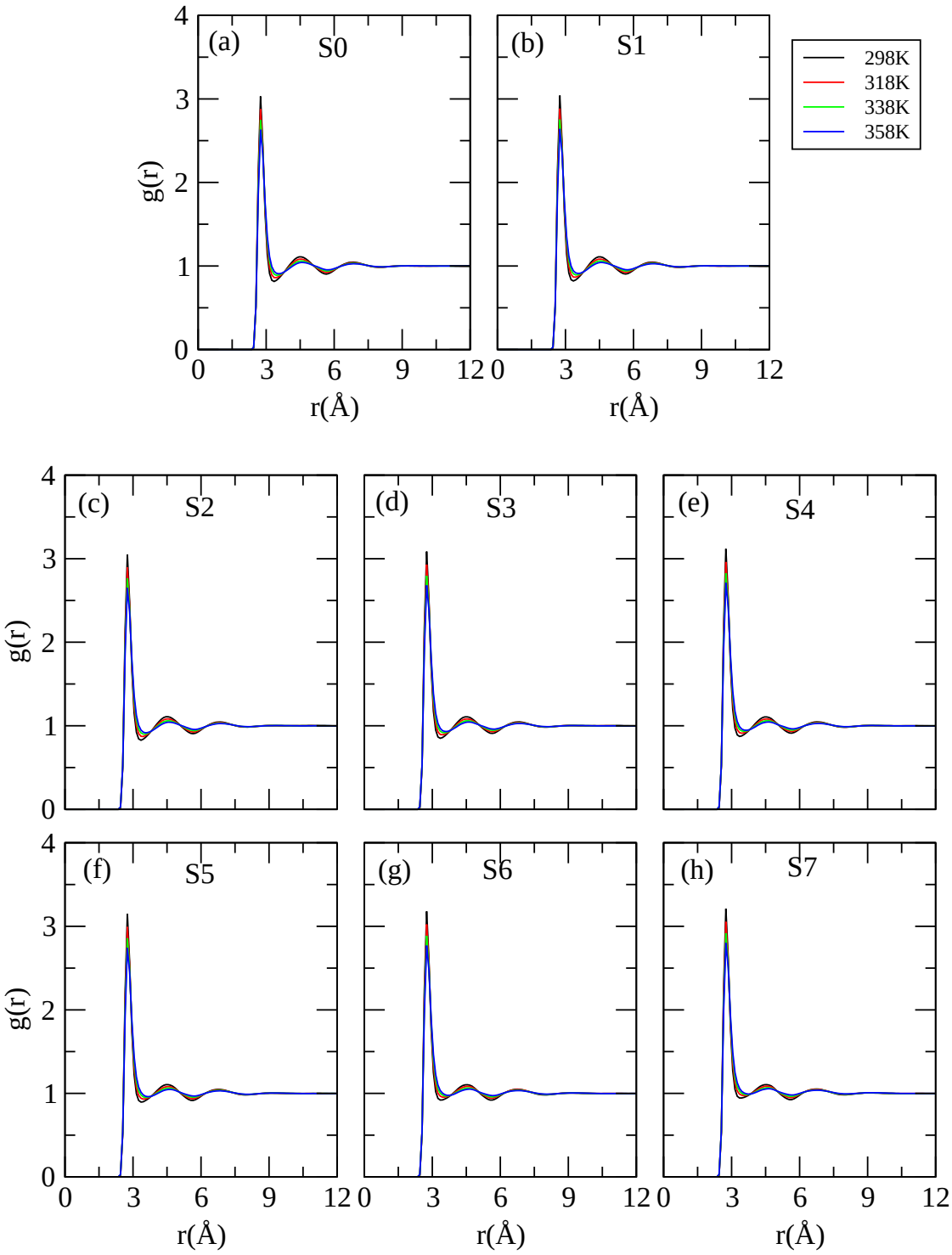

Figure 2A-9. *Site-site radial distribution functions between* $O_w - O_w$.

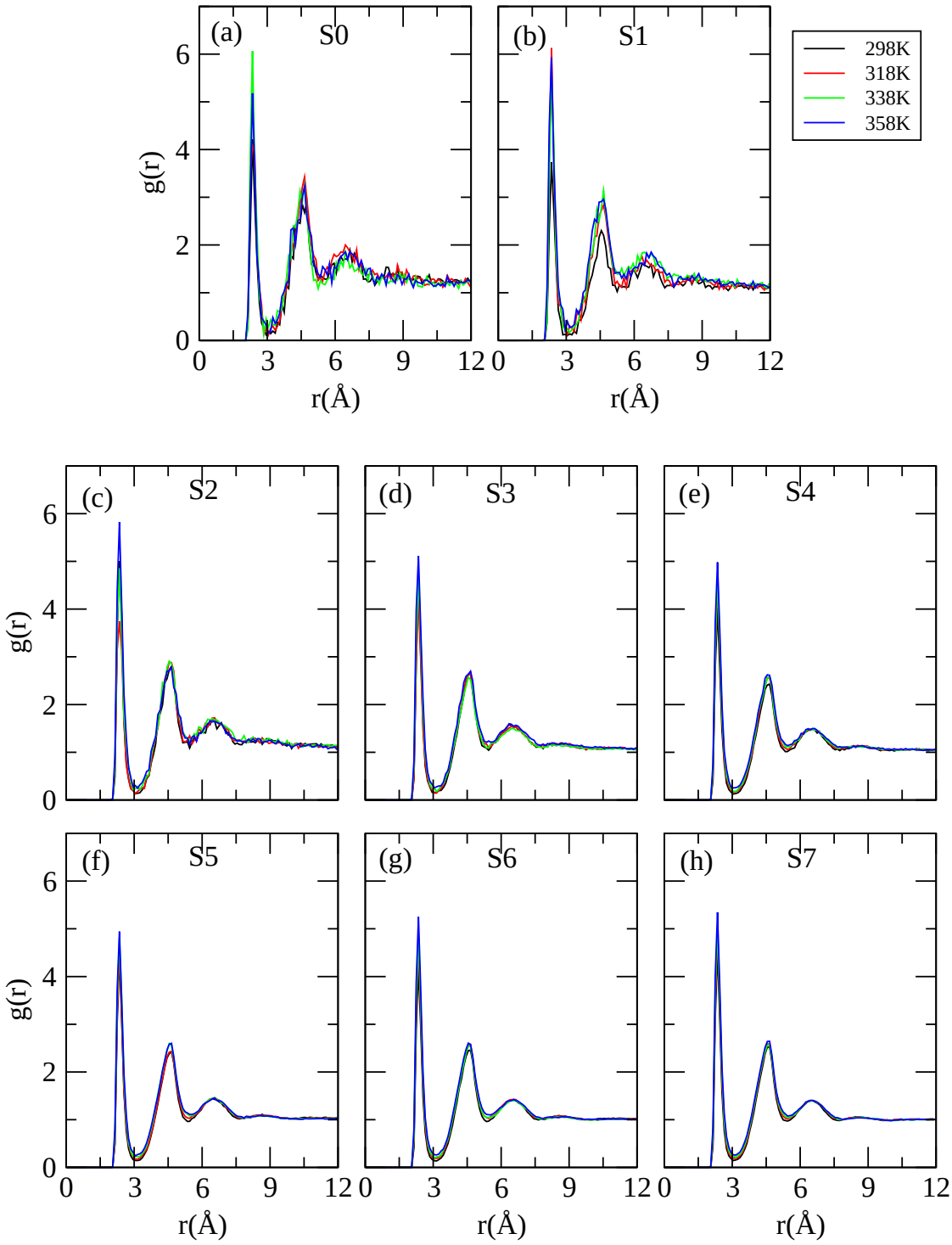

Figure 2A-10. *Site-site radial distribution functions between oxygen atom of polar headgroup of SCS and Na^+ ion.*

Hydrogen-Bond Properties

Because of the presence of oxygen atoms in the sulfonate group of SCS, in aqueous solution it has an ability to act as a hydrogen bond acceptor and forms hydrogen bonds with water molecules. Water structure can be affected by these hydrogen bonds, which can also promote extensive concentration and temperature-dependent aggregation of hydrotropes. Note that because a SCS molecule cannot form hydrogen bonds with like molecules, in aqueous SCS solution two different types of hydrogen bonds are possible, namely, water-water and water-SCS hydrogen bonds. In view of this, following previous works [93-95], we have estimated the average number of hydrogen bonds of each of these types by considering certain geometric criterion. If interatomic distance between hydrotrope oxygen and water oxygen is <3.15 Å and simultaneously the O—O—H angle is $<45^o$, then these two molecules are considered to be hydrogen-bonded. In the case of the water-water hydrogen bond the cutoff distance is <3.35 Å and the angle is the same as that of the water-SCS hydrogen bond. The cutoff distances of these hydrogen bonds are determined from the position of first minimum of the corresponding rdf's. In this context, it is worth noting that the formation of hydrogen bonds between hydrotrope and water molecules depends on the availability of the polar headgroup of SCS for water. If the aggregation of SCS molecules makes its sulfonate group less accessible (due to overlapping of nonpolar and polar groups of SCS) for water molecules to form intermolecular water-SCS hydrogen bonds, then we would observe a depletion in the average number of these hydrogen bonds above MHC level. If the formation of SCS aggregates takes place in such a manner that the availability of its polar sulfonate group is not affected much, then one can expect "no impact" of SCS aggregate formation on the water-SCS hydrogen bond number. In Tables 2A-4 and 2A-5 the average number of hydrogen bonds between water-water and water-SCS (per SCS) for all systems are presented. As per the expectation, temperature-induced breaking of some of the water-water and water-SCS hydrogen bonds causes a depletion in the values of average number of hydrogen bonds. In regard to the effect of added hydrotropes on water-water and water-SCS hydrogen bond numbers, we notice that as concentration increases the values of both of them decrease. Because SCS molecules are capable of hydrogen-bond formation with water (due to the presence of three oxygen atoms in the polar headgroup), some of the water-water hydrogen bonds are replaced by water-SCS hydrogen bonds. As a result, the average number of water-water hydrogen bonds diminishes. For, water-SCS per SCS hydrogen bonds, with increasing concentration because the number of hydrotrope molecules increases (keeping the number of solvent water remains unchanged), we observe a modest

decrease in the average number of this type of hydrogen bond, although the total number of water-SCS hydrogen bonds in the system increases on addition of SCS molecules. Here we note that we did not notice any sharp change in either of these two hydrogen bonds at (and above) MHC level. So at this point it is safe to conclude that it is the hydrophobic tail group of hydrotrope SCS through which the formation of SCS aggregates takes place. Moreover, in the aggregates the accessibility of the polar hydrogen bonding group of a SCS molecule for water remains essentially unaffected.

Table 2A-4. Average Number of Water-Water (per Water) Hydrogen Bonds for Different Systems.

	$HB_{water-water}$			
system	298 K	318 K	338 K	358 K
S0	3.23	3.14	3.05	2.96
S1	3.22	3.13	3.04	2.94
S2	3.21	3.11	3.02	2.93
S3	3.16	3.07	2.98	2.89
S4	3.11	3.03	2.94	2.85
S5	3.07	2.98	2.90	2.81
S6	3.03	2.94	2.85	2.76
S7	2.98	2.90	2.81	2.73

Table 2A-5. Average Number of SCS-Water (per SCS) Hydrogen Bonds for Different Systems.

	$HB_{SCS-water}$			
system	298 K	318 K	338 K	358 K
S0	4.74	4.67	4.50	4.33
S1	4.73	4.54	4.41	4.32
S2	4.62	4.53	4.38	4.30
S3	4.64	4.49	4.36	4.25
S4	4.62	4.47	4.35	4.19
S5	4.57	4.45	4.31	4.17
S6	4.57	4.40	4.29	4.12
S7	4.50	4.36	4.24	4.09

■ SUMMARY AND CONCLUSIONS

Employing classical molecular dynamics simulations, we have investigated the molecular mechanisms of self-aggregation behavior of hydrotrope SCS in aqueous solutions. Eight different SCS concentrations and, for each SCS concentration, four different temperatures have been considered. We also compared our findings with the available experimental results wherever it was necessary. From the calculations of apparent and partial molal volumes of SCS at different concentrations we observed a sudden and dramatic change in the solution structures up to MHC of SCS. In brief, the self-aggregation of SCS molecules starts at 0.185m, and with increasing concentration the growth of SCS molecules leads to an increase in apparent and partial molal volumes of SCS, but above 0.370m concentration the change in these quantities is not very dramatic, suggesting that above this concentration although the number of SCS aggregates in the system increases the size of them does not. Note that the change in the apparent and partial molal volume of SCS with concentrations estimated in this study is in accordance with the experimental findings, albeit qualitatively. Furthermore, in comparison with the typical surfactants, the volume change accompanying the aggregation of SCS is slightly lower, indicating a slightly more closed-packed structure of SCS aggregates. The formation of hydrotrope clusters above MHC is further probed by the estimation of osmotic coefficients value for different systems. Furthermore, in contrast with the experimental findings [29], our calculated molal expansibility at infinite dilution value suggests the water structure breaking ability of SCS molecules.

To examine the origin of SCS aggregate formation above MHC level, we considered different site-site distribution functions of water and SCS molecules. At a fixed temperature, on addition of SCS we found the dehydration of hydrophobic tail of SCS, and the effect is very pronounced above the MHC level. This observation is further confirmed by the atomic mass density analysis. This suggests that it is the interaction between the hydrophobic tails of different SCS molecules that contributes to SCS aggregate formation. The effect of elevated temperature on this dehydration process is also quite visible. As temperature increases, we observed more and more exclusion of water molecules from the hydrophobic atomic sites of SCS, and as a result the aggregation of SCS increases. Interestingly, as suggested by hydrogen-bond analysis, the formation of aggregates does not have much influence on the average number of water-SCS hydrogen bonds, indicating that the accessibility of polar sulfonate headgroup of SCS for water molecules is not greatly

affected. Furthermore, a bimodal type distribution is also observed from the calculation of pair correlation function involving the polar headgroup oxygen of SCS and sodium ion. This suggests the presence of a dual charge layer around the polar headgroup of SCS at two radial distances, and this dual charge layer becomes enhanced as self-aggregation of SCS increases.

Part B:

Hydrotropic Action of Hydrotrope Sodium Cumene Sulfonate on the Solubility of Di-t-Butyl-Methane

Overview: To examine the mechanism of hydrotropic action of hydrotropes on purely hydrophobic molecules, we have carried out classical molecular dynamics simulation of hydrophobic solute di-t-butyl-methane (DTBM) and hydrotrope sodium cumene sulfonate (SCS) in water with a regime of SCS concentrations. Our study demonstrates that, above the minimum hydrotrope concentration (MHC), the self-aggregation of SCS starts, and it creates a micellar-like environment in which the hydrophobic tail part of SCS points inward while its hydrophilic sulfonate group points outward to make favorable contact with water molecules. The formation of the hydrophobic core of SCS cluster creates a hydrophobic environment where the hydrophobic DTBM molecules are encapsulated. Interestingly, the determination of average water-SCS hydrogen bonds further suggests that the aggregate formation of SCS molecules has a negligible influence on it. Moreover, the calculations of Flory-Huggins interaction parameters also reveal favorable interactions between hydrotrope SCS and solute DTBM molecules. The implications of these findings on the mechanism of hydrotrope assisted enhanced solubility of hydrophobic molecules are discussed.

■ INTRODUCTION

The self-aggregation of hydrotrope SCS above its minimum hydrotrope concentration and hydrotrope induced breaking of water structure is discussed in previous chapter (**Chapter 2A**). However, the main limitation that we had in our previous study is that we considered water-SCS binary mixtures without incorporating any third solute. Thus, the underlying mechanism behind the enhanced solubility of a solute in water (in the presence of hydrotropes) could not be explored. This encourages us to examine the role of a hydrotrope on the solubility of a hydrophobic molecule with atomistic detail, and this is the goal of our present study.

Therefore, to examine the mechanism of hydrotropy, we have used di-t-butyl-methane (DTBM) as a model hydrophobic solute (see Figure 2B-1) and SCS as hydrotrope. In order to find out the role of hydrotropes in solubilizing insoluble molecules, we have carried out classical molecular dynamics simulations of DTBM and SCS in water. In this study, first we try to find out the effect of MHC of SCS on the solubilization process of DTBM, and then we extend our analysis toward the microdetails of solubilization of model hydrophobic molecules.

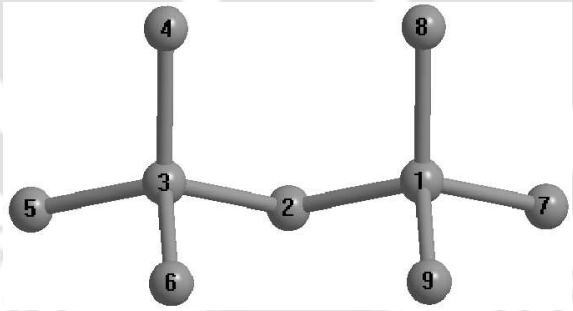

Figure 2B-1. *Structure and atomic number of di-t-butyl-methane applicable for both OPLS/AA and CGenFF models. Hydrogen atoms are left off for clarity.*

The rest of this chapter is divided into three parts. The models and simulation details are presented in next section, then the results are narrated and discussed, and in the last our conclusions are summarized briefly.

■ MODELS AND SIMULATION METHOD

Classical molecular dynamics (MD) simulations of di-t-butyl methane-sodium cumene sulfonate-water ternary mixtures with varying SCS concentrations were carried out at 298 K temperature and at 1 atm pressure. OPLS/AA force field was employed to describe the DTBM molecule [96], and the CHARMM general force field (CGenFF) [78, 79] was used for the SCS molecule. Moreover, in order to examine the robustness of the simulation results presented in this study, we have also considered systems where the CHARMM general force field (CGenFF) [78, 79] is used for DTBM molecules. For water, we have used the SPC/E model [77]. Here we note that, as mentioned in **Chapter 2A**, the identical potential energy functions of CHARMM and AMBER (in case of nonbiological systems) and the application of CHAMBER toolkit [81] make the CHARMM force field AMBER12 compatible. To neutralize the single negative charge of sulfonate group of the hydrotrope molecules, one Na^+ ion was added (for each SCS molecule) in XLEAP of the AMBER12 package [76]. To study the solution properties of the ternary mixtures, 8 different concentrations were considered, and details summarized in Table 2B-1. For the CGenFF model of DTBM molecules we have considered S0, S4, and S7 systems only by keeping the solution mixture compositions exactly same as that for systems containing the OPLS/AA model of DTBM. In those systems, we simply replaced the OPLS/AA model of DTBM with an equal number of CGenFF model DTBM molecules. The initial configurations of all the systems were generated by using the PACKMOL package [82]. All molecular dynamics simulations were performed using the AMBER12 package where the molecules were placed in a cubic box. Periodic boundary conditions were applied in all three directions. We have minimized the energy of the systems for 10000 steps, of which the first 4000 steps are in steepest descent minimization followed by the 6000 steps in conjugate gradient method. All the systems were initially heated slowly from 0 to 298 K for 320 ps in canonical ensemble (NVT). Then, the systems were equilibrated in isothermal-isobaric (NPT) ensemble at 298 K and 1 atm pressure for 5 ns. Then, the production runs were performed in NPT ensemble for 80 ns. In order to get the desired pressure we have used a Berendsen barostat [83] with a pressure relaxation time of 2 ps. The Langevin dynamics method with a collision frequency of 1 ps^{-1} was used in order to control the temperature, and a time step of 2 fs was used for all simulations. The SHAKE algorithm [84] was used to constrain the covalent bonds involving a hydrogen atom. A cutoff distance of 10.0 Å was defined for all nonbonded interactions. The particle mesh Ewald method was used to treat the long-range electrostatic interactions.

Table 2B-1. Overview of Systems[a]

System	N_{DTBM}	N_{scs}	N_{wat}	volume (nm^3)	M_{scs}
S0	8	24	8400	260.34	0.153
S1	8	24	7200	223.31	0.178
S2	8	24	6000	187.18	0.213
S3	8	24	4800	151.50	0.263
S4	8	24	3600	115.72	0.344
S5	8	24	2400	80.11	0.497
S6	8	24	1800	62.24	0.653
S7	8	24	1200	44.28	0.900

[a] N_{DTBM}, N_{scs}, N_{wat} and M_{scs} are the number of Di t-Butyl Methane (OPLS/AA model), Sodium Cumene Sulfonate, Water molecules and molar concentration of the Sodium Cumene Sulfonate respectively for the above system.

For the calculation of Flory-Huggins interaction parameters (discussed in **Chapter 1**) between DTBM and SCS, following earlier work [67], at first we prepared hydrotrope-solute mixtures of two different compositions. The first one consists of 24 hydrotrope SCS molecules and 1 DTBM molecule (in 24:1 ratio), and in the second mixture we consider 24 hydrotrope SCS molecules and 2 DTBM molecules (in 12:1 ratio). For each system, initially all the SCS and DTBM molecules were placed randomly. The initial configurations of each of the DTBM-SCS mixtures were first equilibrated in vacuum. The vacuum simulation run was performed in AMBER12 for 12 ns at 298 K to get the prior compaction of the system. Further, by the use of leap module of AMBER12, a cubic periodic box was generated around the compacted complex, where 0 Å buffer constant in all three directions has been used. The voids, mostly generated at the corners of the cubic box, were filled up by adding 318 and 268 water molecules (SPC/E model) for 24:1 and 12:1 systems, respectively. Then, each DTBM-SCS-water mixture was first energy minimized for 10000 steps of which the first 4000 steps are in steepest descent minimization followed by 6000 steps in conjugate gradient method. Then, the systems were heated in canonical ensemble (NVT) from 0 to 298 K for 320 ps. To relax the density of the system, we have carried out another 4 ns equilibration run in isothermal isobaric (NPT) ensemble at 298 K and 1 atm pressure. At last the system was equilibrated for 20 ns in NPT maintaining the periodic boundary condition at 298 K and 1 atm pressure. A time step of 2 fs has been used. Berendsen barostat (with a pressure relaxation time of 2 ps) and Langevin dynamics (with a collision frequency of 1 ps^{-1}) were used to maintain the pressure and temperature, respectively. SHAKE algorithm was used to constrain the covalent bonds between hydrogen atoms and

heavy atoms while a 10.0 Å cutoff distance was defined for all nonbonded interactions. The long-range electrostatic interactions were treated with particle mesh Ewald method.

■ RESULTS AND DISCUSSION

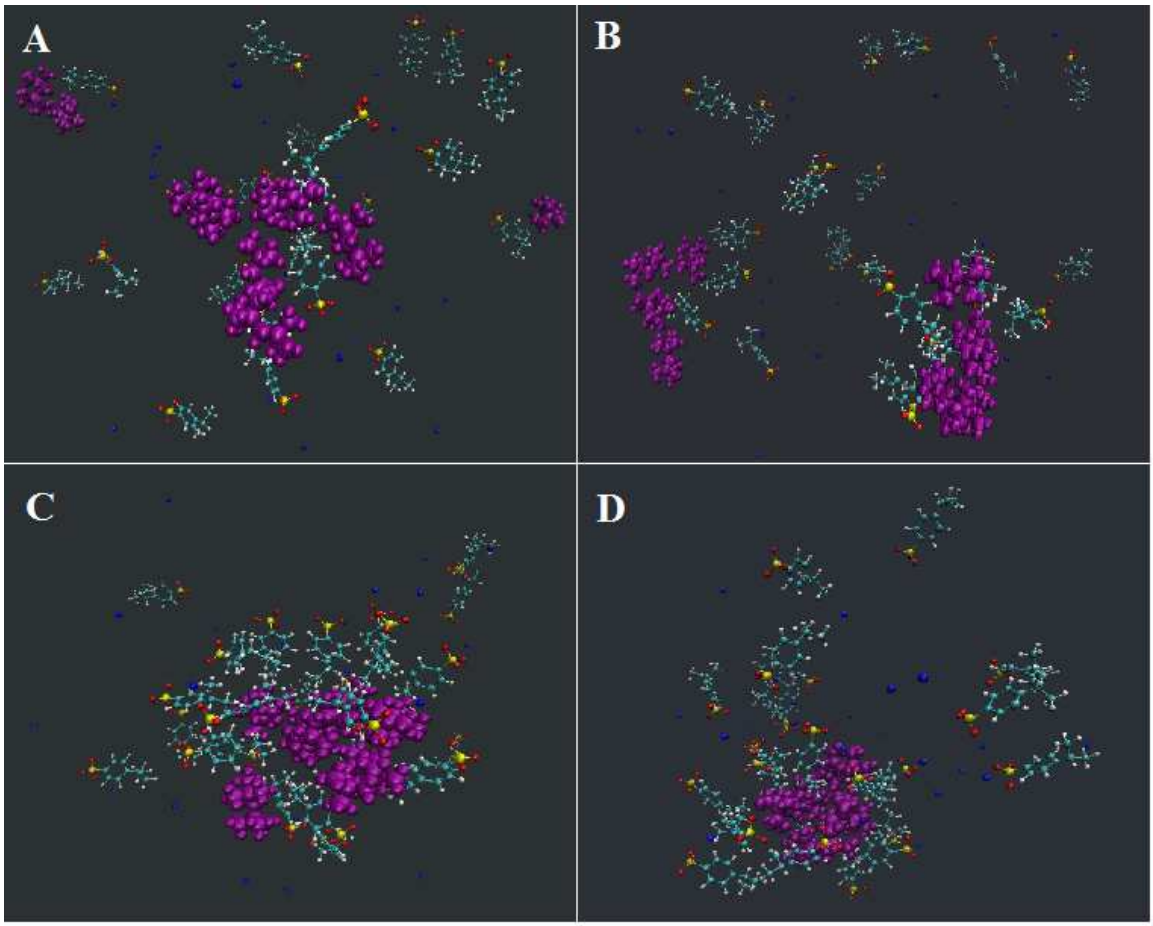

Figure 2B-2. *(A-D) Snapshots for the systems S1, S4, S6, and S7 at 80 ns. Pink balls and blue balls represent DTBM molecules (OPLS/AA model) and sodium ions, respectively. Carbon, Hydrogen, Oxygen and Sulfar atoms of SCS molecules are represented by cyan, white, red and yellow balls respectively. Water molecules are left off for better visual clarity.*

Incorporation of DTBM Molecules inside SCS Clusters

In order to probe the aggregation of SCS molecules, in Figure 2B-2 we present the snapshots of systems S1, S4, S6, and S7. Note that we have chosen the systems in such a manner that at least one concentration of SCS falls below its MHC, one in the MHC region and two are above MHC regions. Furthermore, the water molecules are left off to

enhance the visual clarity of the snapshots. From this figure it is apparent that, as the molarity of the solution increases, a greater and greater number of SCS molecules assembled to form clusters. A close look into these clusters reveals that the hydrophobic tail of the SCS molecule is responsible for this self-assembled process. The mass density map of SCS molecules around a reference SCS, calculated using a visual molecular dynamics (VMD) [85] program, also supports this observation (see Figure 2B-3).

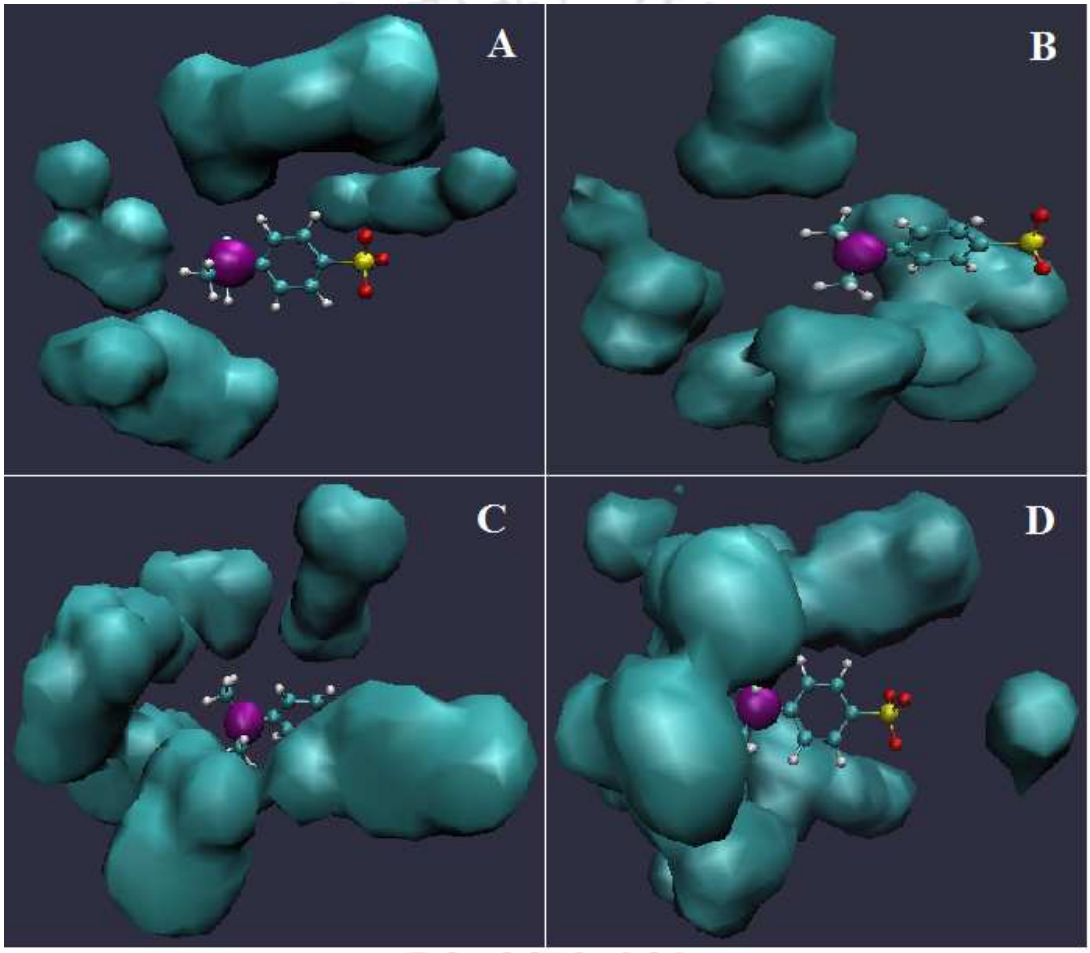

Figure 2B-3. *(A-D) Contours of SCS density within 8.05 Å around a reference SCS molecule for systems S1, S4, S6, and S7 systems, respectively. The large green ball represents the C_7 atom of reference SCS molecule.*

The mass density map is calculated by considering the density of SCS molecules around a reference SCS molecule with a cell side of 0.2 Å and by choosing a C_7-C_7 cutoff distance of 8.05 Å (the choice of this cutoff distance is discussed below). To examine the aggregation behavior of hydrotrope SCS molecules more closely, we have further calculated the mass

density map of the C_7 atom of the SCS molecule around a reference C_7 atom from SCS molecules (for both models of DTBM molecules); the same is presented in Figure 2B-4. This contour diagram shows that the density of the C_7 atomic site of SCS increases with increasing concentration implying that the self-association of SCS takes place through its hydrophobic tail. This finding is per the expectation, and we reported this in our previous study (**Chapter 2A**) of water-SCS binary mixtures. However, what is remarkable is that DTBM molecules also get incorporated inside the core of the clusters of SCS molecules, and the penetration of DTBM molecules into the core of SCS clusters increases with an increase in SCS concentration. Also, this observation is true for both DTBM models (see Figure 2B-5).

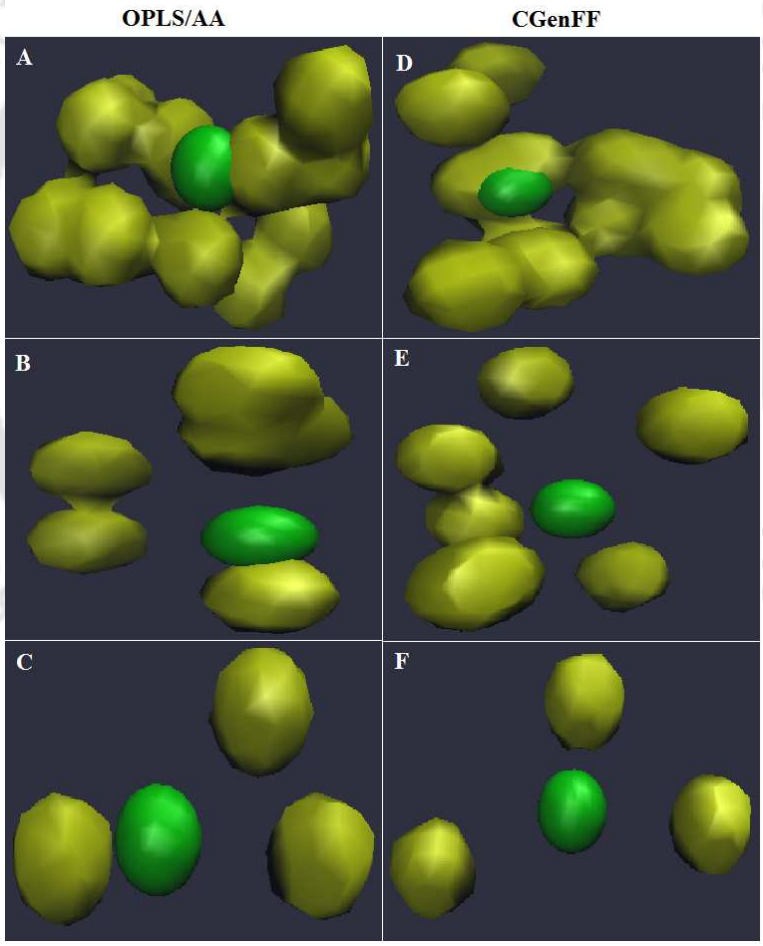

Figure 2B-4. *The contours of C_7 atom of SCS density within 8.05 Å around a reference C_7 atom of SCS molecule for S0, S4, and S7 systems. (A)-(C) are for the systems containing OPLS/AA model of DTBM molecules and (D)-(F) are for the systems containing CGenFF model of DTBM molecules. Large green ball represents the C_7 atom of reference SCS molecule.*

In brief, these snapshots depict the incorporation of DTBM molecules inside the SCS clusters and are qualitatively very similar for both the DTBM models. This suggests that hydrophobic DTBM molecules prefer to stay in a hydrophobic environment over an aqueous medium. Here one remembers that this prediction is purely qualitative in nature because it is based on the observations made from the snapshots of different systems. A more quantitative description of these observations is discussed in the following section.

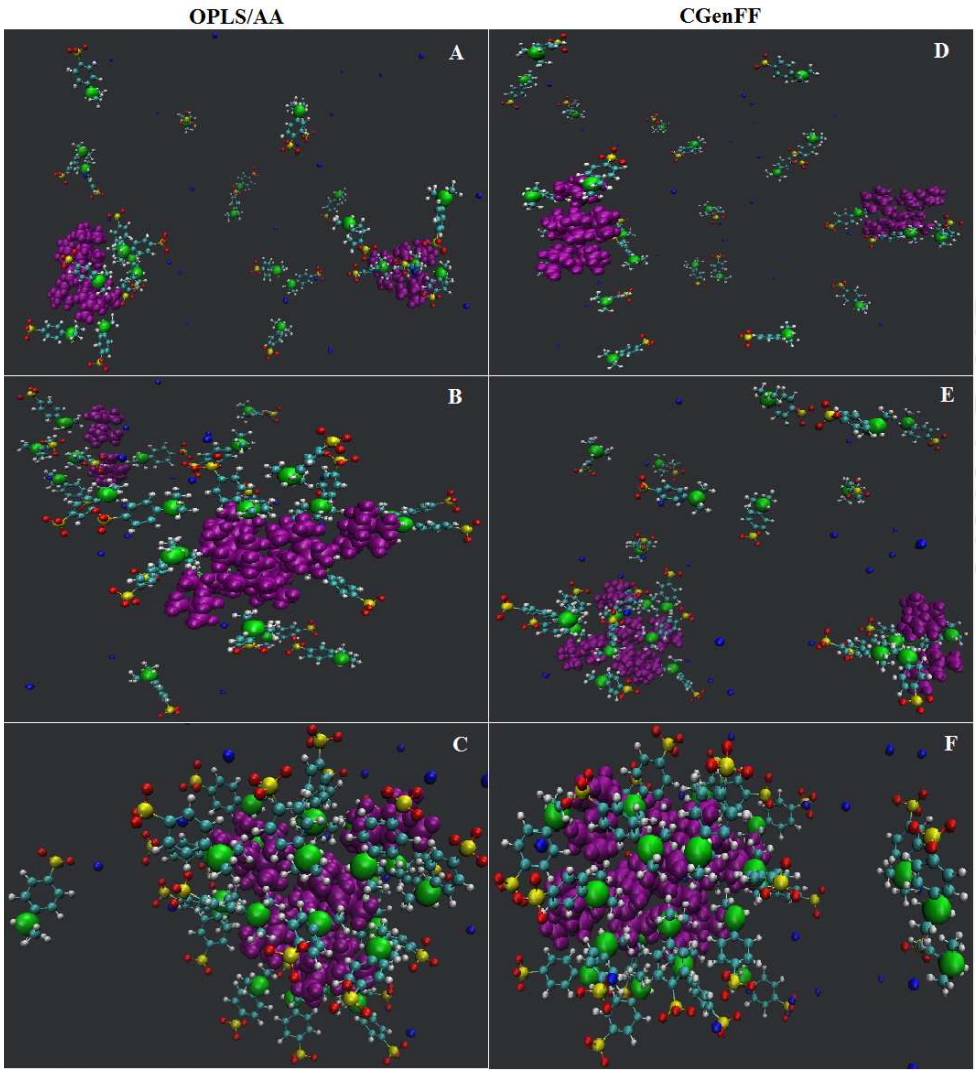

Figure 2B-5. *Snapshots for the systems S0, S4, and S7 at 80ns. (A)-(C) are for the systems containing OPLS/AA model of DTBM molecules and (D)-(F) are for the systems containing CGenFF model of DTBM molecules. Pink balls and blue balls represent DTBM molecules and sodium ions respectively. Water molecules are left-off for better visual clarity.*

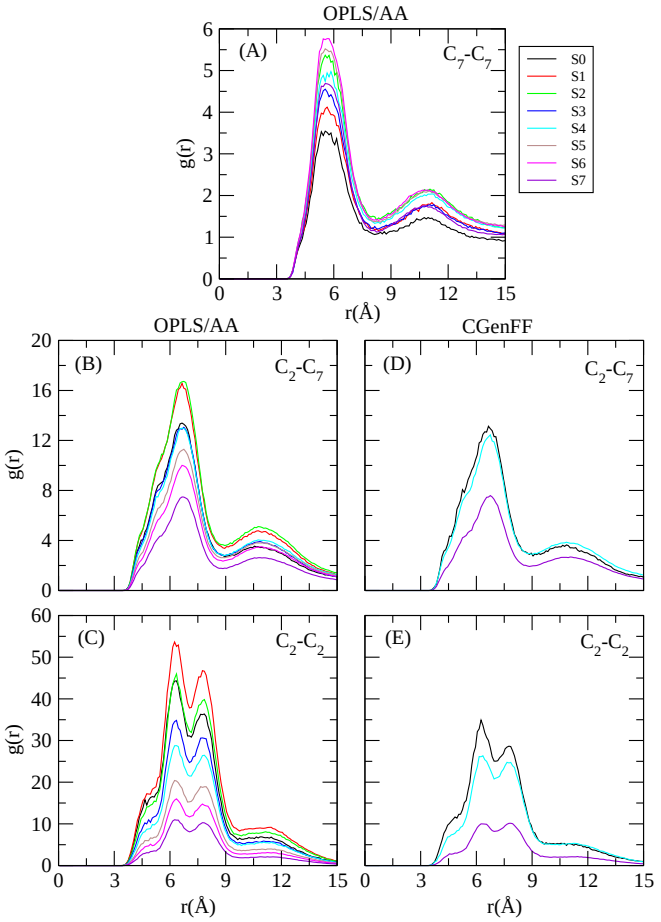

Figure 2B-6. *(A) represents the site-site radial distribution functions between C_7-C_7 (SCS - SCS). (B) and (C) are $C_2 - C_7$ (DTBM - SCS), and $C_2 - C_2$ (DTBM - DTBM) rdfs in which OPLS/AA model of DTBM molecules is considered. (D) and (E) represent the site-site radial distribution functions between $C_2 - C_7$ (DTBM - SCS), and $C_2 - C_2$ (DTBM - DTBM) for CGenFF model of DTBM molecules.*

Cluster Structure Analysis

In this section we first concentrate on the quantitative description of SCS clusters for different systems. Then, we extend our study toward the estimation of the number of DTBM molecules that are present in the core of SCS clusters. Two SCS molecules form a dimer if the C7 atom of one SCS molecule is within a cutoff distance of 8.05 Å of C_7 atom of a neighboring SCS molecule. Similarly, the SCS cluster of size three is obtained if the distance of the C_7 atom of a third SCS molecule is within the cutoff distance of any of the C_7 atom of dimer forming SCS molecules and so on. This cutoff distance is obtained from the position of the first minimum of the C_7-C_7 distribution function of SCS molecules

(see Figure 2B-6), and the choice of C_7 atom is due to the fact that self-aggregation of SCS molecules takes place through its hydrophobic tail (discussed above). Note that we consider the last 16 ns of production run for cluster structure analysis purpose. For all systems considered here, the probability distributions of various sizes of SCS clusters (in percentage) with respect to the total number of SCS molecule present in a given system are shown in Figure 2B-7. We find that the probability of forming higher order clusters increases with increasing SCS concentration. From these histograms it can also be noticed that a clear transition occurs between lower and higher order cluster formation around the MHC region of SCS.

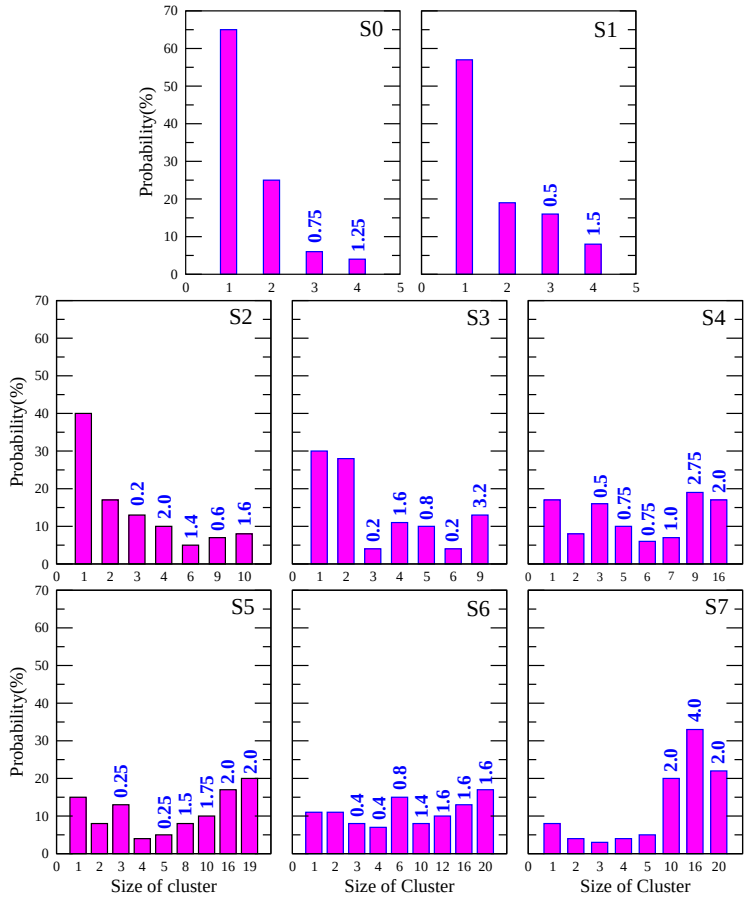

Figure 2B-7. *Probability distribution (in percentage) of SCS clusters of different sizes. The numbers on different bar diagrams represent the average number of DTBM molecules (OPLS/AA model) present in a given SCS cluster.*

Next, we deal with the estimation of the number of DTBM molecules that are present in the core of SCS clusters. Since, the aggregation of SCS takes place through its hydrophobic tail, for this analysis we set up the following criteria: (i) the size of the SCS cluster has to be greater than or equal to three, (ii) the C_2 atom of a DTBM molecule should be within 9.05 Å of C_7 atom of a cluster forming SCS molecule, and simultaneously (iii) two DTBM molecules are considered to be present in the same SCS cluster if the distance between the C_2 atom of one DTBM molecule falls within 9.25 Å of the C_2 atom of a neighboring DTBM molecule and at the same time both the DTBM molecules are present within 9.05 Å of C_7 atom of SCS, which are part of the same cluster. These cutoff distances are taken from the positions of the first minima in the corresponding rdfs shown in Figure 2B-6(B-E). Though these distribution functions depict very similar DTBM-SCS and DTBM-DTBM interactions for both the models of DTBM, a close examination reveals a slight lowering in the peak heights of these rdfs for the CGenFF DTBM model. This suggests that, for the CGenFF model, a slightly weaker interaction between the hydrophobic atomic site C_2 with another C_2 of DTBM and with hydrophobic atomic site C_7 of SCS in which a more prominent effect can be seen in the $C_2 - C_7$ (DTBM-SCS) rdf. The total number of DTBM molecules that are present within the SCS cluster, as calculated for all the systems, are shown in Figure 2B-7. It is apparent that as the probability of formation of higher order cluster of SCS molecules increases, the number of DTBM molecules within that SCS cluster also increases. Below the MHC region, the number of DTBM molecules inside the cluster of SCS is small, but as SCS starts to form higher size clusters around the MHC region, a profound increase in the number of DTBM molecules in the interior of SCS clusters is observed. Moreover, as the self-aggregation of SCS increases, the higher order SCS clusters design more of a hydrophobic environment inside their cores. As a result, the ability of incorporating hydrophobic molecules into interior of these clusters also increases. Further, in order to examine if this encapsulation process is dependent on the choice of DTBM force field, we also estimated the number of the CGenFF model of DTBM molecules inside SCS clusters, and this is shown in Figure 2B-8. Together with this we also show the results for the OPLS/AA model of DTBM molecules for the systems S0, S4, and S7. It can be noticed that both of these molecules show a similar tendency for getting encapsulated in the core of SCS clusters. These observations indicate that, in hydrotrope SCS assisted enhancement in the solubility of solute DTBM molecules, it is the SCS aggregate which plays a significant role (by creating a hydrophobic environment that is favored by the solute molecules). Similar observations have also been made for surfactant assisted solubilization

of hydrophobic molecule [97]. In this context it is important to mention that depending on its chemical structure a drug can be present at different loci of a surfactant micelle. For example, the hydrophilic drugs are adsorbed on the surface of the micelle; the drugs with intermediate solubility are present in the intermediate position between the hydrophilic head groups of micelle forming surfactants or in the intermediate position between the hydrophilic headgroup and the first few carbon atoms of the hydrophobic tail. On the other hand, completely hydrophobic drug molecules are located in the interior of the micelle core [98-100].

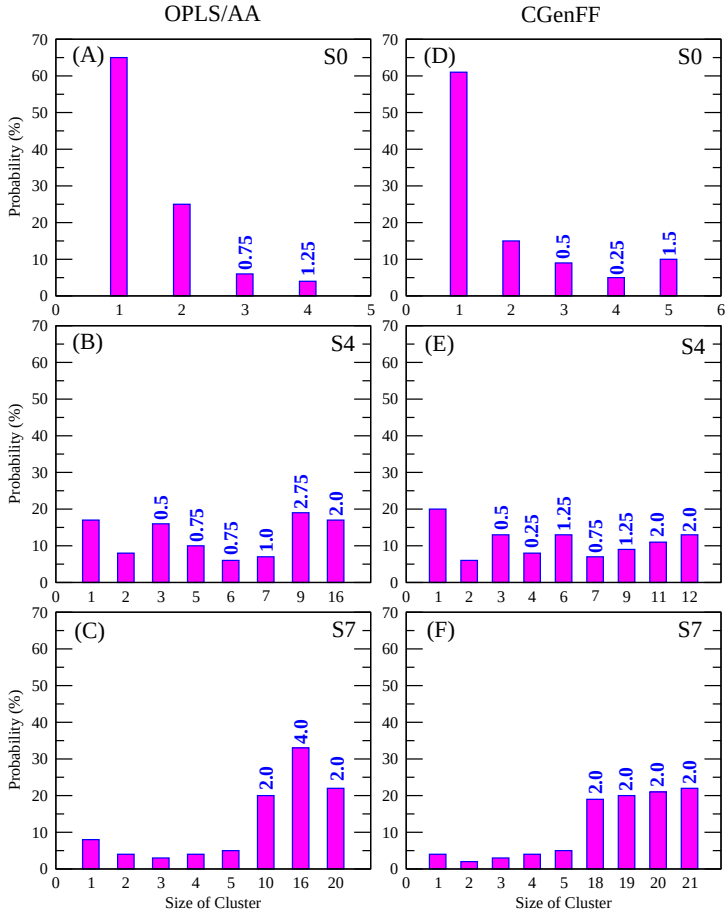

Figure 2B-8. *A, B, and C represent the probability distribution (in percentage) of SCS clusters of different sizes for OPLS/AA model of DTBM molecules D, E, and F are the probability distribution (in percentage) of SCS clusters of different sizes for CGenFF model of DTBM molecules. The numbers on different bar diagrams represent the average number of DTBM molecules present in a given SCS cluster.*

Hydrophobic Hydration

The degree of hydration of the hydrophobic part of a molecule is closely related to the number of water molecules around it. So, to analyze the solvation of DTBM and SCS molecules more clearly, we have estimated the number of first shell water molecules (coordination number, CN) around different hydrophobic moieties of solute DTBM and hydrotrope SCS using Eq. 2.3. In Table 2B-2 we show the number of water molecules that are present in the first coordination shell of different hydrophobic sites of DTBM and SCS. Note that we show the number of first shell water molecules around C_1, C_2 and C_4 atoms of DTBM, and in the same way for SCS we consider C_7 and C_8 atoms. Among different hydrophobic atomic sites of DTBM (and SCS) we chose these sites because they possess different chemical environments. The atomic sites having a similar chemical environment (for example, C_8 and C_9 atoms of SCS) show similar hydration characteristics with respect to change in concentration. In Figure 2B-9, we show the distribution functions involving these atomic sites of DTBM and SCS and water oxygen. As mentioned above, for the estimation of the number of first shell water molecules around these hydrophobic atomic sites, the position of the first minimum in the corresponding rdf is considered. Here it is worth noting that the values of CN for hydrophilic atomic sites of SCS show only a slight change as concentration changes.

Table 2B-2. Number of First Shell Water Molecules around C_7 and C_8 Atom of Sodium Cumene Sulfonate Molecules and C_1, C_2 and C_4 of DTBM (OPLS/AA Model) Molecule[a]

System	C_1	C_2	C_4	C_7	C_8
S0	11.42	19.23	4.56	24.85	13.29
S1	10.85 (11.38)	18.37 (19.17)	4.32 (4.54)	23.47 (24.77)	12.54 (13.25)
S2	10.25 (11.31)	17.57 (19.05)	4.12 (4.52)	22.05 (24.61)	11.81 (13.17)
S3	10.15 (11.21)	17.44 (18.87)	3.93 (4.47)	21.48 (24.39)	11.54 (13.08)
S4	9.26 (10.99)	16.19 (18.51)	3.61 (4.39)	18.97 (23.92)	10.21 (12.80)
S5	8.32 (10.57)	14.73 (17.80)	3.17 (4.22)	16.12 (23.00)	8.67 (12.30)
S6	7.30 (10.22)	13.25 (17.20)	2.86 (4.08)	13.18 (22.23)	7.11 (11.89)
S7	7.01 (9.58)	12.73 (16.13)	2.67 (3.82)	11.66 (20.85)	6.31 (11.15)

[a] The values in the parentheses represent the expected coordination number values due to change in water number density.

From Table 2B-2 it can be observed that the number of first shell water molecules around C_1 and C_2 atoms of DTBM molecule decreases as concentration of the solution

increases, and this effect is more pronounced for systems S4-S7. A very similar trend is also observed for C_7 and C_8 atoms of SCS. Since the number density of water decreases with an increase in SCS concentration, a modest depletion in the coordination number value is expected. In order to negate the effect of reduced water density and to see the effect of SCS aggregation on the number of first shell water molecules around the hydrophobic moieties explicitly, we normalized the coordination number values with respect to that of system S0, and the same are presented in the parentheses of Table 2B-2.

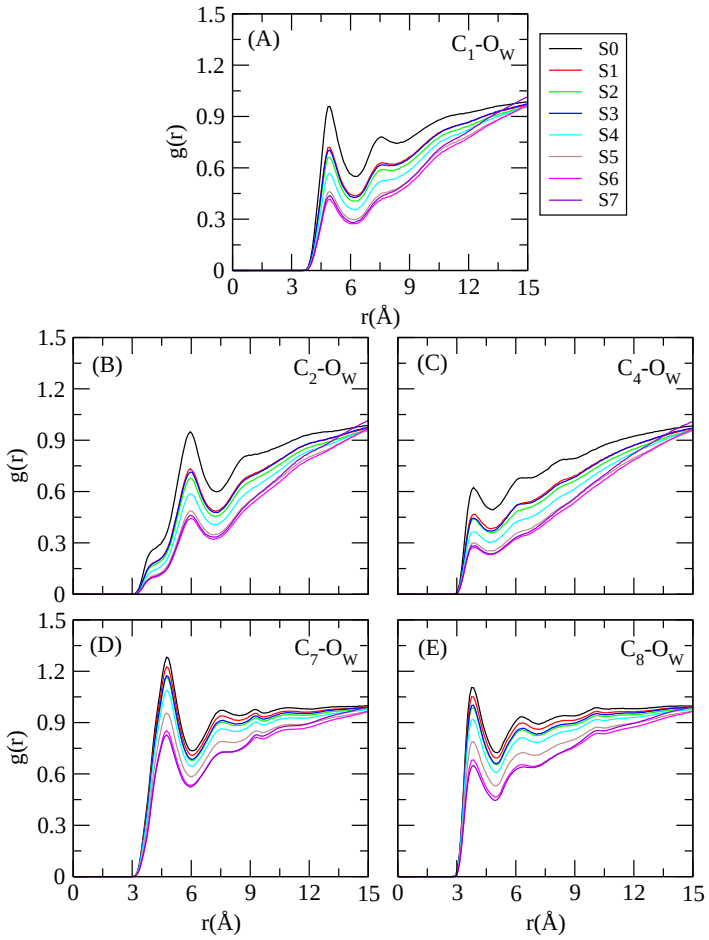

Figure 2B-9. *Site-site radial distribution functions between (A) $C_1 - O_W$ (DTBM - Water), (B) $C_2 - O_W$ (DTBM - Water), (C) $C_4 - O_W$ (DTBM - Water), (D) $C_7 - O_W$ (SCS - Water), and (E) $C_8 - O_W$ (SCS - Water) for different systems. In all the plots, the OPLS/AA model of DTBM is considered.*

It is noticed that the difference between the actual and normalized or expected coordination number is small for below MHC concentration, and this difference begins to rise

from the MHC region. These findings suggest more and more dehydration of hydrophobic tails of both SCS and DTBM molecules as SCS concentration increases, and this is quite similar to the behavior of classical surfactant in solutions above its CMC value [101-103]. For example, the results of a wide Q-range neutron diffraction measurement study and empirical potential structure refinement (EPSR) modeling of aqueous solution of surfactant decyltrimethylammonimum bromide ($C_{10}TAB$) also showed that the hydrophobic tail groups of the surfactant orient themselves to minimize the contact with the solvent water molecules, and they form a hydrophobic core upon micellization [101]. In this context we would also like to mention that neutron diffraction scattering experiments are also useful to study the aggregation propensity of solutes of different sizes including biomolecules [104-107]. For example, by using neutron diffraction with isotropic substitution (NDIS) experiment, Philip et al. examined the aggregation tendency of pyridine molecules in aqueous solution that showed preferential exclusion of water molecules with increasing pyridine concentration [106]. Here, we also note that the results of MD simulations of aqueous solutions of small amphiphilic molecules such as tert-butyl alcohol revealed dehydration of its hydrophobic atomic sites, and self-aggregation takes place through its hydrophobic methyl groups [108-110]. We further note that the number of water molecules around small tail parts of SCS is much lower in comparison to the results from our previous study of SCS-water binary mixture, suggesting that the hydrophobic sites of SCS molecules have been occupied by DTBM molecules. Furthermore, as SCS molecules start to self-aggregate, DTBM molecules commence to enter into the core of aggregated SCS molecules. As a result the number of water molecules around different hydrophobic sites of DTBM molecules decreases, and the effect is more noticeable when SCS molecules get fully aggregated above MHC level.

To get a better idea about water density around DTBM molecules, we have further carried out atomic mass density analysis. Figure 2B-10 displays the mass density map of oxygen atom of water with a cell side of 0.2 Å within 7.25 Å around a randomly chosen DTBM molecule for systems S0, S3, S5, and S7. At low concentration, we observe a very high water density around the DTBM molecule, and as soon as SCS molecules begin to form aggregates, a clear reduction in the water density around the DTBM is observed. This finding suggests the depletion of water molecules from the first solvation shell of DTBM molecules and acts as supportive evidence of what we discussed above. We have also performed atomic mass density analysis of hydrotropes around a DTBM molecule with a cell side of 0.2 Å within 9.05 Å. In Figure 2B-11, we present the mass density map of

SCS molecules around the DTBM molecule for the systems S0, S3, S5, and S7. A low SCS density around DTBM molecules is observed below the MHC region, but with an increase in concentration of SCS, the density of the hydrotrope around DTBM increases. Therefore, these results also uphold the fact that at higher SCS concentrations water molecules are getting replaced by SCS molecules around DTBM molecules.

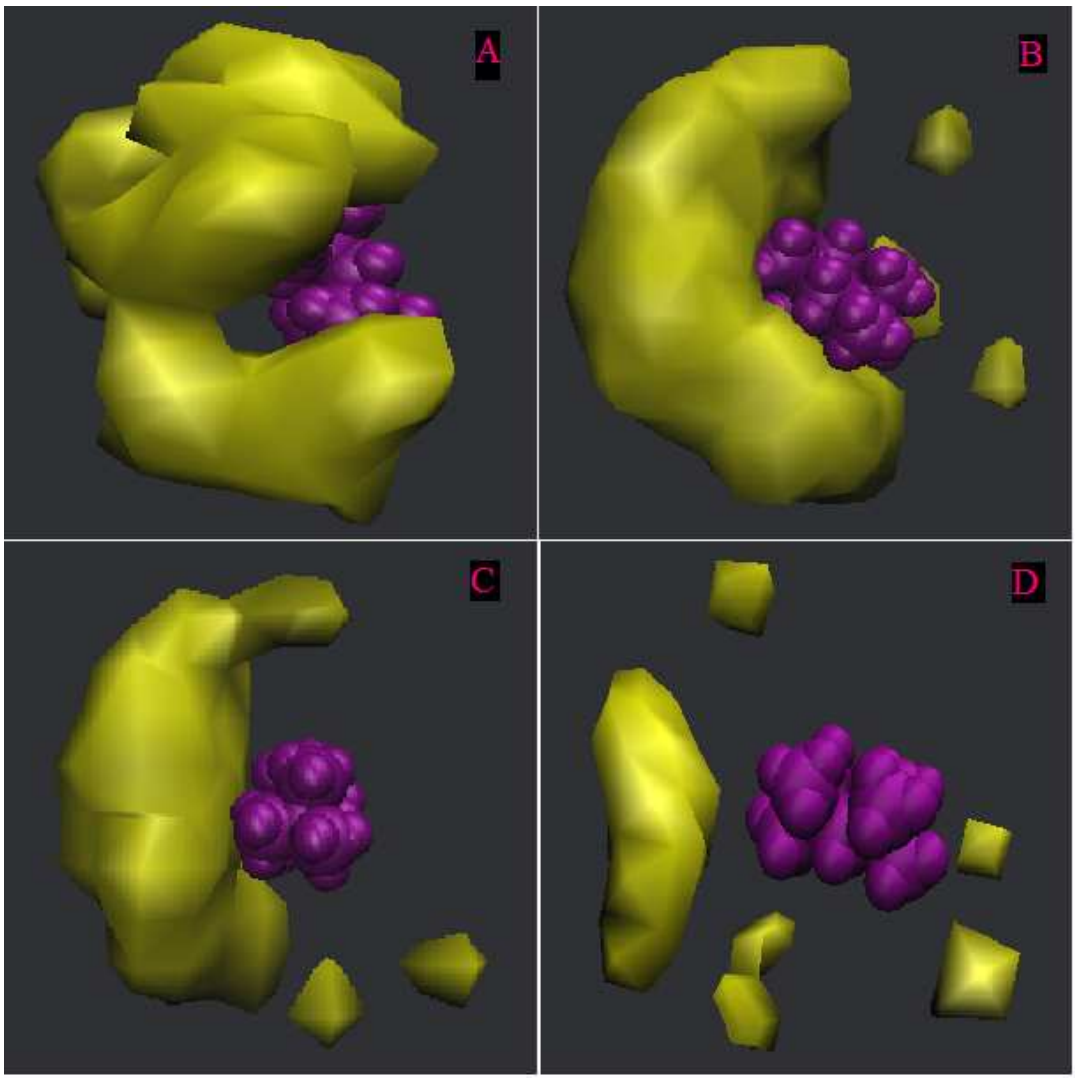

Figure 2B-10. *Contours of solvent water density within 7.25 Å around the OPLS/AA model of the DTBM molecule (pink ball). A, B, C, and D show the results for systems S0, S3, S5, and S7, respectively.*

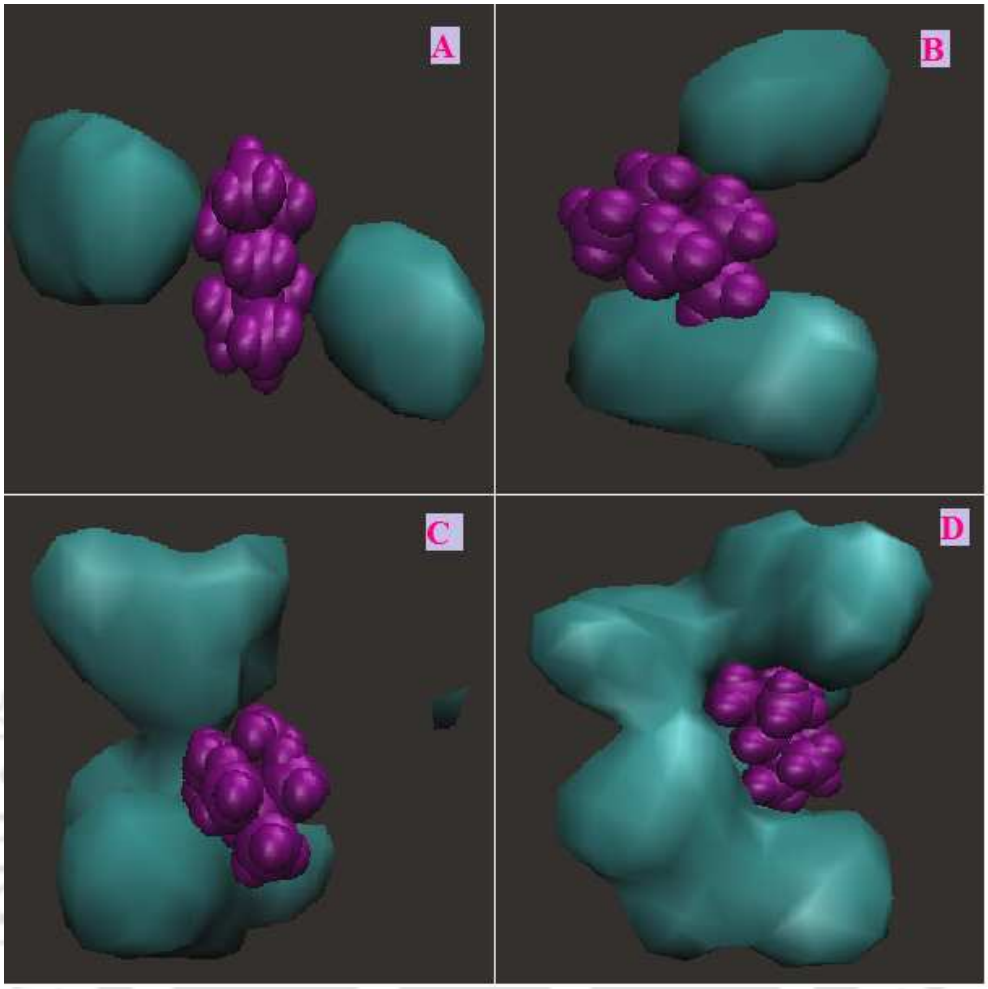

Figure 2B-11. *Contours of hydrotrope SCS density within 9.05 Å around the OPLS/AA model of the DTBM molecule (pink ball). A, B, C, and D show the results for systems S0, S3, S5, and S7, respectively.*

From the above discussions it is evident that as concentration increases in the solvation shell of DTBM, water molecules are replaced by SCS molecules. This prompts us to make an estimation of the number of SCS molecules in the first coordination shell of DTBM molecules in a more quantitative manner. With the help of Eq. 2.3, we have calculated the number of SCS molecules that are present in the first solvation shell of DTBM. For this, we consider the distribution function involving C_1 atom of DTBM and C_7 atom of SCS (see Figure 2B-12). In Table 2B-3 we present the number of first shell SCS molecules around DTBM for different systems considered in this study. We observe that the number of first shell SCS molecules around DTBM increases with increase in concentration, and the effect is more pronounced at and above the MHC level. Thus, as the aggregation of SCS molecules increases from the MHC level with an increase in concentration, water

molecules that were present in the first solvation shell of DTBM molecules are now being replaced by the hydrotropes molecules suggesting the creation of more hydrophobic layers around DTBM molecules.

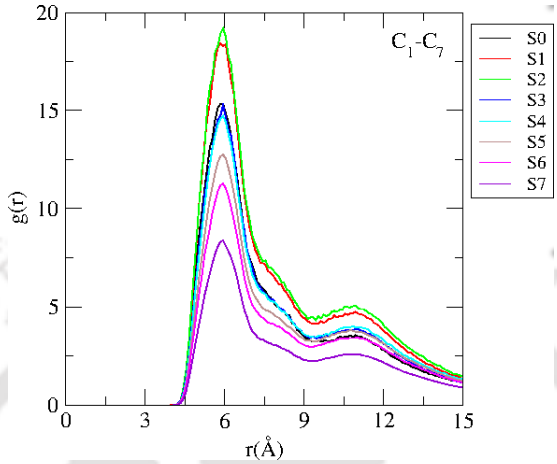

Figure 2B-12. *$C_1 - C_7$ (DTBM - SCS) site site radial distribution functions for different systems. In all the plots, the OPLS/AA model of DTBM is considered.*

Table 2B-3. Number of First Shell Hydrotrope SCS Molecules around Hydrophobic DTBM (OPLS/AA Model) Molecules

system	N_{Hyd}
S0	8.55
S1	8.78
S2	10.90
S3	11.54
S4	13.46
S5	17.22
S6	20.02
S7	21.76

Hydrogen Bond Properties

Due to the presence of oxygen atoms in the sulfonate group, sodium cumene sulfonate has an ability to act as hydrogen bond acceptor and can form hydrogen bonds with a water molecule in aqueous solution. In this section, we present how the presence of a DTBM molecule affects the hydrogen bonding properties of hydrotrope SCS and water. Since DTBM is purely hydrophobic and the SCS molecule cannot form intermolecular SCS-SCS hydrogen bonds between themselves, only two types of hydrogen bonds are possible

(i.e., water-water and water-SCS). Thus, we have estimated the average number of water-water (per water) and water-SCS (per SCS) hydrogen bonds. For this, as reported in earlier works [93-95], we have also considered the following geometric definition in order to define a hydrogen bond. For water-SCS hydrogen bonds, if an interatomic distance between hydrotrope oxygen and water oxygen is less than 3.15 Å and simultaneously the oxygen-oxygen-hydrogen angle is less than 45^o, then they are considered to be hydrogen bonded. In the case of water-water hydrogen bond formation the cutoff distance between oxygen atoms of two different water molecules is less than 3.35 Å and the angle is the same as that of water-SCS hydrogen bonds. These cutoff distances are determined from the appearance of the first minimum of the corresponding rdfs (see Figure 2B-13).

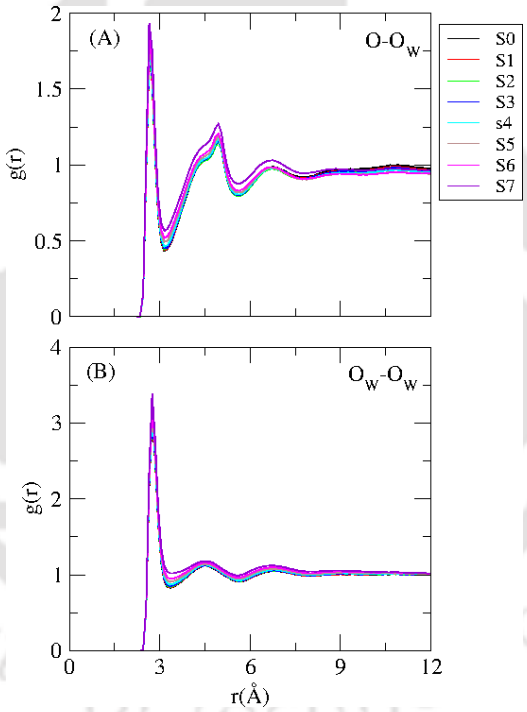

Figure 2B-13. *Site site radial distribution functions between $O - O_W$ (SCS - Water) and $O_W - O_W$ (Water - Water) for different systems.*

For all the systems, the average numbers of hydrogen bonds between water-water and water-SCS are presented in Table 2B-4. With an increase in SCS concentration the average number of both water-water and water-SCS hydrogen bond decreases. As one moves from system S0 to S7, the number of water molecules is getting reduced without altering the number of DTBM and SCS molecules. This results in a modest reduction in the water

number density as SCS concentration increases. Thus, a depletion in these hydrogen bond numbers is expected. In the same table we have also incorporated the expected hydrogen bond numbers due to a change in water density alone (see parentheses of Table 2B-4). A very similar expected and calculated hydrogen bond number suggests that the depletion in these values is mainly attributed to decreased water density. Here, we note that we did not notice any sharp change in these hydrogen bonds numbers at and above MHC level of SCS. Thus, the aggregation of SCS has a negligible influence on the water-SCS hydrogen bonds. This indirectly supports our observations (discussed above) that in SCS self-aggregation it is the hydrophobic tail part which takes part in the process, and the self-aggregation of SCS has a negligible effect on the average number of water-SCS hydrogen bonds.

Table 2B-4. Average Number of Water-Water per Water ($HB_{water-water}$) and SCS-Water per SCS ($HB_{SCS-water}$) Hydrogen Bonds for Different Systems[a]

system	$HB_{water-water}$	$HB_{SCS-water}$
S0	3.28	4.88
S1	3.26 (3.28)	4.79 (4.88)
S2	3.24 (3.26)	4.70 (4.85)
S3	3.21 (3.22)	4.65 (4.79)
S4	3.16 (3.16)	4.62 (4.71)
S5	3.07 (3.05)	4.43 (4.53)
S6	3.01 (2.94)	4.34 (4.37)
S7	2.86 (2.75)	4.14 (4.14)

[a]The values in the parentheses are the expected number of hydrogen bonds due to change in water number density.

Calculations of Flory-Huggins Interaction Parameters for DTBM-SCS interactions

In the vacuum DTBM-SCS mixture, hydrotrope SCS molecules form a reverse micelle-like structure where the hydrophilic part of SCS is pointed inward and its hydrophobic tail part is pointing outward. Not surprisingly, the DTBM molecules are present at the surface (see Figure 2B-14(A-C)). Interestingly, on addition of water, SCS molecules reorient themselves in such a manner that the hydrophobic parts form SCS clusters encapsulating DTBM molecules and the hydrophilic part of SCS molecules is pointing outward for making favorable contacts with water molecules (see Figure 2B-14(D-F)). For 24:1 ratio mixture, the calculated enthalpy of mixing (ΔH_{mix}) and Flory-Huggins interaction parameters for OPLS/AA model of DTBM molecules are -21.09 cal cm^{-3} and -6.02, and the same

for CGenFF model of DTBM molecule, respectively, are -13.9 cal cm^{-3} and -3.96. For the 12:1 ratio these values are -43.44 cal cm^{-3} and -12.39 (for OPLS/AA model) and -25.14 cal cm^{-3} and -7.17 (for CGenFF model), respectively.

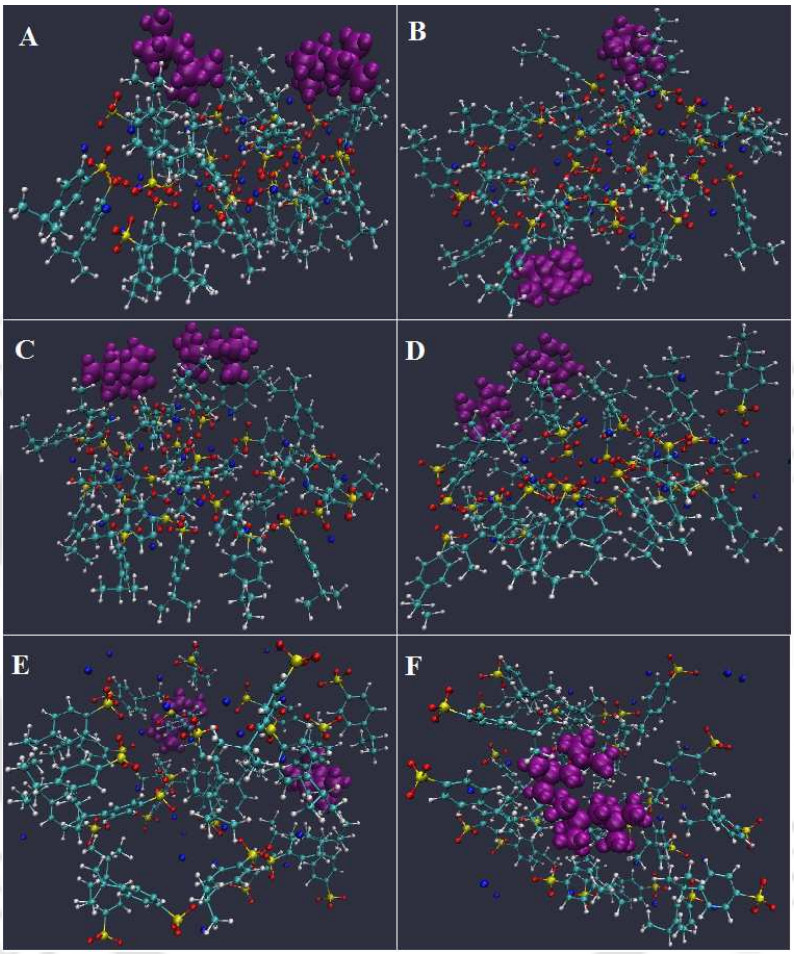

Figure 2B-14. *Snapshots for 12:1 SCS-DTBM mixture in vacuum (A-C) and in the presence of water (D-F) taken at different time intervals. Pink balls represent OPLS/AA model of DTBM molecules. Water molecules are left off for better visual clarity.*

For both mixtures, the relatively smaller χ_{FH} values are for the CGenFF model of the DTBM molecule. A further insight into the different contributions of ΔH_{mix} shows that DTBM-DTBM and DTBM-SCS interactions are responsible for a smaller ΔH_{mix} value for the CGenFF model of DTBM in comparison to OPLS/AA model. This in turn lowers the value of the χ_{FH} value for this model. Nevertheless, for both DTBM models the negative χ_{FH} value suggests favorable SCS-DTBM interactions, and this accounts for the incorporation of DTBM molecules inside the SCS clusters. Further, the DTBM encapsulated SCS clus-

ters are wrapped by the water molecules. Thus, though SCS has a much less hydrophobic part in comparison to polymers or surfactants, but it has an ability to solubilize purely hydrophobic molecules by incorporating the DTBM molecules into the SCS cluster. Note that a very recent theoretical study on the hydrotropic action of non-micellar-type hydrotrope nicotinamide [54] challenged the self-association (of hydrotropes) hypothesis of the solubilization of drug molecules. Rather, it has been claimed that it is the interaction between drug and hydrotrope molecules, which enhances the solubility of the drug molecules. Thus, the underlying mechanisms of hydrotrope SCS assisted solubilization of DTBM molecules that are derived from our findings are apparently somewhat in contrast with the results of Shimizu and co-workers [54]. Here it is to be remembered that the hydrotrope SCS used in this study is micellar-like whereas the one used by Shimizu and co-workers (i.e., nicotinamide) is nonmicellar-type.

■ SUMMARY AND CONCLUSIONS

In this study, we have employed a classical molecular dynamics simulation technique to investigate the underlying mechanism of hydrotropic action of hydrotrope sodium cumene sulfonate (SCS) on purely hydrophobic di-t-butyl methane molecules (DTBM). We considered, altogether, eight different systems with a regime of SCS concentrations at ambient temperature and pressure conditions. Moreover, in order to examine the robustness of our results we consider two different models of DTBM. From the snapshots of different systems we observe that SCS molecules form aggregates at and above the minimum hydrotrope concentration (MHC) level, and in the SCS aggregates it is the hydrotropic tail of the SCS molecule which takes part. This results in creation of the hydrophobic environment in the core of SCS clusters, and not surprisingly, DTBM molecules get accumulated into it. The calculations of first shell coordination number around different hydrophobic moieties of SCS and DTBM also show dehydration of these atomic sites as SCS clusters begin to form. These phenomena are further confirmed by contours of water and contours of SCS density around the DTBM molecule. A quantitative estimation of sizes of different SCS clusters in different systems reveals the formation of higher order clusters at and above the MHC level. A close look into the number of DTBM molecules that are encapsulated in the core of SCS cluster shows a sharp jump as soon as SCS clusters begin to form. Above the MHC region (where the number of hydrotrope aggregates may increase, but the size of its should not change much), almost all DTBM molecules are inside the SCS clusters of size three or higher. Furthermore, the investigation of an average number of water-SCS

hydrogen bonds reveals that self-aggregation of SCS molecules has negligible impact on it.

From the calculation of enthalpy of mixing, ΔH_{mix}, we have further estimated the Flory-Huggins interaction parameter, χ_{FH}, which provides information about the interaction between hydrotrope SCS-hydrophobic solute DTBM in the mixture. The high negative χ_{FH} value for both the DTBM models depicts very favorable SCS-DTBM interactions suggesting the miscibility of a two component system. Moreover, a small positive or negative χ_{FH} value is also characteristic of a stable mixture.

Chapter 3

Hydrotrope Sodium Cumene Sulfonate Assisted Solubilization of Sparingly Soluble Griseofulvin Drug Molecule

"The 'quality' of small-molecule drug candidates, encompassing aspects including their potency, selectivity and ADMET (absorption, distribution, metabolism, excretion and toxicity) characteristics, is a key factor influencing the chances of success in clinical trials. Importantly, such characteristics are under the control of chemists during the identification and optimization of lead compounds."

– John G. Cumming et al. *Nat. Rev. Drug Discov.* **12**, 948 (2013)

Overview: The effect of hydrotrope sodium cumene sulfonate (SCS) on the solubility of a sparingly water-soluble drug, griseofulvin, is studied by employing classical molecular dynamics simulation technique. We mainly focus on the underlying mechanism by which SCS enhances the solubility of a sparingly soluble or insoluble drug griseofulvin in water. The main observations are the following: (a) The self-aggregation of SCS molecules (through its hydrophobic tail) above the minimum hydrotrope concentration (MHC) causes the formation of micellar-like frameworks. Interestingly, though the drug griseofulvin possesses both polar and nonpolar groups, it prefers to get encapsulated inside the hydrophobic core of SCS aggregates. The decomposition of total SCS-drug interaction energy into van der Waals and electrostatic components suggests that the former plays a major role in this interaction. (b) The calculated Flory-Huggins interaction parameter values give a strong indication of the mixing ability of hydrotrope SCS and griseofulvin drug molecules. (c) As expected, we do not observe any strong effect of SCS aggregates on SCS-water and water-water average hydrogen-bond number, but it affects water-drug griseofulvin average hydrogen-bond number. With the help of these observations we try to elucidate the hydrotropic action of hydrotrope SCS on the solubility of drug griseofulvin.

■ INTRODUCTION

The main problem which emerges from the drug discovery program is the poor water solubility of drug molecules. The strategy to accomplish a successful drug delivery for an orally administrated drug is the sufficient dissolution of the drug and its solubility in the gastrointestinal tract. Many newly developed drugs possess poor gastrointestinal tract solubility, which basically limits effective drug development, and the possible worst situation is the termination of a potential candidate [111]. All these problems can be dealt with by the use of nontoxic, water-soluble molecules that act to enhance the solubility of an insoluble or sparingly soluble drug molecule [1, 4, 112, 113]. This phenomenon is familiar as hydrotropy, and the solubilizing agent is known as the hydrotrope. In our previous study (**Chapter 2B**) we have used a purely hydrophobic DTBM molecule as solute to explore the underlying mechanism of hydrotropic action of hydrotrope SCS. Using the similar procedure, here we study hydrotrope assisted enhancement of solubility of a sparingly soluble drug molecule. Here in this study, we consider griseofulvin as a drug molecule (see Figure 3-1) and SCS as a hydrotrope.

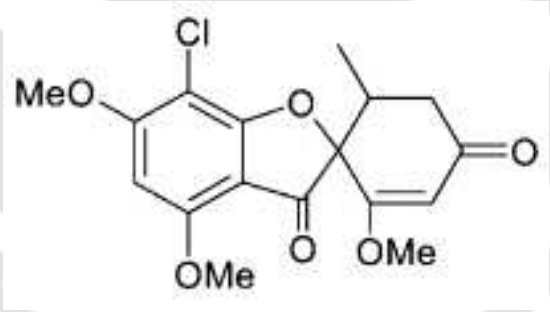

Figure 3-1. *Structure of griseofulvin. Hydrogen atoms are left off for clarity of the structure.*

Griseofulvin is a lipophilic oral administrated fungi-static antibiotic drug [114], and it is believed that it can also act as a potential anticancer drug [115]. Griseofulvin is one of the highly prescribed antifungal drugs, with an annual worldwide business of USD 63.7 million, whereas its annual consumption is 85000 kg [116]. According to the biopharmaceutics classification system griseofulvin falls into Class II drugs that have low-solubility and high-permeability character [117]. In this study, by carrying out classical molecular dynamics simulation of the sparingly soluble drug griseofulvin and hydrotrope SCS in water with a regime of concentrations, we try to examine the mechanism of hydrotropic action of SCS. At first we try to explore the outcome of MHC of SCS on the solubilization action of

the drug griseofulvin. Our analysis is further extended to the microdetails of solubilization of sparingly soluble drug molecules.

The remainder of this chapter is split into three parts. In next section models and simulation details are described, then the results are presented and discussed, and finally our conclusions are outlined concisely.

■ MODELS AND SIMULATION METHOD

Molecular dynamics (MD) simulations of griseofulvin-sodium cumene sulfonate-water ternary mixtures were performed with altering SCS composition at 298 K temperature and 1 atm pressure. Following earlier work [67], the griseofulvin molecule was parameterized using the general AMBER force field (GAFF) [118], and the AM1-BCC [119, 120] calculation method within the antechamber [121] module of AMBER12 [76] was used to compute the partial charges. CHARMM general force field (CGenFF) [78, 79] was taken for the parametrization of SCS molecule. We adopt SPC/E model for water [77]. Note that, as we refer to in our previous works (**Chapter 2A and 2B**) the identical potential energy functions for nonbiological systems in CHARMM and AMBER and the implementation of CHAMBER tool kit [81] make the CHARMM force field AMBER12 reconcilable. One Na^+ ion was added in XLEAP of the AMBER12 package [76] to counterbalance the single negative charge of the sulfonate group of each hydrotrope molecule. To examine the solution properties of the ternary mixtures with a regime of concentrations, we consider eight different concentrations, and the same are presented in Table 3-1. To prepare initial configurations of each of these systems PACKMOL package [82] was used. Each of these simulations was performed using the AMBER12 package [76] and using a time step of 2 fs. For all the systems, molecules were placed in a cubic box, and to remove the edge effect periodic boundary conditions were applied in all three directions. The energy of each of the systems was minimized for 10000 steps in which the steepest descent minimization method is used for the first 4000 steps followed by the 6000 steps in conjugate gradient method. To avoid void formation, each of the systems was then heated slowly over 320 ps from 0 to 298 K in a canonical ensemble (NVT). Thereafter, the systems were equilibrated for 5 ns and followed by 80 ns production runs in isothermal-isobaric (NPT) ensemble at 298 K temperature and 1 atm pressure. We have used the Berendsen barostat [83] with a pressure relaxation time of 2 ps to maintain the physical pressure. Temperature of each of the systems was controlled by the Langevin dynamics method with a collision frequency of 1 ps^{-1}. We have used the SHAKE algorithm [84] to constrain the bonds involving hy-

drogen atom. For all nonbonded interactions, a cutoff distance of 10.0 Å was specified. The long-ranged electrostatic interactions were evaluated by the application of the particle mesh Ewald method.

Table 3-1. Overview of Systems[a]

System	$N_{griseofulvin}$	N_{scs}	N_{wat}	volume(nm^3)	M_{scs}
S0	8	24	8400	261.38	0.152
S1	8	24	7200	224.76	0.177
S2	8	24	6000	188.91	0.211
S3	8	24	4800	152.67	0.261
S4	8	24	3600	116.85	0.341
S5	8	24	2400	81.01	0.492
S6	8	24	1800	63.37	0.629
S7	8	24	1200	45.13	0.883

[a] $N_{griseofulvin}$, N_{scs}, N_{wat} and M_{scs} are the number of Griseofulvin, Sodium Cumene Sulfonate, Water molecules, and molar Concentration of the Sodium Cumene Sulfonate, respectively, for different systems.

Following the recent works [67], primitive hydrotrope-drug mixtures of two dissimilar compositions are constructed. In the first system, we consider 24 hydrotrope SCS molecules and one griseofulvin molecule (in 24:1 ratio), whereas the second mixture consists of 24 hydrotrope SCS molecules and two griseofulvin molecules (in 12:1 ratio). In both the systems, at first we placed all the SCS and griseofulvin molecules randomly. We have first equilibrated the initial configurations for each of the griseofulvin-SCS mixtures in the vacuum to acquire the initial compaction of the mixture. The vacuum simulations run were carried out in AMBER12 for 12 ns at 298 K with a time step of 2 fs. Then, we have generated a cubic box around the compacted complex by using the leap module of AMBER12 using 0 Å buffer constant for all the three directions. To fill up the voids, mainly created at the corners of the cubic box, 405 and 369 SPC/E water molecules were added for the first and second mixture, respectively. Thereafter, we minimized the energy of each griseofulvin-SCS-water mixture for 10000 steps, where the first 4000 steps are in steepest descent minimization method, and this is followed by 6000 steps in the conjugate gradient method. After that, each of the systems was heated slowly from 0 to 298 K for 320 ps in canonical ensemble (NVT). To relax the density of each system, additionally 4 ns equilibration run in an isothermal isobaric (NPT) ensemble at 298 K and 1 atm pressure was carried out. Finally, the systems were equilibrated for 20 ns in NPT at 298 K and 1 atm pressure. Periodic boundary conditions were employed in all the three directions.

■ RESULTS AND DISCUSSION

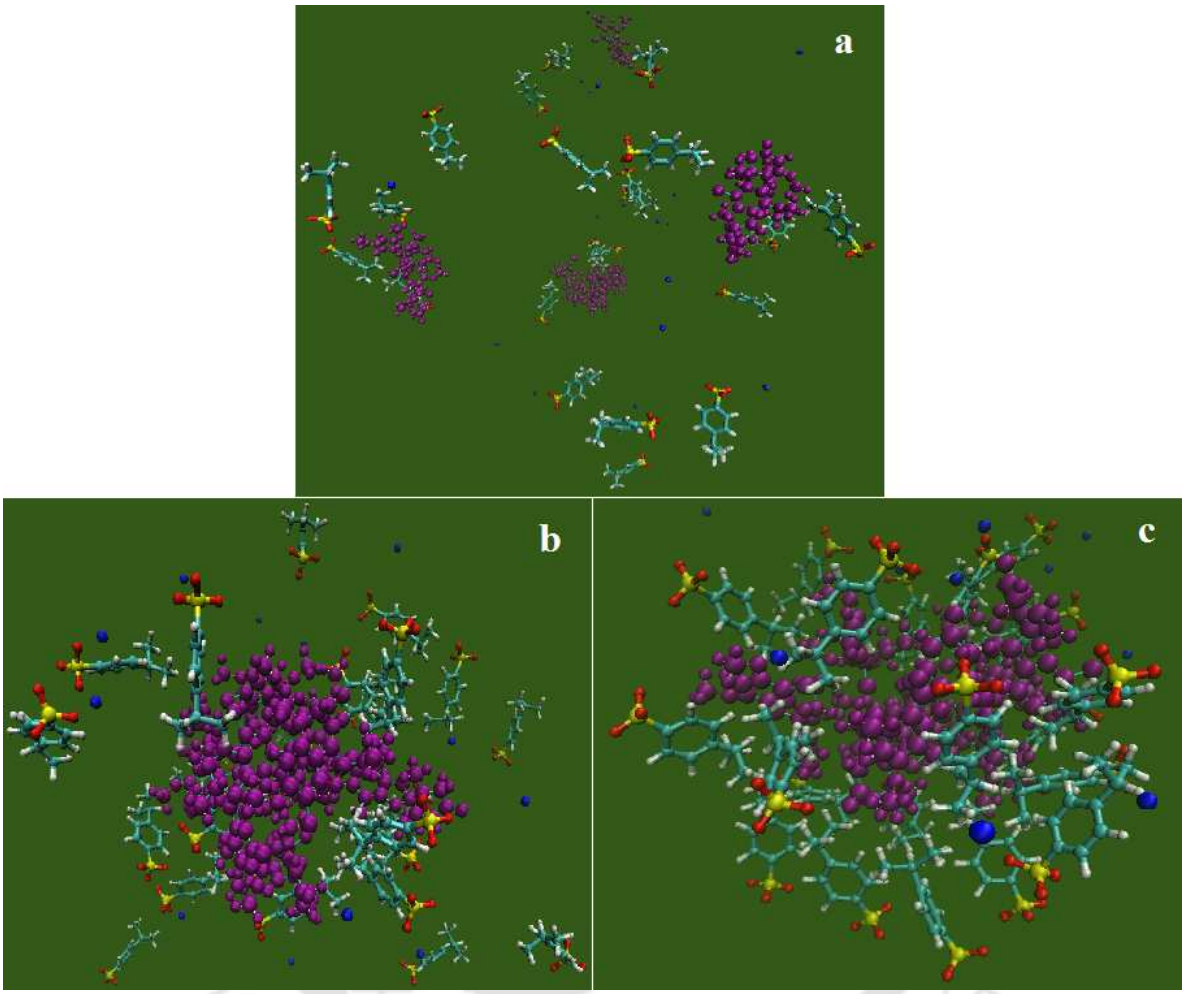

Figure 3-2. *(a), (b), and (c) represent snapshots for systems S0, S4, and S7. Blue balls represent sodium ions and pink ball represents griseofulvin atoms. Water molecules are left-off for better visual clarity.*

Incorporation of Drug Molecules Inside SCS Clusters

Similar to our previous simulation studies (**Chapter 2A and Chapter 2B**), here also we observed a tail-dependent aggregation behavior of SCS (see Figure 3-2), and the self-association of SCS increases with increase in concentration of solution (see Figure 3-3). Another notable observation, made from these visualizing snapshots (Figure 3-2), is that griseofulvin molecules also get successfully enclosed into the lipophilic interior of the aggregates of SCS molecules.

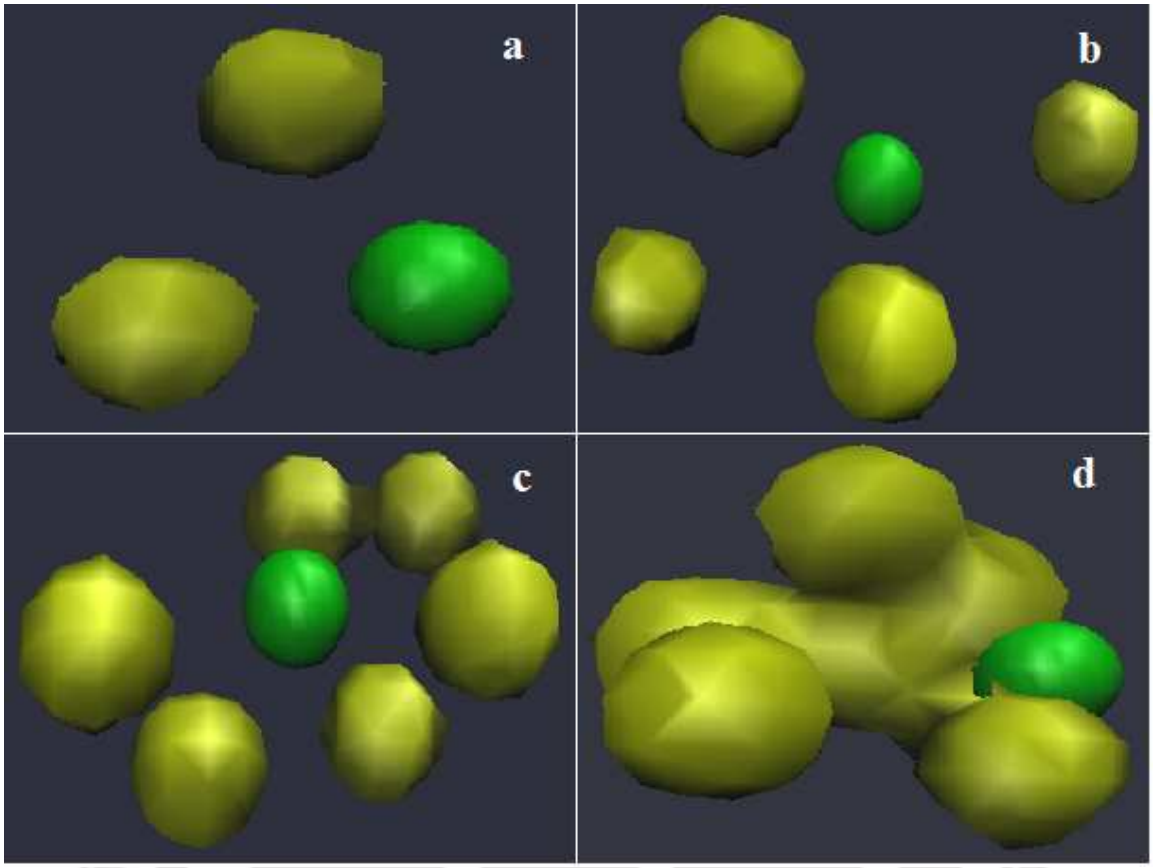

Figure 3-3. *a, b, c and d are the contours of C_7 atom of SCS density within 8.05 Å around a reference C_7 atom of SCS molecule for systems S0, S3, S5, and S7 respectively. Large green ball represents the C_7 atom of reference SCS molecule.*

Moreover, for the estimation of SCS clusters in different systems we performed cluster structure analysis. For this, as used in previous work (**Chapter 2B**), in this study also we apply a geometric criterion in which a cutoff distance between C_7 atoms two neighboring SCS molecules is considered. This cutoff distance is obtained from the C_7-C_7 correlation function of SCS molecules (see Figure 3-4a). In Figure 3-5, we show the probability distributions of different sizes of SCS clusters for all the systems. From these histograms, it can be seen that around the MHC region of SCS, a transition takes place between lower- and higher-order clusters formation and, once the MHC region is crossed, the size of the higher-order SCS aggregates is getting essentially ceased. These findings are very similar to what we found in our previous study (**Chapter 2B**) in which hydrotrope SCS assisted solubilization of hydrophobic di-t-butylmethane (DTBM) is reported. Note that, in the

context of hydrotropic action, the behaviors of hydrotrope SCS molecules are quite contradictory to that of amino acid proline, which is also classified as hydrotrope because of its amphiphilic nature and ability to solubilize hydrophobic solute. Although proline is considered as a hydrotrope, neither experimental nor simulation study evidenced the large-scale proline aggregation in aqueous solution [122, 123].

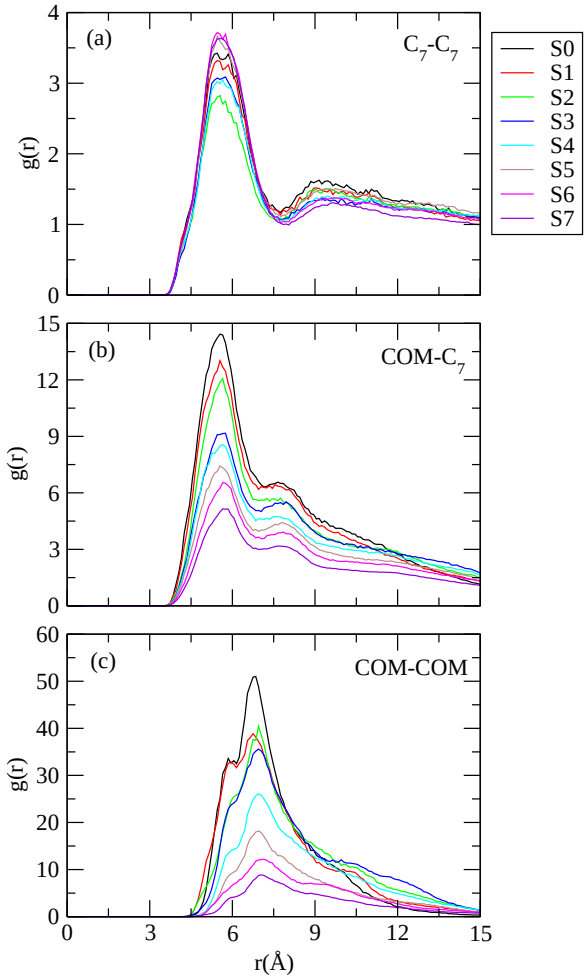

Figure 3-4. *Site site radial distribution functions between (a) C_7-C_7 (SCS - SCS), (b) COM-C_7 (griseofulvin - SCS), and (c) COM-COM (griseofulvin - griseofulvin) for different systems.*

Since our goal is to investigate the role of SCS aggregation on the solubilization of the drug griseofulvin, if any, we extend our analysis further toward the estimation of the number of griseofulvin molecules inside the core of SCS clusters. As before (**Chapter 2B**), for this detailed examination, the following geometric criteria are set: (i) the size of the SCS cluster must be equal to or greater than three, (ii) the cutoff distance between the

center of mass (COM) of a griseofulvin molecule and C_7 atom of a cluster-forming SCS molecule should be within 9.65 Å and at the same time (iii) if the distance between the COM of one griseofulvin molecule is within 8.85 Å of the COM atom of a neighboring griseofulvin molecule (see Figure 3-4, parts b and c) and simultaneously if these two griseofulvin molecules reside within the cutoff distance of C_7 atom of any of the cluster-forming SCS molecules then these two griseofulvin molecules are considered to be located within the same SCS cluster.

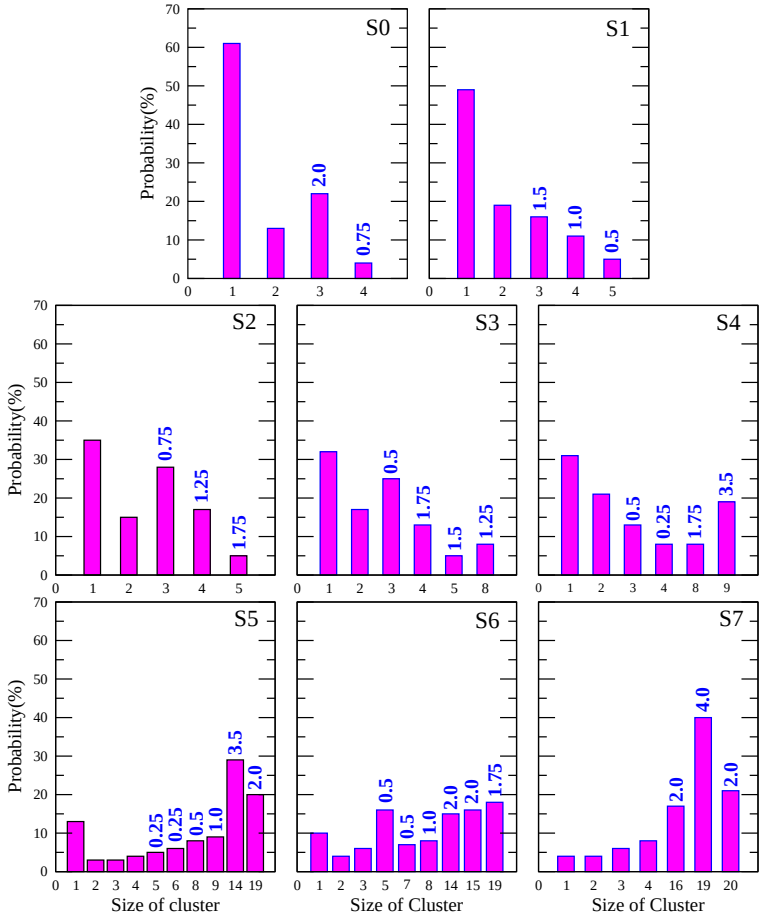

Figure 3-5. *Probability distribution (in percentage) of SCS clusters of different sizes. The numbers on different bar diagrams represent the average number of griseofulvin molecules present in a given SCS cluster.*

Figure 3-5 also displays the total number of griseofulvin molecules that are present in the interior of SCS clusters of different sizes. It is quite apparent that, below the MHC level, the number of griseofulvin molecules within the SCS clusters is in lesser extent, but as

soon as SCS begins to form higher-order aggregates (in the region of the MHC) a prominent increase in the number of griseofulvin molecules in the inner core of hydrotrope clusters is observed. These results indicate the creation of more hydrophobic layer in the interior of higher-order SCS aggregates increases the potential for encapsulating drug molecules into the inner core of these hydrotrope clusters. Here it is to be remembered that, unlike our previous study where pure hydrophobic DTBM molecules were used (**Chapter 2B**) in the present study we used drug griseofulvin which is not purely hydrophobic in nature. But, both DTBM and griseofulvin molecules behave in similar fashion (in the context of their encapsulation into the hydrophobic core of SCS clusters) as is evident from Figure 3-5. These findings further suggest that the aggregated structure of SCS plays a crucial role for the elevation of the solubility of a solute molecule by designing a hydrophobic layer in which the solute is getting encapsulated.

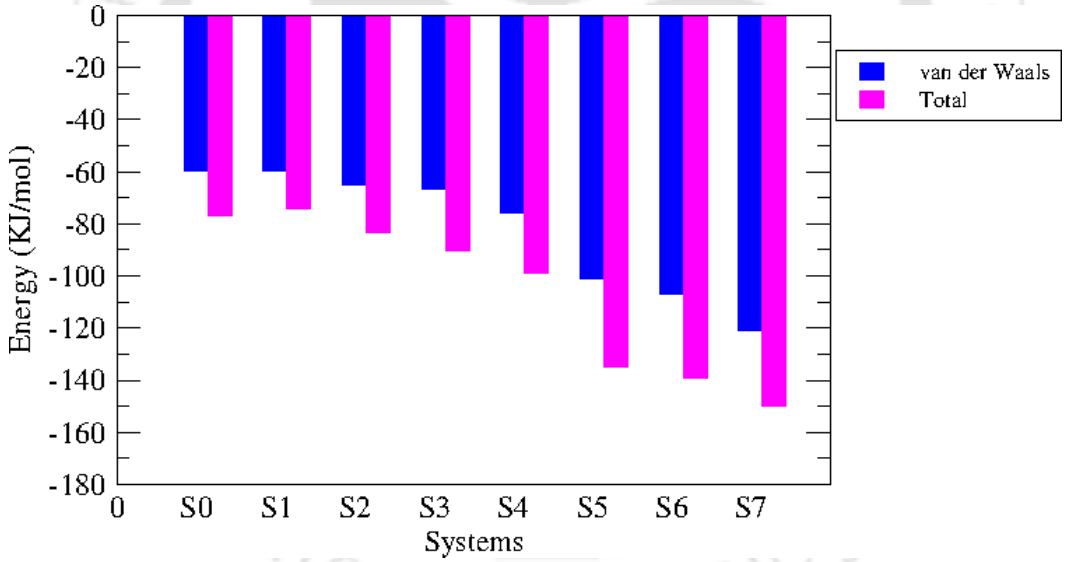

Figure 3-6. *Average van der Waals and total interaction energy between griseofulvin and SCS.*

From the above discussions it is evident that the interactions between griseofulvin drug and SCS molecules play an important role in the encapsulation of the former into the clusters of latter. In order to see the hydrotropes' direct interaction pattern with the drug molecule, following earlier work [124], we have decomposed total griseofulvin-SCS interaction energy into electrostatic and van der Waals energy components for all the systems (S0-S7). Figure 3-6 represents the total interaction energy and van der Waals energy (averaged over the last 60 ns of simulation run) between griseofulvin and SCS

molecules. Here we note that the electrostatic component of griseofulvin-SCS interactions is not a strong function of concentration. Nevertheless, as is evident from this figure, the electrostatic interaction energy component plays a very minor role in griseofulvin-SCS interactions (which is not surprising based on the findings discussed above) and its contribution to total direct interaction energy is also very small compared to van der Waals energy for all the systems (S0-S7) considered here. Hence, it can be inferred that van der Waals energy plays a dominant role in the interaction between hydrotrope and drug molecules. We also find that, with an increase in concentration of SCS, van der Waals interaction energy between griseofulvin and SCS decreases (more negative), but the effect is more noticeable for the systems S4-S7. This can be explained on the basis of the fact that, as the aggregation of SCS starts from the MHC level, the drug incorporation ability into the SCS hydrophobic cores also increases. This makes the van der Waals interaction between griseofulvin and SCS molecules more favorable.

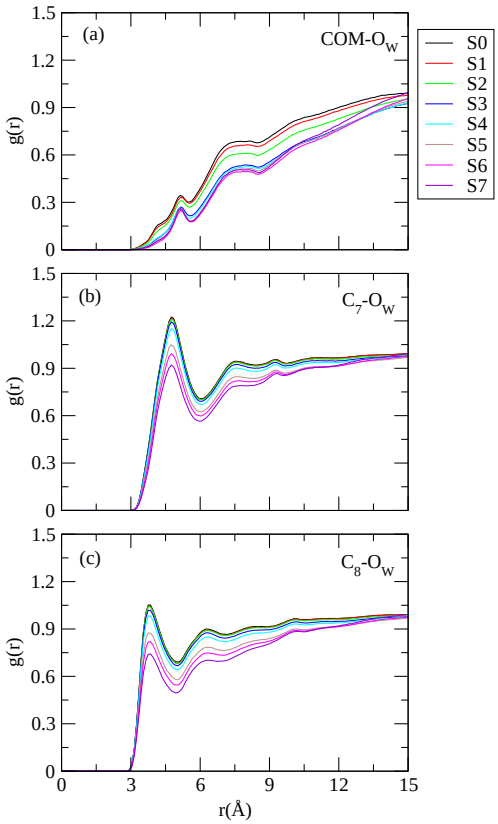

Figure 3-7. *Radial distribution functions between (a) COM-O_W (griseofulvin-water), (b) C_7-O_W (SCS-water), and (c) C_8-O_W (SCS-water).*

Hydrophobic Hydration

As the structural features of hydrotrope SCS and griseofulvin drug molecules in water are reflected in their hydration pattern also, we have additionally extended our investigation toward the radial distribution functions (rdfs) involving the COM of griseofulvin and water molecules and C_7 and C_8 atomic sites of SCS and water molecules. Figure 3-7 exhibits the rdfs between the COM of griseofulvin and oxygen atom of water, the C_7 atom of SCS and oxygen atom of water, and the C_8 atom of SCS and oxygen atom of water, respectively. From Figure 3-7a it is evident that the g(r) value of the system S0 at the first maximum is only 0.35 of the bulk density, and with increase in concentration of the SCS, a depletion in the peak height is observed for the COM-O_W distribution function, but the effect is not remarkable for the systems below the MHC level of SCS. Here the oxygen atom of water is denoted by O_W. In view to the effect of the MHC on C_7-O_W and C_8-O_W distribution functions, we find that with increase in concentration of SCS there is a modest decrease in the first peak height of both the distribution functions and the effect is more prominent for concentrated solution systems. These observations imply that, with an increase in concentration of SCS, the number of water molecules in the first solvation shell of the COM of griseofulvin, the C_7 atom of SCS, and the C_8 atom of SCS decreases.

Table 3-2. Number of First-Shell Water Molecules around the Center of Mass (COM) of Griseofulvin Molecules and the C_7 and C_8 Atoms of Sodium Cumene Sulfonate Molecules[a]

System	COM	C_7	C_8
S0	5.73	25.47	12.93
S1	5.43 (5.71)	24.99 (25.39)	12.73 (12.89)
S2	4.89 (5.68)	24.60 (25.23)	12.60 (12.81)
S3	3.79 (5.60)	23.66 (24.91)	12.09 (12.65)
S4	3.63 (5.50)	22.00 (24.44)	11.31 (12.41)
S5	3.17 (5.28)	18.63 (23.49)	9.63 (11.92)
S6	2.87 (5.07)	16.65 (22.53)	8.61 (11.44)
S7	2.81 (4.75)	13.80 (21.10)	7.16 (10.71)

[a] The values in the parentheses represent the first-shell normalized coordination numbers due to change in the number density of water.

Furthermore, in an attempt to see the degree of solvation of griseofulvin and SCS molecules more perspicaciously, the number of first-shell water molecules (first-shell coordi-

nation number, CN) surrounding the COM of griseofulvin and different hydrophobic sites of hydrotrope SCS is determined. We have calculated the CN from the corresponding site-site correlation functions involving these atomic sites of SCS (and the COM of griseofulvin) and water oxygen atom by using Eq. 2.3. As can be seen from Table 3-2, the number of first solvation shell water molecules around the COM of griseofulvin molecules and the C_7 and C_8 atoms of SCS molecules decreases as the concentration of SCS increases, and the effect is more profound for the systems S3-S7. Note that, as we move from system S0 to system S7, water number density decreases, and this might affect the coordination number values. To nullify the effect of reduced water density we normalized CNs with respect to that for system S0, and these normalized coordination number values are also incorporated in the same table. Below the MHC level of SCS, the difference between the actual and normalized (or expected) coordination number is not very significant, but this difference starts to increase dramatically from the MHC region. These results demonstrate that with increasing SCS concentration more and more dehydration of small hydrophobic tails of SCS and the COM of griseofulvin molecules is taking place. Here we note that a very similar hydration pattern of C_7 and C_8 atoms of hydrotrope SCS has also been observed in previous simulation study (**Chapter 2B**) except for the fact that the number of first solvation shell water molecules surrounding hydrophobic tail parts of SCS is slightly less dehydrated in the presence of the drug griseofulvin. Moreover, as SCS molecules begin to self-aggregate, griseofulvin molecules start to penetrate into the interior of the core of SCS clusters. Therefore, a depletion in the number of first-shell water molecules surrounding the COM of griseofulvin molecules is also observed, and the influence is more pronounced as soon as SCS molecules acquired a more aggregated structure above the MHC region.

To explore the change in water density around griseofulvin molecules upon SCS aggregation more precisely, further, we perform atomic mass density analysis by using the Visual Molecular Dynamics package [85]. In Figure 3-8, we present the mass density map of the oxygen atom of water around a randomly selected griseofulvin molecule with a cell side of 0.5 Å within 5.55 Å . Below the MHC region, a very high water density around the griseofulvin molecule is noticed, but around the MHC region when SCS molecules start to self-aggregate a sharp depletion in the water density around the griseofulvin is perceived. This result can act as a corroborative proof of the preceding discussions.

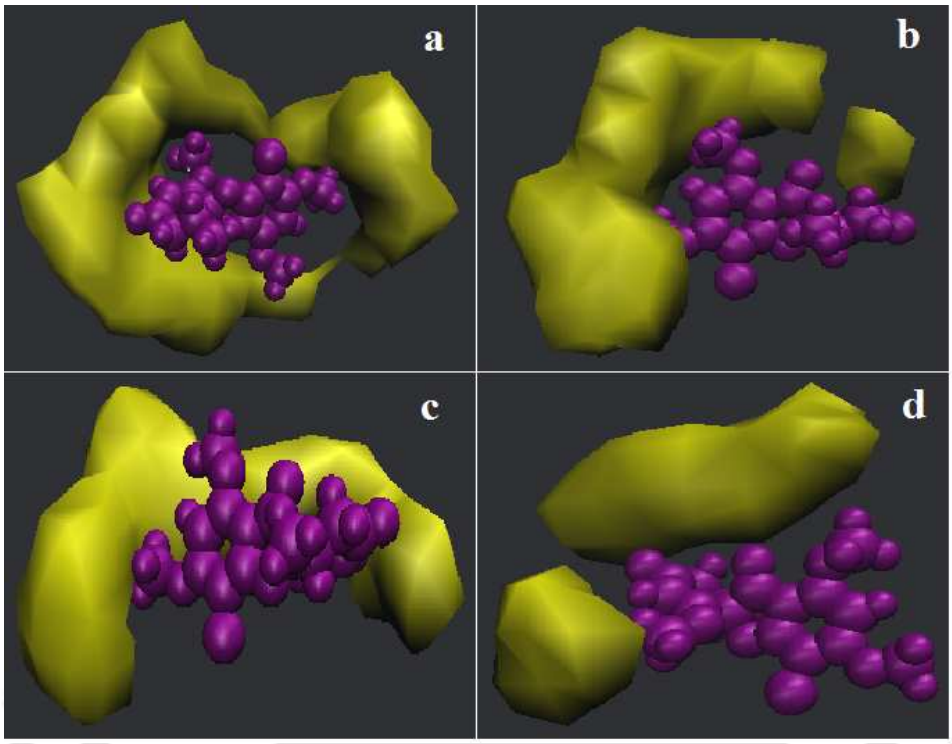

Figure 3-8. *Contours of solvent water density within 5.55 Å around griseofulvin molecule (pink balls). Panels a, b, c, and d are for systems S0, S3, S5, and S7, respectively.*

We also carry out atomic mass density analysis of SCS surrounding a griseofulvin molecule possessing a cell side of 0.5 Å inside 9.65 Å and the same is presented in Figure 3-9. As observed for the DTBM-SCS-water ternary system (**Chapter 2B**), in this study also we observe a low hydrotrope density around the griseofulvin molecule below the MHC region; however, with increasing concentration of hydrotrope, density of SCS around griseofulvin increases. Thus, these results can act as supportive evidence that water molecules are being substituted by SCS molecules around griseofulvin molecules at higher SCS concentrations. Here, we would like to mention that the findings of a recent fluctuation solution theory of hydrotropy argued that it is the excess number of hydrotropes around the solute (i.e., excess coordination number) which causes an enhancement in the solubility of the solute [125]. This excess coordination number arises from the long-ranged changes in the solution structure around the solute. Here we note that the calculated coordination number, CN, is somewhat different from the excess coordination numbers. Although both are calculated by integrating the radial distribution functions, the latter (i.e., excess coordination number) provides information about the deviation from the ideal solvation model.

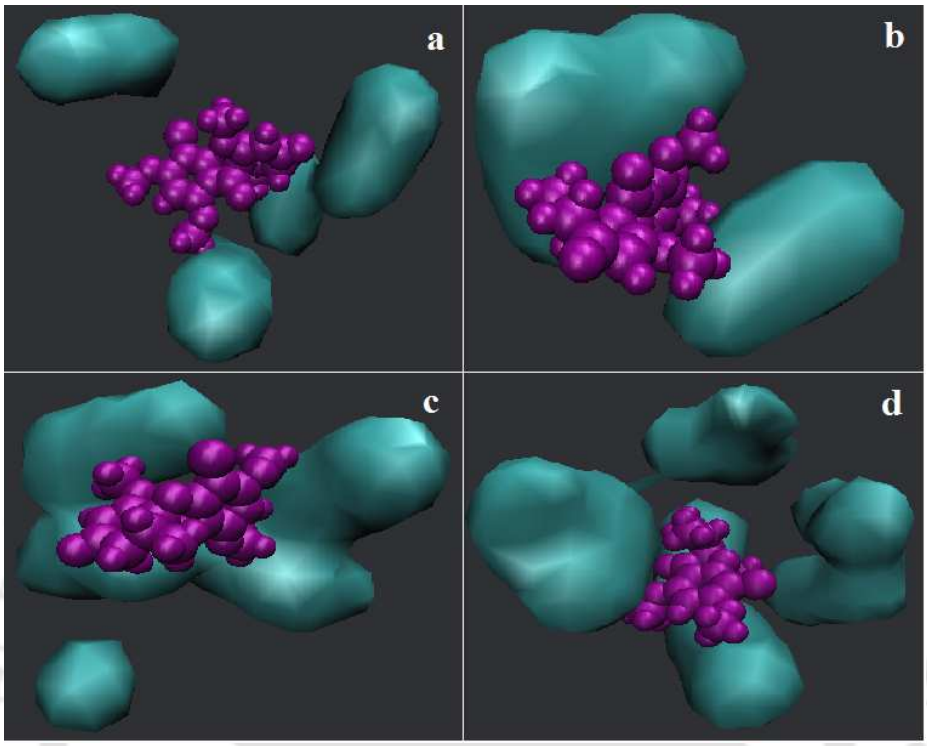

Figure 3-9. *Contours of hydrotrope SCS density within 9.65 Å around griseofulvin molecule (pink balls). Panels a, b, c, and d are for systems S0, S3, S5, and S7, respectively.*

In order to estimate the number of hydrotrope molecules in the first coordination shell of griseofulvin molecule, with the help of Eq. 2.3, we have calculated the number of first solvation shell SCS molecules around the griseofulvin molecule by considering the correlation function between the COM of griseofulvin and the C_7 atom of SCS (see Figure 3-4). From Table 3-3, it can be seen that, with increasing concentration of the solution, the number of first-shell SCS molecules around griseofulvin increases, but a prominent rise in these numbers can only be observed at and above the MHC level. These results, further, infer the formation of more hydrophobic surfaces around griseofulvin molecules. Here, it is worth to mention that Busch et al. [126] studied the concentrated aqueous solution of hydrotrope proline by the use of both neutron and X-ray diffraction (with isotropic substitution and inelastic neutron scattering) experiments as well as empirical potential structure refining (EPSR) and molecular dynamics simulation methods. They found that proline molecules form dimers in water via short-ranged interactions in which the cyclic electrostatic interaction between the CO_2^- group of one proline molecule and the NH_2^+ group of a neighboring proline plays an important role (unlike SCS, proline does not form

a large aggregated structure). Moreover, these proline dimers create small hydrophobic pockets that can associate with nonpolar parts of other solutes. Here it is also important to mention that neutron diffraction scattering experiments have also been carried out to investigate the self-association of different molecules in water [105, 106, 108, 127-130].

Table 3-3. Number of First-Shell SCS Molecules around Griseofulvin Molecules

System	N_{SCS}
S0	10.64
S1	11.31
S2	11.29
S3	11.31
S4	13.50
S5	17.65
S6	19.43
S7	22.28

For example, McLain et al., by employing a combination of neutron diffraction and computer simulation techniques, examined the role of hydrophobic and hydrophilic interactions in the peptide association [128]. For their study they used aqueous solutions of different peptides such as glycyl-l-alanine, glycyl-l-proline, and l-alanyl-l-proline. They argued that hydrophilic interactions play a major role in the peptide association process. Furthermore, by the use of experimental (neutron diffraction) followed by computational (EPSR) methods, Rhys et al. [129] investigated the effect of increased temperature (from 297 to 333 K) on the self-association tendency of glutamine in water. They observed that, in aqueous solution, the hydrophilic interactions are responsible for the self-association of glutamine. This association causes the formation glutamine dimers (mostly), and the effect of temperature on it is very negligible. Furthermore, Mason et al. [130] used a combination of small-angle neutron scattering (SANS) method and MD simulation technique to explore the aggregation property of isopropyl alcohol and pyridine in aqueous solution, and they also examined the impact of guanidinium chloride (GdmCl) on the clustering of these molecules. In specific, in aqueous solution pyridine molecules interact with the like molecules via T-type edge face interactions [106]. The addition of GdmCl into aqueous pyridine solution causes a reduction in the self-aggregation propensity of pyridine molecules, whereas it (GdmCl) has a very negligible effect on the self-association tendency of isopropyl alcohol [130]. They argued that GdmCl interacts weakly with the "lumpy" aliphatic group of the isopropyl alcohol molecule leading to a very minimal effect of GdmCl on isopropyl alcohol aggregation. On the other hand, it (GdmCl) interacts favorably with the planar

aromatic faces of pyridine molecules, which leads to the breaking of pyridine clusters and enhances dissolution of pyridine molecules in water.

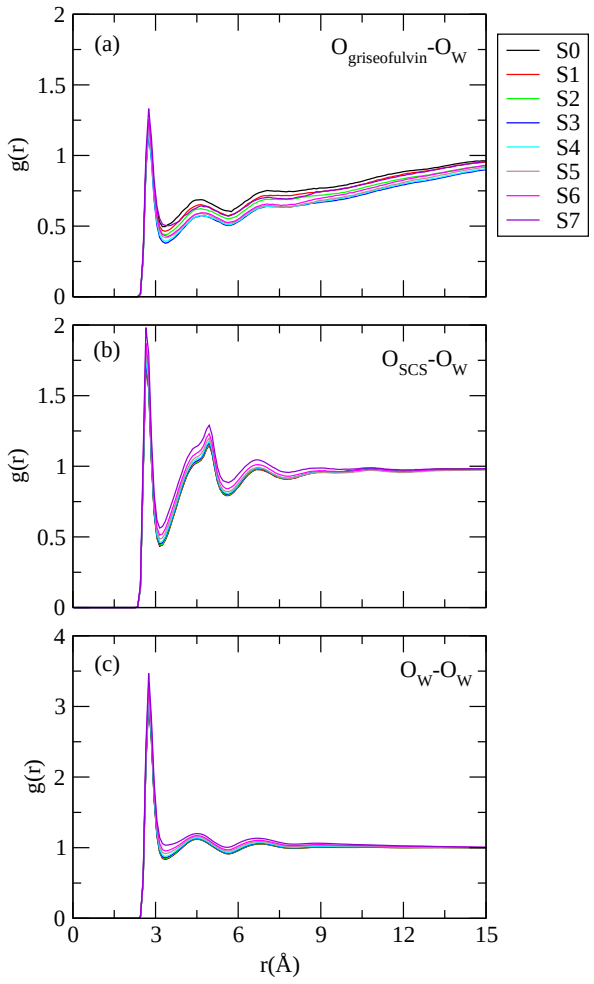

Figure 3-10. *Site site radial distribution functions between (a) $O_{griseofulvin}$-O_W (griseofulvin - Water), (b) O_{SCS}-O_W (SCS - Water), and (c) O_W-O_W (Water - Water) for different systems.*

Hydrogen-Bond Properties

The available electronegative oxygen atoms in the sulfonate group of SCS make it a potential hydrogen-bond acceptor. Thus, in aqueous solution, it can form hydrogen bonds with water molecules. Moreover, because of the presence of carbonyl groups in the griseofulvin molecules, in aqueous solution it also has a potential to act as a hydrogen-bond acceptor and form hydrogen bonds with water molecules. Since the carbonyl group

of griseofulvin molecules and the sulfonate group of SCS molecule both can function only as hydrogen-bond acceptors, so each of these molecules cannot form hydrogen bonds between the like molecules, and also griseofulvin-SCS hydrogen bonds are not possible. Therefore, only three types of hydrogen bonds are possible, namely, water-water, griseofulvin-water, and SCS-water. Following earlier works [93-95], the average number of water-water (per water), griseofulvin-water (per griseofulvin), and SCS-water (per SCS) hydrogen bonds are estimated by considering certain geometric criteria. If the interatomic distance between oxygen atoms of two water molecules is less than 3.35 Å and at the same time the oxygen-oxygen-hydrogen angle is less than 45^o, then the two water molecules are taken as hydrogen-bonded. For griseofulvin-water and SCS-water hydrogen bonds, the cutoff distances are less than 3.25 and 3.15 Å respectively, whereas the angle is the identical as that for water-water hydrogen bonds. We have taken these cutoff distances from the appearance of the first minimum in the corresponding distribution functions (see Figure 3-10). In Table 3-4 the average number of hydrogen bonds between water-water, griseofulvin-water, and SCS-water is presented. It is apparent that the average number of these hydrogen bonds decreases as the concentration of SCS increases. Since, increased concentration causes a depletion in water number density (as mentioned above), a modest decrease in these numbers is expected. To negate this effect, in the parentheses of the same Table 3-4 the expected hydrogen-bond numbers are also included. Negligible differences in the expected and calculated hydrogen-bond numbers are observed for water-water and SCS-water hydrogen bonds for all the systems. Therefore, the availability of the polar hydrogen-bonding group of the SCS molecule for water remains unaffected in the aggregated structure of hydrotropes, indicating that the self-accumulation of SCS has an imperceptible impact on the average number of water-water and water-SCS hydrogen bonds. Similar observations were also reported in which DTBM molecules were used as solute molecules in water-SCS-DTBM ternary system (**Chapter 2B**). But, for griseofulvin-water hydrogen bonds, with increasing concentration, we observed a decrease in the average number of this type of hydrogen bond. We further noticed that the difference of expected and calculated hydrogen-bond numbers is less below the MHC level and this difference starts to rise from the MHC level. This indirectly supports that, although griseofulvin molecule carries hydrophilic parts, it favors to stay in the hydrophobic environment over the hydrophilic aqueous environment.

Table 3-4. Average Number of Water-Water Per Water ($HB_{water-water}$), Griseofulvin-Water Per Griseofulvin ($HB_{griseofulvin-water}$), and SCS-Water Per SCS ($HB_{SCS-water}$) Hydrogen Bonds for Different Systems [a]

System	$HB_{water-water}$	$HB_{griseofulvin-water}$	$HB_{SCS-water}$
S0	3.28	2.59	4.83
S1	3.26 (3.28)	2.45 (2.59)	4.79 (4.83)
S2	3.24 (3.26)	2.18 (2.57)	4.75 (4.80)
S3	3.21 (3.22)	2.03 (2.54)	4.64 (4.74)
S4	3.15 (3.16)	2.02 (2.49)	4.63 (4.65)
S5	3.08 (3.03)	1.82 (2.39)	4.43 (4.47)
S6	3.00 (2.91)	1.67 (2.30)	4.28 (4.29)
S7	2.89 (2.73)	1.56 (2.15)	4.18 (4.01)

[a]The values in the parentheses are the expected number of hydrogen bonds due to change in water number density.

Flory-Huggins Interaction Parameters for Griseofulvin-SCS Interactions

It is noticed that hydrotrope SCS molecules adopt a reverse micelle-like structure (see Figure 3-11(a-c)) in the gas phase (vacuum state) of the griseofulvin-SCS mixture. The griseofulvin molecules possess hydrophilic parts, but they are found at the surface of the reverse micelle structure of SCS. Interestingly, with the addition of water, to make favorable interactions with water molecules, hydrotrope molecules reorganize themselves in such a way that the small hydrophobic parts of SCS aggregates enclose griseofulvin molecules in their core while the hydrophilic part of SCS molecules is directing toward solvent water molecules (see Figure 3-11(d-f)). As mentioned above, for the calculations of Flory-Huggins interaction parameters we consider two different drug-hydrotrope mixtures with varying compositions. The calculated values of enthalpy of mixing (ΔH_{mix}) and Flory-Huggins interaction parameters (χ_{FH}) for the first mixture (24:1 ratio) are -30.83 cal cm^{-3} and -8.99, respectively, whereas for the second mixture (12:1 ratio) they are -55.37 cal cm^{-3} and -16.16, respectively. The negative χ_{FH} values that we obtain for both the mixtures suggest the favorable hydrotrope SCS-drug griseofulvin interactions. Besides this, the griseofulvin encapsulated SCS clusters are tightly wrapped by the water molecules. Thus, we can infer that, though SCS contains a much shorter hydrophobic chain in contrast to classical surfactants or long chain polymers, its ability to incorporate the griseofulvin molecules into its cluster makes it a potential drug solubilizer. Here it is worth mentioning that the χ_{FH} and ΔH_{mix} values for both the SCS-griseofulvin mixtures are more negative

when compared to that for the respective SCS-DTBM mixtures (**Chapter 2B**), indicating a much higher mixing ability for the former mixtures than the latter.

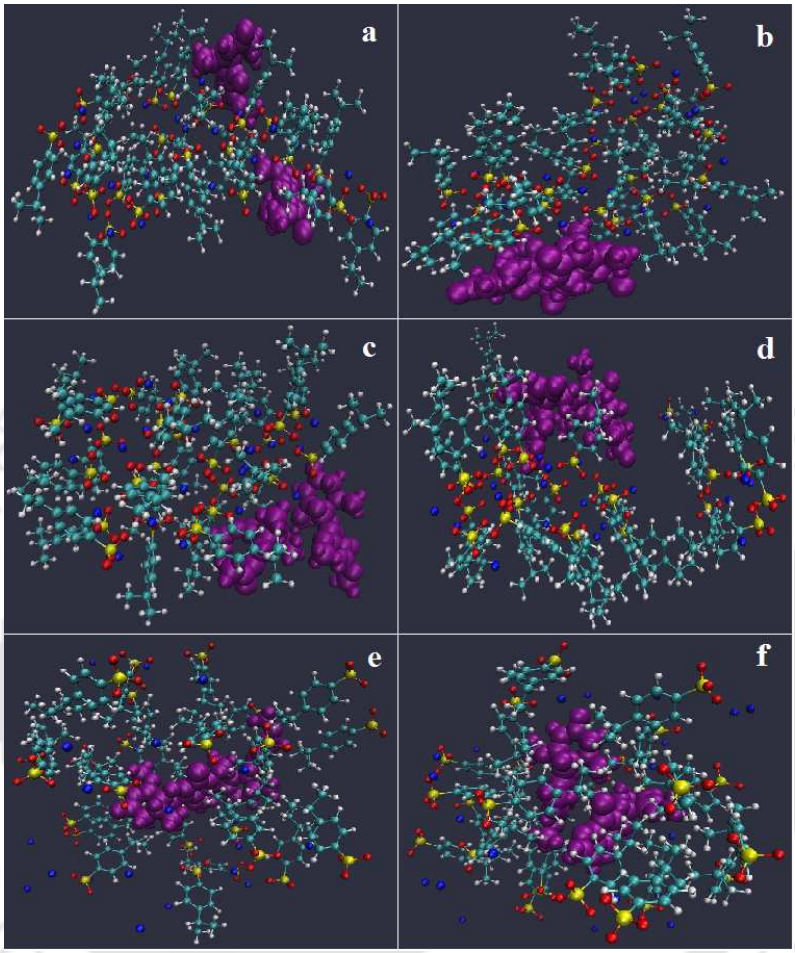

Figure 3-11. *Snapshots for 12:1 SCS-griseofulvin mixture in vacuum (a-c) and in presence of water (d-f) taken at different time intervals. Pink balls represent griseofulvin molecules while blue balls represent sodium ions. Water molecules are left off for better visual clarity.*

■ SUMMARY AND CONCLUSIONS

Employing classical molecular dynamics simulation and the MM-GBSA method, the basic mechanism of hydrotropic action of hydrotrope sodium cumene sulfonate on sparingly soluble griseofulvin drug molecules is studied. Eight different systems with varying SCS concentrations at ambient temperature and pressure conditions are considered. The snapshots of different systems show that the SCS molecules start to self-aggregate through their small hydrotropic tail parts at and above minimum hydrotrope concentration (MHC)

and drug griseofulvin molecules get incorporated into the inner core of SCS clusters. As concentration increases, the exclusion of water molecules from the first shell of different hydrophobic moieties of SCS and the *COM* of griseofulvin molecules has also been observed, and this effect is more prominent above the MHC level of SCS. These observations are further probed by the atomic mass density analysis of water and SCS density around the griseofulvin molecule. At and above the MHC level, the formation of higher-order SCS clusters is confirmed by cluster structure analysis. Furthermore, when SCS molecules start to form higher-order clusters, the number of incorporated griseofulvin molecules within the inner core of SCS aggregates exhibits a prominent enhancement, and above the MHC level, nearly all griseofulvin molecules are encapsulated into the SCS aggregates. The decomposition of drug-hydrotrope interactions into electrostatic and van der Waals components implies that the contribution of the latter is more significant in spite of the fact that the drug griseofulvin possesses both polar and nonpolar moieties. Interestingly, the estimation of average number of hydrogen bonds suggests that, though the self-association of SCS molecules has insignificant effect on water-SCS hydrogen bonds, it influences the water-griseofulvin hydrogen bonds. Furthermore, Flory-Huggins interaction parameter (χ_{FH}) successfully explains the reason behind the incorporation of drug griseofulvin into the core of SCS clusters. In this regard, we would like to mention that the recent studies of statistical thermodynamic theory of hydrotropic action, which is based upon the rigorous Kirkwood-Buff theory of solution, reported that the MHC of hydrotrope is caused by the solute (drug) persuaded increment of hydrotrope aggregation and bulk phase self-association of hydrotropes causes a reduction in the solubilization efficiency [53, 54]. It has further been claimed that it is the nonstoichiometric accumulation of the hydrotrope molecules around the drug which is responsible for its enhanced solubility in water [54]. In this study also, though we observe a sharp increase in the number of SCS molecules in the first solvation shell of griseofulvin above the MHC level, our results are somewhat different from the findings of refs 53 and 54, where it has been reported that the preferential interactions between solute molecules and hydrotropes play a major role for the solubilization of solutes, not the aggregation of hydrotropes.

Chapter 4

Hydrotropic Action of Cationic Hydrotrope p-Toluidinium Chloride on the Solubility of Sparingly Soluble Gliclazide Drug Molecule

"The application of guidelines linked to the concept of drug-likeness, such as the 'rule of five', has gained wide acceptance as an approach to reduce attrition in drug discovery and development. However, despite this acceptance, analysis of recent trends reveals that the physical properties of molecules that are currently being synthesized in leading drug discovery companies differ significantly from those of recently discovered oral drugs and compounds in clinical development. The consequences of the marked increase in lipophilicity - the most important drug-like physical property - include a greater likelihood of lack of selectivity and attrition in drug development. Tackling the threat of compound-related toxicological attrition needs to move to the mainstream of medicinal chemistry decision-making."

— P. D. Leeson and B. Springthorpe *Nat. Rev. Drug Discovery* **6**, 881 (2007)

Overview: We perform classical molecular dynamics simulations of sparingly soluble drug gliclazide (GLC) and hydrotrope p-toluidinium chloride (PTOL) in water with a regime of PTOL concentrations. Our results demonstrate that PTOL starts to self-aggregate above its minimum hydrotrope concentration (MHC). Further, these PTOL aggregates create a mixed micellar-like framework in which the hydrophobic small tail part of most of the PTOL molecules direct toward the inside, whereas in order to make favorable contact with water molecules, its hydrophilic ammonium group points outward. But, in order to make hydrogen bonds with GLC molecules, the polar groups of a few of the PTOL hydrotropes direct inward also. This provides an environment for the incorporation of the drug molecules into the mixed environment (hydrophobic as well as hydrophilic core) of PTOL clusters. The average number of hydrogen bond calculations indicate that PTOL aggregate does not have much effect on the average number of water-PTOL hydrogen bonds, but it has an influence on the average number of water-GLC, GLC-GLC, and GLC-PTOL hydrogen bonds. Both electrostatic and van der Waals energy components of drug and hydrotrope interactions play vital roles in the solubilization process. Furthermore, the estimation of Flory-Huggins interaction parameters also suggests favorable interactions between hydrotrope PTOL and GLC drug molecules.

■ INTRODUCTION

In our previous studies (**Chapter 2A, 2B and 3**) the self-aggregation behavior of an anionic hydrotrope above its minimum hydrotrope concentration has been reported, and we have also supported the moderate water structure breaking hypothesis. Like surfactants or polymer micelles, the organized self-assembly of hydrotropes is believed to act as a vehicle for drug solubilization [131, 132]. In pharmaceutical formulation, hydrophobic drugs are loaded inside micellar cores, and these drug-incorporated micelles are solubilized by the hydrophilicity of the micellar corona. Here, it is worth mentioning that the loading of lipophilic drugs in sufficient concentration in pharmaceutical formulation is also a major challenge.

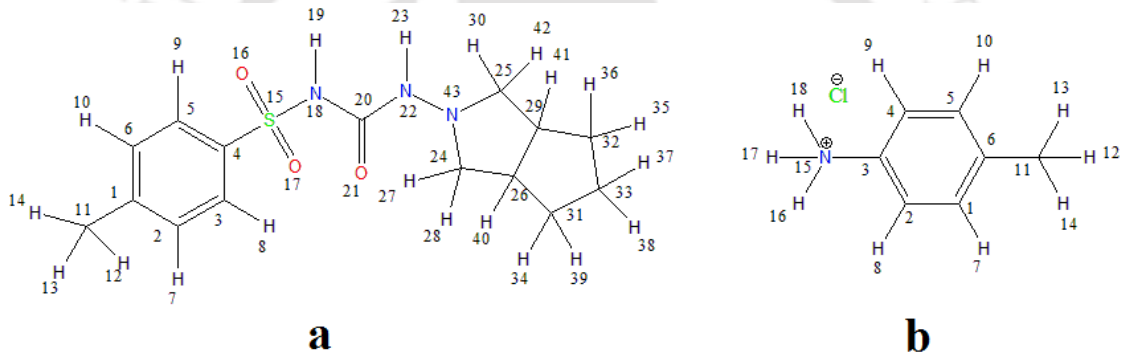

Figure 4-1. *Structure and atomic numbers of (a) gliclazide and (b) p-toluidinium chloride.*

Though hydrotropes can be anionic, cationic, or neutral depending on the charge of its polar headgroup, hydrotropes composed of a cationic headgroup, such as salts of aromatic amines and so on, are hardly studied. Here, we have studied the mechanism of hydrotropic action of p-toluidinium chloride (PTOL) on the sparingly soluble drug gliclazide (GLC) molecule (Figure 4-1). In our previous studies (**Chapter 2A, 2B and 3**), we have explored the mechanism of hydrotropy by using anionic hydrotrope sodium cumene sulfonate (SCS), but in this study to determine the molecular mechanism of a hydrotrope, we used cationic hydrotrope PTOL, which is barely studied. GLC is an oral hypoglycemic drug, which is used to treat noninsulin-dependent diabetes mellitus. Being a Class II drug (according to the Biopharmaceutics Classification System) with low aqueous solubility [133-135], GLC exhibits an unpredictable and slow absorption rate that may in turn reflect considerable intra- and intersubject variability [136]. In order to increase the solubility of GLC molecules in aqueous solution by the formulation of hydrotropes and to check the

microdetails of solubilization, we perform classical molecular dynamics simulations of GLC and PTOL in water. Here, we would like to mention that hydrotrope-induced solubilization of a drug molecule depends strongly on drug-hydrotrope interactions. This implies that a particular type of hydrotrope cannot be responsible for enhanced solubility of all different types of drug molecules.

The rest of the chapter is divided into three sections. Next section we present models and simulation details. The results are described and discussed after that. Our conclusions are summarized briefly in the last.

■ MODELS AND SIMULATION METHOD

In this work, we adopted the classical molecular dynamics (MD) simulation approach to simulate gliclazide-p-toluidinium chloride-water ternary mixtures. The geometry of drug gliclazide (GLC) and hydrotrope p-toluidinium (PTOL) were optimized separately with the HF/6-31G^* level of theory using Gaussian 09 [137]. The RESP (restrained electrostatic potential) [121, 138] module of AMBER12 was used for fitting the partial charges of all the atomic sites of both molecules. The rest of the parameters of drug and hydrotrope molecules were then parametrized using the General AMBER Force Field (GAFF) [118] with the ANTECHAMBER [121] module of AMBER12. The developed atomic partial charges for both molecules are shown in Table 4-1. To neutralize the ammonium group of a hydrotrope molecule, one Cl^- counterion was added in XLEAP of the AMBER12 package. For water, the SPC/E model was employed [77]. For the present study, we have constructed seven different systems by varying p-toluidinium chloride concentrations, and these are summarized in Table 4-2. Starting from system S0, we have prepared different systems by decreasing the number of water molecules keeping the number of both PTOL and GLC molecules unchanged. Also note that these systems are chosen in such a manner that at least one system falls below the MHC region of the hydrotrope PTOL (system S0), three systems fall within the MHC region (systems S1-S3), and the other three systems, i.e., systems S4-S6, fall above MHC regions (below we have defined the MHC region of hydrotrope PTOL). In order to construct the initial configurations for all the simulated systems, PACKMOL package [82] was used. All the simulations were carried out using the AMBER12 package [76] at 298 K temperature and 1 atm pressure. Initially, all the molecules were placed randomly in a cubic box, and periodic boundary conditions were implemented in all the three directions. For each of the systems, energy was minimized (10000 steps) with the steepest descent method (4000 steps) followed by the conjugate

Table 4-1. Atomic Numbers and Partial Charges of GLC and PTOL Molecules

GLC		PTOL	
Atomic Numbers	Partial Charges	Atomic Numbers	Partial Charges
C1	0.372761	C1	-0.198716
C6	-0.305592	H7	0.204934
C5	-0.110863	C2	-0.325133
H9	0.174104	H8	0.214056
H10	0.179746	C3	0.356963
C11	-0.531053	N15	-0.779890
H12	0.154225	H16	0.450952
H13	0.154225	H17	0.450952
H14	0.154225	H18	0.450952
C2	-0.305592	C4	-0.325133
H7	0.179746	H9	0.214056
C3	-0.110863	C5	-0.198716
H8	0.174104	H10	0.204934
C4	-0.126190	C6	0.269711
S15	1.272923	C11	-0.426323
O16	-0.606611	H12	0.145467
O17	-0.606611	H13	0.145467
N18	-0.794035	H14	0.145467
H19	0.416152		
C20	0.857889		
O21	-0.637499		
N22	-0.301690		
H23	0.323002		
N43	-0.171062		
C24	-0.203742		
C26	0.197069		
C29	0.197069		
C25	-0.203742		
H30	0.080850		
H42	0.080850		
C32	-0.292282		
C33	0.027368		
C31	-0.292282		
H34	0.076694		
H39	0.076694		
H37	0.029972		
H38	0.029972		
H35	0.076694		
H36	0.076694		
H41	0.037491		
H40	0.037491		
H27	0.080850		
H28	0.080850		

gradient method (6000 steps). The minimized structures were then heated gradually from 0 to 298 K in a canonical ensemble (NVT). Next, the systems were equilibrated for 5 ns in an isothermal-isobaric (NPT) ensemble at 298 K temperature and 1 atm pressure. The production runs were further performed for 80 ns in an NPT ensemble with the pressure maintained at 1 atm and the temperature at 298 K. For all simulations, the physical pressure was controlled using the Berendsen barostat [83] with a pressure relaxation time of 2 ps. In order to control the temperature, we used the Langevin dynamics method [139] with a collision frequency of 1 ps^{-1}. All the simulations were conducted with a 2 fs time step. All covalent bonds involving hydrogen atoms were constrained using the SHAKE algorithm [84]. A cutoff distance of 10.0 Å was used for all short-ranged nonbonded interactions. The particle mesh Ewald (PME) method [140] was used to calculate the long-ranged electrostatic interactions with a grid spacing of 1.0 Å spline order of 4, and relative tolerance of 10^{-5}.

Table 4-2. Overview of Systems[a]

System	N_{GLC}	N_{PTOL}	N_{wat}	Box volume (nm^3)	M_{PTOL}
S0	8	24	10000	307.86	0.129
S1	8	24	7200	224.56	0.177
S2	8	24	4800	152.35	0.261
S3	8	24	3600	116.34	0.342
S4	8	24	2400	79.93	0.498
S5	8	24	1800	62.31	0.639
S6	8	24	1200	44.36	0.898

[a] N_{GLC}, N_{PTOL} and N_{wat} are the number of gliclazide, p-toluidinium chloride and water molecules respectively and M_{PTOL} refers to molar concentration of the p-toluidinium chloride.

In order to calculate Flory-Huggins interaction parameter, we have considered two different hydrotrope-solute simulation systems. We have constructed the first mixture by using 24 hydrotrope PTOL molecules and 1 GLC molecule (in a 24:1 ratio), and for the second one, we consider 24 hydrotrope PTOL molecules and 2 GLC molecules (in 12:1 ratio). In both systems, initially all PTOL and GLC molecules arranged randomly. To obtain the initial compactness of each of the systems, the initial configurations of each GLC-PTOL mixture was equilibrated in vacuum. The vacuum simulations were conducted in AMBER12 for 15 ns at a 298 K temperature. A cubic periodic box was generated around the compacted complex in the leap module of AMBER12 and 0 Å a buffer constant was used in all three directions. The voids, mostly generated at the corner of the cubic box, were filled with 319 and 404 SPC/E water molecules for the 24:1 and 12:1 systems,

respectively. Then, the systems were subjected to energy minimization of 4000 steps in the steepest descent method and thereby 6000 steps in the conjugate gradient method. Next, the systems were heated gradually from 0 to 298 K in canonical ensemble (NVT). In order to relax the density of the systems, another 4 ns equilibration run was performed in an isothermal isobaric (NPT) ensemble at 298 K and 1 atm pressure. This is followed by an equilibration run of 20 ns in NPT (at 298 K and 1 atm pressure) carried out by maintaining periodic boundary conditions. All the simulation runs were performed in AMBER12 with a time step of 2 fs. The temperature was maintained using the Langevin dynamics method, and the pressure was maintained by the application of a Berendsen barostat. The SHAKE algorithm was used to constrain all of the bonds that involve hydrogen atoms. The particle mesh Ewald method was employed to treat the long-ranged electrostatic interactions, and a cut off distance of 10.0 Å was defined for all nonbonded short-ranged interactions.

■ RESULTS AND DISCUSSION

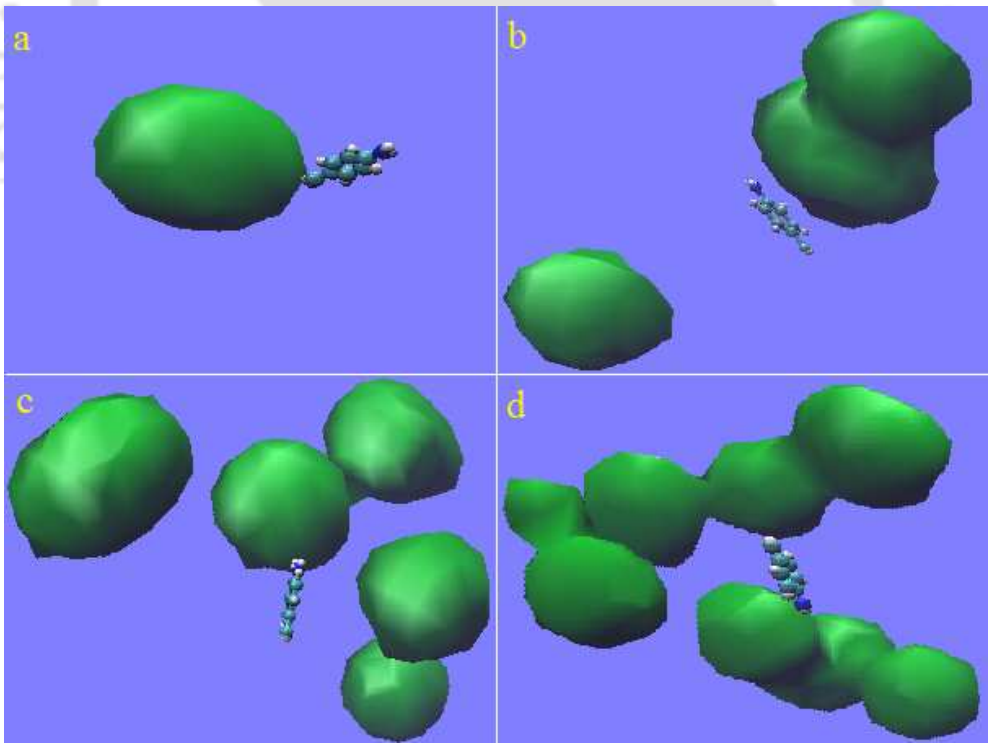

Figure 4-2. *Panels a, b, c, and d are contours of average PTOL density (averaged over last 10 ns of simulated trajectory) within 6.55 Å around a reference PTOL molecule for systems S0, S2, S4, and S6, respectively.*

Incorporation of GLC Molecules inside PTOL Clusters

In order to obtain information about the aggregation behavior of PTOL molecules, we have calculated the mass density maps of PTOL molecules around a reference PTOL molecule for the systems S0, S2, S4, and S6, and the same are presented in Figure 4-2. These maps are plotted by choosing a C_{11}-C_{11} cutoff distance of 6.55 Å. The choice of this cutoff distance is made from the position of the first minimum in C_{11}-C_{11} distribution function (Figure 4-3).

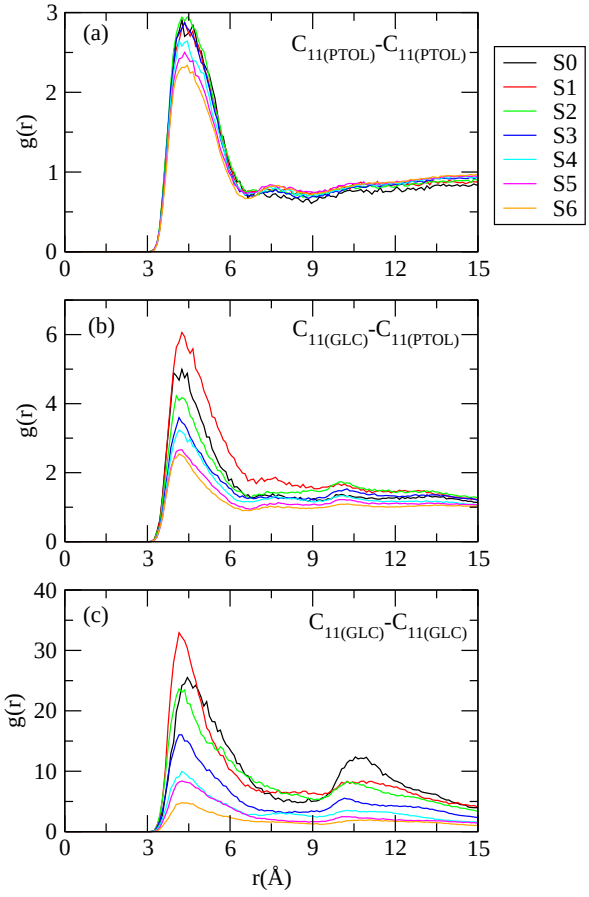

Figure 4-3. *Site site radial distribution functions between (a) C_{11}-C_{11} (PTOL - PTOL), (b) C_{11}-C_{11} (GLC - PTOL), and (c) C_{11}-C_{11} (GLC - GLC) for different systems.*

For each simulation, the average PTOL density maps are generated by using the Volmap plugin tool of VMD with a cell side of 0.5 Å. A mass density map is created by considering

the weighted atomic density at each grid point. In brief, for different systems, the average PTOL densities are created by using the Volmap plugin tool of VMD that produced the density maps (3D grids of values-in this case, the occupancy of a C_{11} atom of a PTOL molecule) of the PTOL molecules found in a specified region at each MD snapshot, which were then averaged over the last 10 ns of the MD trajectory. For system S0, we observe a very low PTOL density around a reference PTOL molecule. As the molarity of the solution is increased, the density of PTOL molecules around the reference PTOL molecule increases. This suggests the aggregation propensity of PTOL molecules at higher PTOL concentration.

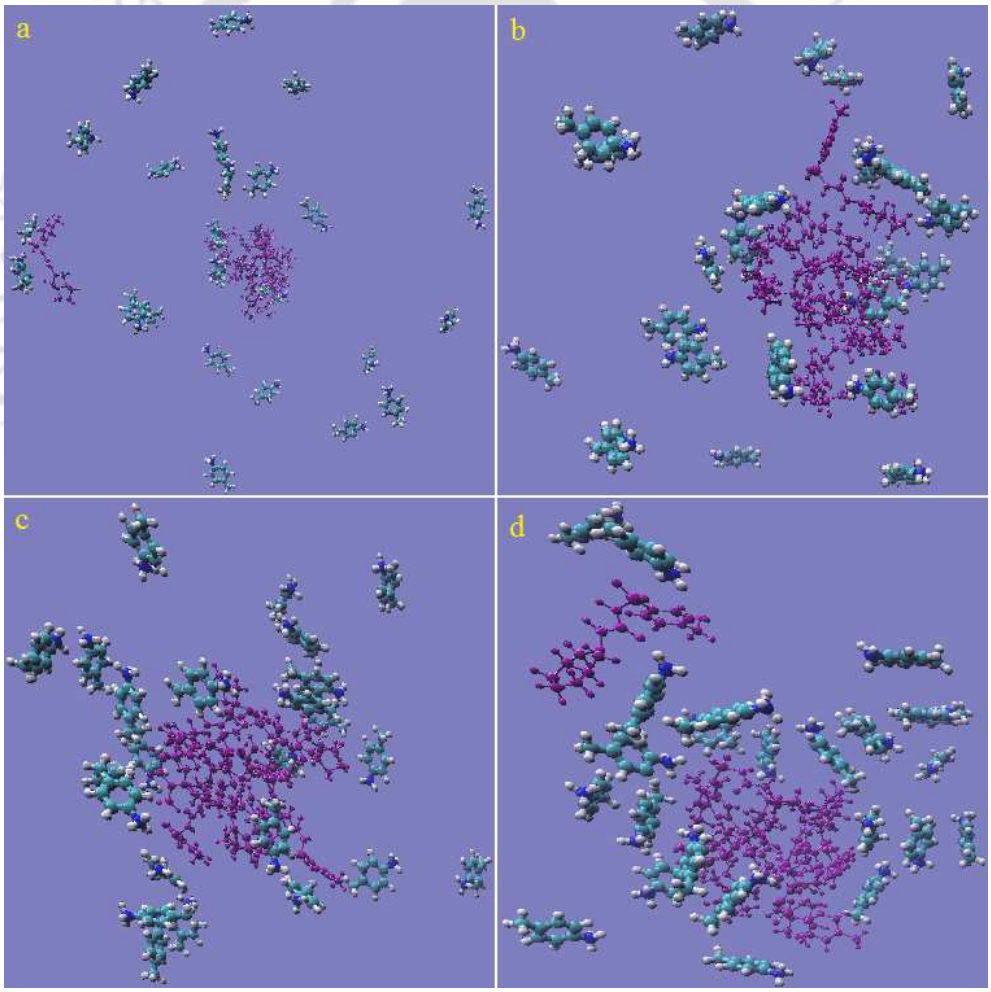

Figure 4-4. *Panels a, b, c, and d represent snapshots for systems S0, S2, S4, and S6, respectively, at 80 ns. Gliclazide molecules are represented by the pink color. Water molecules and chloride ions are left off for better visual clarity.*

To study the effects of PTOL aggregate formation as the solubilization of GLC and distribution of the latter through the different sites of PTOL clusters, we have taken visualizing snapshots for different systems (Figure 4-4). In order to obtain the proper visual clarity of the snapshots, the water molecules are left off. As is shown, in system S0, all PTOL molecules are dispersed in the solution, and as soon as molarity of the solution increases, more and more PTOL molecules assemble to form clusters. From Figure 4-4, it is also apparent that when hydrotrope PTOL molecules start to form a self-aggregated structure GLC drug molecules also start to penetrate inside the core of PTOL clusters. A closer look into these clusters reveals that although the small hydrophobic tail of the amphiphilic PTOL molecule participates in this self-aggregation process (by pointing inward) some polar head groups of PTOL molecules also are directing inward to make favorable interactions with drug molecules (discussed below) (Figure 4-5).

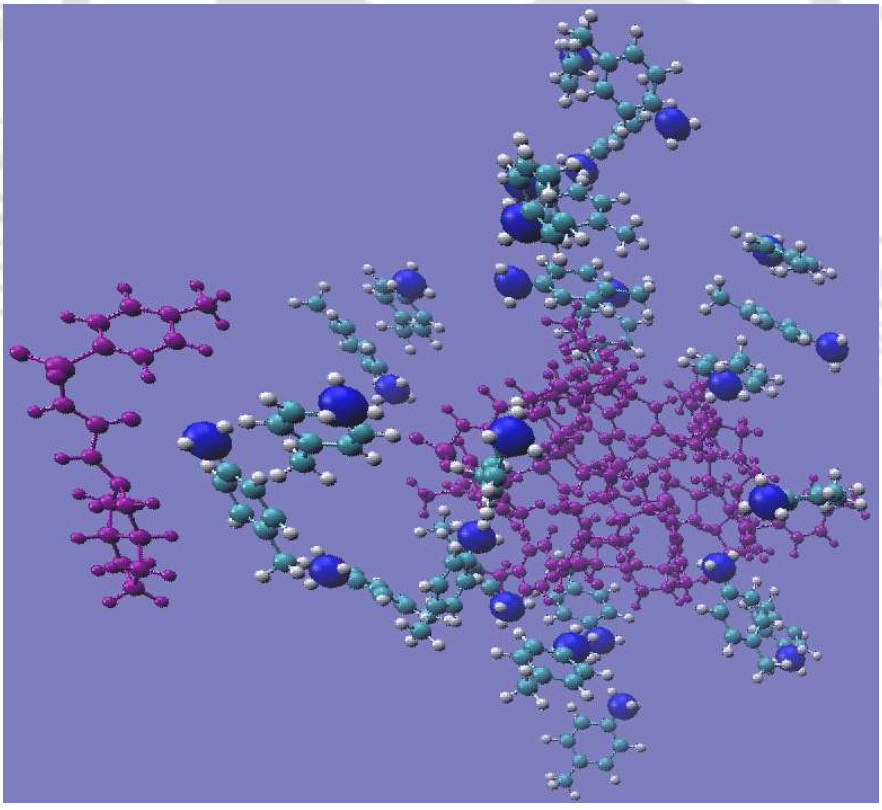

Figure 4-5. *Close view of clustering of PTOL molecules and encapsulation of GLC molecules (represent by purple color) of system S6, where some polar head group (nitrogen atoms represent by large blue balls) directed inwards.*

These results are little bit different from our previous study (**Chapter 2B and 3**) where the self-aggregation of anionic hydrotrope SCS was seen to occur solely through the small hydrophobic tail of an SCS molecule, but the polar part of the hydrotrope was directing outward to make favorable contact with water molecules. In an attempt to examine the aggregation tendency of hydrotrope PTOL molecules more precisely, we have additionally computed the mass density map of C_{11} atoms of PTOL molecules around a reference C_{11} atom of a like molecule for the last 10 ns using the method discussed above. Figure 4-6 represents the average mass density map of C_{11} atoms of PTOL molecules within 6.55 Å of a reference C_{11} atom of PTOL molecules. This atomic density map qualitatively suggests the enhancement of C_{11} density with increasing PTOL concentration. This result further implies that the self-aggregation of PTOL occurs mainly through the small hydrophobic tail of PTOL molecules. Bear in mind that these observations are made from the visualizing snapshots (Figure 4-4) and average mass density (Figures 4-2 and 4-6) of different systems, so this prediction is entirely qualitative. A more quantitative analysis of these observations has also been performed and is presented in the following subsection.

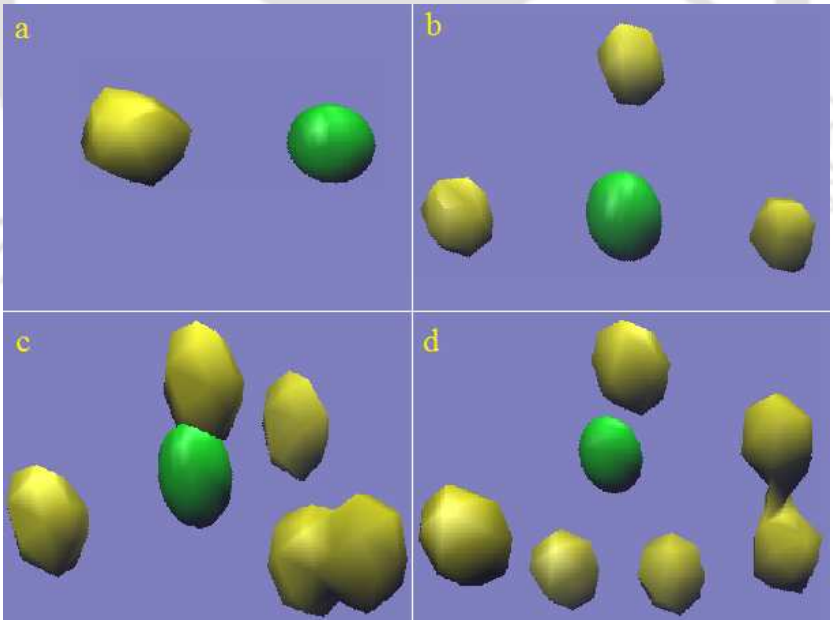

Figure 4-6. *Panels a, b, c, and d are contours of C_{11} atom density (averaged over last 10 ns of simulated trajectory) of PTOL molecules within 6.55 Å around a reference C_{11} atom of a PTOL molecule for systems S0, S2, S4, and S6 systems, respectively. Large green balls represent the C_{11} atom of the reference PTOL molecule.*

Cluster Structure Analysis

In this subsection, first, we present the quantitative proof of clustering of PTOL molecules for all systems considered in this study. Furthermore, our analysis is extended apropos to the estimation of the number of GLC molecules inside the core of PTOL clusters. The numbers of PTOL clusters and their average sizes are determined for all systems. Following earlier works (**Chapter 2B and 3**), it is assumed that two PTOL molecules construct a dimer if the distance between the C_{11} atom of one PTOL molecules falls within a cutoff distance of 6.55 Å of a C_{11} atom of a neighboring PTOL molecule. Likewise, a trimer PTOL cluster can be acquired if the distance of a C_{11} atom of a third PTOL molecule falls within the cutoff distance of the C_{11} atom of either of the two PTOL molecules of cluster size two and so on. The choice of this cutoff distance was discussed above. Figure 4-7 displays the probability distributions of different sizes of PTOL clusters (in percentage) that are present in a particular system. Here, the last 16 ns of production phase trajectories are considered for this quantitative analysis purpose. At low concentrations (systems S0 and S1), PTOL molecules are not aggregated, and the percentage of monomers are quite high. As the concentration of hydrotrope increases, the probability of forming higher order clusters increases. In systems S2 and S3, PTOL clusters gradually grow in size at the expense of the monomers. For systems of S4-S6, the sizes of PTOL clusters increases further, and for system S6, we observe a noticeable probability of the formation of a 22-mer. From these histograms, it can also be seen that a clear transition occurs between lower and higher order cluster formation. To be specific, the cluster distributions of systems S1 and S2 are quite similar, but a sharp increase in the formation of higher order cluster is observed as one moves from systems S2 to S3. These observations further indicate that 0.177 to 0.342 molar is the MHC region of a PTOL molecule.

In order to examine the effect of PTOL aggregation on GLC solubilization, we have, further, estimated the number of GLC molecules within the core of different PTOL clusters. For this purpose, we consider certain geometric criteria: (i) The size of the PTOL cluster has to be greater than or equal to three. (ii) The distance between a C_{11} atom of a GLC molecule should be within 6.45 Å of a C_{11} atom of a cluster-forming PTOL molecule (Figure 4-3b). Concurrently, (iii) the cutoff distance between a C_{11} atom of one GLC molecule should be within 9.25 Å of a C_{11} atom of a neighboring GLC molecule (Figure 4-3c), and simultaneously, if both of these two GLC molecules stay within the cutoff distance of a C_{11} atom of PTOL molecules that are part of the same cluster, then the two GLC molecules are considered to be present within the same PTOL cluster.

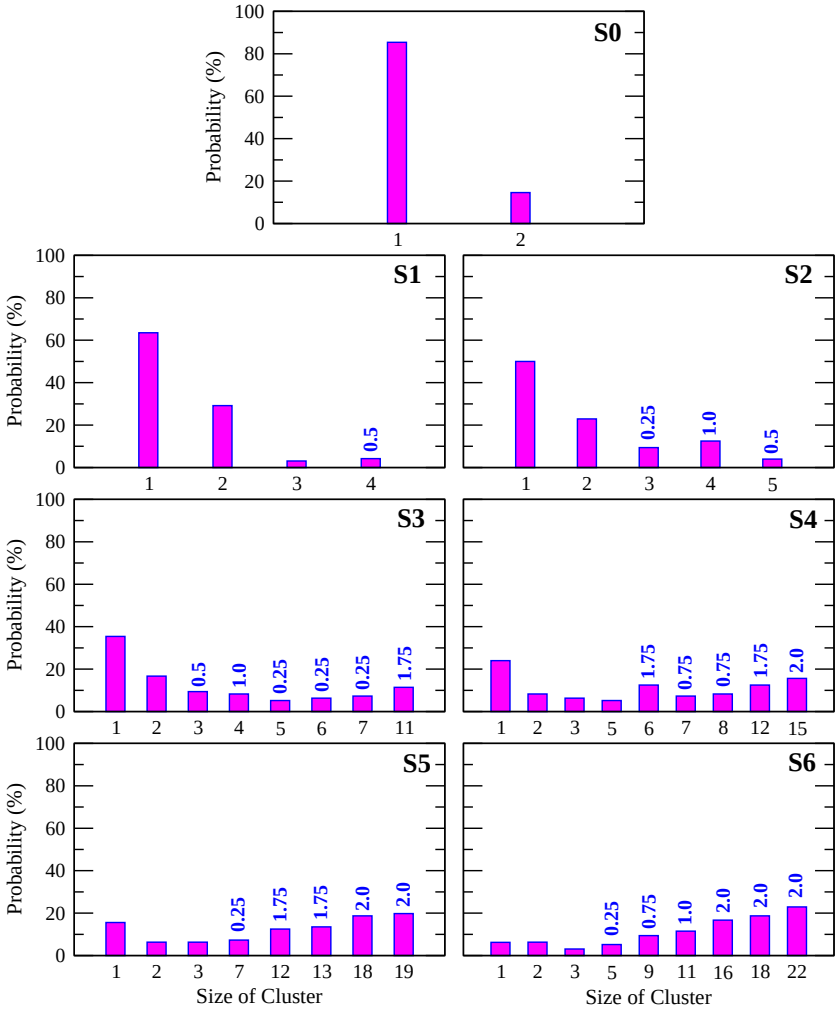

Figure 4-7. *Probability distributions (in percentage) of PTOL clusters of different sizes. Numbers on different bar diagrams represent the average number of GLC molecules present in a given PTOL cluster.*

Figure 4-7 shows the average number of GLC molecules that are located within the core of different sizes of PTOL clusters. As can be seen that the incorporation of GLC molecules within the PTOL clusters increases with an increase in the probability of formation of a higher order cluster of PTOL molecules. Below the MHC level, GLC molecules do not start to penetrate inside the core of PTOL clusters, whereas at and above the MHC level, as PTOL starts to construct higher size clusters, GLC molecules start to penetrate the interior of PTOL clusters.

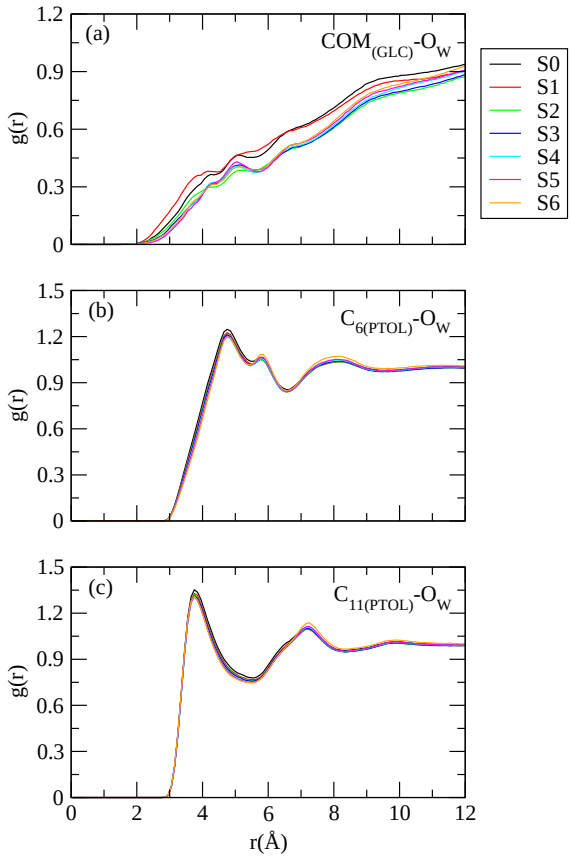

Figure 4-8. *Site site radial distribution functions between (a) COM-O_W (GLC - Water), (b) C_6-O_W (PTOL - Water), and (c) C_{11}-O_W (PTOL - Water) for different systems.*

Hydrophobic Hydration

Indirect information on self-aggregation of hydrotrope PTOL molecules can be obtained from the estimation of the number water molecules that are present in the first solvation shell of its different hydrophobic moieties. To be specific, it is expected that as a result of aggregation some of the water molecules should be excluded from the PTOL surface with an increase in molarity of the hydrotrope. Thus, it is important to estimate the average number of first shell water molecules (coordination number, CN) around different hydrophobic moieties of solute GLC and hydrotrope PTOL. CNs are calculated by integrating radial distribution functions (rdfs) involving different hydrophobic moieties of these molecules and oxygen atom of water molecules by using Eq. 2.3 (Figure 4-8).

Table 4-3. Number of First Shell Water Molecules around Center of Mass (COM) of Gliclazide Molecules and C_6 and C_{11} Atom of p-Toluidinium Chloride Molecules[a]

System	COM	C_6	C_{11}
S0	9.49	20.67	22.02
S1	8.60 (9.37)	19.85 (20.42)	21.19 (21.75)
S2	7.34 (9.20)	19.00 (20.03)	20.26 (21.34)
S3	7.23 (9.02)	18.33 (19.65)	19.55 (20.94)
S4	7.06 (8.76)	16.97 (19.08)	18.09 (20.33)
S5	6.69 (8.44)	16.04 (18.38)	17.04 (19.58)
S6	6.42 (7.88)	14.27 (17.17)	15.21 (18.29)

[a] Values in the parentheses represent the first shell normalized coordination numbers due to change in the number density of water.

The average number of first shell water molecules present around different hydrophobic sites of PTOL and the center of mass of (COM) of GLC molecules is shown in Table 4-3. Note that we show only the coordination numbers for C_6 and C_{11} atomic sites of the PTOL molecule because the CN values for other hydrophobic atomic sites and hydrophilic atomic sites show only a slight change with a change in concentration of hydrotrope molecules. It can be seen that the number of first shell water molecules around COM of GLC molecules decreases as molarity of the solution increases, but the effect is much more pronounced for systems S2-S6. The CN values of C_6 and C_{11} atomic sites of PTOL molecules also display similar trends. This result also supports our previous observation that the MHC region of PTOL molecules starts from system S2. Here, it is worth mentioning that as we move from systems S0 to S6, the number density of water decreases, and therefore, a small decrease in the first shell coordination number value is expected. In an attempt to rule out the effect of reduced water density, the coordination number values are normalized with a reference to that of system S0, and the same are also included in the parentheses of Table 4-3. We find that the difference between the actual and normalized or expected coordination numbers are small for below the MHC level of PTOL, but above the MHC region the difference between them starts to rise dramatically. This finding indicates that as the molarity of the solution increases, more and more reduction in the number of water molecules in the first solvation shell of C_6 and C_{11} atomic sites of a PTOL molecule and COM of GLC molecules is occurring.

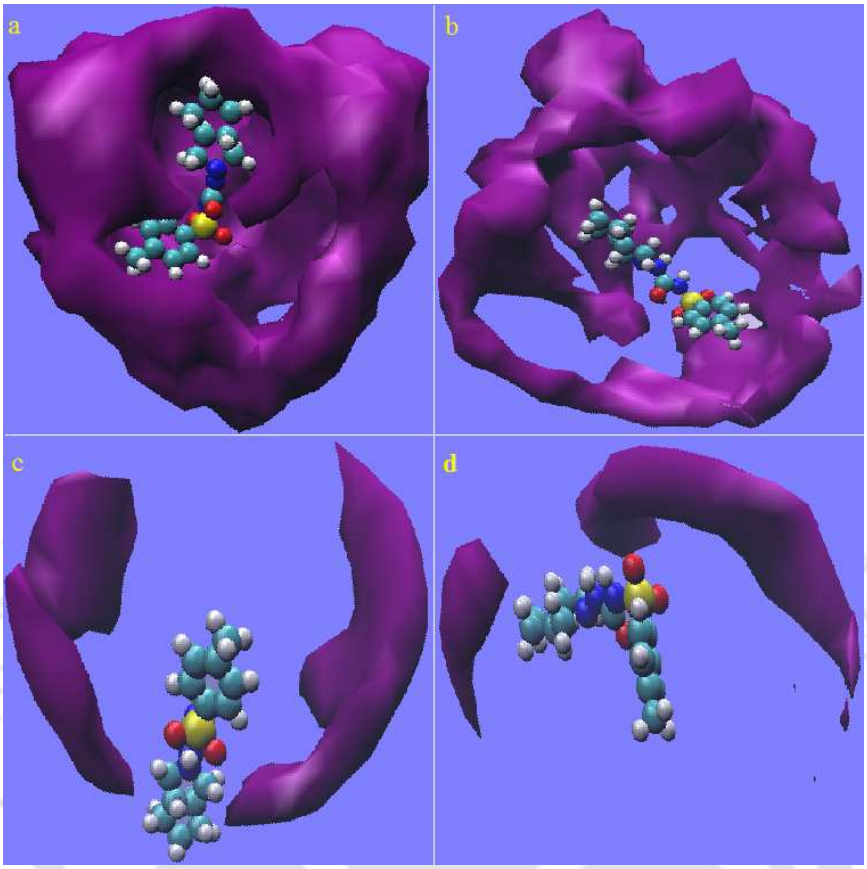

Figure 4-9. *Contours of solvent water density (averaged over last 10 ns of simulated trajectory) within 5.55 Å around GLC molecule. Panels a, b, c, and d are for systems S0, S2, S4, and S6, respectively.*

In an attempt to gather more information about water density around GLC molecules, atomic mass density analyses have been performed using VMD. The average mass density maps of an oxygen atom of water with a cell side of 0.5 Å within 5.55 Å around a randomly selected GLC molecule for systems S0, S2, S4, and S6 are shown in Figure 4-9. The average water density maps are computed with the Volmap plug-in of VMD and averaged over the last 10 ns of a simulated trajectory. At low concentration (below MHC level), a very high water density around the GLC molecule is observed. Above the MHC region, as PTOL molecules begin to self-accumulate, a clear reduction in the water density around GLC is observed. This acts as corroborative evidence of the above discussions. To gain insight on the average hydrotrope density (averaged over last 10 ns) around the GLC molecules, we have also carried out atomic mass density analysis of hydrotropes around a randomly chosen GLC molecule with a cell side of 0.5 Å within 6.45 Å . The mass density maps of PTOL molecules around a GLC molecule for systems S0, S2, S4, and

S6 are displayed in Figure 4-10. Below MHC region, we have observed a low hydrotrope density around GLC molecules, but with an increase in the molarity of hydrotrope, density of PTOL around GLC increases. Thus, these results support the fact that water molecules are being replaced by PTOL molecules around GLC molecules at and above the MHC level of this cationic hydrotrope.

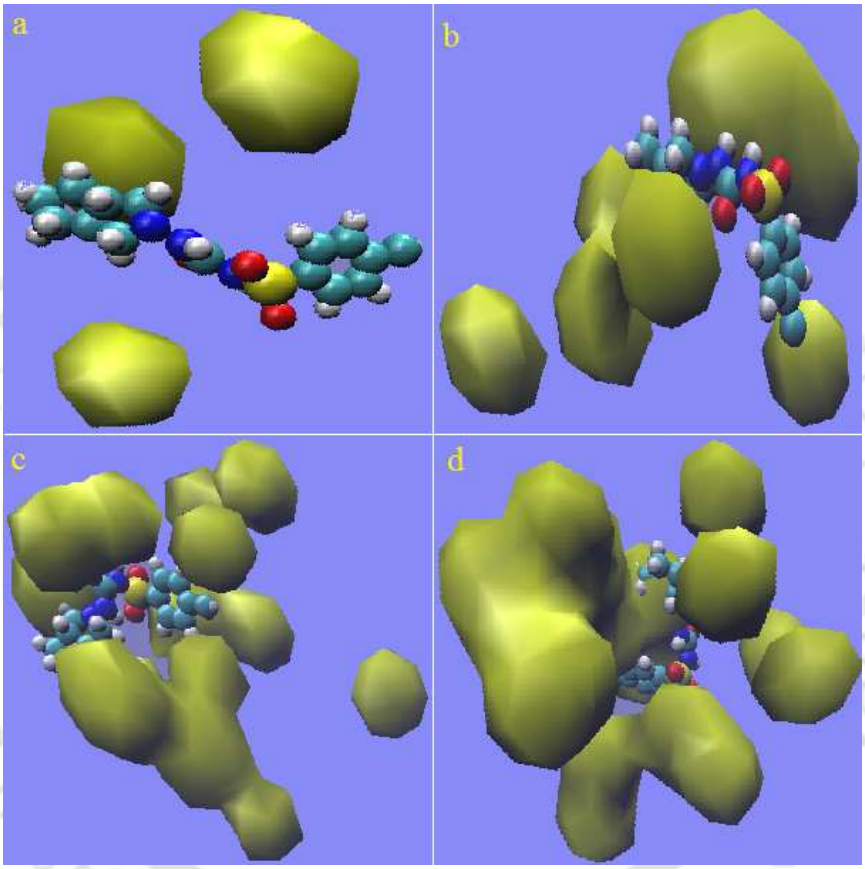

Figure 4-10. *Contours of hydrotrope PTOL density (averaged over last 10 ns of simulated trajectory) within 6.45 Å around GLC molecule. Panels a, b, c, and d are for systems S0, S2, S4, and S6, respectively.*

From the above analysis, it is clearly understood that as the concentration of the solution increases water molecules are replaced by PTOL molecules from the first solvation shell of GLC molecules. This encourages us to carry out estimation (in a more quantitative manner) of a number of PTOL molecules in the first coordination shell of a GLC molecule. We have estimated the number of first solvation shell PTOL molecules around the GLC molecules by using Eq. 2.3. The average number of PTOL molecules present in the first solvation shell of GLC is calculated by considering the distribution function involving C_{11} of GLC and C_{11} atom of PTOL (Figure 4-3b). The average numbers of first shell PTOL

molecules around GLC for different systems considered in this study are presented in Table 4-4. We find that with increasing molarity of the solution the number of first shell PTOL molecules around GLC increases, and a sharp jump in these numbers is noticed at and above the MHC level of the hydrotrope.

Table 4-4. Number of First Shell Hydrotrope PTOL Molecules around GLC Drug Molecules (CN_{Hyd})

system	CN_{Hyd}
S0	3.99
S1	5.01
S2	6.08
S3	7.33
S4	9.98
S5	11.49
S6	14.47

Hydrogen Bond Properties

As PTOL molecules possess a nitrogen atom (as NH_3^+), one may expect that in aqueous solution it can act as a hydrogen bond donor and can involve hydrogen bonding interactions with water molecules. Again, in drug GLC, the presence of amide linkage and oxygen atoms attached to sulfur makes it both a potential hydrogen bond acceptor as well as donor. Therefore, it can form hydrogen bonds with water molecules and also with hydrotrope molecules. Again, GLC molecules can also form intermolecular GLC-GLC hydrogen bonds between themselves. Since PTOL molecules can only act as donors, an intermolecular PTOL-PTOL hydrogen bond is not possible. Thus, five types of hydrogen bonds are possible, viz., water-water, water-PTOL, water-GLC, PTOL-GLC, and GLC-GLC. As was carried out in the previous reports [93-95] here also, the average numbers of these hydrogen bonds are calculated considering certain geometric criteria. If interatomic distance between the donor (D) and acceptor (A) atoms of a hydrogen bonding pair (already mentioned above) is less than 3.4 Å and the concurrent angle D—A—H is less than 45^o, then the pairs are considered to be hydrogen bonded. The average numbers of hydrogen bonds between all the possible pairs are shown in Table 4-5. It can be seen that with increasing hydrotrope concentration the average number of hydrotrope-water, drug-water, and water-water hydrogen bond decreases. As mentioned above, as concentration increases, the number of water molecules decreases, as a result of which a modest reduction in the

water number density is observed as we move from system S0 to system S6. Thus, a reduction in the number of these hydrogen bonds is expected. In an attempt to rule out the effect of reduced water density, we have also calculated the expected hydrogen bond numbers, and the same are included in parentheses of Table 4-5.

Table 4-5. Average Number of Water-Water per Water ($HB_{water-water}$), Gliclazide-Water per Gliclazide ($HB_{GLC-water}$), PTOL-Water per PTOL ($HB_{PTOL-water}$), Gliclazide-Gliclazide ($HB_{GLC-GLC}$), and Gliclazide-PTOL ($HB_{GLC-PTOL}$) Hydrogen Bonds for Different Systems[a]

System	$HB_{water-water}$	$HB_{GLC-water}$	$HB_{PTOL-water}$	$HB_{GLC-GLC}$	$HB_{GLC-PTOL}$
S0	3.34	3.97	2.46	5.92	0.49
S1	3.30 (3.30)	3.76 (3.92)	2.40 (2.43)	5.86	0.71
S2	3.25 (3.24)	3.01 (3.85)	2.35 (2.38)	5.82	0.85
S3	3.20 (3.18)	2.91 (3.77)	2.28 (2.34)	5.73	0.93
S4	3.12 (3.08)	2.82 (3.66)	2.23 (2.27)	5.66	1.09
S5	3.05 (2.97)	2.71 (3.53)	2.18 (2.19)	5.01	1.15
S6	2.93 (2.74)	2.63 (3.30)	2.08 (2.04)	4.59	1.21

[a]The values in the parentheses are the *expected* number of hydrogen bonds due to change in water number density.

We found a very small difference between the expected and calculated PTOL-water and water-water hydrogen bond numbers, which suggest that the decreased water density mainly causes depletion in the average number of these hydrogen bonds. In this context, it is worth mentioning that we do not observe any severe change in these hydrogen bond numbers at and above the MHC region of PTOL. Thus, the results indicate that the self-aggregation of PTOL has a slight or no impact on the PTOL-water and water-water hydrogen bonds. On the other hand, with an increase in PTOL concentration, the discrepancies between the expected and calculated GLC-water hydrogen bond number started to rise, and the difference is more pronounced at and above the MHC level. This suggests that as PTOL molecules start to self-aggregate at and above the MHC level the drug molecules begin to enter into the cage of the hydrotrope cluster. With an increase in concentration of hydrotrope, the intermolecular hydrogen bonds between the drug molecules (GLC-GLC) decrease, but the average number of hydrogen bonds between PTOL and GLC increases modestly. This can be described on the basis of the following: (i) With an increase in concentration of the ternary mixtures, PTOL starts to self-aggregate, and drug molecules also start to enter into the interior of the PTOL clusters. (ii) Hydrophilic parts of a few

hydrotrope molecules are directing inward, i.e., toward the encapsulated drug molecules (Figure 4-5) in the cluster conformation, and it increases above the MHC. As a result, interaction between drug and hydrotrope increases, and the formation of hydrogen bonds between PTOL and GLC also increases.

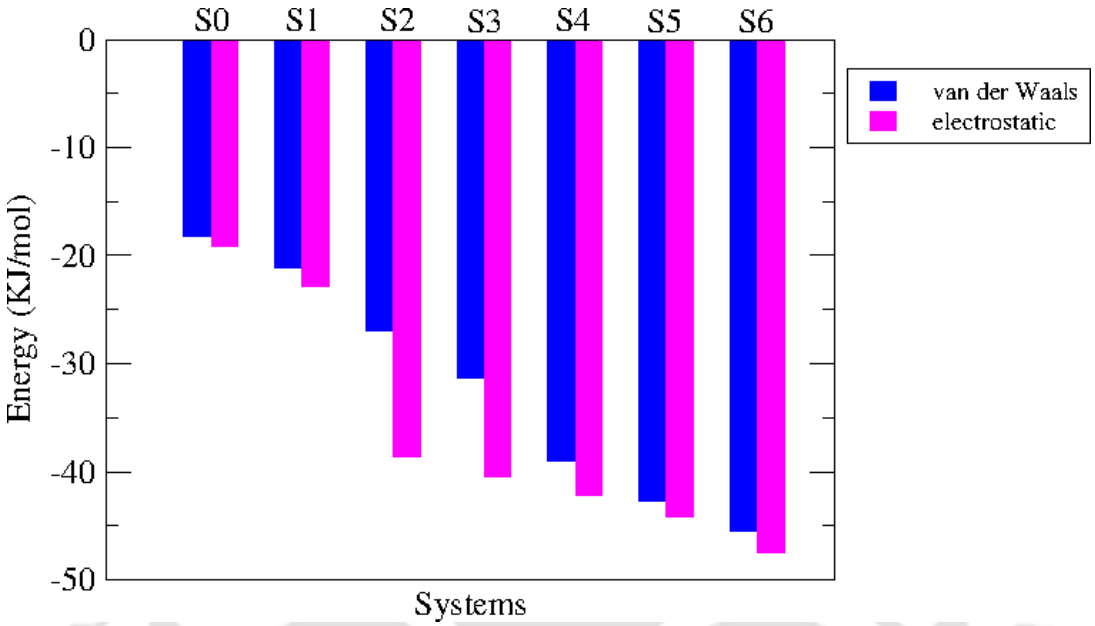

Figure 4-11. *Average van der Waals and electrostatic interaction energies between GLC and PTOL.*

GLC-PTOL Interactions

The above discussions suggest that the interactions between GLC drug molecules and PTOL hydrotrope molecules have a great influence in the solubilization of the former into the interior of the latter by virtue of hydrophobic or hydrophilic interactions in solutions. To get an idea about the direct interaction pattern between GLC and the PTOL molecule, total GLC-PTOL nonbonded interaction energies are decomposed into electrostatic and van der Waals (vdW) energy components for all systems. The electrostatic interaction energy between GLC and PTOL either comes from hydrogen bonding interactions between these molecules or from other types of electrostatic interactions. On the other hand, dispersion interactions between PTOL and GLC contribute to the van der Waals energy between these two molecules. The last 60 ns of production phase trajectory is taken for calculation purposes, and the results are shown in Figure 4-11. It is evident that both electrostatic and van der Waals energies play important roles in the interaction

between hydrotrope and drug molecules. Electrostatic interaction energy between GLC and PTOL contributes a little more in comparison to van der Waals interaction energy. It has also been observed that with an increase in concentration of PTOL both electrostatic and van der Waals energy components become more favorable, and the effect is more pronounced from the MHC level of the hydrotrope molecules. As the self-association of PTOL begins from the MHC level, the drug assimilation ability into the PTOL hydrophobic cores also increases. Again, as PTOL starts to form clusters, the hydrophilic sites of some of the PTOL molecules are moving inward to make favorable interactions and to form hydrogen bonds with GLC molecules. All of these factors make the electrostatic as well as van der Waals interaction between drug and hydrotrope molecules favorable. An important examination into these energy components further reveals that once the hydrotrope PTOL starts aggregate formation with the like molecules (system S2) a favorable jump of electrostatic energy component is observed. But, for systems S3-S6, it is the vdW component of the PTOL-GLC interaction which is responsible more for the encapsulation of GLC molecules inside the PTOL clusters (vdW energy changes from -28 kJ/mol for system S2 to -46 kJ/mol for system S6).

Flory-Huggins Interaction Parameters for GLC-PTOL Interactions

As described above, to calculate the Flory-Huggins interaction parameters between GLC and PTOL, two different drug-hydrotrope mixtures of different stoichiometric ratios are considered. The estimated enthalpy of mixing (ΔH_{mix}) and Flory-Huggins interaction parameters (χ_{FH}) are -62.38 cal cm^{-3} and -15.08 for a 24:1 ratio and -107.12 cal cm^{-3} and -25.91 for 12:1 ratio, respectively. The negative χ_{FH} value suggests favorable PTOL-GLC interactions. Thus, it can be inferred that PTOL clusters have an ability to incorporate GLC molecules inside clusters. Therefore, though PTOL molecule contains a smaller hydrophobic part in comparison to classical surfactants or polymers, it can solubilize the drug GLC molecules by incorporating them into its cluster.

■ SUMMARY AND CONCLUSIONS

The underlying mechanism of the hydrotropic action of hydrotrope p-toluidinium chloride (PTOL) on sparingly soluble gliclazide (GLC) drug molecules is investigated using classical molecular dynamics simulation and MM-GBSA techniques. We have studied the molecular interactions for the hydrotrope and drug in seven different systems with a regime of PTOL concentrations at ambient temperature and pressure conditions. From the snap-

shots of different systems, it is found that PTOL molecules self-aggregate at and above the minimum hydrotrope concentration (MHC) level. We have also observed the aggregation of hydrotrope occurs through the small hydrophobic tail of PTOL molecules, and GLC drug molecules also get accumulated into the core of PTOL clusters. These observations are further established by atomic mass density analyses of PTOL density around a reference PTOL molecule and C_{11} atom density of PTOL molecules around a reference C_{11} atom of a PTOL molecule. The estimated values of the first shell hydration number around different hydrophobic moieties of PTOL and GLC indicate the exclusion of water molecules from these atomic sites, and the effect is more pronounced above the MHC level of PTOL. The atomic mass density analysis of water and the PTOL density around the GLC molecule also supports this observation. The formation of a large size of PTOL clusters above the MHC level is suggested by cluster structure analysis. The number of GLC molecules inside the cluster of PTOL molecules increases from the MHC level of PTOL molecules, and above the MHC level, almost all GLC molecules are accumulated inside the PTOL clusters. Both electrostatic and van der Waals interaction energies between GLC and PTOL play vital roles in the solubilization of drug molecules, although the contribution of the former is slightly more pronounced than the latter. Above MHC, it is the favorable PTOL-GLC vdW interaction which is mainly responsible for the encapsulation of the drug molecules inside the hydrotrope clusters. The electrostatic component of the PTOL-GLC interaction plays a minor role in this. The average numbers of hydrogen bonds between all the possible pairs show that the self-aggregation of PTOL molecules has negligible impact on water-water and water-PTOL hydrogen bonds, but it affects the water-GLC, GLC-GLC, and GLC-PTOL hydrogen bonds. From the estimated value of enthalpy of mixing, ΔH_{mix}, the Flory-Huggins interaction parameter (χ_{FH}) is calculated, which provides detailed information about the favorable interaction between the hydrotrope PTOL-drug GLC in the mixture. A highly negative χ_{FH} value indicates very favorable interactions between PTOL and GLC molecules and explains successfully the reason behind the accumulation of drug GLC into the core of PTOL clusters.

Chapter 5

Hydrotropic Solubilization of Sparingly Soluble Riboflavin Drug Molecule in Aqueous Nicotinamide Solution

"Molecular recognition, binding and catalysis are often mediated by non-covalent interactions involving aromatic functional groups. Although the relative complexity of these so-called π interactions has made them challenging to study, theory and modelling have now reached the stage at which we can explain their physical origins and obtain reliable insight into their effects on molecular binding and chemical transformations. This offers opportunities for the rational manipulation of these complex non-covalent interactions and their direct incorporation into the design of small-molecule catalysts and enzymes."

— Andrew J. Neel et al. *Nature* **543**, 637 (2017)

Overview: We study the effect of non ionic hydrotrope nicotinamide on the solubilization of sparingly soluble riboflavin drug molecule. Nicotinamide molecules self-associate through stacking of their pyridine rings and they also form complexes with riboflavin molecules. Water molecules only prefer to stay at the periphery of the riboflavin molecules and they are replaced by the hydrotrope molecules with increasing concentration of the solution. The analyses of orientation distributions and distance measurements reveal that the riboflavin and nicotinamide molecules form 1:2 sandwich complexes. It is also demonstrated that the self-aggregation of nicotinamide and the complexation between riboflavin and nicotinamide does not have much influence on the number of water-water average hydrogen bonds but they influence the riboflavin-water, nicotinamide-water, riboflavin-riboflavin, riboflavin-nicotinamide and nicotinamide-nicotinamide hydrogen bonds. Favorable van der Waals interaction energy between riboflavin and nicotinamide plays an important role in the 1:1 or 1:2 complex formation between drug and hydrotrope molecules. The electrostatic energy component of drug and hydrotrope interaction also contributes to the solubilization process. The negative Flory-Huggins interaction parameter value suggests the favorable interactions between the hydrotrope and drug molecules.

■ INTRODUCTION

Solubilization is the process of dissolution of solute molecules in solvent to produce a homogeneous system. Increasing the water solubility of insoluble or sparingly soluble drugs is a major challenging problem in recent years. The poor aqueous solubility of drugs causes slow drug absorption leading finally to insufficient and variable bio-availability. Due to the ease of administration, oral route is the most convenient and commonly employed route of drug delivery. Since solid oral dosages forms like tablets, capsules have many advantages over other types of oral dosage forms, therefore, it is important that these forms of drugs endure sufficient dissolution in the gastrointestinal fluids. For a newly developed orally administered drug, the gastrointestinal tract solubility of it is the most important one rate-limiting parameter to reach the desired concentration in systemic circulation for proper pharmacological response. Problem of low solubility of drug is a major challenge for formulation scientist. In our previous studies, we have reported the self-aggregating nature of anionic hydrotrope sodium cumene sulfonate (SCS) above minimum hydrotrope concentration and the same hydrotrope also breaks the tetrahedral network of water structure. Anionic hydrotrope SCS attributed to the increase in solubilizing effect by forming organized self aggregates, which encapsulate the insoluble solute molecules inside their hydrophobic cage (**Chapter 2A, 2B and 3**). The self-aggregation behavior of cationic p-toluidinium chloride (PTOL) hydrotrope above MHC has also been studied. Their behavior is different from that of the anionic hydrotrope. In the organized self assembly of PTOL both hydrophobic and hydrophilic sites of hydrotropes play crucial role to the solubilization of insoluble drug molecules (**Chapter 4**).

The use of neutral hydrotrope nicotinamide (NIC), a non toxic vitamin B_3, as a solubilizing agent has already been reported in the literature [51, 141-143]. NIC is a very useful complexing or formulating agent because it possesses good solubilizing ability and low in toxicity. NIC molecules undergoing stacking interactions with drug molecules has commonly been proposed as NIC induced-drug solubilization mechanism [42, 144-146]. By using molecular orbital calculation, it has been shown that the complex can be formed between nicotinamide and heteroatomic drug molecules via π-donor and π-acceptor mechanism [147, 148]. Rasool et al. reported that the aromaticity of the pyridine ring is responsible for stacking interactions [51]. Although, the drug and the complex forming molecules do not possess any direct affinity towards each other but still they can be stacked with each other to reduce their exposure to water. Stacking can take place between the two like

molecules (self-association) or two different molecules (co-association). Through stacking interactions a simple 1:1 complex can be formed by one drug and one complexing agent whereas, for a 1:2 sandwich complex formation two complexing agent molecules are necessary on the two sides of the planar hydrophobic regions of the drug molecule. It has also been observed that the electrostatic interactions between the donor-acceptor type plays an important role in the complexation [149]. Though hydrogen bonding interactions between the drug and complexing agent in stacking interactions also plays a crucial role but its role is yet to be established [150]. Besides this, it has been suggested that nicotinamide molecules can behave like a chaotrope, i.e., it can break the tetrahedral network of water [151]. It has also been proposed that nicotinamide molecules form self-aggregated structures and the water insoluble drugs are incorporated into these clusters [43, 152]. Various experimental techniques have also been employed previously to explore the mechanism of neutral hydrotrope NIC-induced drug solubilization. These techniques consist of direct (spectral studies such as UV, IR, NMR, thermal studies such DSC, and fluorescence quenching) [151, 153] and indirect (solubility studies and measurement of thermodynamic parameters associated with the process) [145] approaches. Here it is to be mentioned that the results from the direct approaches are often inconclusive because it is difficult to examine the existence of a complex in a dissolved state from such experimental techniques.

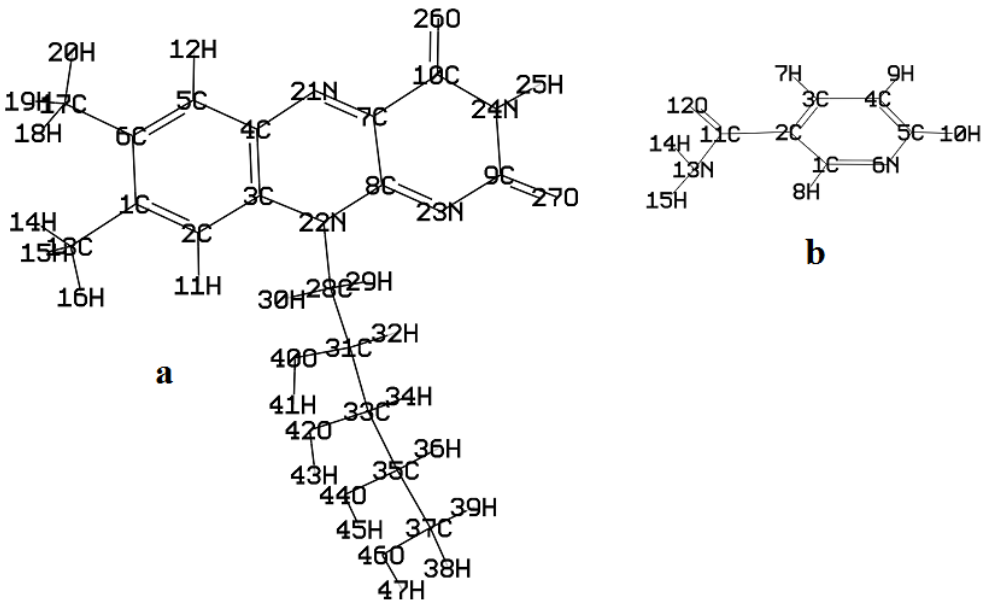

Figure 5-1. *The structures and atomic numbers of (a) riboflavin and (b) nicotinamide.*

In this study, we focus on the molecular mechanisms by which hydrotrope NIC increases the solubility of the sparingly soluble drug riboflavin (RIB) molecule (Figure 5-1). RIB, commonly known as vitamin B_2, is an important biological molecule. RIB is a poorly soluble drug and in deionized water, the solubility of RIB is up to 0.08 mg mL^{-1} at room temperature. In 2003, Wollensak et al. reported that RIB can be used as a drug that is typically administered to the eyes in order to mediate UV-induced corneal cross-linking in the treatment of keratoconus [154]. As RIB possesses low aqueous solubility, therefore, there is a clear need to develop novel formulations that could enhance its aqueous solubility. In order to study the mechanism of hydrotropy, we have carried out classical molecular dynamics simulation of RIB and NIC in water. In this study, first we have attempted to examine the effect of change in concentration of NIC on the solubility of drug RIB. Then we extend our analysis towards the atomistic details of NIC-induced solubilization of sparingly soluble RIB molecules.

The rest of the chapter is organized as follows. Simulation details are provided in section models and simulation method. Then results are discussed and the last section includes the conclusion of the present work.

■ MODELS AND SIMULATION METHOD

In the present work, the atomistic classical molecular dynamics (MD) simulation technique was employed to study the solution properties of riboflavin-nicotinamide-water ternary mixtures. The geometry optimizations of drug riboflavin and hydrotrope nicotinamide were carried out using Gaussian 09 [137] with the HF/6-31G^* basis set. The RESP (Restrained Electrostatic Potential) charges [121, 138] of drug and hydrotrope were generated from the HF/6-31G^* quantum mechanical data by fitting with the RESP module of AMBER12 [76]. Assignment of the force field parameters of all the atomic sites of both the molecules were performed using the general AMBER force field (GAFF) of ANTECHAMBER [118, 121] suite of AMBER12. The derived partial charges of riboflavin and nicotinamide are presented in Table 5-1. The water model employed was SPC/E [77]. In the present study by changing the hydrotrope concentration, eight different systems were prepared and these are presented in Table 5-2. PACKMOL package [82] was used to generate the starting configurations for each of the simulated systems. All simulations were performed with the aid of the AMBER12 package at 298 K temperature and 1 atm pressure. All the molecules were positioned at initial random positions in a cubic simulation box and also the periodic boundary conditions were applied in all the three directions.

Table 5-1. Atomic numbers and partial charges of different atomic sites of riboflavin and nicotinamide molecules.

Riboflavin		Nicotinamide	
Atomic Numbers	Partial Charges	Atomic Numbers	Partial Charges
C1	0.198470	C1	0.577879
C6	0.160873	H8	0.027267
C5	-0.451760	C2	-0.560573
C4	0.520975	C11	0.865803
N21	-0.545193	C3	0.356963
C7	0.120165	O12	-0.613661
C8	0.557262	N13	-0.960238
N23	-0.908993	H14	0.403268
C9	1.140068	H15	0.403268
N24	-0.906471	C3	0.340982
C10	0.847377	H7	0.086431
O26	-0.614826	C4	-0.613092
H25	0.425022	H9	0.217465
O27	-0.692034	C5	0.552662
H12	0.235627	H10	0.040728
C17	-0.340983	N6	-0.768188
H18	0.107628		
H19	0.107628		
H20	0.107628		
C13	-0.428271		
H14	0.130276		
H15	0.130276		
H16	0.130276		
C2	-0.424282		
H11	0.310033		
C3	-0.090653		
N22	0.037897		
C28	-0.213630		
H29	0.133260		
H30	0.133260		
C31	0.221186		
H32	0.085003		
O40	-0.627621		
H41	0.403993		
C33	0.124447		
H34	0.067987		
O42	-0.638028		
H43	0.446167		
C35	0.196338		
H36	0.001674		
O44	-0.626963		
H45	0.431491		
C37	0.192701		
H38	0.026588		
H39	0.026588		
O46	-0.707683		
H47	0.459226		

Each system was energy minimized for 10000 steps (4000 steps of steepest descent method followed by 6000 steps of conjugate gradient method). Initially, the temperature of the minimized structures was gradually increased from 0 to 298 K in a canonical ensemble (NVT). Then, the systems were then equilibrated for 5 ns at 298 K temperature and 1 atm pressure in isothermal-isobaric (NPT) ensemble. The simulations were then extended for another 80 ns production runs in NPT ensemble with the temperature and pressure maintained at 298 K and 1 atm respectively. Berendsen barostat [83] with a pressure relaxation time of 2 ps was used to control the pressure of all the systems. The simulation temperature was regulated using the Langevin dynamics method [139] with a collision frequency of 1 ps^{-1}. The SHAKE algorithm [84] was applied to constrain all covalent bonds involving hydrogen atoms and the simulation time step of 2 fs was used for all the simulations. All MD simulations were run with a 10 Å cutoff for calculating all short-ranged nonbonding interactions. Particle mesh Ewald (PME) method [140] was employed for an adequate treatment of long-ranged non bonding electrostatic interactions.

Table 5-2. Overview of Systems[a]

System	N_{RIB}	N_{NIC}	N_{wat}	Box volume (nm^3)	M_{NIC}
S0	8	24	10000	307.35	0.130
S1	8	24	7200	222.16	0.179
S2	8	24	6000	186.42	0.214
S3	8	24	4800	150.62	0.264
S4	8	24	3600	114.99	0.346
S5	8	24	2400	78.36	0.508
S6	8	24	1800	60.66	0.657
S7	8	24	1200	42.78	0.931

[a] N_{RIB}, N_{NIC} and N_{wat} are the number of riboflavin, nicotinamide and water molecules respectively and M_{NIC} represents the molar concentration of the nicotinamide.

To study the miscibility of the drug-hydrotrope mixtures, following our previous studies here also we have considered two different hydrotrope-drug simulation systems. In the first mixture, we choose to simulate with 24 hydrotrope NIC molecules and 1 RIB molecule (in 24:1 ratio) and in the second mixture the simulation is carried out with 24 hydrotrope NIC molecules and 2 RIB molecule (in 12:1 ratio). In both the systems, initially all the RIB and NIC molecules are positioned randomly. In order to get the initial compactness of each of the systems, at first we have equilibrated the initial configurations of each of the RIB-NIC mixtures in vacuum. For this, a 12 ns simulation run is performed

for each of these two mixtures in AMBER12 at 298 K temperature. For each system, to incorporate the solvent, a cubic periodic box is generated around the compacted complex. We have constructed the box in leap module of AMBER12 and a 0 Å buffer constant is used in all three directions. For 24:1 and 12:1 systems, 398 and 371 number of SPC/E water molecules are added respectively to the voids that were mostly at the corner of the cubic box. This is followed by a 10000 steps of energy minimization is carried out of which first 4000 steps in steepest descent followed by 6000 steps in conjugate gradient method. Temperature is then gradually increased from 0 to 298 K in canonical ensemble (NVT). A 4 ns equilibration run is performed in isothermal isobaric (NPT) ensemble at 298 K and 1 atm pressure to allow the system to relax towards its equilibrium structure. Each of this two simulations is extended for another 20 ns in NPT ensemble (at 298 K and 1 atm pressure) by applying periodic boundary conditions in all the directions. All the MD simulations are performed using the AMBER12 package with a time step of 2 fs. The bonds involving hydrogen atoms are constrained by SHAKE algorithm. A 10.0 Å cut off distance is used for all non bonded short-ranged interactions. The particle mesh Ewald method (PME) is applied for the treatment of long-ranged non bonded electrostatic interactions.

■ RESULTS AND DISCUSSION

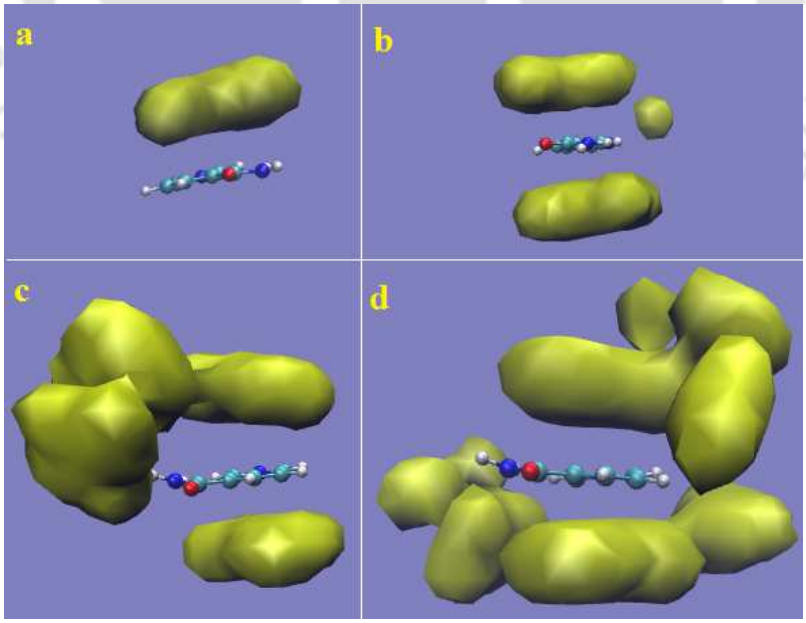

Figure 5-2. *a, b, c and d are the contours of NIC density within 3.25 Å around a reference NIC molecule for systems S0, S3, S5 and S7 respectively.*

Complexation between RIB and NIC molecules

To explore the interactions among NIC molecules, the mass density maps of NIC molecules around a reference NIC molecule is examined for the systems S0, S3, S5 and S7 and they are shown in Figure 5-2. The mass density maps are built using the Visual Molecular Dynamics (VMD) [85] program, with a cell side of 0.5 Å . We have calculated the mass density maps by choosing a cut off distance of 3.25 Å . This cut off distance criterion is taken from the position of the first minimum of the center of mass (COM) - center of mass (COM) distribution function of NIC molecules (see Figure 5-3 (a)).

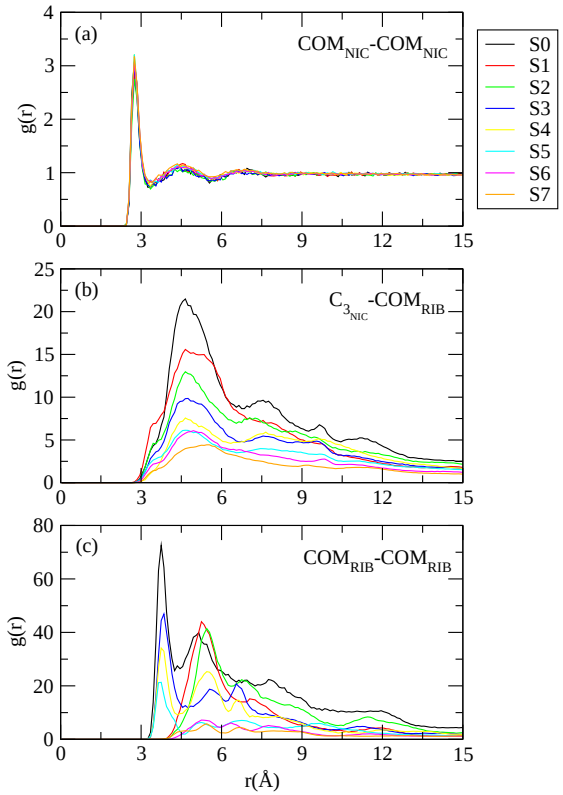

Figure 5-3. *Site site radial distribution functions between (a) COM-COM (NIC - NIC), (b) COM-C_3 (RIB - NIC), and (c) COM-COM (RIB - RIB) for different systems.*

As can be seen from Figure 5-2, for system S0 a very low NIC density around the reference NIC molecule is appeared. The enhancement in the NIC density around reference NIC molecule is also observed as the molarity of the solution increases. This finding indicates

that the interactions between the neutral hydrotrope increases as the concentration of the solution increases. Another important observation can be made from these mass density maps is that the self association of NIC occurs through stacking interactions. At the lowest concentration (system S0), the density of one NIC molecule is observed around the reference NIC molecule and these two NIC molecules are paired up by stacking interaction. But for the systems S3, S5 and S7, the hydrophobic faces of the reference NIC molecule are paired up with two NIC molecules through stacking interactions in such a manner that the central reference NIC molecule is surrounded on its two sides by the density of another two NIC molecules.

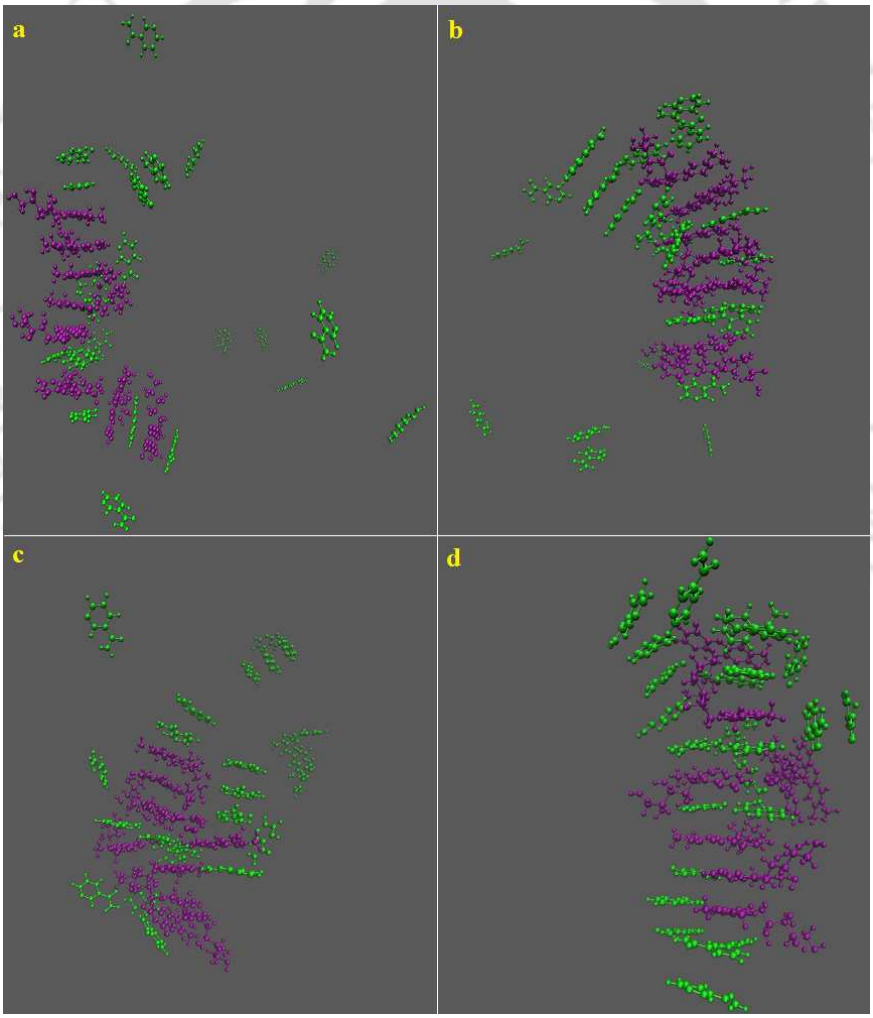

Figure 5-4. *a, b, c and d refer to snapshots for the systems S0, S2, S4 and S7 respectively at 80 ns. RIB and NIC molecules are represented by magenta and green colors respectively. Water molecules are left-off for better visual clarity.*

To gather more information about the self aggregation behavior of NIC molecules and its effect on the solubilization of RIB drug molecules, we have additionally considered the visualizing snapshots for different systems and the same are presented in Figure 5-4. The water molecules are left-off to obtain the proper visual clarity of the snapshots. It is seen that NIC molecules self-aggregate through stacking interactions of their pyridine rings. Furthermore, the polyaromatic rings of RIB molecules self associate through π-stacking interactions and that lead to the formation of RIB clusters and some of the RIB molecules also form NIC-RIB clusters with hydrotrope molecules. At low concentration (system S0), most of the NIC molecules are dispersed in the solution and few of them are in the dimeric form. As the concentration of the solution is increased, the self association of hydrotropes through stacking of their pyridine rings also increases. We also find that with increase in molarity of the solution, the complexation between RIB and NIC also increases. Furthermore, a close examination of these clusters reveals that small NIC clusters are arranged laterally (in parallel or perpendicular fashions) around the RIB clusters.

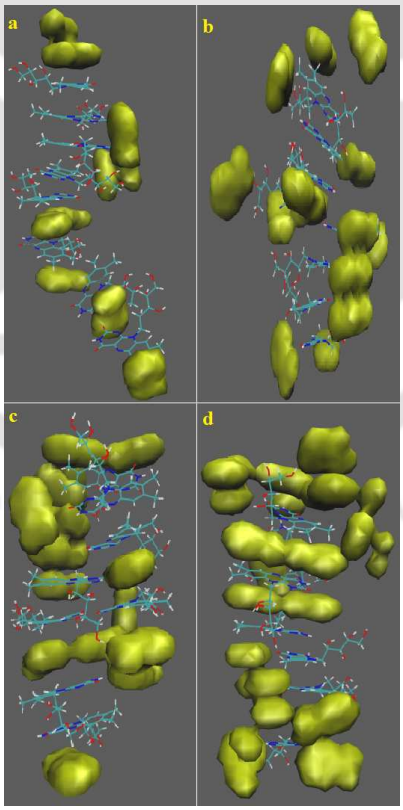

Figure 5-5. *Contours of hydrotrope NIC density within 6.55 Å around RIB molecule. a, b, c and d are for systems S0, S2, S4 and S7 respectively.*

In order to examine the complexation between NIC and RIB molecules, further we have calculated the mass density maps of NIC molecules around the RIB clusters with a cell side of 0.5 Å and within a cut-off distance of 6.55 Å and they are shown in Figure 5-5. The choice of the cut-off distance is made from the position of the first minimum of the correlation function involving COM of RIB and C_3 atom of NIC (see Figure 5-3b). We have observed that the hydrophobic faces of RIB drug molecules are paired up with the NIC molecules through stacking interactions. The clouds of aggregated hydrotrope density around the periphery of RIB clusters can also be seen from Fig. 5-5. At the lowest concentration (system S0) two RIB molecules form complex with NIC molecules in 1:2 RIB to NIC ratio and 3 drug molecules form 1:1 complex with the hydrotrope molecules through stacking type interactions. But, the density of NIC molecules around the periphery of the RIB clusters is very low at this concentration. The complexation between the RIB and NIC molecules either in 1:1 or 1:2 ratio is increased substantially with increasing the concentration of the solution. Again, with increase in molarity of the solution as NIC molecules start to self-aggregate through stacking of their pyridine rings, the density of aggregated NIC around the periphery of RIB clusters also increases.

Although the results discussed above are qualitative in nature but the following observations can be made: (i) Self association of NIC molecules occurs through stacking of their pyridine rings, (ii) RIB molecules form clusters with like molecules by stacking of their polyaromatic rings and (iii) RIB and NIC molecules form 1:1 or 1:2 complexes through hydrophobic stacking interactions. To provide the direct evidences about these three stacking types of interactions, we have calculated the orientational distribution between two respective molecular planes. In order to get an idea about the orientational preference of aromatic plane of a hydrotrope molecule with that of another hydrotrope NIC molecule, we have determined the distribution of the angle ϕ between their molecular planes. For different systems the distributions, P(ϕ), of the angles, ϕ, made by the plane normal vectors of two NIC molecules are shown in Figure 5-6(a). The appearances of the peaks near 0^o reveal that the parallel orientations of the two NIC molecules is highly preferred. As the concentration of the solution changes, there is no noticeable change in the peak heights and the position of their appearances. Further in the same figure, we have also shown the probability distributions of the angles ϕ between the normal vectors of the planes of RIB molecules. As expected, we have observed that the preferred arrangement of two RIB planes is parallel, indicating the polyaromatic stackings of RIB molecules one above another in parallel fashion. Moreover, the change in peak heights is unaware of the

change in molarity of the solutions. Furthermore, we have also calculated the distributions of the angles ϕ formed by the plane normal vector of RIB and NIC molecules (see Figure 5-6(c)). We find a peak close to 0^o implying almost parallel stacking orientation between RIB and NIC moieties.

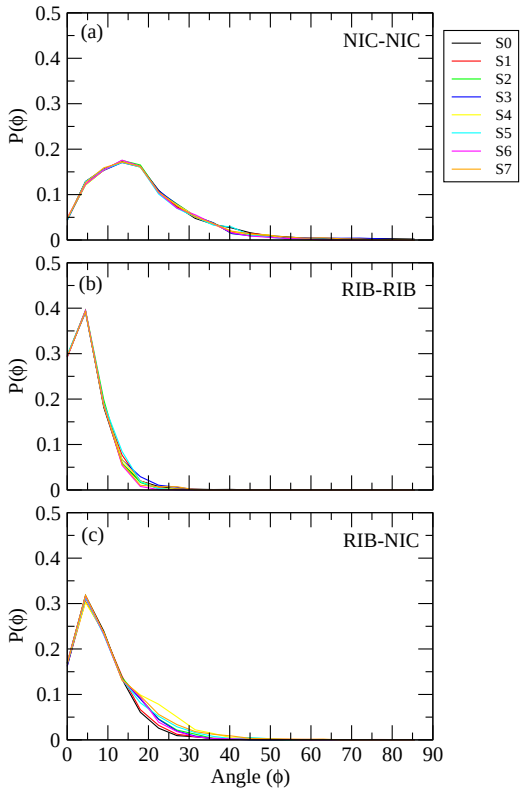

Figure 5-6. *Distributions $P(\phi)$ of the angles ϕ made by the normal vectors of two molecular planes of (a) NIC and NIC, (b) RIB and RIB and (c) RIB and NIC.*

To gain more information about the 1:2 sandwiched type complexation between RIB and NIC molecules, we have, further, performed distance and orientational analyses between the hydrotrope and drug molecules by putting some geometric criteria. A 1:2 sandwich complex is formed if these three criteria are satisfied simultaneously. (i) The plane normal vector of central RIB (RIB_{cen}) drug molecule and two complexing NIC molecules (NIC_1 and NIC_2) are in parallel orientation individually, (ii) the angle ϕ between the two molecular planes of the same two complexing NIC molecules (NIC_1 and NIC_2) is close to zero, and (iii) the distance between these two NIC (NIC_1 and NIC_2) molecules equals

to (or less than) the sum of their individual distances with RIB_{cen} molecule. Here it is important to mention that for the calculation of distance and angle between RIB and NIC molecules we do not consider those hydrotrope NIC molecules that are arranged laterally to the RIB clusters. Figure 5-7 displays the variations in the angles and distances between RIB_{cen} and NIC_1, RIB_{cen} and NIC_2 and NIC_1 and NIC_2 as the time progresses for the systems S6 and S7 (last 20 ns simulation time is considered for both these systems). We choose only the concentrated systems (S6 and S7) because in these systems, complexes (1:2) are stable for longer simulation time. The inter plane orientational angle between RIB_{cen} and NIC_1, RIB_{cen} and NIC_2 and NIC_1 and NIC_2 are close to zero. Moreover, the distance between these two complex forming NIC molecules is slightly lower than that of sum of their individual distances with central RIB molecule. So the orientational analysis alone supports the fact that RIB and NIC molecules can form simple 1:1 complex and the combination of both orientational and distance analyses lead us to conclude that RIB and NIC molecules also form 1:2 sandwiched type complex.

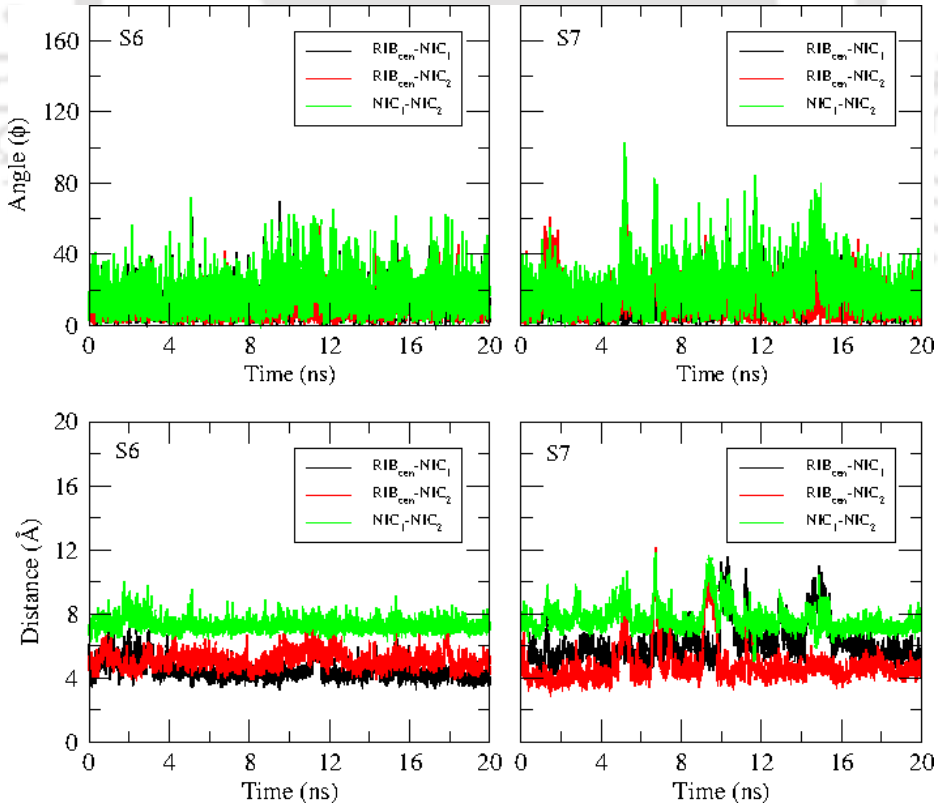

Figure 5-7. *Variations of angles and distances of complex forming central RIB and two NIC molecules for systems S6 and S7 vs simulation time.*

Cluster Structure Analysis

In order to obtain a more quantitative proof about the clustering of NIC molecules, we carry out cluster structure analysis by considering certain geometric criteria. We have estimated the number of NIC clusters and their average sizes for all the systems considered in this study. Two NIC molecules can be presumed to form a dimer if the distance between one *COM* of NIC falls within a cut-off distance of 3.25 Å of *COM* of a neighboring NIC molecule. In the same way, a trimer can be formed if the distance of *COM* of a third NIC molecule falls within the cut-off distance of the *COM* of either of the two NIC molecules of cluster size two and so on. This cut-off distance criterion is taken from the appearance of the first minimum of *COM-COM* pair-correlation function of NIC molecules. For all the systems, the distributions of different sizes of NIC clusters with respect to the total number of NIC molecules (in percentage) are shown in Figure 5-8.

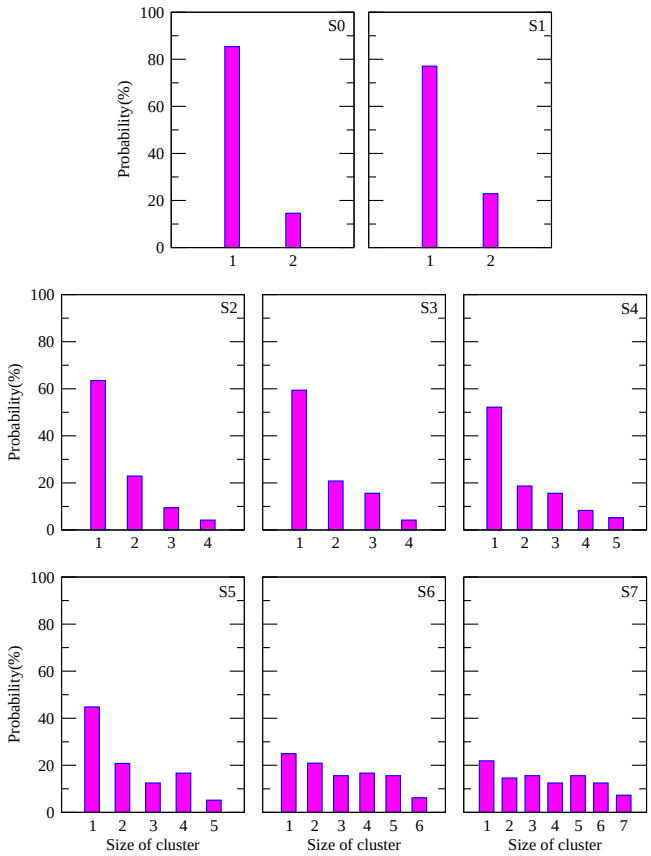

Figure 5-8. *Probability distributions (in percentage) of NIC clusters of different sizes.*

At the lowest concentration (system S0), percentage of monomers is quite high, which infers that almost all the NIC molecules are dispersed in solution. From the histograms of different systems, it is apparent that with increasing NIC concentration the probability of formation of higher order clusters (dimer, trimer, tetramer etc.) increases. Here it is to be mentioned that unlike our previous studies of anionic and cationic hydrotropes (**Chapter 2B, 3 and 4**), neutral hydrotropes do not form any large cluster. As concentration increases, NIC clusters gradually grow in size at the expense of the monomers. In this context, it is also worth to mention that we do not observe any sharp change in these cluster formations with change in concentration. Therefore, we can safely conclude minimum hydrotrope concentration (MHC) of NIC falls in a broad concentration region.

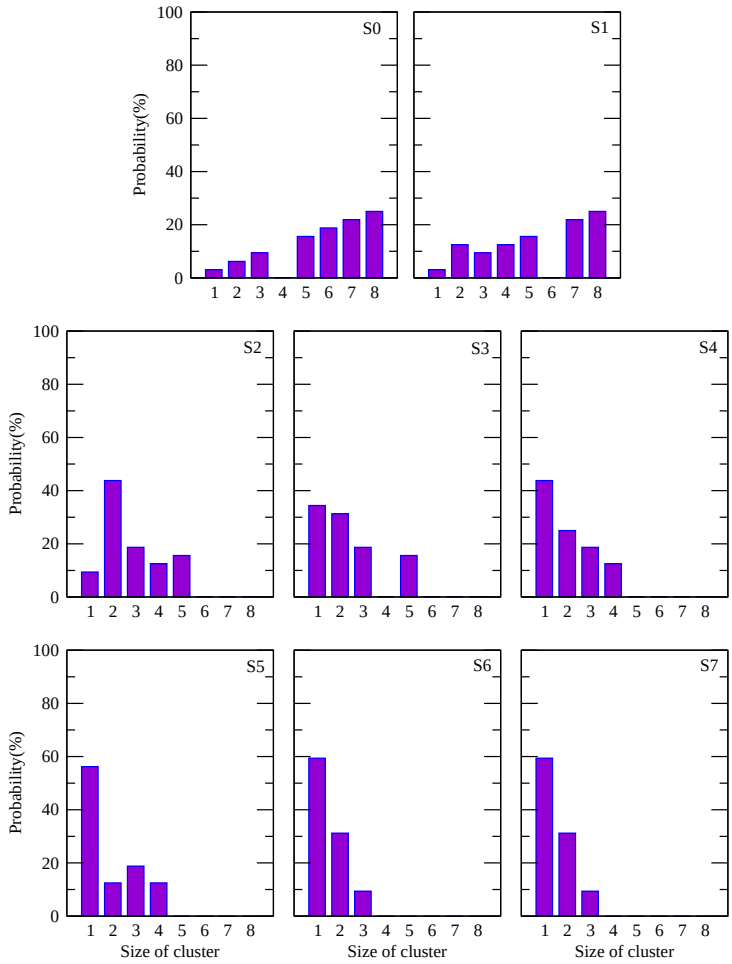

Figure 5-9. *Probability distributions (in percentage) of RIB clusters of different sizes.*

Next, we estimate the probability of formation of different sizes of RIB clusters. The calculation of different sizes of RIB clusters gives us an idea about the number of complex forming RIB molecules. In order to calculate the number of RIB clusters and their average sizes, we consider certain cut-off distance criterion. If the distance of one COM of RIB is within 4.25 Å of COM of a second RIB molecule then these two RIB molecules are considered as dimer. Similarly, a trimer RIB cluster can be acquired if the distance of COM of a third RIB molecule falls within the cut-off distance of the COM atom of either of the two RIB molecules of cluster size two and so on. We have taken this cut-off distance criterion from the position of the first minimum of COM-COM distribution function of RIB molecules (See Figure 5-3). In Figure 5-9, the distributions of different sizes of RIB clusters with respect to the formation of RIB clusters are shown. It is apparent that in system S0, the percentage of monomer is quite low and the percentage of higher order RIB clusters is quite high. But as the concentration of the solution increases, the probability of higher order cluster formation decreases whereas the percentage of RIB monomer increases. This results indicates that initially RIB molecules form clusters with themselves through stacking of their polyaromatic ring but as the concentration of the solution increases NIC molecules start to form complex with RIB molecules that causes to break the RIB clusters.

Hydrophobic Hydration

Although NIC is semi-standard non-polar molecule but it shows moderately high aqueous solubility. In order to form stacked arrangement, the exposure of the planar hydrophobic parts of NIC or RIB to water should be reduced. Therefore, to get information about the hydration of different hydrophobic moieties of hydrotrope NIC, it is important to calculate the average number water molecules that are present in the first solvation shell of a reference atomic site (coordination number, CN). The CNs are calculated by integrating the corresponding pair correlation functions using Eq. 2.3 (See Figure 5-10). In Table 5-3 we show the average number of first shell water molecules that are present around the different atomic sites of NIC molecules. It is to be mentioned that, for different systems the co-ordination numbers of C_2, C_3, C_{11} and N_{13} atomic sites of NIC molecules are only shown here since the CN values of other hydrophobic and hydrophilic atomic sites of NIC exhibit very little change with the change molarity of the solutions. It is observed that the number of first shell water molecules around the different hydrophobic and hydrophilic sites decreases with increase in concentration of the hydrotrope molecules. Remember that as we decrease the number of water molecules (to change the concentration of the systems),

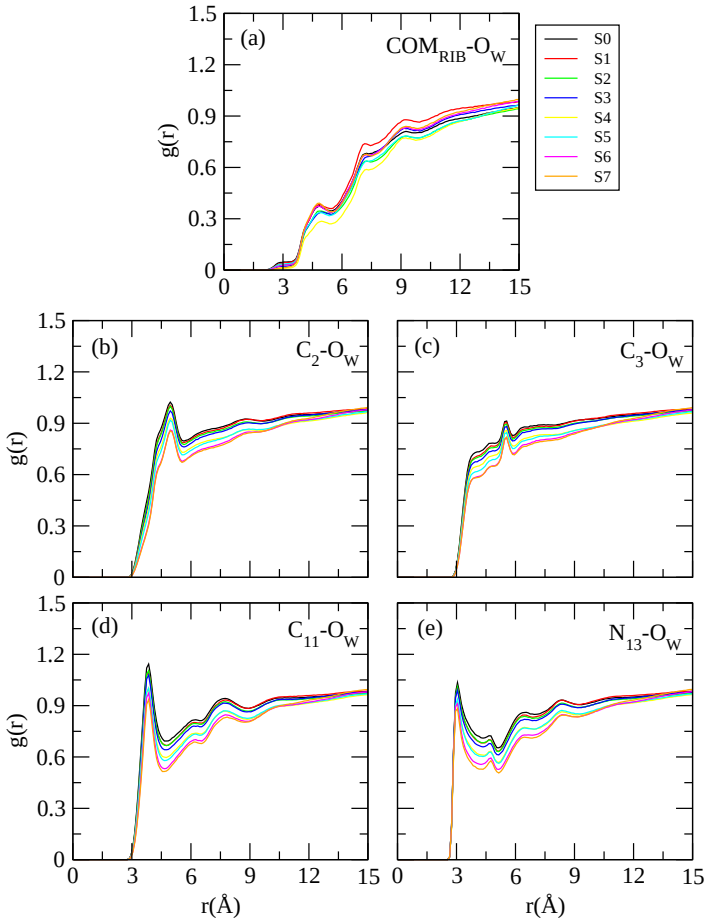

Figure 5-10. *Site site radial distribution functions between (a) COM-O_W (RIB - Water), (b) C_2-O_W (NIC - Water), (c) C_3-O_W (NIC - Water), (d) C_{11}-O_W (NIC - Water), and (e) N_{13}-O_W (NIC - Water) for different systems.*

the box volume decreases. This causes a reduction in the number density of water as one moves from system S0 to system S7. Thus a small decrease in these hydration number values is expected due to decrement in the number density of water. In order to nullify this effect, we normalize the coordination number values of different systems with reference to that of system S0 and these are also included in the parentheses of Table 5-3. With increase in molarity of the solution the difference between the *actual* and *normalized or expected* hydration number starts to rise. From this observation it is apparent that, as NIC starts to self associate through stacking of their planar hydrophobic regions, the average number of first shell water molecules around the different hydrophobic sites of NIC molecule also

decreases. Moreover, as the concentration of NIC increases, the number of first shell water molecules around the hydrophilic sites of NIC also decreases. This implies fact that as NIC begins to form clusters and surrounds the RIB clusters, the polar parts of NIC molecules also start to reorient themselves to make hydrogen bonds (or to make favorable electrostatic interaction) with RIB molecules (discussed in the following sections).

Table 5-3. Number of first shell water molecules around C_2, C_3, C_{11} and N_{13} atoms of nicotinamide molecules[a]

System	C_2	C_3	C_{11}	N_{13}
S0	17.43	22.26	9.20	7.85
S1	16.59 (17.38)	21.25 (22.19)	8.66 (9.17)	7.45 (7.82)
S2	16.09 (17.27)	20.55 (22.05)	8.57 (9.11)	7.38 (7.78)
S3	15.16 (17.11)	19.43 (21.85)	8.14 (9.03)	7.06 (7.70)
S4	13.78 (16.79)	17.74 (21.44)	7.32 (8.86)	6.36 (7.56)
S5	12.63 (16.41)	16.18 (20.96)	6.86 (8.66)	6.05 (7.39)
S6	11.04 (15.93)	14.45 (20.34)	6.14 (8.41)	5.46 (7.17)
S7	10.00 (15.02)	13.12 (19.18)	5.45 (7.93)	4.85 (6.76)

[a] The values in the parentheses indicate the first shell *normalized* coordination numbers due to change in the number density of water.

In order to gain further insight into the distribution of water density around RIB, the atomic mass density analysis is carried out. In Figure 5-11 we present the mass density maps of water oxygen atom with a cell side of 0.5 Å within 5.45 Å around eight RIB molecules for systems S0, S2, S4 and S7. For this, the correlation function involving COM of RIB and O atom of water (see Figure 5-10) is considered. We find that the water density around the stacked RIB molecules is not symmetric and water molecules prefer to stay at the periphery of RIB molecules. Water density around the hydrophobic faces above and below the stack is not observed because these faces are occupied by the stacked hydrotrope molecules. The appearance of a high water density around the periphery of the stacked RIB molecule is also observed at low concentration, which starts breaking as concentration is increased. This suggests that with increase in molarity of the solution, the water molecules around the peripheral position of RIB clusters are replaced by NIC molecules.

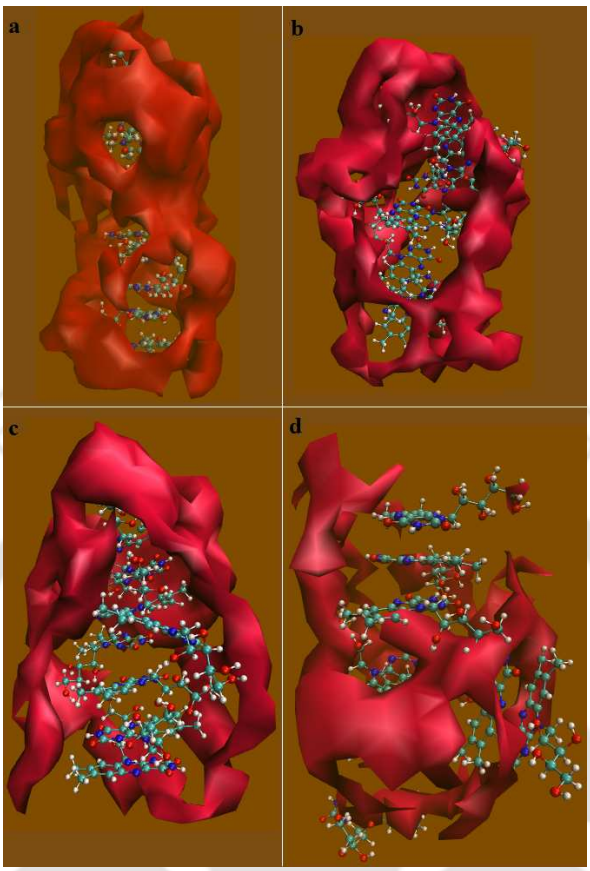

Figure 5-11. *Contours of solvent water density within 5.45 Å around RIB molecule. a, b, c and d are for systems S0, S2, S4 and S7 respectively.*

Thus, the result presented in this chapter so far demonstrates that with increase in molarity of the solution, higher order complex formation between RIB and NIC takes place and the number of NIC molecules within the first solvation shell of RIB molecules increases. This encourages us to accomplish a quantitative estimation of the number of hydrotrope NIC molecules around the first coordination shell of RIB molecules. With the help of Eq. 2.3, for different systems, the average number of NIC molecules present in the first solvation shell of RIB is calculated (see Table 5-4). To determine the average number of first shell NIC molecules around the drug molecules, we have considered the pair-correlation function involving COM of RIB and C_3 atomic sites of NIC molecule. The maximum number NIC molecules that can embed within the solvation shell of RIB is governed by the molecular geometry of NIC and the packing of RIB clusters. From the Table 5-4 it can be seen that with increasing molarity of the solution, the number of first shell hydrotrope molecules around drug increases.

Table 5-4. The number of first shell hydrotrope nicotinamide molecules around hydrophobic riboflavin molecules (CN_{Hyd}).

system	CN_{Hyd}
S0	7.84
S1	11.14
S2	13.29
S3	14.98
S4	16.71
S5	19.18
S6	21.87
S7	22.38

Hydrogen Bond Properties

The presence of –C=O and $–NH_2$ groups makes NIC to act as both hydrogen bond acceptor as well as hydrogen bond donor. Thus, NIC can form hydrogen bonds with both water and RIB molecules. Moreover, NIC-NIC hydrogen bond is also possible. The presence of two nitrogen atoms and two carbonyl groups of RIB molecule makes it a potential hydrogen bond acceptor. Again the presence of hydroxyl groups and the hydrogen atoms attached to -NH group make RIB a hydrogen bond donor also. Therefore, besides intermolecular RIB-RIB hydrogen bonds, RIB-NIC and RIB-water hydrogen bonds are also possible. Thus, six types of hydrogen bonds are possible viz. RIB-RIB, RIB-water, RIB-NIC, NIC-NIC, NIC-water and water-water. Following earlier works [93-95], we calculate the average numbers of hydrogen bonds by considering its geometric definition. If interatomic distance between the donor and acceptor atoms of a hydrogen bonding pair is less than 3.4 Å and at the same time D—A—H angle is less than 45^o, then they are considered as hydrogen bonded. In Table 5-5 we have shown the average number of hydrogen bonds between all the possible pairs. It is apparent that the average number of drug-drug, drug-water, hydrotrope-water and water-water hydrogen bonds decreases with increasing hydrotrope concentration. As already mentioned in the previous section that as we move from system S0 to S7, a modest reduction in the water number density is observed. Therefore, one can expect a modest reduction in the number of the hydrogen bonds that involve water molecules. In an attempt to nullify the effect of reduced water density, the *expected* hydrogen bond numbers are also calculated (see the parentheses of the Table 5-5). A close look into the *expected* and calculated hydrogen bond numbers reveals a very small difference between water-water hydrogen bonds. It infers that the decreased water density

mainly causes the depletion in the average number of water-water hydrogen bonds. As NIC starts to self associate and occupy the peripheral positions of the RIB clusters (by replacing the water molecules), the difference between *expected* and calculated RIB-water, NIC-water hydrogen bond number starts to rise. This makes us to propose that the high accumulation of NIC around RIB causes the exclusion of water molecules from RIB surface and this, in turn, decreases the RIB-water, NIC-water hydrogen bonds. The decrease of RIB-water and NIC-water hydrogen bonds are also somewhat compensated by the formation of RIB-NIC hydrogen bonds. A modest increase in the average number of hydrogen bonds between RIB and NIC molecules has also been observed with increase in concentration of the solution.

Table 5-5. Average number of water-water ($HB_{wat-wat}$), riboflavin-water ($HB_{RIB-wat}$), nicotinamide-water ($HB_{NIC-wat}$), riboflavin-riboflavin ($HB_{RIB-RIB}$), nicotinamide-nicotinamide ($HB_{NIC-NIC}$) and riboflavin-nicotinamide ($HB_{RIB-NIC}$) hydrogen bonds for different systems[a]

System	$HB_{wat-wat}$	$HB_{RIB-wat}$	$HB_{NIC-wat}$	$HB_{RIB-RIB}$	$HB_{NIC-NIC}$	$HB_{RIB-NIC}$
S0	3.35	8.80	3.42	0.97	0.07	0.48
S1	3.32 (3.34)	8.43 (8.77)	3.28 (3.41)	0.93	0.08	0.50
S2	3.30 (3.32)	7.89 (8.72)	3.25 (3.39)	0.90	0.09	0.56
S3	3.28 (3.28)	7.37 (8.64)	3.08 (3.36)	0.87	0.10	0.60
S4	3.25 (3.23)	6.46 (8.47)	2.84 (3.29)	0.77	0.11	0.70
S5	3.18 (3.15)	6.20 (8.29)	2.75 (3.22)	0.74	0.13	0.82
S6	3.12 (3.06)	6.01 (8.04)	2.66 (3.13)	0.68	0.14	0.94
S7	3.02 (2.89)	5.79 (7.58)	2.46 (2.95)	0.63	0.16	1.00

[a]The values in the parentheses are the *expected* number of hydrogen bonds due to change in water number density. The hydrogen bonds are shown with respect to the first species (i.e., $HB_{RIB-water}$ represents the average number of RIB-water hydrogen bonds per RIB molecule and so on).

RIB-NIC Interactions

It has been previously reported that charge transfer interactions, electrostatic forces, induction forces, hydrogen bonding and hydrophobic interactions between the complexing agent controls the complex formation [150]. It has also been observed that the electron donor-acceptor interactions (charge transfer interactions) and hydrophobic interactions are the major controlling factors in water soluble complex formations [147, 148]. Therefore, to obtain further evidence on the interactions between RIB drug molecules and NIC hydrotrope molecules in water, the total RIB-NIC nonbonded interaction energies are decomposed into van der Waals and electrostatic energy components [124]. The last 60 ns

of the production phase trajectory is considered for the analysis purpose and the results are plotted in Figure 5-12. The contribution of the electrostatic energy to the total interaction energy is lower than that of the van der Waals energy. Thus, it is the van der Waals energy, which contributes profoundly in the hydrotrope and drug interactions. This results strongly supports the fact that hydrophobic stacking interactions between RIB and NIC is contributing significantly to the RIB-NIC complex formation. We have also observed that with increasing hydrotrope concentration, both van der Waals and electrostatic components of energy become more favorable. A possible explanation is that the aggregation of NIC is enhanced by its planar hydrophobic parts, which leads to inclusion of RIB molecules into these aggregates. Again, as the concentration of NIC increases, the probability of formation of higher order complexes between RIB and NIC molecules also increases. All of these factors make the van der Waals interaction between the drug and hydrotrope molecules more favorable as hydrotrope concentration is increased. On the other hand, as NIC starts to self associate and occupy the peripheral positions of RIB clusters, the hydrophilic sites of NIC molecules also reorient themselves into inward direction to form hydrogen bonds with RIB molecules, which, in turn, strengthen the electrostatic interaction between RIB and NIC molecules.

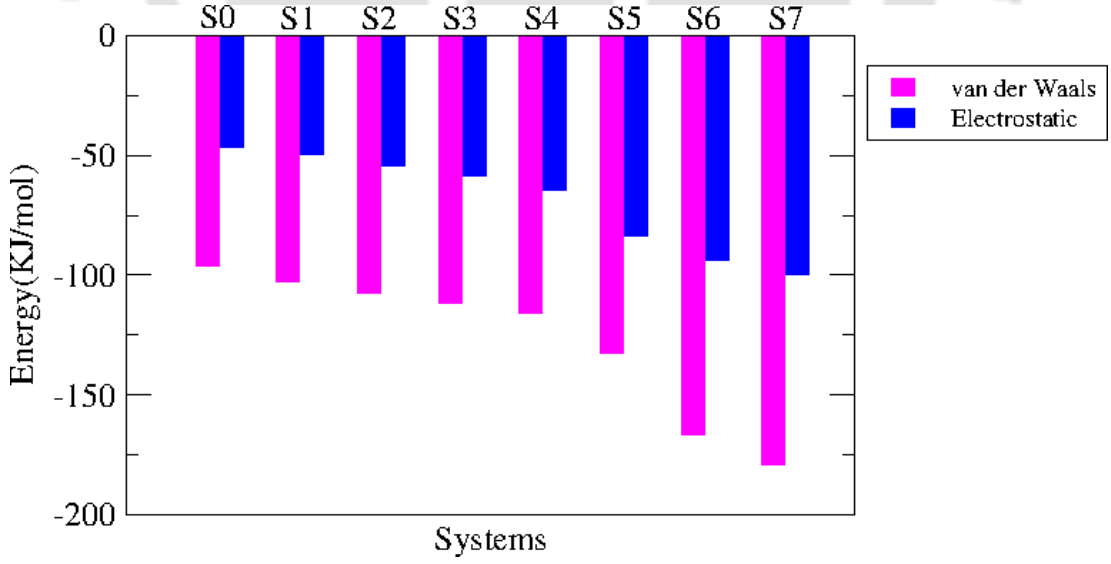

Figure 5-12. *Average van der Waals and electrostatic interaction energy between RIB and NIC.*

Flory-Huggins Interaction Parameters for RIB-NIC interactions

In order to examine the miscibility of drug-hydrotrope mixtures, we have calculated the Flory-Huggins interaction parameters between RIB and NIC molecules. As mentioned above that for this calculation, two different RIB-NIC mixtures of different stoichiometric ratios are used. The values of enthalpy of mixing (ΔH_{mix}) and Flory-Huggins interaction parameters (χ_{FH}) are -323.52 cal cm^{-3} and -47.66 respectively for 24:1 ratio whereas for the 12:1 mixture the same are -523.51 cal cm^{-3} and -77.13 respectively. Thus, in both the mixtures, we find ΔH_{mix} is negative, which implies favorable RIB-NIC interactions and the miscibility of drug-hydrotrope mixtures.

■ SUMMARY AND CONCLUSIONS

Using both classical MD simulation and MM-GBSA method, the underlying mechanisms of hydrotropic action of hydrotrope nicotinamide (NIC) on sparingly soluble riboflavin (RIB) drug molecules are investigated. In order to elucidate the effects of NIC concentration on the solubilization of RIB drug molecules, we have considered RIB-NIC-water ternary mixture of eight different NIC concentrations ranging from 0.130 to 0.931 molar of NIC at normal temperature and pressure condition. The snapshots of different systems infer that NIC molecules self-aggregate at high concentration. It also reveals that the self association of NIC occurs through stacking of their pyridine rings. We have also observed RIB and NIC complex formation in 1:1 ratio and 1:2 ratio through stacking interactions. These observations are further established by the atomic mass density analyses of NIC density around a reference NIC molecule and NIC density around the RIB clusters. Analyses of the orientational distributions between two molecular planes of NIC further supports the parallel arrangements of two NIC molecules. Combination of both orientational and distance analyses confirms the formation of 1:2 sandwich complexes between RIB and NIC molecules. From the cluster structure analysis it has also been observed that with increasing concentration, the probability of formation of higher order NIC clusters increases but the probability of large size RIB clusters formation decreases. Water molecules are also excluded from the first solvation shell of different atomic sites of the NIC molecules as concentration is increased. Atomic mass density of water around RIB clusters suggests that water molecules prefer to occupy the available hydrogen bonding sites around the periphery of RIB molecules. Furthermore, when hydrotrope starts to form clusters, water molecules that are present at the periphery of RIB clusters are replaced by the NIC

molecules. van der Waals' interaction between RIB and NIC molecules plays a vital role in the 1:1 and 1:2 complex formation between them whereas the electrostatic interaction energy also plays a crucial role in the solubilization of drug molecules. Self-association of NIC and RIB-NIC complex formation do not affect the average number of water-water hydrogen bonds. The average number of RIB-water, NIC-water hydrogen bonds decreases steadily with increasing concentration. Flory-Huggins interaction parameter (χ_{FH}) values provide a direct evidence of favorable NIC-RIB interactions.

Chapter 6

Binding Sites and Binding Mechanisms of Hydrotrope Sodium Cumene Sulfonate Encapsulated Griseofulvin Drug on γ-Tubulin Protein

"One of the most effective ways of administering a drug is to package it up in a form that can be transported around the body, and to release it exactly when and where it is needed. Many prototype drug-delivery systems have been tested, but there are still a whole host of design problems to be overcome."

– Helen Phillips *Nature News* (6 August 1998)

Overview: The protein γ-tubulin plays an important role in centrosomal clustering and this makes it an attractive therapeutic target for treating cancers. Griseofulvin, an anti-fungal drug, has recently been used to inhibit proliferation of various types of cancer cells. It can also affect the microtubule dynamics by targeting the γ-tubulin protein. So far, the binding pockets of γ-tubulin protein are not properly identified and the exact mechanism by which the drug binds to it is an area of intense speculation and research. The aim of the present study is to investigate the binding mechanism and binding affinity of griseofulvin on γ-tubulin protein using classical molecular dynamics simulations. Since the drug griseofulvin is sparingly soluble in water, here we also present a promising approach for formulating and achieving delivery of hydrophobic griseofulvin drug via hydrotrope sodium cumene sulfonate (SCS) cluster. We observe that the binding pockets of γ-tubulin protein are mainly formed by the H8, H9 helices and S7, S8, S14 strands and the hydrophobic interactions between the drug and γ-tubulin protein drive the binding process. The release of the drug griseofulvin from the SCS cluster is confirmed by the coordination number analysis. We also find hydrotrope-induced alteration of the binding sites of γ-tubulin protein and the weakening of the drug-protein interactions.

■ INTRODUCTION

Cancer is defined as a group of diseases involving uncontrolled cell growth and the spread of cells that can affect any other part of the body [155]. In recent times this disease spreads universally and it has appeared as one of the most dreaded miseries. Cancer causes about millions of death every year. 8 million lives had been devoured by this disease in 2010. The occurrence of cancer increases by 38 % since the last 20 years [156]. According to the world cancer report, around 14.1 million new cases of cancer arise worldwide [157]. As per the report of GLO-BOCAN, by 2030, the global burden is expected to grow to 21 million new cancer cases [158].

Figure 6-1. *The secondary structure of γ-tubulin protein.*

Centrosome commonly alludes to as polar corpuscle. In animal cell it functions as the microtubule organizing center. During kinesis it can administer spindle formation that assures a uniform distribution of genome [159]. Normal functioning of centrosome and successful spindle formation of non-transformed cells is controlled by the gamma tubulin (γ-tubulin) protein (See Figure 6-1), centrin etc [160]. The presence of multiple centrosome causes the multipolar spindle formation that direct the cell toward apoptosis. Presence of multiple centrosome within the same cell create a condition that is often referred to as supernumerary centrosomes. It is a crucial indication of most form of cancers [161]. The

general scheme of cells with supernumerary centrosomes to persevere and cause destruction by its demonstration as cancer is its capability to experience a phenomenon called as centrosomal clustering or centrosome clustering [162]. Thus, it becomes very important to recognize the centrosomal clustering process to prepare the strategies for its destruction. The long search for inhibitors that can inhibit the centrosomal clustering is still in its early stage of development. There are numbers of natural origin compounds reported previously that can inhibit centrosomal clustering in tumor cell both in vitro as well as in vivo [161]. In an attempt to inhibit the centrosomal clustering, the inhibitors attack the main molecular targets, which are: (1) tubulin polymerization, (2) cell cycle regulation, (3) spindle tension, and (4) ability to affect mitotic spindle. In order to get a polarized, radial array of microtubules, localization of γ-tubulin to the spindle is necessary that helps to reorganize minus end of microtubule [163]. This process confirms the natural cell divisions [164]. Hence, an effective way to inhibit the centrosomal clustering is to target the γ-tubulin protein.

Griseofulvin is a lipophilic orally active fungi-static antibiotic drug (See Figure 3-1) [114]. Recently, griseofulvin has attracted a significant interest as a potential anticancer drug because of its low toxicity and has an efficiency to inhibit the proliferation of various types of cancer cells [165-168]. It can also inhibit the growth of tumor in athymic mice [165]. It has ability to induce apoptosis in many cancer cell lines [169]. It has been observed that the griseofulvin can selectively kill the cancer cells without affecting any normal healthy cells [167]. It has also been reported that griseofulvin can inhibit the growth of fungal, plant and mammalian cells mostly by inducing unnatural mitosis and also by blocking the cells at G2/M phase of cell cycle [165-167, 170-172]. As griseofulvin shows different affinity to dissimilar tubulin, therefore, various organisms display non-identical degrees of sensitivity to griseofulvin [170, 173]. Since griseofulvin possesses much higher affinity towards fungal tubulin than the mammalian tubulin, so the concentration needed to inhibit the growth of fungal cells is much lower than the mammalian cells [170, 174-176]. Previously, it has been reported that griseofulvin can interact with tubulin [166, 176-180] and also with microtubule associated protein [177, 181]. Although, there are several studies on the $\alpha\beta$-tubulin [182, 183] suggested that tubulin is the primary target of griseofulvin but the binding mechanism, binding activity or the binding sites of novel anticancer drugs towards γ-tubulin is mostly unexplored.

Here, in this study our aim is to understand the potential binding mechanism and binding sites for griseofulvin on γ-tubulin protein. Our particular interest in this

study is that whether griseofulvin can bind with γ-tubulin protein if initially griseofulvin is in the cage of SCS clusters. We focus on this particular aspect because of the fact that griseofulvin alone (without any hydrotrope) is poorly soluble in water. Since, the presence of hydrotrope SCS molecules enhances its aqueous solubility (**Chapter 3**) it would be interesting to look at: (i) in solution whether the drug griseofulvin is released from SCS cluster and (ii) how does the presence of SCS cluster affect the drug-protein interaction provided the condition (i) is fulfilled. To understand these we perform both all atom classical molecular dynamics simulation as well as drug-protein binding free energy calculations using MM-GBSA methods. We expect that the detailed understanding of the γ-tubulin and griseofulvin interactions provide some useful insights for designing better analogues in future.

The remaining of the chapter divided into four sections. Simulation and free energy calculation details are described in simulation and methods and the methodology of binding free energy calculations sections respectively. Then results are presented and discussed and in the last section our conclusions are outlined concisely.

■ MODELS AND SIMULATION METHOD

In this study classical molecular dynamics (MD) simulation was performed to investigate the binding ability of griseofulvin drug molecules to γ-tubulin protein in presence and in absence of hydrotrope SCS. The different systems considered in this study are tabulated in Table 6-1. The initial crystal structure of γ-tubulin was downloaded from the protein data bank (PDB ID 3CB2 [184, 185]). The Insight II graphics package [186] was used to add the coordinates of the missing residues of γ-tubulin. The hydrogens attached to heavy atoms were added by using the leap program of AMBER12 package [76]. To neutralize the negatively charged γ-tubulin, 15 Na^+ counter ions were added and the N- and C- termini of γ-tubulin were capped with acetyl and methyl groups respectively, using XLEAP of AMBER12 program. The model single chain of modified γ-tubulin consists of 474 amino acid residues. The AMBERff99 force field [187] parameters were adopted for the different atomic sites of the protein molecule. For the different atomic sites of the drug griseofulvin, we used the force field parameters and the partial charges that were developed in our earlier work (**Chapter 3**). CHARMM General Force Field (CGenFF) was adopted for SCS molecules [78, 79]. To counterbalance the single negative charge carried by the sulfonate group of SCS molecule, one Na^+ counter ion was added using the XLEAP of AMBER12 package. The SPC/E model was chosen for the water molecules [77]. The stability of the

protein in pure water was investigated by immersing the protein in water in absence of any cosolute molecules (system P0). Then three different systems were prepared that contain griseofulvin drug molecule in the cage of SCS clusters (systems P4-P6) and three without SCS aggregates (systems P1-P3). In order to prepare the griseofulvin encapsulated SCS clusters, following our previous work (**Chapter 3**), initially a system was constructed that consisted of 24 hydrotrope SCS molecules and one griseofulvin molecule (in 24:1 ratio). At first all the SCS and griseofulvin molecules were placed randomly. The initial configuration of the hydrotrope-drug mixture was equilibrated in the vacuum. The vacuum simulation run was carried out in AMBER12 for 12 ns at 298 K with a time step of 2 fs. Next, a cubic box around the compacted complex was generated with the help of leap module of AMBER12 using 0 Å buffer constant in all the three directions. The voids mainly created at the corners of the cubic box, were filled up by 405 SPC/E water molecules. Then, energy of the system was minimized for 10000 steps, where first 4000 steps were performed in steepest descent minimization method and this was followed by another 6000 steps in conjugate gradient method. Thereafter, the system was heated slowly from 0 K to 298 K in a canonical ensemble (NVT). Finally, the system was subjected to 24 ns equilibration in isothermal isobaric (NPT) ensemble at 298 K and 1 atm pressure. At the end of the simulation the hydrotrope molecules adopt a micelle like structure where small hydrophobic part of SCS aggregates around the griseofulvin molecule, whereas the hydrophilic part of SCS molecule is directing towards water molecules (**Chapter 3**). From the last step of the simulated trajectory, the coordinates for SCS and griseofulvin molecules were extracted. Finally, after checking the insulation of the drug in the cage of hydrotrope cluster, these coordinates were used to prepare the systems P4-P6 for this study. In the initial starting configurations, the γ-tubulin and griseofulvin molecules were placed randomly in close contact for the systems P1-P3. In the same way, the protein and griseofulvin containing SCS cluster were placed randomly closed to each other in systems P4-P6. In each and every simulations, protein was fixed at the center of the simulation box. Therefore, a total of 7 MD simulation runs were performed with the AMBER12 package at 298 K temperature and 1 atm pressure. Using PACKMOL software [82], the initial configurations of each of these systems was constructed and the molecules were placed in a cubic box. For all the systems periodic boundary conditions were applied in all the three directions. For all the systems, to obtain proper initial structures following the methods stated above, 10000 steps of energy minimization were performed. Note that during the energy minimization, two-step minimizations were performed to relieve bad van der Waals contacts. At first the

protein was held fixed by using harmonic restraints (force constant = 6000.0 kcal mol^{-1} $Å^{-2}$) and then withdrawing the restraints on the protein. Subsequently, each of the energy minimized systems was then gradually heated from 0 K to 298 K in NVT ensemble for 320 ps using a 2 fs time step. The systems were then equilibrated for 25 ns and then the equilibrated structures were further simulated for 100 ns to generate production phase trajectories in NPT ensemble, at 298 K and 1 atm pressure. The SHAKE algorithm was used to constrain bonds involving hydrogen and heavy atoms [84]. During the simulation, the temperature of the simulation box was controlled by the Langevin dynamics method with a collision frequency of 1 ps^{-1}. In addition, the pressure was controlled by Berendsen barostat [83] using a pressure relaxation time of 2 ps. The particle mesh Ewald method was used to treat the non-bonded long ranged electrostatic interactions and for all short-ranged nonbonded interactions a cut-off distance of 12.0 Å was used.

Table 6-1. Overview of Systems[a]

System	$N_{Protein}$	N_{GSV}	N_{SCS}	N_{Water}	Box Volume(nm^3)
P0	1			25000	812.95
P1	1	1		25000	814.78
P2	1	1		25000	813.89
P3	1	1		25000	815.22
P4	1	1	24	25000	821.68
P5	1	1	24	25000	821.44
P6	1	1	24	25000	822.08

[a] N_{Protein}, N_{GSV}, N_{SCS} and N_{Water} are the number of γ-tubulin protein, griseofulvin drug, hydrotrope sodium cumene sulfonate, and water molecules respectively.

■ BINDING FREE ENERGY CALCULATIONS

In order to explore the differential binding affinity of γ-tubulin protein with griseofulvin drug molecule, for different systems binding free energies were calculated using MM-GBSA method [69]. Each of the MM-GBSA calculations was carried out with the help of Python script MMPBSA.py of AMBER12 package. The binding free energies for different systems were calculated using last 4 ns of the corresponding production phase trajectories. The free energy of complex, receptor and ligand can be estimated using the series of following equations: [183]

$$\Delta G_{bind} = G_{complex} - G_{receptor} - G_{ligand} \tag{6.1}$$

The ΔG_{bind} (without entropic contribution) can be calculated from the changes in molecular mechanical energies (ΔE_{MM}) and solvation free energy ΔG_{solv} as follows: [182]

$$\Delta G_{bind} = \Delta E_{MM} + \Delta G_{solv} \tag{6.2}$$

ΔE_{MM} is the sum of van der Waals (ΔE_{vdw}) and electrostatic (ΔE_{ele}) energies.

$$\Delta E_{MM} = \Delta E_{vdw} + \Delta E_{ele} \tag{6.3}$$

ΔG_{solv} can be calculated as (see **Chapter 1**)

$$\Delta G_{solv} = \Delta G_{GB} + \Delta G_{NP} \tag{6.4}$$

The polar component of free energy change (ΔG_{GB}) was calculated by the use of generalized-Born (GB) approach [71]. On the contrary non polar part (ΔG_{NP}) of the solvation free energy was determined by the use of following equation: [67, 71]

$$\Delta G_{NP} = \gamma(SASA) + \beta \tag{6.5}$$

where γ=0.0072 kcal/Å^2 and β=0.0, and SASA is the solvent accessible surface area.

■ RESULTS AND DISCUSSION

Root Mean Square Deviation (RMSD)

In order to examine the conformational stability of the protein during the MD trajectories, the atom positional root mean square deviations (RMSDs) of the C_α backbone atoms of the residues of γ-tubulin protein are calculated for all the systems considered here and the same are shown in Figure 6-2. The downloaded original crystal structure of γ-tubulin 3CB2 does not contain C-terminal region in its template structure. Thus, the RMSD of γ-tubulin protein of the last 28 C-terminal amino acid region of γ-tubulin displays a large increased and more fluctuated RMSD. Therefore, the RMSDs (eliminating the C-terminal region) of C_α backbone atoms starting from amino acid GLY-446 are calculated. A comparison of the RMSD values of the different systems implies that the γ-tubulin protein undergoes structural changes and its conformation deviates significantly from the initial starting conformation. The relative fluctuation in the RMSD values of C_α atom of the protein is very small for all the systems once the equilibration is attained, indicating the convergence of simulations. Further, it can also be seen that the RMSD of

γ-tubulin in pure aqueous system (P0) is almost similar with that of drug containing systems without SCS molecules (i.e., systems P1-P3), which indicates that the conformations of γ-tubulin in systems P1-P3 are almost similar to that for system P0. Concentrating on the systems with SCS-cluster encapsulated drug molecule (systems P4-P6) we observe a moderate deviation of the protein conformation from its initial conformation. Therefore, γ-tubulin conformation has achieved more stability in the drug bound states in absence of SCS molecules than the drug bound protein in presence of SCS molecules. Since, in order to check the reliability of our results, we have simulated the same system composition three times with different initial configurations and in all the cases excellent agreements have observed indicating the results presented here are trustworthy.

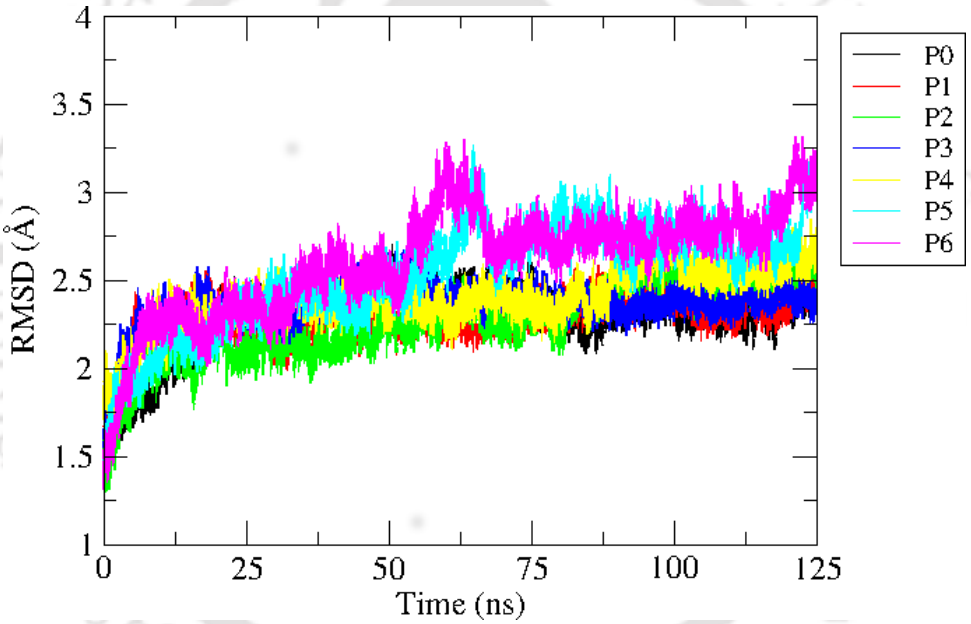

Figure 6-2. *Variations of Root Mean Square Deviations (RMSDs) of the backbone C_α-atoms of different residues of γ-tubulin protein as simulation progresses.*

Radius of Gyration

To get an idea about the compactness of γ-tubulin structure, we have further determined the radius of gyration (R_g) of γ-tubulin during the production phase MD trajectories for all the systems. R_g values actually give information about the size of the protein and that can be employed to achieve an insight to the stability of a protein throughout MD simulation trajectory. Figure 6-3 displays the R_g values versus simulation time of γ-tubulin both in pure water (system P0) and in drug bound state (systems P1 to P6). It is observed

that R_g values are stable during the simulation for all the systems. So the results basically confirm that the overall compactness and stability of γ-tubulin protein are maintained during the simulation. A comparison of all seven R_g values show that the most packed γ-tubulin structures are acquired when protein is bound with griseofulvin in absence of hydrotrope SCS molecules (systems P1-P3) and in pure aqueous system (system P0). The moderately higher R_g values of the protein for the systems P4-P6 suggest the expansion of protein conformation in the presence of hydrotrope molecules.

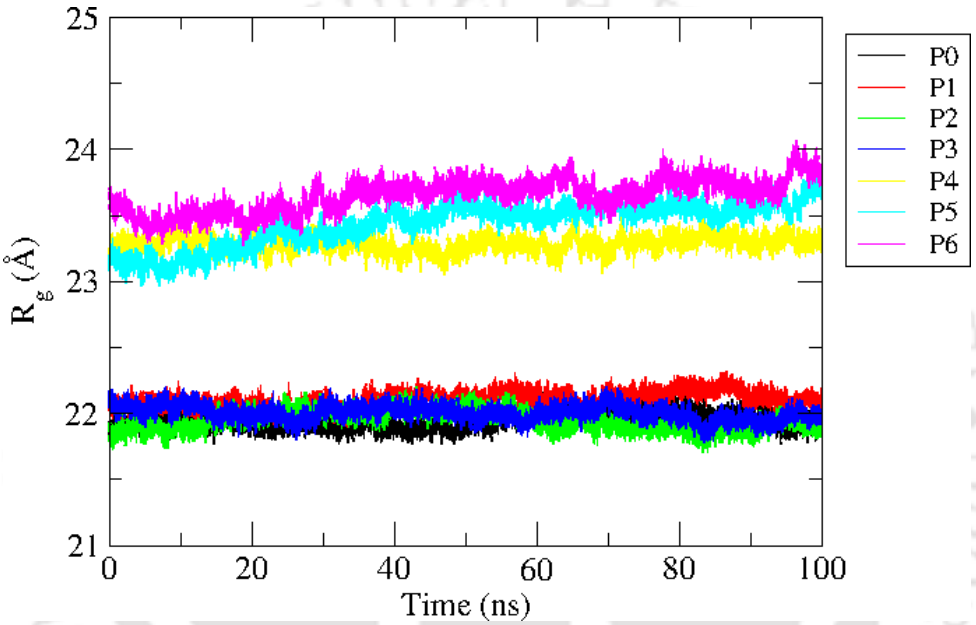

Figure 6-3. *Radius of gyration (R_g) of γ-tubulin in different systems versus simulation time.*

Solvent Accessible Surface Area (SASA)

The solvent accessible surface area (SASA) provides quantitative estimation of the surface area of the solute protein that is available to the solvent molecules. Using the Visible Molecular Dynamics (VMD) software [85], the SASA values of γ-tubulin protein for all the systems are calculated by considering a spherical probe radius of 1.4 Å throughout the protein surface. In Table 6-2 we have shown the average SASA values for all the systems. In the parentheses of the same table we have also included the standard errors of different SASA values. These standard errors are calculated by dividing the total simulation runs into five equal blocks. Then by considering independent SASA value of each block the standard errors are estimated. It is apparent that the maximum SASA value is achieved by the protein γ-tubulin for the system P6 and its smallest value is acquired for the system

P2. The smaller SASA values for the systems P0-P3 than the systems P4-P6 indicate that the protein experiences more solvent exposure in presence of hydrotrope molecules. These findings imply that SCS molecules deliver some flexibility to protein conformation that ultimately leads to a possible expansion in γ-tubulin conformation. These observations are in accordance with the estimated RMSD and R_g values of different systems discussed above.

Table 6-2. Solvent Accessible Surface Area (SASA) for different Systems[a]

System	$SASA$ (Å^2)
P0	21713.26 (±59.01)
P1	21717.26 (±59.00)
P2	21389.54 (±72.49)
P3	21569.55 (±59.44)
P4	26445.36 (±59.87)
P5	26702.29 (±41.59)
P6	26984.05 (±70.94)

[a] The numbers inside the parentheses represent standard errors that are estimated by dividing the total simulation runs into five independent blocks (see text for details).

Root Mean Square Fluctuation (RMSF)

Root mean square fluctuation (RMSF) gives important information about the local structure transformation of each residue of γ-tubulin protein. RMSF actually determines the amount of deviation of C_α atoms of each residue from its average position. It is expected that the regions of the protein that are highly flexible will display high RMSF values whereas the constrained regions will exhibit low RMSF values. For different systems, RMSFs of all C_α atoms of γ-tubulin are calculated (see Figure 6-4). For all the systems the RMSFs of C_α atoms of all the residues of γ-tubulin fall within the range of 6.0 Å. Furthermore, it is clear that γ-tubulin protein in the drug bound state either in presence of SCS molecules or in absence of SCS molecules adopts very different dynamic behavior compared to that in pure aqueous solution. The fluctuations of RMSFs of C_α atoms of most of the residues of γ-tubulin for systems P1-P6 are higher than that of system P0. A comparison of different plots of RMSFs for different systems also suggests that the γ-tubulin displays higher fluctuations in presence of SCS molecules (systems P4-P6) than that for the systems devoid of SCS. The loop joining the S9 strand and H10 helix is very flexible. As our initial γ-tubulin protein PDB structure (3CB2) does not contain 278-283

residues, therefore this loop (residue 274-289) exhibits more flexibility. Again, the opening of this loop also helps the griseofulvin drug molecule to penetrate into the binding sites that also makes it more flexible. From Figure 6-4, it is also apparent that loops joining the S7 strand and H6 helix, S13 and S14 strands, and H11 helix and S13 strand also experience increased flexibility. It is also observed that the loops joining the H7 and H8 helices, H8 and H9 helices, and S10 and S11 strands display moderate flexibility. The adjacent regions i.e., H6, H7, H8, H9, H11 helices and S7, S11, S13, S14 strands also show significant flexibility. Therefore, it can be proposed that the functionally relevant loops and adjacent helices and strands can act as drug binding sites and exhibit large RMSF values.

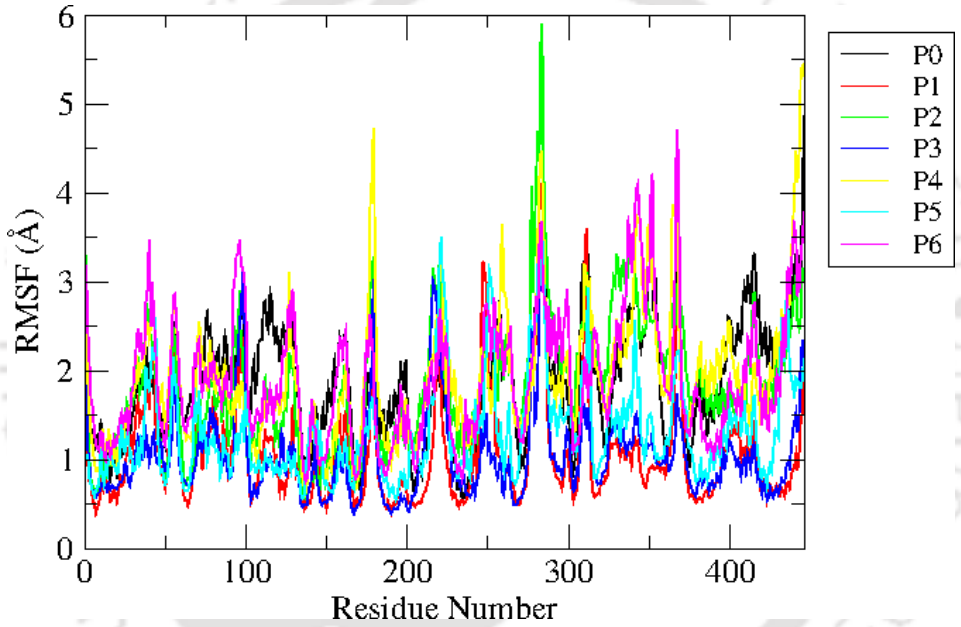

Figure 6-4. *Root Mean Square Fluctuations (RMSFs) of C_α-atoms of all residues of γ-tubulin for different systems.*

In Figure 6-5, we have presented a detailed structural comparison of γ-tubulin for the systems P0, P3 and P6. We created this figure by stereo superposition of the averaged structure of the protein for the systems P0, P3 and P6. We have considered these three systems because of the fact that one system is pure aqueous protein solution (system P0), one system contains only drug molecules (system P3) and the third one consists of encapsulated drug molecule by hydrotrope SCS. By considering the C_α atoms of γ-tubulin protein the average structure is calculated from the last 12 ns of simulation trajectories. In this figure, we highlight only those γ-tubulin residues for which the most significant structural changes occur. Larger fluctuations are perceived in the functionally relevant

residues of γ-tubulin for the systems P3 and P6 than that for the pure aqueous system i.e. system P0. The loops joining the S7 strand and H6 helix (residues 174-183), H8 and H9 helices (residues 241-252), S9 strand and H10 helix (residues 275-289), S10 and S11 strands (residues 306-314), H11 helix and S13 strand (residues 344-354), and S13 and S14 strands (residues 363-372), that are significant sites for drug binding (discussed later), exhibit maximum deviations for the systems P3 and P6. In pure aqueous system, the loops of γ-tubulin protein stay in a stable inward conformation while in other drug containing systems (systems P3 and P6) the loops extend to the outward conformation. Some other helices and strands also display small variations, which are not shown to maintain the visual clarity of the figure. We note that findings are in accordance with RMSF analyses discussed above.

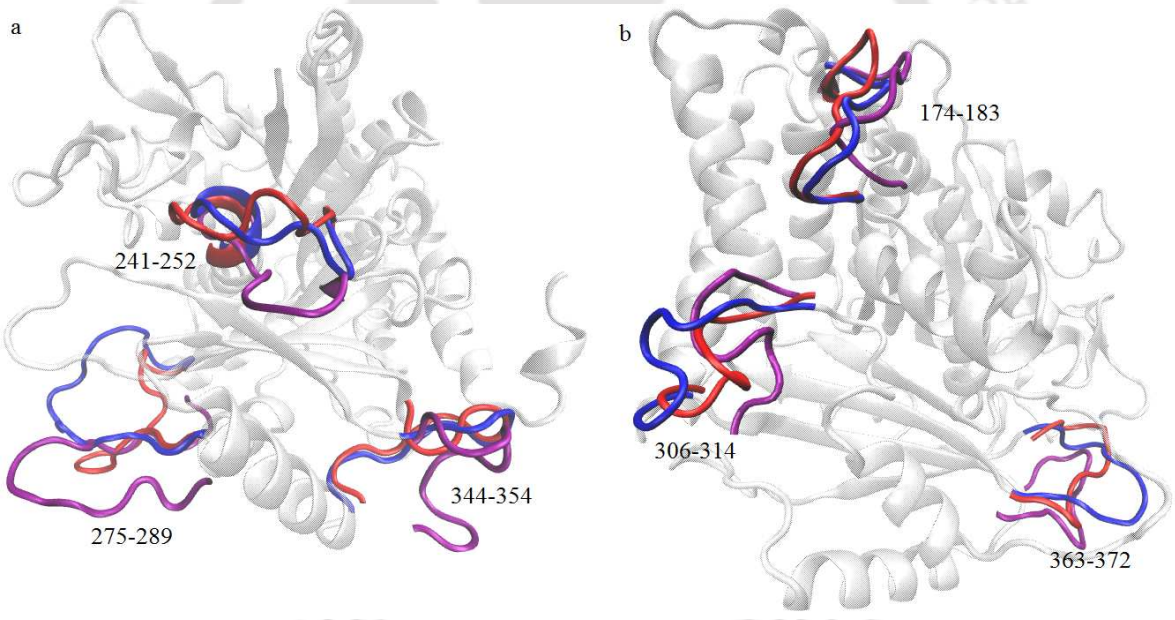

Figure 6-5. *Structural changes of γ-tubulin with respect to system P0. Time averaged structures of γ-tubulin of systems P3 and P6 are superposed on the time averaged structure of γ-tubulin of system P0. To maintain the clarity of the picture, the most significant conformational changes of γ-tubulin protein are highlighted in both the structure (a) and (b). Blue, red and purple colors refer to the different sites of the protein γ-tubulin for systems P0, P3 and P6 respectively.*

Coordination Number

In order to facilitate the interaction between drug griseofulvin and different residues of the protein γ-tubulin, the former has to be released from inside of the SCS core. This can be captured qualitatively (and indirectly) by calculating the average number of first shell SCS molecules (first shell coordination number, CN) around the drug griseofulvin for different systems. The CNs can be estimated from the site-site pair-correlation function involving center of mass (COM) of griseofulvin and C_7 atomic site of SCS molecules using Eq. 2.3. For different systems first solvation shell CNs are calculated by considering r_1=0 and r_2=the position of first minimum of the corresponding pair-correlation function and the same are shown in Table 6-3.

Table 6-3. Number of first shell SCS molecules (N_{SCS}), water molecules (N_{Water}) and γ-tubulin protein residues ($N_{Protein-Res}$) for different systems.

System	N_{SCS}	N_{Water}	$N_{Protein-Res}$
P0			
P1		1.13	20.69
P2		0.86	21.22
P3		0.74	22.02
P4	3.14	6.70	10.38
P5	2.46	6.47	11.27
P6	2.32	6.06	12.62

As stated above, in systems P4-P6, we begin the simulation with a cluster of hydrotrope comprised of 24 SCS molecules and one griseofulvin drug molecule that reside inside the cage of the cluster. From Table 6-3 it can be seen that for these systems the average number of hydrotrope molecules that are present in the first coordination shell of the drug griseofulvin are 3.14, 2.46 and 2.32 respectively. This implies that the drug molecule is being released from the cage of SCS clusters for systems P4-P6. Interestingly, though we have started with different initial configurations for systems P4-P6 but they exhibit almost similar results.

Now the question is after moving out from the cage of hydrotrope cluster whether griseofulvin molecule prefers to stay in the hydrophilic aqueous environment or in the binding pocket of γ-tubulin protein. To find out the answer of this question, we further determine the average number of first shell water molecules and average number of γ-tubulin residues around the COM of griseofulvin molecule. With the help of Eq. 2.3, we have estimated the number of first shell water molecules as well as the average number of

γ-tubulin residues that are present within 4 Å of drug molecule (see Table 6-3). We find that the numbers of first shell water molecules around the *COM* of griseofulvin are very low for the systems P1-P3 and in presence of hydrotrope molecules (systems P4-P6) these numbers increase moderately. Table 6-3 also depicts that in absence of SCS molecules the average number of protein residues around the drug molecule are 20.69, 21.22 and 22.02 for systems P1, P2 and P3 respectively, on the other hand for systems P4, P5 and P6 the same are 10.38, 11.27 and 12.68 respectively. These results clearly suggest that large number of protein residues are surrounding the drug molecule in absence of SCS molecules. A detailed comparison of the results indicate that the average number of protein residues around the griseofulvin is higher for the systems (P1-P3) that are devoid of hydrotrope molecules than the systems consist of hydrotrope SCS molecules (systems P4-P6). As in the initial configurations of the systems P4-P6, the drug containing hydrotrope cluster and γ-tubulin protein are in close contact, so the complete release of the drug molecule from the hydrotrope cluster is inhibited by the protein molecule. Moreover, since the distance between the drug and the protein in systems P4-P6 is relatively higher (due to encapsulation) than that for the systems P1-P3, the interactions of griseofulvin with possible binding residues of γ-tubulin protein is getting reduced for the former systems as a result of which number of protein residues around the drug griseofulvin molecule decreases. Nevertheless, we find that there are considerable number of protein residues in the first solvation shell of the drug molecules for the systems P4-P6. This clearly suggests that the drug griseofulvin once released from the hydrotrope encapsulation can interact with the protein residues.

In order to gather information about the possible binding pockets of γ-tubulin protein, we have considered the residues of γ-tubulin protein that are within 4 Å distance of griseofulvin. In an attempt to do so, we have implemented certain criteria. The cut-off distance between the *COM* of the griseofulvin molecule and any heavy atom of a residue of the protein should be within 4 Å and simultaneously, the residence time of a residue of γ-tubulin protein (which is lying within 4 Å distance of the griseofulvin molecule) should be more than 2.5% of the production phase trajectory. Table 6-4 shows the residues that fulfill these two criteria simultaneously for systems P1-P6. Residence times of different residues allow us to compare the most probable binding sites of γ-tubulin protein with griseofulvin. Note that, Efferth et al. [161] did the molecular docking study of γ-tubulin protein and griseofulvin drug molecules. They reported that the griseofulvin drug molecule binds with ASN-250 and LEU-360 residues of γ-tubulin protein.

Table 6-4. Residues of γ-tubulin that are present within the 4 Å distances of griseofulvin molecule[a]

System	
P1	LEU-164 (56.83), GLN-166 (94.27), TYR-168 (22.99), ASP-199 (17.42), CYS-200 (99.98), SER-238 (90.27), THR-241 (86.48), LEU-242 (29.85), TYR-247 (26.13), MET-248 (2.63), ASN-250 (45.37), ASP-251 (60.43), LEU-252 (99.99), ILE-253 (24.60), LEU-255 (99.63), ILE-256 (99.99), LEU-259 (80.83), ILE-260 (80.22), HIE-266 (73.34), LEU-268 (99.99), ALA-318 (46.46), ILE-319 (41.64), LEU-320 (99.99), ILE-322 (93.86), ALA-358 (75.00), MET-377 (99.72), ASN-379 (42.32)
P2	ARG-2 (77.37), GLU-3 (98.44), ILE-4 (99.77), THR-6 (9.59), PHE-20 (93.29), VAL-49 (42.83), PHE-50 (98.78), GLU-132 (99.93), GLY-133 (92.89), PHE-134 (64.16), VAL-135 (99.91), LEU-164 (33.82), GLN-166 (99.95), THR-167 (61.85), TYR-168 (99.96), CYS-200 (28.25), LEU-201 (28.38), VAL-202 (99.96), MET-235 (99.31), SER-238 (99.93), THR-239 (99.96), THR-240 (21.73), THR-241 (97.61), LEU-242 (99.95), LEU-252 (99.97), LEU-255 (61.01), ILE-256 (83.44), LEU-259 (4.53), MET-377 (78.65)
P3	ILE-4 (41.06), THR-6 (91.92), PHE-20 (71.16), PHE-50 (99.95), VAL-135 (99.93), LEU-136 (4.36), CYS-137 (11.21), GLN-166 (97.86), TYR-168 (99.83), THR-167 (4.85), CYS-200 (53.85), VAL-202 (99.95), ILE-234 (99.98), MET-235 (99.85), SER-238 (99.98), THR-239 (99.97), THR-241 (48.08), LEU-242 (99.96), ASN-250 (5.01), LEU-252 (99.52), LEU-255 (99.76), ILE-256 (99.88), LEU-259 (74.47), LEU-268 (99.99), MET-269 (4.94), THR-270 (99.91), ILE-322 (4.23), LEU-375 (87.77), MET-376 (3.70), MET-377 (99.98), ALA-378 (3.40)
P4	ARG-2 (45.55), GLU-132 (42.73), LYS-162 (3.18), LYS-163 (3.09), LYS-164 (99.99), VAL-165 (4.28), GLN-166 (89.52), TYR-168 (52.96), ASP-199 (60.42), CYS-200 (83.06), LEU-252 (99.93), ILE-253 (97.97), GLY-254 (15.02), ILE-256 (76.07), ALA-257 (94.52), PRO-263 (64.81)
P5	ARG-310 (19.22), ASN-313 (6.09), HIE-314 (6.30), CYS-315 (98.40), ILE-317 (8.29), ALA-343 (4.20), ASN-346 (21.03), PHE-347 (25.49), ILE-348 (96.58), PRO-349 (99.70), TRP-350 (99.99), THR-381 (76.44), SER-382 (19.70), ASN-434 (64.15), HIE-435 (14.42), ALA-437 (97.68), THR-438 (99.15), ARG-439 (94.51), PRO-440 (97.88)
P6	PRO-261 (6.45), THR-262 (6.69), LEU-265 (72.37), ARG-310 (5.93), HIE-314 (20.94), CYS-315 (70.98), TYR-316 (7.13), ILE-317 (99.96), ALA-343 (5.02), ALA-345 (88.08), ASN-346 (95.07), PHE-347 (91.09), ILE-348 (99.90), PRO-349 (83.56), TRP-350 (81.19), ASN-379 (9.88), THR-381 (92.66), SER-382 (6.08), ALA-437 (86.33), THR-438 (97.14), ARG-439 (80.64), PRO-440 (88.80)

[a]Values in the parentheses represent the percentage of residence time of the corresponding residues of γ-tubulin protein around the drug.

Other than this study, since there is no conclusive evidence of the binding sites, therefore, the simulations presented here constitute an extensive search for griseofulvin binding sites of γ-tubulin protein. We have found multiple binding sites of γ-tubulin protein for griseofulvin drug in different systems. In system P1, griseofulvin binds to H8, H9 helices and S7, S8, S9, S11, S13, and S14 strands. Griseofulvin is also observed to bind with loops joining the H6 helix and S8 strand, H8 and H9 helices and H9 helix and S9 strand in system P1. Binding to H1, H8, H9 helices and S1, S6, S7, S8, S14 strands is also observed in system P2. As, shown in Table 6-4, griseofulvin can also bind with loops joining the H1 helix and S2 strand, H8 and H9 helices. In system P3, we notice that γ-tubulin protein contains a binding pocket surrounded by β sheets S1, S6, S7, S8, S9, S12, and S14, alpha helices H8 and H9 and loops joining the helices H8 and H9. Although systems P1, P2 and P3 possess different initial starting configurations but they show similar binding patterns. In system P4, binding sites of griseofulvin are three beta sheets S6, S7 and S8, one helix H9, and two loops joining the H8 and H9 helices and H9 helix and S9 strand. S11, S14 strands and H13 helix, and loops joining the S10 and S11 strands and H11 helix and S13 strand come in close contact with griseofulvin drug molecule in system P5. In system P6, the griseofulvin drug molecule makes a contact with S11, S14 strands and H13 helix, and loops joining the H9 helix and S9 strand, S10 and S11 strands and H11 helix and S13 strand. Here also we have found an agreement in the griseofulvin binding sites of γ-tubulin for systems P4, P5 and P6. It is interesting to note that though all the binding sites of griseofulvin on γ-tubulin protein are not the same in all the systems (P1-P6) but they possess major similarity. Moreover, here it is worth to mention that our simulated results are in accordance with molecular docking results published elsewhere [161]. We also find that griseofulvin binding sites are remarkably consistent with that for colchicine binding on γ-tubulin protein [188].

Binding sites are also identified by constructing visualizing snapshots, averaged over frames from the last 12 ns of the simulation (see Figure 6-6). In system P1, the most probable contact residues lies in H8, H9 helices, S7, S8, S9, S11, S13, S14 strands and loops joining the H6 helix and S8 strand, H8 and H9 helices and H9 helix and S9 strand. From Figure 6-6(b) it can be seen that griseofulvin's most preferable location is in a core that is surrounded by H1, H8, H9 helices and S1, S6, S7, S8, S14 strands. Moreover, the loops joining the H1 helix and S2 strand, H8 and H9 helices of the γ-tubulin are in close contact with griseofulvin drug molecule. In system P3, the griseofulvin is found to occupy almost the similar position in γ-tubulin protein cage that we have found in systems P1 and P2.

Figure 6-6(d) shows that S6, S7 and S8 strands H9 helix and loops joining the H8 and H9 helices and H9 helix and S9 strand are in close contact with griseofulvin drug molecule. In system P5, contact residues located in S11, S14 strands and H13 helix, and loops joining the S10 and S11 strands and H11 helix and S13 strand. Figure 6-6(f) displays that the binding sites for griseofulvin in system P6 are consistent with that for system P5.

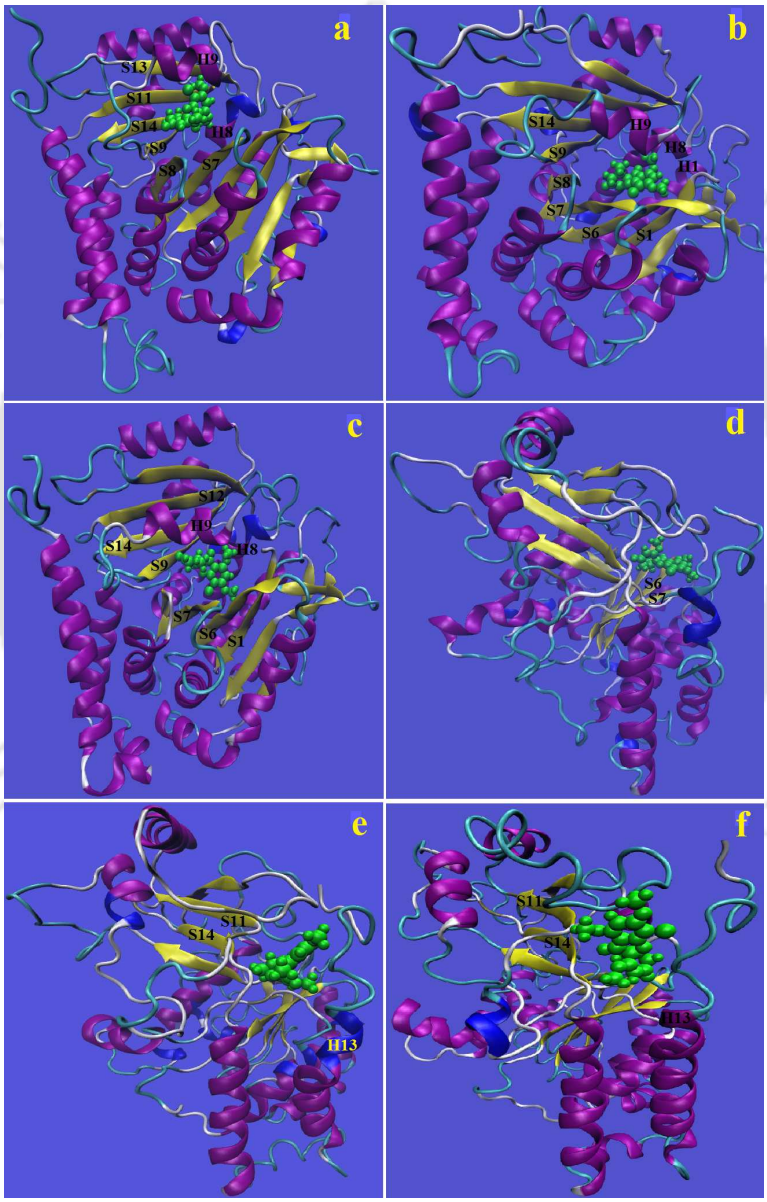

Figure 6-6. *Binding motif of griseofulvin in γ-tubulin. The drug-protein complex is created by averaging the last 12 ns of simulated trajectory. (a) System P1, (b) system P2, (c) system P3, (d) system P4, (e) system P5 and (f) system P6.*

Hydrogen Bond Properties

To obtain more direct information about the interactions between the drug and protein binding sites, we have carried out hydrogen bond analysis between these two moieties. Our analysis reveals the key amino acids at the active binding centers of γ-tubulin protein with which griseofulvin forms hydrogen bonds. Only those hydrogen bonds are included in the Table 6-5 whose occupancy is more than 1%.

Table 6-5. Hydrogen bonding interactions between griseofulvin (GSV) and different residues of γ-tubulin protein[a]

System	Hydrogen Bonding Interactions			
	Atoms Involved 1-2-3	Bond Distance	Bond Angle	Occupancy
P1	GSV-O2-HE22-NE2-GLN-166	2.916	31.82	34.68
	GSV-O4-HE21-NE2-GLN-166	3.164	47.94	9.79
	GSV-O2-HE21-NE2-GLN-166	2.961	35.16	9.14
	GSV-O4-HG-OG-SER-238	3.224	46.78	1.14
P2	GSV-Cl-HE22-NE2-GLN-166	3.274	43.20	18.24
	GSV-Cl-HE21-NE2-GLN-166	3.233	41.58	11.95
	GSV-O1-HE21-NE2-GLN-166	3.249	46.71	5.46
	GSV-O2-HG-OG-SER-238	3.038	32.89	2.23
P3	GSV-O6-HG-OG-SER-238	3.177	36.73	4.32
	GSV-O2-HG-OG-SER-238	2.909	30.83	3.86
	GSV-O4-HG-OG-SER-238	3.159	34.03	1.72
	GSV-O1-HE21-NE2-GLN-166	3.142	38.13	1.16
P4	GSV-O5-HE22-NE2-GLN-166	2.962	37.98	4.32
	GSV-O5-HE21-NE2-GLN-166	2.995	36.95	1.64
	GSV-O2-HE21-NE2-GLN-166	3.195	45.79	1.09
P5	GSV-O3-HD21-ND2-ASN-346	3.113	22.75	5.54
	GSV-O5-HE2-NE2-HIE-314	3.052	41.04	3.94
	GSV-Cl-HE1-NE1-TRP-350	3.293	53.32	2.46
	GSV-O5-HG1-OG1-THR-381	2.969	21.94	1.06
P6	GSV-O3-HG1-OG1-THR-381	3.115	36.29	10.35
	GSV-Cl-HG1-OG1-THR-381	3.304	36.03	8.99
	GSV-O5-HD21-ND2-ASN-346	3.029	31.27	4.54
	GSV-O5-HG-OG-SER-382	3.358	59.27	1.32
	GSV-O4-HE1-NE1-TRP-350	3.258	37.54	1.06

[a]Bond distance (in Å) refers to donor-acceptor cut-off distance and the bond angle (in Degree) is donor - H - acceptor cut-off angle. Occupancy (in %) represents percentage of simulation time occupied by a particular hydrogen bond.

The analysis shows that in absence of hydrotrope molecules (i.e., systems P1-P3) griseofulvin bounds with GLN-166 and SER-238 residues of γ-tubulin protein through hydrogen

bonding interactions. In system P1, griseofulvin forms three hydrogen bonds with GLN-166 and one hydrogen bond with SER-238 residue. Of the four hydrogen bonds, the carbonyl group that is attached to five membered heterocyclic ring of griseofulvin drug molecule forms the most stable hydrogen bonds (occupancy 34.68%). In system P2 and P3, griseofulvin also form four hydrogen bonds with GLN-166 and SER-238 residues but they exhibit relatively low occupancy. A close examinations of these results reveal that it is mainly the GLN-166 residue of γ-tubulin protein which shows maximum hydrogen bonding interactions ability with griseofulvin drug molecules in absence of hydrotrope SCS molecules. In contrast griseofulvin forms hydrogen bonds with multiple residues of γ-tubulin protein in presence of hydrotrope SCS molecules (systems P4-P6). Moreover, these hydrogen bonds display very low occupancy. Only in system P6, griseofulvin forms moderately stable hydrogen bonds with THR-381 residue of γ-tubulin. These results further infer that hydrotrope molecules hinder the hydrogen bonding interactions and weaken the polar interactions between the γ-tubulin protein and griseofulvin drug molecule.

Binding Free Energy

The binding free energy (ΔG_{bind}) between γ-tubulin protein and griseofulvin for different systems are tabulated in Table 6-6. The binding energy between the drug and protein is more favorable for systems without hydrotrope than that containing hydrotropes. This supports our coordination number analysis discussed above. As the number of protein residues around the drug griseofulvin increases binding ability between protein and drug also increases. Moreover, the drug griseofulvin alters its binding motif to γ-tubulin in presence of SCS clusters. In systems P4-P6 as the protein and SCS cluster are in close contact, the complete release of drug from hydrotrope clusters is difficult. Therefore, the binding ability of griseofulvin to γ-tubulin protein is getting decreased for systems P4-P6. Remarkably, pure drug containing systems i.e systems P1-P3 show very similar binding energies and in presence of hydrotrope molecule i.e for systems P4-P6 the binding energies between the γ-tubulin protein and griseofulvin are also close to each other.

Table 6-6 also lists the values of the components of the binding free energy (ΔG_{bind}). The van der Waals energy component (ΔE_{vdw}) of drug-protein interactions makes the maximum contribution to the binding free energy. The electrostatic energy (ΔE_{ele}) and the nonpolar solvation free energy (ΔG_{NP}) are also favorable for binding. On the contrary the polar component of the solvation free energy (ΔG_{GB}) is unfavorable for binding. Although, both van der Waals and electrostatic energy components play significant roles in binding free

energy but it is mainly the hydrophobic contacts between the protein residues and the drug that make the binding favorable. As the number of first shell hydrotrope molecules around griseofulvin increases, the hydrophobic contacts between protein and drug also decreases. It explains the reason behind the lower (less favorable) van der Waals interaction energy for systems P4-P6 compared to that for systems P1-P3. Interestingly, the contribution ΔE_{ele} to ΔG_{bind} for hydrotrope containing systems P4-P6 is negligible. This finding acts as a corroborative evidence of what we have observed in the calculations of drug-protein hydrogen bonds discussed above.

Table 6-6. Binding free energies (ΔG_{bind}) of γ-tubulin protein with griseofulvin for different systems[a]

System	ΔE_{vdw}	ΔE_{ele}	ΔG_{GB}	ΔG_{NP}	ΔG_{bind}
P1	-45.09	-9.36	16.36	-4.95	-43.04
P2	-47.33	-11.32	20.08	-5.75	-44.32
P3	-51.39	-11.14	20.80	-5.65	-47.38
P4	-31.22	-3.10	11.92	-2.89	-25.29
P5	-32.28	-2.12	11.00	-3.19	-26.59
P6	-32.97	-2.93	11.66	-3.63	-27.87

[a] ΔE_{vdw} and ΔE_{ele} are the van der Waals and electrostatic energies respectively, whereas ΔG_{GB} and ΔG_{NP} represent the polar and non-polar solvation free energies respectively. All values are in kcal mol^{-1} unit.

■ SUMMARY AND CONCLUSIONS

In this study, we have investigated the drug binding ability and drug binding mechanism of γ-tubulin protein in presence and in absence of hydrotrope molecules using all atom MD simulations. Results give the details of structural changes of γ-tubulin protein due to interactions with hydrotrope or binding with drug molecule. Detailed analysis of the results suggests that the γ-tubulin proteins are more flexible in presence of hydrotrope molecules than when devoid of hydrotropes. Remarkably, in absence of hydrotrope molecules the conformational stability of protein is almost same as that in pure aqueous solution. Radius of gyration and SASA analysis also showed that γ-tubulin protein achieved more stable conformation in absence of hydrotrope molecules. The most noticeable changes in γ-tubulin protein, caused due to binding of drug griseofulvin, is observed in the functionally relevant loops of the protein. RMSF and average structure analysis showed that loops joining the S7

strand and H6 helix, H8 and H9 helices, S9 strand and H10 helix, S10 and S11 strands, H11 helix and S13 strand, and S13 and S14 strands undergo the largest conformational changes. These loops are crucial for binding of griseofulvin drug molecules. From the analysis of coordination number it can be inferred that the hydrotrope SCS cage does not prevent the drug from interacting with the protein. Further, these analyses also implies that the number of protein residues surrounding the griseofulvin drug molecule is higher in absence of hydrotrope molecules, indicating the stronger drug receptor interactions. The residues around the griseofulvin in different systems also predict the possible binding pockets of drug molecule. We further find more information about the binding pockets and binding motifs of griseofulvin with γ-tubulin protein from hydrogen bond analysis. The calculations of MM-GBSA suggest that the van der Waals, electrostatic and non polar solvation free interactions play important roles in the binding of griseofulvin with γ-tubulin protein for all the systems considered in this study. But, it is the drug-protein van der Waals interaction, which plays a dominant role. We find that the initial distance between the protein and drug could affect their binding interactions and the hydrotrope cluster also causes weakening of the drug-protein interactions. Thus, our results clearly demonstrate that the drug-protein interaction is not affected much in presence of SCS molecules. The only effect that one could see due to the encapsulation is that, the presence of SCS cluster in the starting configurations for systems P4-P6 causes the binding of the drug to different binding pockets of the protein when compared to systems without SCS clusters (systems P1-P3). Bearing in mind that there is no conclusive definitive answer for the possible binding sites of the protein γ-tubulin for the drug griseofulvin. In our opinion, proper systematic experimental works must be carried out in order to identify the actual binding sites of the protein for the drug griseofulvin. Remember that the drug griseofulvin used in this study is sparingly soluble in water and in our previous study we showed the enhancement in its solubility in water in presence of hydrotrope SCS (see **Chapter 3**). Thus, the results presented in this chapter can definitely shed some lights on how does the encapsulation alter the drug-protein interactions. Nevertheless, our study not only provides molecular level mechanism and binding affinities of griseofulvin drug molecule in different systems but also delivers a detailed insight about the drug releasing ability of hydrotropic clusters. The results presented here could help in the drug designing and drug delivery approaches in future.

Chapter 7

Summary and our View on the Hydrotrope-Induced Solubilization of Sparingly Soluble Drug Molecules

"The appeal of MD simulations is due to their ability to provide realistic descriptions of the actual molecular motions, and the ability to simulate the time evolution of reactive trajectories is very useful. Furthermore, MD simulations appear to provide a simple and effective way of averaging over protein configurations and obtaining the free energies that control biological functions."

– Arieh Warshel *Acc. Chem. Res.* **35**, 385 (2002)

The aim of this work is to gain an insight and a deeper understanding of the effect of hydrotrope on the solubility of sparingly soluble drug molecules. To explore the mechanisms of hydrotropy we have investigated different structural and thermodynamical properties of the drug-hydrotrope mixtures. Interaction energies between the drug and hydrotrope and interactions with the solution species of the hydrotrope and the drug are explored as well. Flory-Huggins theory has been employed which has helped us to achieve the reason behind the enhanced solubilization.

We have started the investigations by classical MD simulation of an anionic hydrotrope SCS in pure aqueous solution. In literature the experimental study on the self-aggregation behaviors of SCS against concentration and temperature are available. MHC of the anionic hydrotrope is studied by estimating partial and apparent molal volumes of SCS solution. The study reveals that MHC region of SCS falls within the range of 0.185 to 0.370 m. The study also finds that SCS aggregates form more close packed structure than the classical surfactant. In support of this, we have shown osmotic coefficients value for different systems. The calculations of molal expansibility at infinite dilution confirms the water structure breaking ability of SCS molecules. In support of this, we have shown rdfs between oxygen atoms of water. To explain the origin of self-aggregation above MHC level, we have calculated site-site distribution functions of water and SCS molecules. We found that at a fixed temperature, there is a depletion in the number of water molecules around the small hydrophobic tail of SCS molecules with increasing concentration of binary mixture. We also notice the dehydration of hydrophobic tail of SCS with increasing temperature. A further investigation of solvent water density around the hydrophobic tail of SCS molecules suggests that the interaction between the hydrophobic tails of different SCS molecules contributes to SCS aggregate formation. As temperature increases, we have observed more self-accumulation of SCS molecules. The investigation of hydrogen bonds formed by the SCS and water molecules showed that SCS aggregates do not affect the water-water or SCS-water hydrogen bonds. A bimodal type distribution between the polar headgroup oxygen of SCS and sodium ion indicate the presence of a dual charge layer around the polar headgroup of SCS. The overall conclusion from the study can be given as follows. Anionic hydrotrope molecules self-associate among themselves through their small hydrophobic tail to form organized aggregates or clusters in bulk solution above the MHC.

To obtain atomic-level picture of the mechanism of hydrotropic action of hydrotropes on purely hydrophobic molecules, classical MD simulation of the anionic hydrotrope SCS and hydrophobic solute DTBM is carried out. To explain the concentration

dependent self-aggregation behavior of SCS different structural properties are analyzed first. To be more specific above MHC, SCS starts to self-associate and it creates a miceller like structure where the hydrophobic tail part of SCS points inward while its hydrophilic sulfonate group points outward to make favorable contact with polar solvent water molecules. Our study reveals that SCS clusters create a hydrophobic core and DTBM molecules get incorporated into this hydrophobic environment. This encourages us to examine the size of SCS clusters and the number of DTBM molecules that are encapsulated in SCS clusters. We observe that the formation of higher order SCS clusters at and above the MHC level and the number of DTBM molecules that are incorporated in the core of SCS cluster shows a sharp jump as soon as SCS clusters begin to form. Exclusion of water molecules from the DTBM solvation shell is observed with increasing hydrotrope concentration. Water density around hydrophobic solute decreases due to the replacement of water molecules from this region by SCS molecules. SCS aggregates do not affect the hydrogen bond properties of water. The Flory-Huggins interaction parameter calculations confirm the very favorable SCS-DTBM interactions and the miscibility of a two component system. The significant importance in the context of hydrotrope-induced DTBM solubilization is the hydrotrope aggregates that promote the solubility of the insoluble molecules by incorporating the insoluble solutes into the cage of these hydrotrope clusters.

The MD simulation study on the effect of anionic SCS hydrotrope on the solubility of sparingly soluble griseofulvin drug molecules under eight different concentration gives rise to following conclusions. MHC of SCS in aqueous phase is found to be essential for the initiation of the hydrotropic solubilization of griseofulvin. The solubilization effect of hydrotrope increases with increase in hydrotrope concentration. The increase in the solubilizing effect of hydrotropes SCS with increase in hydrotrope concentration is due to the availability of more SCS clusters for incorporation of the insoluble griseofulvin molecules. It is also noticed that the hydrotropic small tail of SCS molecules contribute to SCS aggregate formation. This suggests the formation of a more hydrophobic environment in the inner core of SCS clusters and drug griseofulvin molecules get incorporated into it. Furthermore, when SCS start to form cluster, the number of encapsulated griseofulvin molecules in the inner core of SCS cluster exhibits a sharp jump. Above MHC level almost all griseofulvin molecules are encapsulated into the SCS clusters of size three or higher. We have observed that water molecules are replaced from griseofulvin surface by the SCS molecules. These results indicate direct interaction of griseofulvin with SCS has an important role in the solubilization process. van der Waals interaction energy between the

drug and hydrotrope molecules guides the solubilization process. The analyses of hydrogen bond properties of SCS and griseofulvin with the water molecules show that though SCS aggregate does not have much effect on the average number of water- SCS hydrogen bonds but it has an influence on the average number of water-griseofulvin hydrogen bonds. From the estimated value of enthalpy of mixing, Flory-Huggins interaction parameter has been calculated, which extends the details about the favorable interaction between hydrotrope SCS-drug griseofulvin in the mixture. The high negative χ_{FH} value indicates a very favorable interactions between SCS and griseofulvin molecules and explains successfully the reason behind the incorporation of drug griseofulvin into the core of SCS clusters. So the overall conclusion from this study is that the unprecedent increase in the solubilizing effect of anionic SCS hydrotropes above MHC is due to the formation of organized aggregates of hydrotrope molecules at this particular concentration.

Next we explore the mechanism of cationic hydrotrope PTOL induced solubilization of sparingly soluble GLC drug molecules using classical MD simulation technique. Cationic hydrotrope PTOL shows tremendous potential to undergo self-association in water. On the same lines, a threshold value, which is nothing but MHC is found necessary to increase the solubility of insoluble solutes. MHC values of PTOL range between 0.177 to 0.342 molar. It is observed that the aggregation of PTOL increases with increase in hydrotrope concentration and a mixed miceller like environment is created in which GLC molecules get incorporated. The hydrophobic small tail part of most of the PTOL molecule direct towards the inside whereas in order to make favorable contact with water molecules its hydrophilic ammonium group points outward. But, in order to make hydrogen bonds with GLC molecules the polar groups of few of the hydrotropes direct inward also. A quantitative estimation of sizes of different PTOL clusters in different systems reveals the formation of higher order clusters at and above the MHC level. A close look into the number of GLC molecules that are encapsulated in the core of PTOL cluster shows a sharp jump as soon as PTOL clusters begin to form. The calculations of first shell water molecules around different hydrophobic moieties of PTOL and GLC show dehydration of these atomic sites as PTOL clusters begin to form. These phenomena are further confirmed by contours of water and contours of PTOL density around the GLC molecule. The decomposition of drug-hydrotrope interactions into electrostatic and van der Waals components indicates that both these interactions are significant in the solubilization process. Cationic hydrotrope has significant effect on the average number of water-GLC, GLC-GLC and GLC-PTOL hydrogen bonds. The estimation of Flory-Huggins interaction param-

eter successfully explains the reason behind the incorporation of GLC into the core of PTOL clusters. These observations direct us to propose that self-aggregation of cationic hydrotrope is the main reason behind increased solubility.

The influence of the nonionic hydrotrope NIC on the solubilization of sparingly soluble RIB drug molecule is evaluated using classical MD simulation. To shed the light on the mechanism of hydrotropy of nonionic hydrotrope we examine various structural and Flory-Huggins interaction parameters. Analyses of the orientational distributions between two molecular planes of NIC supports that the NIC molecules form clusters through stacking of their pyridine ring. Furthermore, it is also found that NIC forms 1:1 (RIB:NIC) and 1:2 (RIB:NIC) stacking complexes with hydrophobic drug molecules. On the other hand, it is found that the average size of NIC clusters is not more than 7. Furthermore, with increase in concentration, as NIC molecules start to self-associate through stacking interactions, accumulation of NIC clusters around RIB molecules also increases. NIC aggregates prefer to occupy the peripheral position of RIB clusters. Cluster structure analyses also support that with increasing concentration, the probability of formation of higher order NIC clusters increases but the probability of large size RIB clusters formation decreases. Complexation between RIB and NIC (in 1:1 and 1:2 ratio) increases with increasing concentration of the hydrotrope. The estimated values of the first shell hydration number around different hydrophobic and hydrophilic moieties of RIB and NIC indicate the exclusion of water molecules from these atomic sites. Water molecules prefer to stay at the periphery of the RIB molecules and water density around the hydrophobic faces above and below the stack is not observed because these faces are occupied by the stacked hydrotrope molecules. Both electrostatic and van der Waals interaction energies between RIB and NIC play vital roles in the solubilization of drug molecules. The average numbers of hydrogen bonds between all the possible pairs show that the self-association of NIC molecules has negligible impact on water-water and water-NIC hydrogen bonds, but it affects the water-RIB, RIB-RIB, NIC-NIC and RIB-NIC hydrogen bonds. A highly negative χ_{FH} value indicates a very favorable interaction between RIB and NIC molecules. This observation supports the fact that complexation between drug and hydrotrope molecules is the main reason behind increased solubility of the former.

We have investigated the structural features of γ-tubulin protein through all-atom MD simulation. In this study, we propose a new target and new formulation method to inhibit microtubule assembly. Our strategy is to identify and validate binding sites at γ-tubulin protein and the release of griseofulvin drug molecule from SCS cluster and binds

on the specific sites of γ-tubulin protein. In this study we provide atomic-level description of the conformational changes of the protein caused by drug binding. Detailed analyses indicate that the γ-tubulin protein, in presence of hydrotrope molecules, is more flexible than in absence of hydrotrope molecules. The dominant effect due to griseofulvin binding is observed in the possible binding pockets. It alters the conformation of loops joining the H7 and H8 helices, H8 and H9 helices, and S10 and S11 strands and also the adjacent regions i.e., H6, H7, H8, H9, H11 helices and S7, S11, S13, S14 strands. These helices, loops and strands are crucial for binding of drug griseofulvin. We have found that griseofulvin is released from the hydrophobic core of hydrotrope clusters and binds to the γ-tubulin protein. We have also observed the existence of binding pockets at H8, H9 helices and S7, S8, S14 strands region. GLN-166 and SER-238 residues of γ-tubulin protein are important for hydrogen bonding interactions with the griseofulvin drug molecule. Results from MM-GBSA analyses imply that the hydrotrope alters the binding motif of griseofulvin and weakens the drug-protein interactions. It is the hydrophobic interactions between the drug and protein which mainly control the binding phenomenon.

Hydrotropy, we conclude, is a collective molecular effect which operates above the minimal hydrotrope concentration. A hydrotrope solution, above its MHC, contains noncovalent self-aggregates of the molecules. It can self-aggregate through hydrophobic interactions or through stacking interactions. The assembled structure of hydrotrope is different from that of a classical surfactant micelle. It appears that the insoluble solute molecules after finding their way through the interface of hydrotrope aggregates are encapsulated into the hydrophobic core of hydrotrope aggregates or held hidden in the hydrotropic stack. We support all the three hypothesis viz. (i) self-aggregation (ii) water structure breaking and (iii) complexation by which hydrotrope can solubilize insoluble or sparingly soluble molecules. So the hydrotropic mechanism depends upon the type of structure of hydrotrope. As hydrotropes possess a broad range of structures, therefore it is very difficult to propose a general mechanism of hydrotropy.

Bibliography

1. Neuberg, C. *Biochem. Z.* **76**, 107 (1916).
2. Freundlich, H. and Slottman, G. *Biochem. Z.* **188**, 101 (1927).
3. Traube, J.; Schning, I. and Weber, L. J. *Eur. J. Inorg. Chem.* **60**, 1808 (1927).
4. Hodgdon, T. K. and Kaler, E. W. *Curr. Opin. Colloid Interface Sci.* **12**, 121 (2007).
5. Balasubramanian, D. and Friberg, S. E. *In Surface and Colloid Science*, Matijevic, E., Ed.; Plenum Press: New York, Vol. 15 (1993).
6. Lomax, E. G. *Amphoteric Surfactants*, Ed.; Marcel Dekker, Inc: New York, 2nd edn, (1996).
7. Woolfson, A. D.; McCafferty, D. F. and Launchbury, A. P. *Int. J. Pharm.* **34**, 17 (1986).
8. Jain, N. K.; Patel, V. V. and Taneja, L. N. *Pharmazie* **43**, 254 (1988).
9. Osborne, D. W. *Colloids Surf.* **30**, 13 (1988).
10. Koparkar, Y. P. and Gaikar, V. G. *J. Chem. Eng. Data* **49**, 800 (2004).
11. Sherje, A. P. and Desai, K. J. *Indian J Pharm Sci.* **73**, 579 (2011).
12. Gaikar, V. G. and Sharma, M. M. *Solv. Extr. Ion Exch.* **4**, 839 (1986).
13. Agarwal M. and Gaikar V. G. *Sep. Technol.* **2**, 79 (1992).
14. Mahapatra A.; Gaikar, V. G. and Sharma, M. M. *Sep. Sci. Technol.* **23**, 429 (1988).
15. Raney, K. H. and Miller, C. A. *J. Colloid. Interface Sci.* **119**, 539 (1987).
16. Styan, G. E. and Bramhall, A. E. *Pulp Pap. Can.* **80**, 74 (1979).
17. Dandekar, D. V. and Gaikar, V. G. *Sep. Sci. Technol.* **38**, 1185 (2003).
18. Raman, G. and Gaikar, V. G. *Ind. Eng. Chem. Res.* **41**, 2966 (2002).
19. Sadvilkar, V. G.; Samant, S. D. and Gaikar, V. G. *J. Chem. Technol. Biotechnol.* **62**, 405 (1995).

20. Heldt, N.; Zhao, J.; Friberg, S.; Zhang, Z.; Slack, Y. and Li, Y. *Tetrahedron* **56**, 6985 (2000).

21. Friberg, S. E.; Yang, J. and Huang, T. A *Ind. Eng. Chem. Res.* **35**, 2856 (1996).

22. Guo, R.; Zhang, Q.; Qian, J. and Zou, A. *Colloids Surf. A: Physicochem. Eng. Aspects* **196**, 223 (2002).

23. McKee, R. H. *Ind. Eng. Chem.* **38**, 382 (1946).

24. Maheshwari, R. K. and Singh. M. *Asian J. Chem.* **2**, 4922 (2008).

25. Danielson, I. and Stenius, P. *J. Colloid Interface Sci.* **37**, 264 (1971).

26. Hopkins H. M.; Eastoe, J.; Dowding, P. J.; Rogers, S. E.; Heenan, R. K. and Dyer, R. *Langmuir* **27**, 12346 (2011).

27. Kim, J. Y.; Kim, S.; Papp, M.; Park, K. and Pinal, R. *J. Pharm. Sci.* **99**, 3953 (2010).

28. Bauduin, P.; Renoncourt, A.; Kopf, S.; Touraud, D. and Kunz, W. *Langmuir* **21**, 6769 (2005).

29. Wagle, V. B.; Kothari, P. S. and Gaikar, V. G. *J. Mol. Liq.* **133**, 68 (2007).

30. Balasubramanian, D. and Srinivas, V. *Langmuir* **14**, 6658 (1998).

31. Bancroft, W. D. *Science* **82**, 388 (1935).

32. Booth, H. S. and Everson, H. E. *Ind. Eng. Chem.* **40**, 1491 (1948).

33. Winsor, P. A. *Trans. Faraday Soc.* **44**, 376 (1948).

34. Licht, W. and Wiener, L. D. *Ind. Eng. Chem.* **42**, 1538 (1950).

35. Deno, N. C. and Spink, C. H. *J. Phys. Chem.* **67**, 1347 (1963).

36. Ueda, S. *Chem. Pharm. Bull.* **14**, 22 (1966).

37. Rath, H. *Tenside* **2**, 1 (1965).

38. Rawat, S and Jain, N. K. *Indian Drugs* **43**, 565 (2006).

39. Poochikian, G. K. and Cradock, J. C. *J. Pharm. Sci.* **68**, 728 (1979).

40. Badwan, A. A. *Intern. J. Pharm.* **13**, 67 (1983).

41. Balasubramanian, D.; Srinivas, V.; Gaikar, V. G. and Sharma, M. M. *J. Phys. Chem.* **93**, 3865 (1989).

42. da Silva, R. C.; Spitzer, M.; da Silva, L. S. H. M.; and Loh, W. *Thermochim. Acta* **328**, 161 (1999).

43. Coffman, R. E. and Kildsig, D. O. *J. Pharm. Sci.* **85**, 951 (1996).

44. Balasubramanian, D.; Srinivas, V.; Rodley, G. A.; Ravikumar, K.; Robinson, W. T. and Turnbull, M. M. *Langmuir* **13**, 3235 (1997).

45. Triolo, R.; Ho, P. C. and Johnson, J. S. *J. Phys. Chem.* **99**, 9581 (1995).

46. Ferreira, G.; Perigo, D. M.; Politi, M. J. and Schreier, S. *Photochem. Photobiol.* **63**, 755 (1996).

47. Frank, H. S. and Franks, F. *J. Chem. Phys.* **48**, 4746 (1968).

48. Sanghi, R.; Evans, D. and Yalkowsky, S. H. *Int. J. Pharm.* **336**, 35 (2007).

49. Cui, Y. *Int. J. Pharm.* **397**, 36 (2010).

50. Korenman, Y. I. *J. Phys. Chem.* **48**, 653 (1974).

51. Rasool A. A.; Hussain A. A. and Dittert L. W. *J. Pharm. Sci.* **80**, 387 (1991).

52. Booth, J. J.; Abbott, S. and Shimizu, S. *J. Phys. Chem. B* **116**, 14915 (2012).

53. Shimizu, S. and Matubayasi, N. *J. Phys. Chem. B* **118**, 10515 (2014).

54. Booth, J. J.; Omar, M.; Abbott, S. and Shimizu, S. *Phys. Chem. Chem. Phys.* **17**, 8028 (2015).

55. Bauduin, P.; Testard, F. and Zemb, Th. *J. Phys. Chem. B* **112**, 12354 (2008).

56. Ponder J. W. and Case D. A. *Adv. Prot. Chem.* **66**, 27 (2003).

57. Lennard-Jones, J. E. *Proc. R. Soc. London, Ser. A* **106**, 463 (1924).

58. van der Waals, J. D. *Verhandelingen der Koninklijke Akademie der Wetenschappen* **1**, 1 (1893).

59. Coulomb, C. A. *Collection de ḿemoires relatifs à la physique* Gauthier-Villars, 569-638 (1884).

60. Verlet, L. *Phys. Rev.* **159**, 98 (1967).

61. Hockney, R. W. *Meth. Comp. Phys.* **9**, 136 (1970).

62. Flory, P. J. *J. Chem. Phys.* **10**, 51 (1942).

63. Huggins, M. L. *J. Chem. Phys.* **9**, 440 (1941).

64. Huynh, L.; Grant, J.; Leroux, J.-C.; Delmas, P. and Allen, C. *Pharm. Res.* **25**, 147 (2008).

65. Case, F. H. and Honeycutt, D. J. *TRIP* **2**, 256 (1994).

66. Patel, S.; Lavasanifar, A. and Choi, P. *Biomacromolecules* **9**, 3023 (2008).

67. Kasimova, O. A.; Pavan. M. G.; Danani. A.; Modan. K.; Cristiani, A.; Scapozza, L.; Gurny, R. and Moller, M. *J. Phys. Chem. B* **116**, 4338 (2012).

68. Xiang,T.X. and Anderson, B. D. *J. Pharm. Sci.* **102**, 876 (2013).

69. Srinivasan, J.; Cheatham, T. E.; Cieplak, P.; Kollman, P. A. and Case, D. A. *J. Am. Chem. Soc.* **120**, 9401 (1998).

70. Jayaram, B.; Sprous, D. and Beveridge, D. L. *J. Phys. Chem. B* **102**, 9571 (1998).

71. Onufriev, A.; Bashford, D. and Case, D. A. *Proteins. Struct. Funct. Bioinf.* **55**, 383 (2004).

72. Neumann, M.G.; Schmitt, C. C; Prieto, K. R. and Goi, B. E. *J. Colloid Interface Sci.* **315**, 810 (2007).

73. Hassan, P. A.; Raghavan, S. R. and Kaler, E. W. *Langmuir* **18**, 2543 (2002).

74. Mishra, S. P. and Gaikar, V. G. *Ind. Eng. Chem. Res.* **43**, 5339 (2004).

75. Mathew, D. S. and Gaikar, V. G. *Ind. Eng. Chem. Res.* **44**, 434 (2005).

76. Case, D. A.; Darden, T. A.; Cheatham, III, T. E.; Simmerling, C. L.; Wang, J.; Duke, R. E.; Luo, R.; Walker, R. C.; Zhang, W.; Merz, K. M.; Roberts, B.; Hayik, S.; Roitberg, A.; Seabra, G.; Swails, J.; Gtz, A. w.; Kolossvry, I.; Wong, K. F.; Paesani,

F.; Vanicek, J.; Wolf, R. M.; Liu, J.; Wu, X.; Brozell, S. R.; Steinbrecher, T.; Gohlke, H.; Cai, Q.; Ye, X.; Wang, J.; Hsieh, M. J.; Cui, G.; Roe, D. R.; Mathews, D. H.; Seetin, M. G.; Salomon-Ferrer, R.; Sagui, C.; Babin, V.; Luchko, T.; Gusarov, S.; Kovalenko, A. and Kollman P. A. AMBER 12, University of California, San Francisco (2012).

77. Berendsen, H. J. C.; Grigera, J. R. and Straatsma, T. P. *J. Phys. Chem.* **91**, 6269 (1987).

78. Vanommeslaeghe, K.; Hatcher, E.; Acharya, C.; Kundu, S.; Zhong, S.; Shim, J.; Darian, E.; Guvench, O.; Lopes, P.; Vorobyov, I. and Mackerell Jr, A. D. *J. Comput. Chem.* **31**, 671 (2010).

79. e, X.; Guvench, O.; MacKerell, A. D. and Klein, M. L. *J. Phys. Chem. B* **114**, 9787 (2010).

80. Mark, P. and Nilsson, L. *J. Phys. Chem. A* **105**, 9954 (2001).

81. Crowley, M. F.; Williamson, M. J. and Walker, R. C. *J. Comput. Chem.* **109**, 3767 (2009).

82. Martinez L.; Andrade R.; Birgin E. G. and Martinez J. M. *J. Comput. Chem.* **30**, 2157 (2009).

83. Berendsen, H. J. C.; Postma, J. P. M.; van Gunsteren, W. F.; DiNola, A. and Haak, J. R. *J. Chem. Phys.* **81**, 3684 (1984).

84. Ryckaert, J. P.; Ciccotti, G. and Berendsen, H. J. C. *J. Comput. Phys.* **23**, 327 (1927).

85. Humphrey, W.; Dalke, A. and Schulten, K. VMD: Visual Molecular Dynamics. *J. Molec. Graphics.* **14**, 33 (1996).

86. Wandrey, C.; Bartkowiak, A. and Hunkeler, D. *Langmuir* **15**, 4062 (1999).

87. Leduc, P. A.; Fortier, J. L. and Desnoyers, J. E. *J. Phys. Chem.* **78**, 1217 (1974).

88. Goolam, M. M.; Gerald, P. and Jacques, E. D. *J. Colloid Interface Sci.* **54**, 80 (1976).

89. Musbally, M. G.; Perron, G. and Denoyers, J. E. *J. Colloid Interface Sci.* **48**, 494 (1974).

90. Gaikar, V. G. and Wagle, V. B. *J. Chem. Eng. Data* **51**, 886 (2006).

91. Sharma, B. and Paul, S. *J. Chem. Phys.* **139**, 194504 (2013).

92. Chowdhury, S. and Chandra, A. *J. Chem. Phys.* **115**, 3732 (2001).

93. Luzar. A. and Chandler, D. *Phys. Rev. Lett.* **76**, 928 (1996).

94. Chandra, A. *Phys. Rev. Lett.* **85**, 768 (2000).

95. Chandra, A. *J. Phys. Chem. B* **107**, 3899 (2003).

96. W. L. Jorgensen, D. S. Maxwell and J. Tirado-Rives *J. Am. Chem. Soc.* **118**, 11225 (1996).

97. Edwards, D. A.; Luthy, R. G. and Liu, Z. *Environ. Sci. Technol.* **25**, 127 (1991).

98. Gref, R.; Minamitake, Y.; Peracchia, MT.; Trubetskoy, V.; Torchilin, V. and Langer R. *Science* **263**, 1600 (1994).

99. Torchilin, V. P. *J. Control. Rel.* **73**, 137 (2001).

100. Rosen, M. J. *Surfactants and interfacial phenomena*, 2ed., John Wiley & Sons, New York, (1989).

101. Hargreaves, R.; Bowron, D, T.; Edler, K. *J. Am. Chem. Soc.* **133**, 16524 (2011).

102. Jorge, M. *J. Mol. Struc. (THEOCHEM)* **946**, 88 (2010).

103. Wang, Z. W. and Larson, R. G. *J. Phys. Chem. B* **113**, 13697 (2009).

104. Gillams, R. J.; Busto, J. V.; Busch, S.; Goni, F. M.; Lorenz, C. D. and McLain, S. E. *J. Phys. Chem. B* **119**, 128 (2015).

105. Malardier-Jugroot, C.; Bowron, D. T.; Soper, A. K.; Johnson, M. E. and Head-Gordon, T. *Phys. Chem. Chem. Phys.* **12**, 382 (2010).

106. Mason, P. E.; Neilson, G. W.; Dempsey, C. E.; Price, D. L.; Saboungi, M-L. and Brady, J. W. *J. Phys. Chem. B* **114**, 5412 (2010).

107. Mason, P. E.; Neilson, G. W.; Price, D.; Saboungi, M-L. and Brady, J. W. *Food Biophys.* **6**, 210 (2011).

108. Bowron, D. T.; Finney, J. L. and Soper, A. K. *J. Phys. Chem. B* **102**, 3551 (1998).

109. Fornili, A.; Civera, M.; Sironi, M. and Fornili, S. L. *Phys. Chem. Chem. Phys.* **5**, 4905 (2003).

110. Paul, S. and Patey, G. N. *J. Phys. Chem. B* **110**, 10514 (2006).

111. Leeson, P. D. and Springthorpe, B. *Nat Rev Drug Discov.* **6**, 881 (2007).

112. Subbarao, C. V.; Chackravarthy, I. P. K.; Sai Bharadwaj, A. V. S. L. and Prasad, K. M. M. *Chem. Eng. Technol.* **35**, 225 (2012).

113. Saleh, A. M. and Elkhordagui, L. K. *Int. J. Pharm.* **24**, 231 (1985).

114. Chan, Y. C. and Friedlander, S. F. *Curr. Opin. Infect. Dis.* **17**, 97 (2004).

115. Panda, D.; Rathinasamy, K.; Santra, M. K. and Wilson, L. *Proc. Natl. Acad. Sci. U.S.A.* **102**, 9878 (2005).

116. Thomson Reuters *NEWPORT* database, (2011).

117. Kasim, N. A.; Whitehouse, M.; Ramachandran, C.; Bermejo, M.; Lennerna, H.; Hussain, A. S.; Junginger, H. E.; Stavchansky, S. A.; Midha, K. K.; Shah, V. P. and Amidon, G. L. *Mol. Pharmaceutics* **1**, 85 (2004).

118. Wang, J.; Wolf, R. M.; Caldwell, J. W.; Kollman, P. A. and Case, D. A. *J. Comput. Chem.* **25**, 1157 (2004).

119. Jakalian, A.; Bush, B. L.; Jack, D. B. and Bayly, C. I. *J. Comput. Chem.* **21**, 132 (2000).

120. Jakalian, A.; Jack, D. B. and Bayly, C. I. *J. Comput. Chem.* **23**, 1623 (2002).

121. Wang, J.; Wang, W.; Kollman, P. A. and Case, D. A. *J. Mol. Graphics Modell.* **25**, 247 (2006).

122. Troitzsch, R. Z.; Martyna, G. J.; McLain, S. E.; Soper, A. K. and Crain, J. *J. Phys. Chem. B* **111**, 8210 (2007).

123. McLain, S. E.; Soper, A. K.; Terry, A. E. and Watts, A. *J. Phys. Chem. B* **111**, 4568 (2007).

124. Paul, S. and Paul, S. *J. Phys. Chem. B* **119**, 10975 (2015).

125. Shimizu, S.; Booth, J. J. and Abbott, S. *Phys. Chem. Chem. Phys.* **15**, 20625 (2013).

126. Busch, S.; Lorenz, C. D.; Taylor, J.; Pardo, L. C. and McLain, S. E. *J. Phys. Chem. B* **118**, 14267 (2014).

127. Mason, P. E.; Neilson, G. W.; Price, D.; Saboungi, M.-L. and Brady, J. W. *Food Biophys.* **6**, 210 (2011).

128. McLain, S. E.; Soper, A. K.; Daidone, I.; Smith, J. C. and Watts, A. *Angew. Chem. Int. Ed.* **47**, 9059 (2008).

129. Rhys, N. H.; Soper, A. K. and Dougan, L. *J. Phys. Chem. B* **119**, 15644 (2015).

130. Mason, P. E.; Dempsey, C. E.; Neilson, G. W.; Kline, S. R. and Brady, J. W. *J. Am. Chem. Soc.* **131**, 16689 (2009).

131. Zaheer, A.; Naveen, M.; Santosh, M. K. and Imran, K. *Int. J. Pharm. Tech.* **3**, 807 (2011).

132. Nidhi, K.; Indrajeet, S.; Khushboo, M; Gauri, K and Sen, D. J. *Int. J. Drug. Dev. Res.* **3**, 26 (2011).

133. Alkhamis, K. A.; Allaboun, H. and Al-Momani, W. Y. *J. Pharm. Sci.* **92**, 839 (2003).

134. Varshosaz, J.; Talari, R.; Mostafavi, S.A. and Nokhodchi, A. *Powder Technol.* **187**, 222 (2008).

135. Saharan, V. A. and Choudhury, P. K. *Acta Pharm.* **61**, 323 (2011).

136. Palmer, K. J. and Brogden, R. N. *Drugs* **46**, 92 (1993).

137. Frisch, M. J.; Trucks, G. W.; Schlegel, H. B.; Scuseria, G. E.; Robb, M. A.; Cheeseman, J. R.; Scalmani, G.; Barone, V.; Mennucci, B.; Petersson, G. A.; Nakatsuji, H.; Caricato, M.; Li, X.; Hratchian, H. P.; Izmaylov, A. F.; Bloino, J.; Zheng, G.; Sonnenberg, J. L.; Hada, M.; Ehara, M.; Toyota, K.; Fukuda, R.; Hasegawa, J.; Ishida, M.; Nakajima, T.; Honda, Y.; Kitao, O.; Nakai, H.; Vreven, T.; Montgomery, Jr., J. A.; Peralta, J. E.; Ogliaro, F.; Bearpark, M.; Heyd, J. J.; Brothers, E.; Kudin, K. N.; Staroverov, V. N.; Kobayashi, R.; Normand, J.; Raghavachari, K.; Rendell, A.;

Burant, J. C.; Iyengar, S. S.; Tomasi, J.; Cossi, M.; Rega, N.; Millam, J. M.; Klene, M.; Knox, J. E.; Cross, J. B.; Bakken, V.; Adamo, C.; Jaramillo, J.; Gomperts, R.; Stratmann, R. E.; Yazyev, O.; Austin, A. J.; Cammi, R.; Pomelli, C.; Ochterski, J. W.; Martin, R. L.; Morokuma, K.; Zakrzewski, V. G.; Voth, G. A.; Salvador, P.; Dannenberg, J. J.; Dapprich, S.; Daniels, A. D.; Farkas, .; Foresman, J. B.; Ortiz, J. V.; Cioslowski, J. and Fox, D. J. Gaussian 09, Revision A.1, Gaussian, Inc., Wallingford CT, (2009).

138. Bayly, C.I.; Cieplak, P.; Cornell, W.D. and Kollman, P.A. *J. Phys. Chem.* **97**, 10269 (1993).

139. Hunenberger, P. H. *Adv. Polym. Sci.* **173**, 105 (2005).

140. Essmann, U.; Perera, L.; Berkowitz, M. L.; Darden, T.; Lee, H. and Pedersen, L. J. *J. Chem. Phys.* **103**, 8577 (1995).

141. Lee, J.; Lee, S. C.; Acharya, G.; Chang, C. and Park, K. *Pharm. Res.* **20**, 1022 (2003).

142. Lim, L. and Go, M. *Eur. J. Pharm. Sci.* **10**, 17 (2000).

143. Agrawal, S.; Pancholi, S. S.; Jain, N. K. and Agrawal, G. P. *Int. J. Pharm.* **274**, 149 (2004).

144. Hussain, M. A.; Diluccio, R. C. and Maurin, M. B. *J. Pharm. Sci.* **82**, 77 (1993).

145. Suzuki, H. and Sunada, H. *Chem. Pharm. Bull.* **46**, 125 (1998).

146. Chen, A. X.; Zito, S. W. and Nash, R. A. *Pharm. Res.* **11**, 398 (1994).

147. Hata, S.; Mizuno, K. and Tomioka, S. *Chem. Pharm. Bull.* **15**, 1719 (1967).

148. Fawzi, M. B.; Davison, E. and Tute, M. S. *J. Pharm. Sci.* **69**, 104 (1980).

149. Badwan, A. A.; El-Khordagui, L. K.; Saleh, A. M. and Khalil, S. A. *Int. J. Pharm.* **13**, 67 (1983).

150. Kenley, R. A.; Jackson, S. E.; Winterle, J. S.; Shunko, Y. and Visor, G. *J. Pharm. Sci.* **75**, 648 (1986).

151. Coffman, R. E. and Kildsig, D. O. *Pharm. Res.* **13**, 1460 (1996).

152. Yong, C.; Chenyue, X. and Yingqing, R. *J. Pharm. Sci.* **99**, 3048 (2010).

153. Oberoi, L. M.; Alexender, K. S. and Riga, A. T. *J. Pharm. Sci.* **94**, 93 (2005).

154. Wollensak, G.; Spoerl, E. and Seiler, T. *Am. J. Ophthalmol.* **135**, 620 (2003).

155. http://www.who.int/topics/cancer/en/index.html

156. Lozano, R.; Naghavi, M.; Foreman, K.; Lim, S.; Shibuya, K.; Aboyans, V.; Abraham, J.; Adair, T.; Aggarwal, R.; Ahn, S. Y. and AlMazroa, M. A. et al. *Lancet* **380**, 2095 (2012).

157. Bray, F.; Ren, J. S.; Masuyer, E. and Ferlay, J. *Int. J. Cancer* **132**, 1133 (2013).

158. Hussain, S. A. and Sullivan, R. *Jpn. J. Clin. Oncol.* **43**, 1159 (2013).

159. Bornens, M. *Science* **335**, 422 (2012).

160. Gergely, F. and Basto, R. *Genes Dev.* **22**, 2291 (2008).

161. Guha, D. B.; Saeed, M. E. M.; Greten, H. J. and Efferth. T. *Curr. Med. Chem.* **22**, 685 (2015).

162. Krmer, A.; Maier, B. and Bartek, J. *Mol. Oncol.* **5**, 324 (2011).

163. OToole, E.; Greenan, G.; Lange, K.I.; Srayko, M. and Muller-Reichert, T. *PLoS ONE* **7**, e29795 (2012).

164. Nguyen, C. L.; Eichwald, C.; Nibert, M. L. and Mnger, K. *J. Virol.* **81**, 13533 (2007).

165. Ho, Y. S.; Duh, J. S.; Jeng, J. H.; Wang, Y. J.; Liang, Y. C.; Lin, C. H.; Tseng, C. J.; Yu, C. F.; Chen, R. J. and Lin, J. K. *Int. J. Cancer.* **91**, 393 (2001).

166. Panda, D.; Rathinasamy, K.; Santra, M. K. and Wilson, L. *Proc. Nat. Acad. Sci. USA.* **102**, 9878 (2005).

167. Rebacz, B.; Larsen, T. O.; Clausen, M. H.; Ronnest, M. H.; Loffler, H.; Ho, A. D. and Krmer, A. *Cancer Res.* **67**, 6342 (2007).

168. Singh, P.; Rathinasamy, K.; Mohan, R. and Panda, D. *IUBMB Life* **60**, 368 (2008).

169. Uen, Y. H.; Liu, D. Z.; Weng, M. S.; Ho, Y. S. and Lin, S. Y. *J. Cell. Biochem.* **101**, 1165 (2007).

170. Czymmek, K. J.; Bourett, T. M.; Shao, Y.; DeZwaan, T. M.; Sweigard, J. A. and Howard, R. J. *Protoplasma* **225**, 23 (2005).

171. De, C. L. and Larizza, L. *Muta. Res.* **195**, 91 (1988).

172. Brown, R. C. and Lemmon, B. E. *J. Cell. Sci.* **103**, 1031 (1992).

173. Voutsinas, G.; Zarani, F. E. and Kappas, A. *Cell. Biol. Int.* **21**, 411 (1997).

174. Brian, P. W. *Annals of Botany* **13**, 59 (1949).

175. Barros, M. E. d. S.; de Assis, S. D. and Hamdan, J. S. *J. Med. Microbiol.* **56**, 514 (2007).

176. Chaudhuri, A. R. and Luduena, R. F. *Biochem. Pharmacol.* **51**, 903 (1996).

177. Wehland, J.; Herzog, W. and Weber, K. *J. Mol. Biol.* **111**, 329 (1977).

178. Roobol, A.; Gull, K. and Pogson, C. I. *FEBS Lett.* **67**, 248 (1976).

179. Sloboda, R. D.; Van, B. G.; Creasey, W. A.; Rosenbaum. J. L. and Malawista, S. E. *Biochem. Biophys. Res. Commun.* **105**, 882 (1982).

180. Weber, K.; Wehland, J. and Herzog, W. *J. Mol. Biol.* **102**, 817 (1976).

181. Roobol, A.; Gull, K. and Pogson, C. I. *Biochem. J.* **167**, 39 (1977).

182. Kumbhar, B. V.; Borogaon, A.; Panda, D. and Kunwar, A. *PLoS ONE* **11**, e0156048 (2016).

183. Natarajan, K. and Senapati, S. *PLoS ONE* **7**, e42351 (2012).

184. Rice, L. M.; Montabana, E. A. and Agard, D. A. *Proc. Natl. Acad. Sci. Usa* **105**, 5378 (2008).

185. Madej, T.; Lanczycki, C. J.; Zhang, D.; Thiessen, P. A.; Geer, R. C.; Marchler-Bauer, A. and Bryant S H. *Nucleic Acids Res.* **42(Database issue):D297-303** (2014).

186. Insight II, Accelrys Inc. San Diego CA (1996).

187. Hornak, V.; Abel, R.; Okur, A.; Strockbine, B.; Roitberg, A. and Simmerling, C. *Proteins.* **65**, 712 (2006).

188. Friesen, D. E.; Barakat, K. H.; Semenchenko, V.; Perez-Pineiro, R.; Fenske, B. W.; Mane, J.; Wishart, D. S. and Tuszynski, J. A. *Chem Biol Drug Des* **79**, 639 (2012).

List of Publications

1. Shubhadip Das and Sandip Paul, Exploring Molecular Insights into Aggregation of Hydrotrope Sodium Cumene Sulfonate in Aqueous Solution: A Molecular Dynamics Simulation Study *J. Phys. Chem. B* **119**, 3142-3154 (2015).

2. Shubhadip Das and Sandip Paul, Mechanism of Hydrotropic Action of Hydrotrope Sodium Cumene Sulfonate on the Solubility of Di-t-Butyl-Methane: A Molecular Dynamics Simulation Study *J. Phys. Chem. B* **120**, 173-183 (2016).

3. Shubhadip Das and Sandip Paul, Computer Simulation Studies of the Mechanism of Hydrotrope-Assisted Solubilization of a Sparingly Soluble Drug Molecule *J. Phys. Chem. B* **120**, 3540-3550 (2016).

4. Shubhadip Das and Sandip Paul, Hydrotropic Action of Cationic Hydrotrope p-Toluidinium Chloride on the Solubility of Sparingly Soluble Gliclazide Drug Molecule: A Computational Study *J. Chem. Inf. Model.* **57**, 1461-1473 (2017).

5. Shubhadip Das and Sandip Paul, Hydrotropic Solubilization of Sparingly Soluble Riboflavin Drug Molecule in Aqueous Nicotinamide Solution *J. Phys. Chem. B* **DOI: 10.1021/acs.jpcb.7b05774** (2017).

6. Shubhadip Das and Sandip Paul, Exploring the Binding Sites and Binding Mechanism for Hydrotrope Encapsulated Griseofulvin Drug on γ-Tubulin Protein *PLOS ONE* (Manuscript Under Revision).

Conferences Attended

1. Presented a poster entitled "Concentration Dependent Aggregation Behavior of Hydrotrope Molecules" in the conference "Current Trends in Theoretical Chemistry (CTTC-2013)" held at Bhabha Atomic Research Centre Mumbai.

2. Presented a poster entitled "Exploring Molecular Insights of Aggregation of Hydrotrope Sodium Cumene Sulfonate in Aqueous Solution: A Molecular Dynamics Simulation Study" in the conference "Theoretical Chemistry Symposium (TCS-2014)" held at NCL-Pune and IISER Pune.

2. Presented a poster entitled "Mechanism of Hydrotropic Action of Hydrotrope Sodium Cumene Sulfonate on the Solubility of Di-t-Butyl-Methane: A Molecular Dynamics Simulation Study" in the conference "Chem Convene (2015)" held at IIT Guwahati.

4. Presented a poster entitled "Computer Simulation Studies of the Mechanism of Hydrotrope Assisted Solubilization of Sparingly Soluble Drug Molecule" in the conference "Theoretical Chemistry Symposium (TCS-2016)" held at University of Hyderabad.